AD-A072 644 COLORADO UNIV BOULDER DEPT OF ELECTRICAL ENGINEERING F/G 13/8
QUANTITATIVE SYNTHESIS OF MULTIPLE LOOP FEEDBACK SYSTEMS WITH L--ETC(U)
JUN 79 T WANG, I HOROWITZ AFOSR-76-2946

UNCLASSIFIED AFOSR-TR-79-0880 NL

1 OF 3
AD A072644

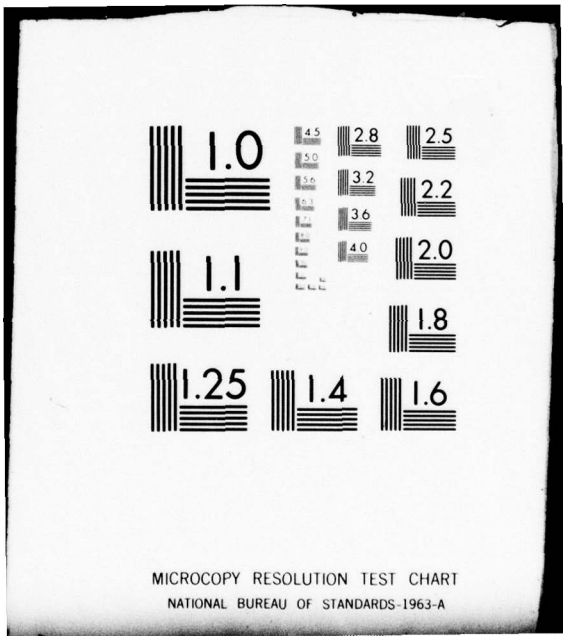
1.0
1.1
1.25
1.4
1.6
1.8
2.0
2.2
2.5
2.8
3.2
3.6
4.0
4.5
5.0
5.6
6.3
7.1
8.0
9.0
MICROCOPY RESOLUTION TEST CHART
NATIONAL BUREAU OF STANDARDS-1963-A

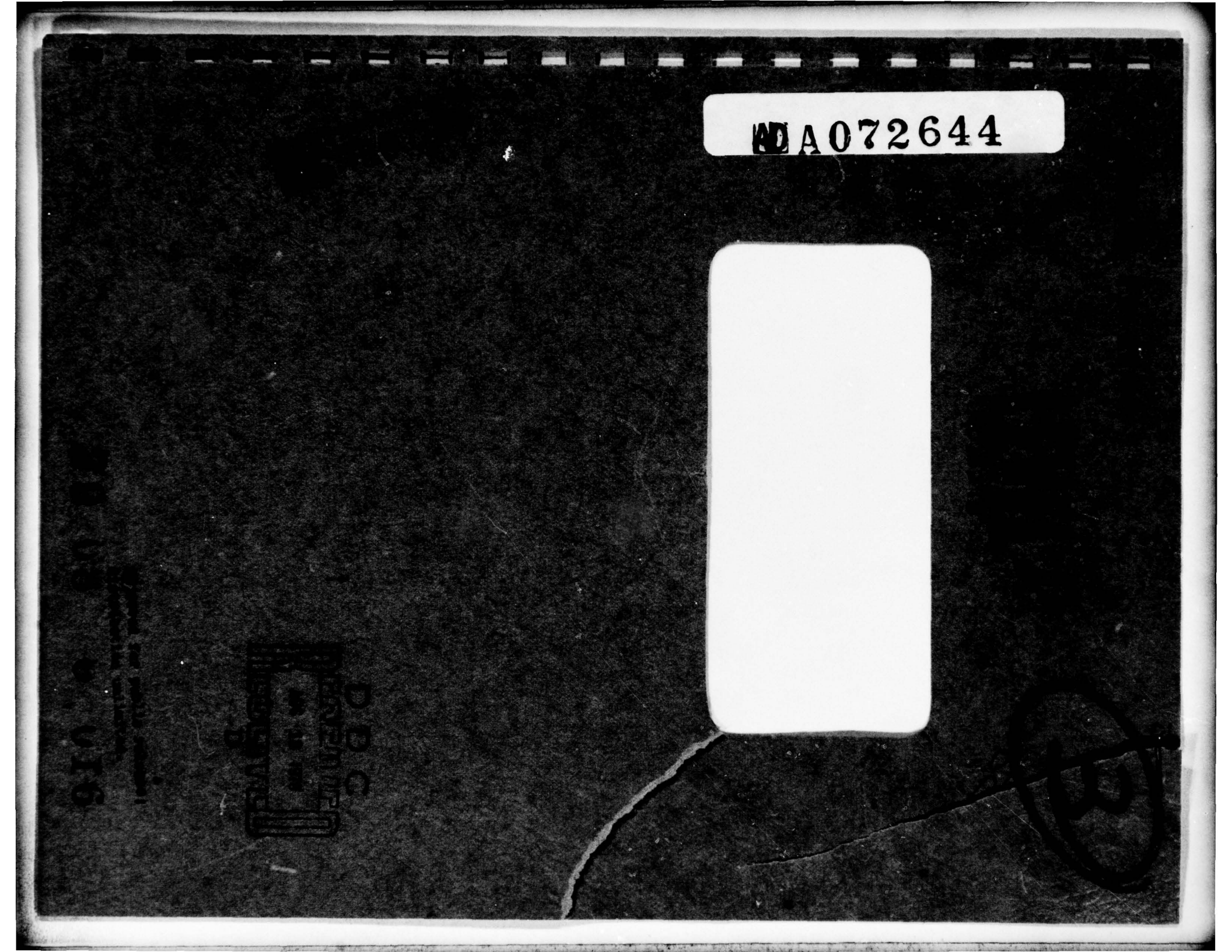

LEVEL II

3

QUANTITATIVE SYNTHESIS OF MULTIPLE LOOP FEEDBACK SYSTEMS WITH LARGE PLANT UNCERTAINTY

by

Te-Shing Wang
Isaac Horowitz

Department of Electrical Engineering
University of Colorado
Boulder, Colorado 80309

This research was supported in part by the
AIR FORCE OFFICE OF SCIENTIFIC RESEARCH
under Research Grant AFOSR-76-2946C

June 1979

UNCLASSIFIED

SECURITY CLASSIFICATION OF THIS PAGE (When Data Entered)

REPORT DOCUMENTATION PAGE	READ INSTRUCTIONS BEFORE COMPLETING FORM
1. REPORT NUMBER: AFOSR-TR-79-0880	2. GOVT ACCESSION NO. / 3. RECIPIENT'S CATALOG NUMBER
4. TITLE (and Subtitle): QUANTITATIVE SYNTHESIS OF MULTIPLE LOOP FEEDBACK SYSTEMS WITH LARGE PLANT UNCERTAINTY.	5. TYPE OF REPORT & PERIOD COVERED: Interim rept.
	6. PERFORMING ORG. REPORT NUMBER
7. AUTHOR(s): Te-Shing Wang, Isaac Horowitz	8. CONTRACT OR GRANT NUMBER(s): AFOSR-76-2946
9. PERFORMING ORGANIZATION NAME AND ADDRESS: Department of Electrical Engineering, University of Colorado, Boulder, Colorado 80309	10. PROGRAM ELEMENT, PROJECT, TASK AREA & WORK UNIT NUMBERS: 61102F 2304 A1
11. CONTROLLING OFFICE NAME AND ADDRESS: Air Force Office of Scientific Research/NM, Bolling AFB, Washington, D.C. 20332	12. REPORT DATE: June 1979 / 13. NUMBER OF PAGES: 186 (194p)
14. MONITORING AGENCY NAME & ADDRESS (if different from Controlling Office)	15. SECURITY CLASS. (of this report): UNCLASSIFIED / 15a. DECLASSIFICATION/DOWNGRADING SCHEDULE

16. DISTRIBUTION STATEMENT (of this Report)

Approved for public release; distribution unlimited.

17. DISTRIBUTION STATEMENT (of the abstract entered in Block 20, if different from Report)

18. SUPPLEMENTARY NOTES

19. KEY WORDS (Continue on reverse side if necessary and identify by block number)

Multiple loop feedback systems uncertain feedback systems

20. ABSTRACT (Continue on reverse side if necessary and identify by block number)

This work extends single input-output linear time invariant minimum-phase "quantitative feedback synthesis" to two new complex plant structures with internal sensing points. One is the triangular structure. The second consists of parallel branches, each with cascaded sections. Due to uncertainty, the plant parameters are elements of given sets. The system response must satisfy specified time or frequency domain tolerances. The basic problem is how to divide the feedback burden among the available loops so as to minimize the net rms effect at the plant input, of the various sensor noise sources.

DD FORM 1 JAN 73 1473

088 440

JOB

Abstract

This work extends single input-output linear time invariant minimum-phase "quantitative feedback synthesis" to two new complex plant structures with internal sensing points. One is the triangular structure. The second consists of parallel branches, each with cascaded sections. Due to uncertainty, the plant parameters are elements of given sets. The system response must satisfy specified time or frequency domain tolerances. The basic problem is how to divide the feedback burden among the available loops so as to minimize the net rms effect at the plant input, of the various sensor noise sources.

Frequency-response formulations are presented which provide a deep understanding of the trade-off among the feedback loops. One vital feature is "free uncertainty", wherein a loop optimized to cope with uncertainty U_1, may in fact for some frequency ranges, handle uncertainty $U >> U_1$. A second is "bandwidth propagation", wherein the loops take turns in dominating the design over the frequency range. Together, they locate the frequency regions in which the respective loops dominate, and the key trade-off parameters among them. "Design Perspective" then enables the designer to very rapidly find a close approximation to the precise design based on any choice of these parameters. Numerous design examples with very large uncertainty, illustrate the design procedures and the advantages of multiple-loop design.

TABLE OF CONTENTS

CHAPTER 1

STATEMENT OF PROBLEM AND PRELIMINARY BACKGROUND

1.1 Introduction

This work deals with the problem of making a system perform satisfactorily despite uncertainty, in the following context:

Equipment has been assembled by specialists in the area of concern, in order to achieve certain objectives, for example, an airframe and engine for accomplishment of certain aeronautical objectives, a chemical plant for production of certain chemicals, etc. This assembly of equipment is denoted as the plant. The plant has the ability, the muscle so to speak, to achieve the objectives. However, it does not have the accuracy needed. This is manifested by uncertainty in the parameters of the mathematical relations describing the plant. For example in Figure 1.1, suppose the relation

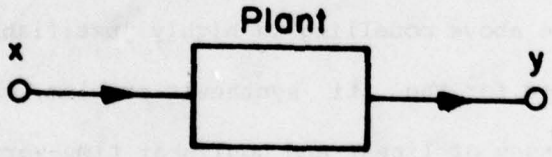

Figure 1-1. Plant

between plant output y and input x is given by a linear time-invariant (lti) ordinary differential equation

$$y^{(n)} + A_1 y^{(n-1)} + \ldots + A_n y = K[x^{(m)} + B_1 x^{(m-1)} + \ldots + B_m x] \qquad (1.1\text{-}1)$$

i.e., the A_i , B_j are constants. There are q physical parameters $k_1,\ldots,k_q$ and K , A_i , B_j are functions of these parameters. The values of these parameters are not known precisely, but it is known that they lie within certain bounds $k_i \in [k_i^1, k_i^2]$. Hence, each possible parameter vector k , each combination of k_i values $i = 1,\ldots,q$, gives a different plant transfer function, generating a set $\mathcal{P} = \{P(s)\}$ of possible plant transfer functions.

Such a formulation of the uncertainty problem may appear naive because one might argue that often the parameter values change with time-giving uncertain linear time-varying relations, because the rate of variation is uncertain. Also, the lti description is usually an approximation of a nonlinear relation. We are really assuming lti relations with the above uncertainty form, in order to be able to rigorously use Laplace transforms and frequency response methods. However, it has been rigorously proven [H1] that a large class of practical uncertain linear time-varying plant problems is reducible to the above lti uncertainty form, and even uncertain nonlinear time-varying plants to a certain extent [H2], can be so reduced. Hence the above modelling is highly justifiable, because the techniques developed for the lti synthesis problem, can be rigorously used for these classes of linear and nonlinear time-varying synthesis problems. Finally, one must begin somewhere with the development of a scientific synthesis theory for uncertain systems, and "scientific" implies "quantitative". The lti case is obviously where to start.

The objective is to achieve certain apriori specified performance objectives $\forall\, P \in \mathcal{P}$. Since the overall system is to be lti , it can be characterized by its response to any input, and the

step response is very popular because it combines within it both the fastest kind of input (an abrupt change) and the slowest (no change). Time domain specifications are reasonable in many cases, as in Figure 1.2a, the step response is to be inside the bounds b_1 , b_2 $\forall$ p $\in$ $\mathcal{D}$, with additional bounds of similar nature on the

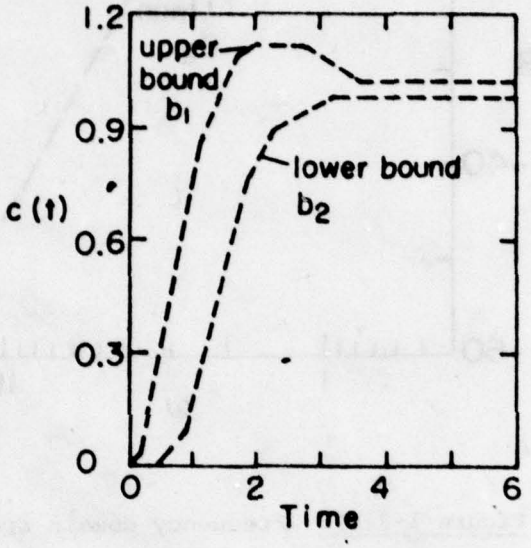

Figure 1-2(a). Time domain step response specification.

first and perhaps higher derivatives. Our design technique is in the frequency-domain, so we must translate such t-domain bounds into "equivalent" ω-domain bounds on the system frequency response $T(j\omega)$. If the system is minimum-phase [H3], $|T(j\omega)|$ suffices and we restrict ourselves here to such systems. This translation is, as of this date, an engineering art rather than a science. Advice on how to translate is scattered in the literature [H3, K1, S1]. Very good results have been obtained with only moderate effort. We shall

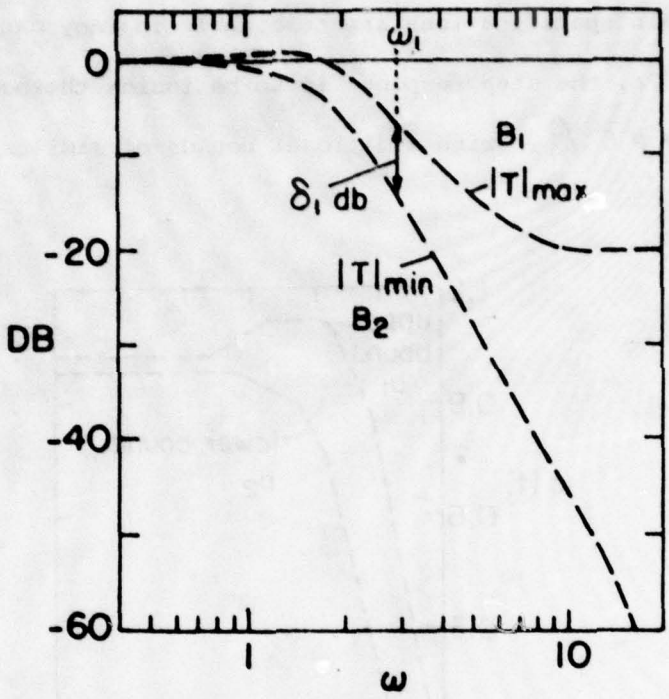

Figure 1-2(b). Frequency domain specification.

assume in this work that the translation has already been done. It is worth noting that it has been shown [H2] that for minimum-phase systems, time-domain specifications on the step response and on its derivatives of the following nature

$$b_2^{(i)}(t) \leq c^{(i)}(t) \leq b_1^{(i)}(t) \quad , \quad i = 0,1,\ldots,n \quad , \quad t \in [0,\infty) \qquad (1.1\text{-}2)$$

can always be satisfied by means of ω-domain bounds of the following nature

$$B_2(\omega) \leq |T(j\omega)| \leq B_1(\omega) \quad . \qquad (1.1\text{-}3)$$

In our work, the bounds on system performance will have this form.

1.1.1. Previous work.

The quantitative aspect of our work cannot be over-emphasized. The sensitivity reduction capability of feedback is very well-known. Hundreds of books and thousands of papers have been written on the subject, but the number of these which are quantitative in nature is extremely small, i.e., with uncertainty bounds and performance bounds explicitly included in the problem statement. It is as if the mere use of a feedback configuration around the uncertain plant, suffices to scare it into docile behavior. In the vast majority of the techniques the uncertainty is completely ignored, and there are none or extremely crude performance specifications. One presumably emerges with the same design whether the parameter uncertainty is x% or 1000x%, and irrespective of whether the bounds B_1 , B_2 in Figure 1-2(b) are narrow or wide apart. There is no concern with the 'cost of feedback' - which, aside from the sensors, lies in the bandwidth of the loop transfer function, and little concern with the extremely important matter of sensor noise [see Sec. 1.2]. These points have been emphasized in [H4, H12].

Our work follows closely in the tradition of 'quantitative synthesis' recently established [H3-6, W1]. To appreciate the present work, it is important to be aware of the highlights of this previous work. Quantitative synthesis was first developed for a plant with only one variable, the plant output $c(t)$ in Figure 1-3, available for feedback [H3]. The system command input $r(t)$ was also assumed accessible, so the processing of these two signals provides two independent compensation functions to the designer. An infinitude of canonical two-degree-of-freedom

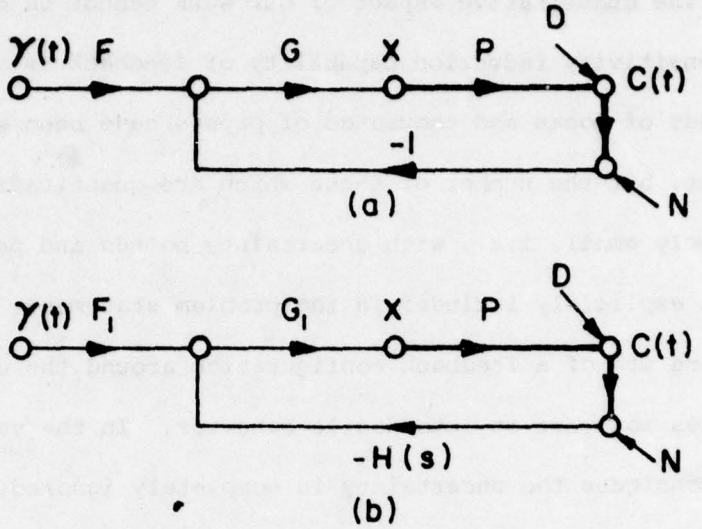

Figure 1-3. Structures of 2-D.O.F. system.

structure may be used [H7]. The design procedure developed in [H3] used Figure 1-3(a), but suppose the sensor transfer function is $H(s)$, then one can use Figure 1-3(b), letting G_1H (of Figure 1-3(b)) = G (of Figure 1-3(a)), in order to have the same loop transmission function $L(s) = GP = G_1PH$, and $F_1G_1 = FG$ in order to have the same system transfer function

$$T(s) = \frac{FGP}{1+GP} = \frac{F_1G_1P}{1+G_1PH} \quad . \tag{1.1-4}$$

1.1.2. A 2-degree-of-freedom structure with 2-loop implementation.

Suppose large loop feedback bandwidth is needed and it is found that an independent sensor measuring $\dot{c}(t)$ (e.g., a tachometer in a position servo) gives less noise than the differentiation

of a position sensor, so both sensors are used, as in Figure 1-4, with the two sensor transfer functions H_1 , H_2 , and say the structure in Figure 1-4 is used. This is a two-loop structure

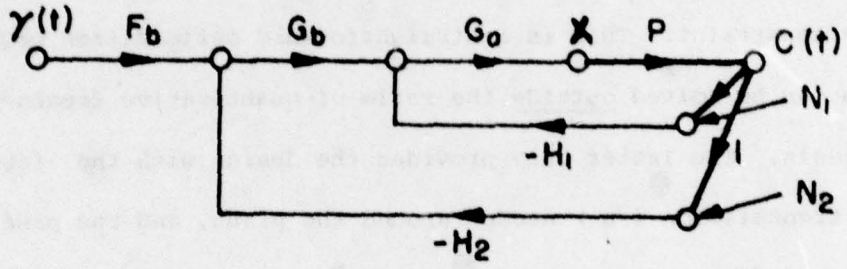

Figure 1-4. 2-loop, 2-D.O.F. structure.

physically, but in terms of fundamental feedback design it is a two-degree-of-freedom system, so the quantitative design theory of Figure 1-3(a) is used, giving G and F . It is required that the loop transmission around P , be the same in both cases, i.e.,

$$L = PG \text{ (Fig.1-3(a))} = P[G_a(H_1+G_bH_2) \tag{1.1-5}$$

and

$$T = F\frac{GP}{1+GP} \text{ (Fig.1-3(a))} = F_b\frac{G_bG_aP}{1+P[G_a(H_1+G_bH_2)]} \tag{1.1-6}$$

so

$$G = G_a(H_1+G_bH_2) \ , \quad FG = F_bG_bG_a \ . \tag{1.1-7}$$

H_1, H_2 are known, so one must decide how to split $G = G_a(H_1+G_bH_2)$ between G_a and G_b . This is done by considering the effect of sensor noise N_1 , N_2 at the plant input,

$$-X_N(j\omega) = \frac{G_a(H_1N_1+H_2G_bN_2)}{1+P[G_a(H_1+G_bH_2)]} \tag{1.1-8}$$

given that

$$G = \frac{L}{P}(j\omega) = G_a(H_1+H_2G_b) \qquad (1.1\text{-}9)$$

is fixed by the quantitative design technique of [H3].

The objective is to minimize $\int_0^\infty |X_N|^2 \, d\omega$, subject to the above constraint. This is a straightforward optimization problem which can be solved outside the realm of quantitative feedback synthesis. The latter only provides the design with the feedback loop transmission (L) needed around the plant, and the prefilter (F) needed to process the command input r(t) . The state-of-the-art in sensors and in filter synthesis determines how L and F are to be realized. In fact, in the above context one might consider use of an accelerometer in a 3-loop feedback structure. But from our point of view the structure remains that of a two-degree-of-freedom system and we shall continue to associate the latter with a single-loop system.

1.2 Review of Two-Degree-of-Freedom Quantitative Design Theory

Figure 1-3(a) is used with $T = F\frac{GP}{1+GP}$. It is assumed that the compensation network, whose power level can be very low (as the plant contains the power elements), can be constructed with negligible uncertainty in their transfer functions. Hence, due to the uncertainty in P ,

$$\Delta \ln T = \Delta \ln \frac{GP}{1+GP} = \Delta \ln \frac{L}{1+L} , \quad L = GP \qquad (1.2\text{-}1)$$

and

$$\Delta \ln |T(j\omega)| = \Delta \ln \left|\frac{L(j\omega)}{1+L(j\omega)}\right| . \qquad (1.2\text{-}2)$$

Given that the specifications require that $\Delta \ell n |T(j\omega)| \leq \delta_1 db$ at ω_1 in Figure 1-2(b), what are the resulting constraints on $L(j\omega_1)$? It is convenient to pick a "nominal" plant $P_o(s)$, and derive the bounds on the resulting "nominal" loop function $L_o = P_o G$. These bounds can be found by means of a digital computer, but it is very useful for insight to see it done on the Nichols' chart (logarithmic complex plane with abscissa in degrees, ordinate in decibels = 20 $\log_{10}$). The procedure is illustrated for the case

$$P(s) = \frac{ka}{s(s+a)} \quad ; \quad k \in [1,10] \quad , \quad a \in [1,10] \quad , \qquad (1.2\text{-}3)$$

and say $k = 1$, $a = 10$ are chosen as nominal, giving $P_o = 10/(s(s+10))$. At $\omega = 2$ rps , $P(j2)$ lies within the boundaries given by ABCD in Figure 1-5. Since $\ell n\, L = \ell n\, G + \ell n\, P$, the pattern outlined by

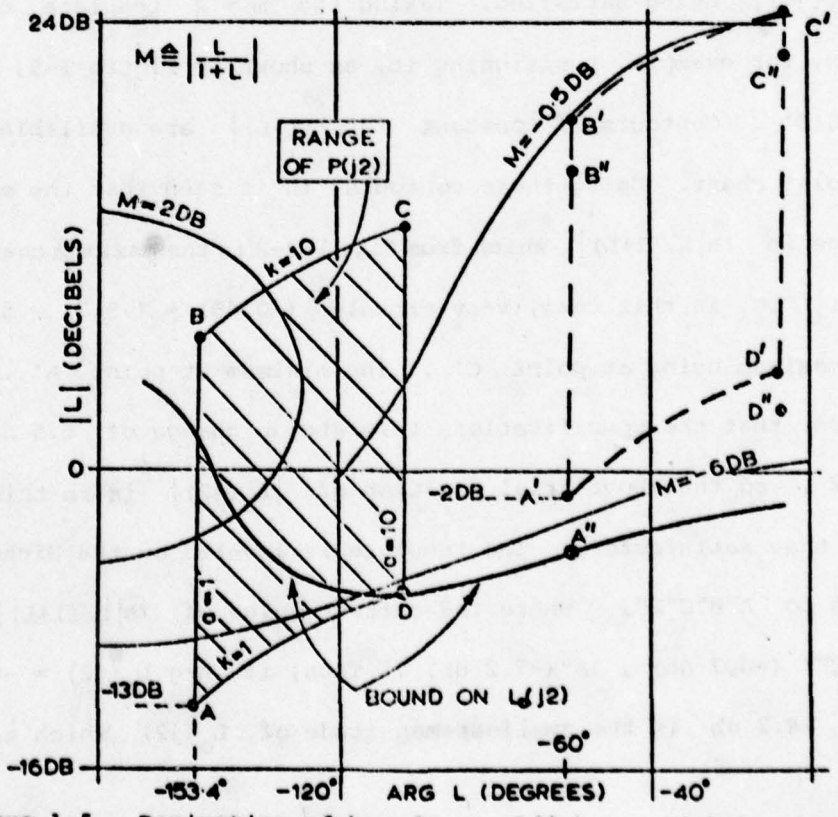

Figure 1-5. Derivation of bounds on $L(j\omega)$ on Nichols chart.

ABCD may be translated, but not rotated, on the Nichols' chart, the amount of translation being given by the value of $\ell n\ G(j2)$. For example, if a trial design of $L(j2)$ corresponds to the template $P(j2)$ at A'B'C'D' in Figure 1-5, then

$$|G(j2)|_{db} = |L(j2)|_{db} - |P(j2)|_{db}$$
$$= (-2.0) - (-13.0) = 11.0 \text{ db} \qquad (1.2\text{-}4)$$

$$\text{Arg } G(j2) = \text{Arg } L(j2) - \text{Arg } P(j2)$$
$$= (-60°) - (-153.4°) = 93.4° \ . \qquad (1.2\text{-}5)$$

1.2.1. Bounds on $L(j\omega)$ in the Nichols' chart.

The templates of $P(j\omega)$ are manipulated to find the position of $L(j\omega)$ which results in the specifications of Figure 1-2(b) on $\ell n\ |T(j\omega)|$ being satisfied. Taking the $\omega = 2$ template, one tries, for example, positioning it, as shown in Figure 1-5, at A'B'C'D' . Contours of constant $\ell n|L/(1+L)|$ are available on the Nichols' chart. Using these contours, it is seen that the maximum change in $\ell n|L/(1+L)|$ which from Fig. 1.2-2 is the maximum change in $\ell n\ |T|$ is, in this case, very closely (-0.49) - (-5.7) = 5.2 db , the maximum being at point C' , the minimum at point A' . Suppose that the specifications tolerate a change of 6.5 db at $\omega = 2$, so the above trial position of $|L_o(j2)|$ is in this case more than satisfactory. The template is lowered on the Nichols' chart to A"B"C"D", where the extreme value of $\ell n|L/(1+L)|$ are at C" (-0.7 db) , A"(-7.2 db) . Thus, if Arg $L_o(j2) = -60°$, then -4.2 db is the smallest magnitude of $L_o(j2)$ which satis-

fies the 6.5 db specification for $\Delta \ln |T|$. Any larger magnitude is satisfactory but represents over-design at that frequency. The manipulation of the $\omega = 2$ template is repeated along a new vertical line, and a corresponding new minimum of $|L_o(j2)|$ found. Sufficient points are obtained in this manner to permit drawing a continuous curve of the bound on $L_o(j2)$, as shown in Figure 1-5. The above is repeated at other frequencies, resulting in a family of boundaries of permissible $L_o(j\omega)$.

1.2.2. Nature of the bounds on $L_o(j\omega)$.

A typical set of bounds is shown in Figure 1-6. The bounds

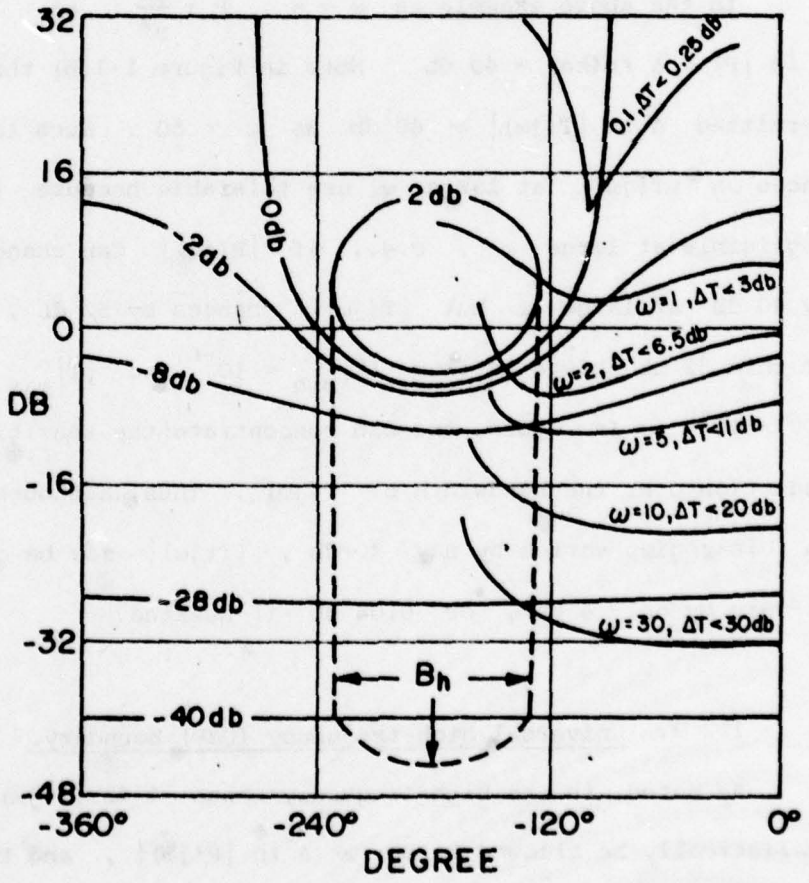

Figure 1-6. Typical bounds on L_o in Nichols' chart.

tend to move down in the Nichols' chart (become less onerous), obviously because as ω increases, greater change in $|T(j\omega)|$ is permitted, as in Figure 1-2(b). It is in fact essential that at large enough ω, the uncertainty in $|T(j\omega)|$ (i.e., the bounds on $|T(j\omega)|$) be greater than the uncertainty in $P(j\omega)$, because the net sensitivity reduction is always zero in any practical system as was long ago [B1] shown by Bode,

$$\int_0^\infty \ln |S_P^T(j\omega)| d\omega = -\int_0^\infty \ln |1+L(j\omega)| \, d\omega = 0 \qquad (1.2\text{-}6)$$

where $S_P^T = \frac{\partial T/T}{\partial P/P}$ is the sensitivity function.

In the above example as $\omega \to \infty$, $P \to \frac{ka}{s^2}$, so $\Delta \ln |P| \to \Delta \ln(ka) = 40$ db. Note in Figure 1-2(b) that the permitted $\Delta \ln |T(j\omega)| \gg 40$ db as $\omega > 50$. Such large tolerances on $|T(j\omega)|$ at large ω are tolerable because $|T(j\omega)|$ is negligible at large ω, e.g., if $|P(j\omega)|$ can change at most by 40 db at large ω but $|T(j\omega)|$ changes by 52 db, who cares if this 52 db change is from $|T|_{min} = 10^{-6}$ to $|T|_{max} = 400 \times 10^{-6}$. In return, one can concentrate the sensitivity reduction over the bandwidth of $T(j\omega)$. Thus, although $|P(j\omega)|$ in this region varies by say 40 db, $|T(j\omega)|$ may be controlled to vary by only 4 db, or 0.04 db if desired.

1.2.3. Universal high-frequency (UHF) boundary.

As noted, in the high-frequency range $\Delta \ln |T(j\omega)|$ must realistically be allowed to be $\gg \Delta \ln |P(j\omega)|$, and this is reflected in the bounds on $L_o(j\omega)$ tending to a very narrow pencil B_ν^p

in the arithmetic complex plane (if $P_o \to \frac{k \min}{s^e}$ as $s \to \infty$) as in Figure 1-7(a) and as in 1-7(b) in the Nichols' chart. In

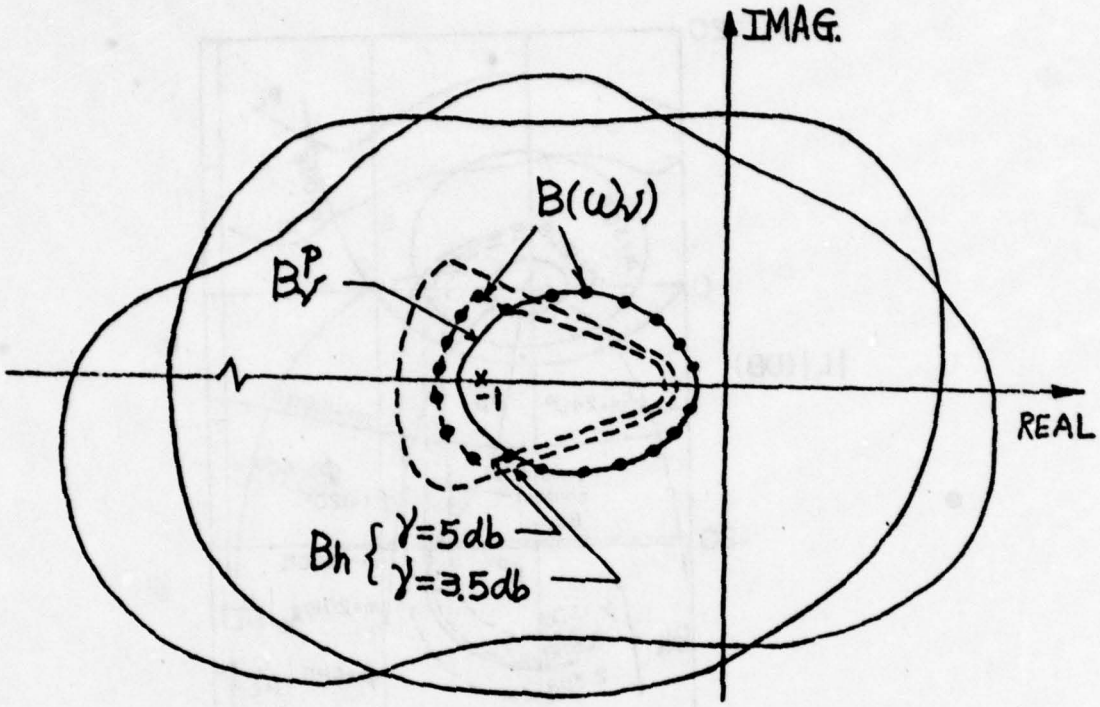

Figure 1-7(a). Typical bounds on $L_o(j\omega)$ in a complex plane.

Figure 1-7(b), the boundary B_ν^p is drawn for the case $\Delta \ln L = \Delta \ln k =$ 20 db, $\Delta \ln |T(j\omega)| = \Delta \ln |L/(1+L)| \leq 23$ db at ω_ν. However, the resulting peak value of $|L/(1+L)|$ is 23 db = 14.1 arithmetic at $k = k_{max}$, indicating a highly under-damped pole pair at the corresponding frequency with damping ratio $\xi = 0.034$, when $k = k_{max}$. This tremendous peaking does not appear in the system response to the command inputs R, because it is filtered out by the pre-filter F in Figure 1-3(a). But the system response to a disturbance D in Figure 1-3, is given by $T_d = \frac{C}{D} = (1+L)^{-1}$. Disturbance attenuation generates its own requirements on L, which may lead

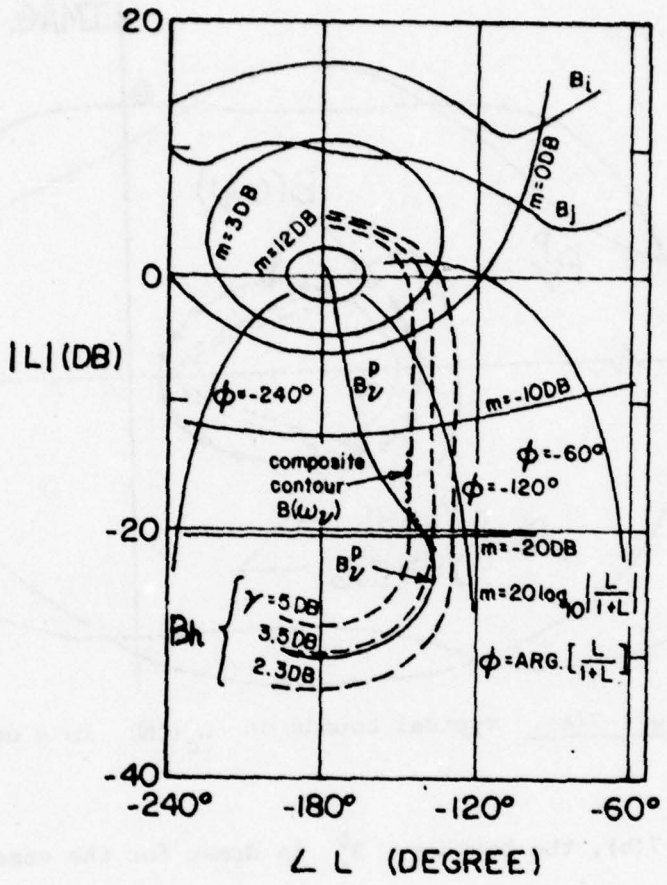

Figure 1-7(b). Bounds on $L(j\omega)$ on Nichol's chart.

to more stringent bounds on L than those due to $T(j\omega)$. The final contours used in the design [H3] must be the most stringent composite of the two. However, even if D is very small, it is usually certain that a peak $|T_d|$ of 14.1 is intolerable. It is reasonable to add a requirement $\left|\frac{L}{1+L}\right| \leq \gamma$ a constant, for all ω and over the whole range of P parameter values. The resulting constraining contours denoted by B_h are shown in Figure 1-7(b)

for the case $\Delta \ell n\, k = 20$ db , and for $\gamma = 2.3, 3.5, 5$ db (all those contours are symmetrical with respect to the vertical Arg $L = -180°$ on the Nichols' chart). If $\gamma = 5$ db is used, then $B(\omega_\nu)$ indicates the composite contour shown in Figure 1-7(b). For $\omega > \omega_\nu$, $|\Delta\, T(j\omega)|$ increases while γ remains the same, so that sooner or later there is reached a frequency $\omega_\gamma \ni B(\omega) = B_h(\gamma)$, $\forall\, \omega \geq \omega_\gamma$. This boundary B_h is called the "universal high frequency" (UHF) boundary.

1.2.4. The optimum $L(j\omega)$.

It has been shown [H6, H8] that a realistic definition of optimum in the ℓti system is the minimization of k , defined by $\lim_{s\to\infty} L(s) = k\, s^{-e}$, where e is the excess of poles over zeros assigned to $L(s)$.

It has been proven [H6, H8] that the optimum L lies on its boundary B_i at each ω_i and that such an optimum exists and is unique. Most important for the present purpose, is that in significant plant ignorance problems the ideal optimal L has the properties shown in Figure 1-8, i.e., over a significant range it follows B_h along UV up to the point J at which it abruptly jumps to infinity along WW'W" and returns on the vertical line YZ , whose phase is $(-90°)\, e$. Such an ideal $L(j\omega)$ is, of course, impractical. A practical suboptimum L is shown in Figure 1-8 (see Section 1.4.3, for more discussion).

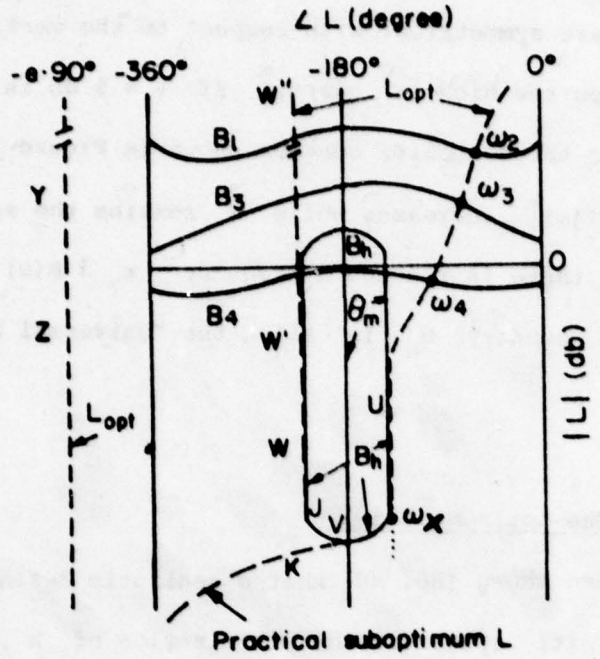

Figure 1-8. Bounds on L and Optimum L on Nichols' Chart.

Some results of a numerical design example are shown in Figure 1-9. They were derived for the following problem.

1.2.5. Numerical example. (Figure 1-3(a)).

Plant: $P = P_1P_2 = P_1(P_2'P_3')$

Plant ignorance:

$$P_1 = \frac{K_1}{S^2 + 2\xi\omega_n S + \omega_n^2} \quad , \quad -3 \leq \xi\omega_n \leq 5$$

$$2 \leq \omega_n\sqrt{1-\xi^2} \leq 10 \quad , \quad 4 \leq K_1 \leq 1250$$

$$P_2' = \frac{AK_2'}{S+A} \quad , \quad 1 \leq A \leq 3 \quad , \quad 10 \leq K_2' \leq 33.3$$

$$P_3' = \frac{BK_3'}{S+B} \quad , \quad 10 \leq B \leq 20 \quad , \quad 100 \leq K_3' \leq 158$$

Performance Specification: Shown in Figure 1-2(b), were originally derived from time domain bounds [S1].

Disturbance response: $\gamma \leq 3.0$ db .

This example is used later in a demonstration of the advantages of multiple-loop design. The L_{i0} transfer functions are given in Appendix 1 of this chapter.

1.3 Cost of Feedback and Effect of Sensor Noise

In significant plant ignorance problems, there is a strong tendency for the design to be such that N , in Figure 1-2(a), is so highly amplified as to saturate the plant input at X . The noise response function is (see Figure 1-3(a))

$$T_N \triangleq \frac{X}{N} = \frac{-G}{1+GP} = \frac{-L/P}{1+L}$$

$$\approx -L/P \quad \text{in h.f. range where} \quad |L| << 1 \ . \qquad (1.3\text{-}1)$$

N represents the square root of the noise power spectrum. The noise response of the numerical design example of the last section is shown in Figure 1-10. Notice that the noise component at x , in Figure 1-2(a), is most important in the high-frequency range where the useful command and disturbance components, due to R and D_i are relatively small, rather than in the low frequency range where the latter are relatively large. This is further enhanced by the fact that arithmetic scales, shown in Figure 1-11, must be used to find

$$(x_N)_{rms} = \sqrt{\int_0^\infty (|T_N|^2 \cdot \Phi_N) d\omega} \ , \ \Phi_N = N^2 : \text{noise power spectrum} \qquad (1.3\text{-}2)$$

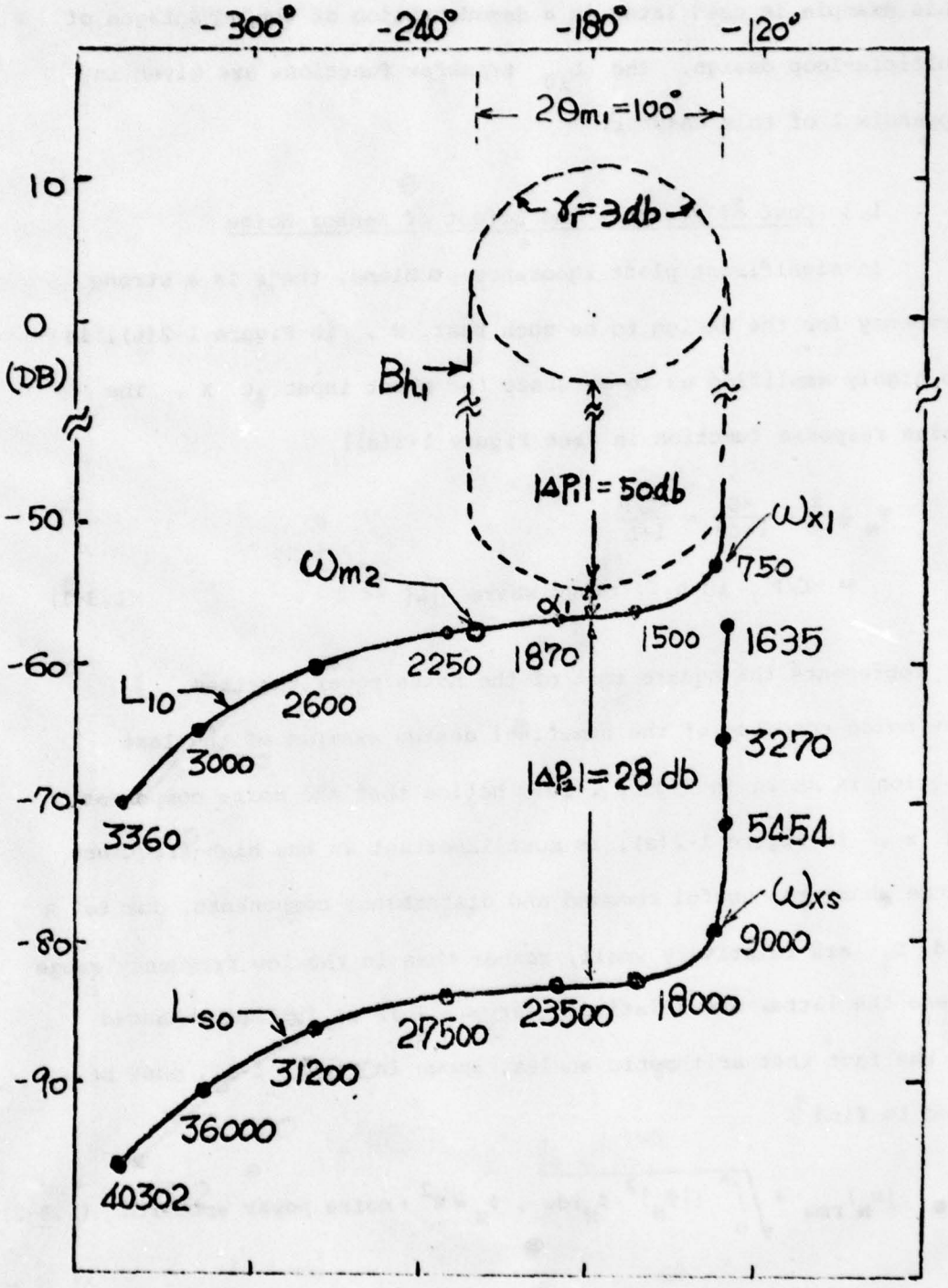

Figure 1-9a. Single loop L_{s0} and outer loop L_{10} of the numerical example in Section 1.2.5.

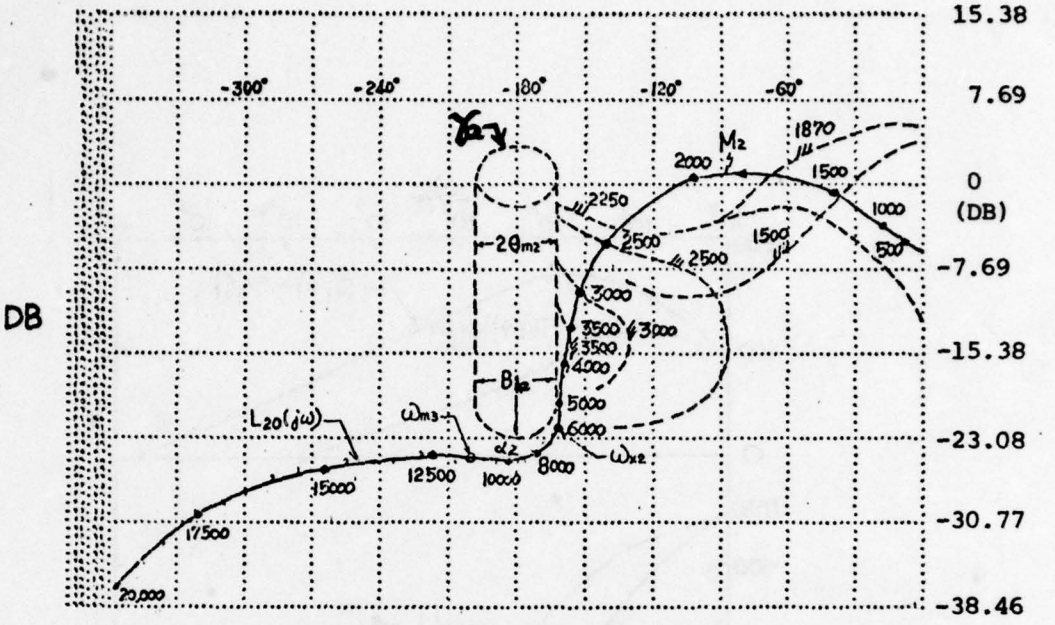

Figure 1-9b. The bounds and loop of first inner loop of the numerical example.

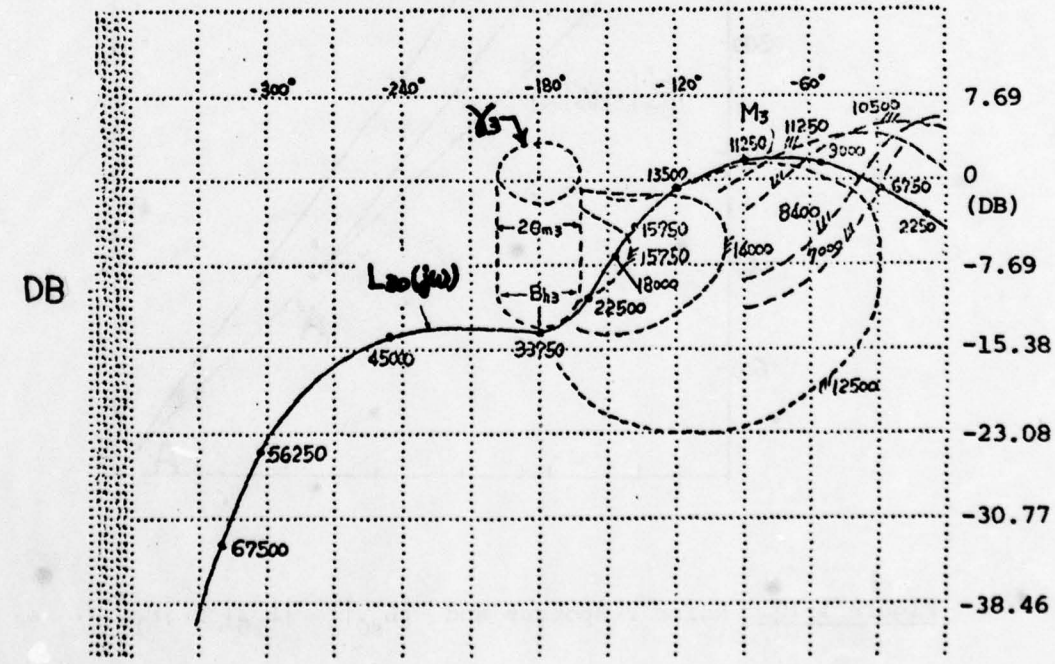

Figure 1-9c. The bounds and loop of second inner loop of the numerical example.

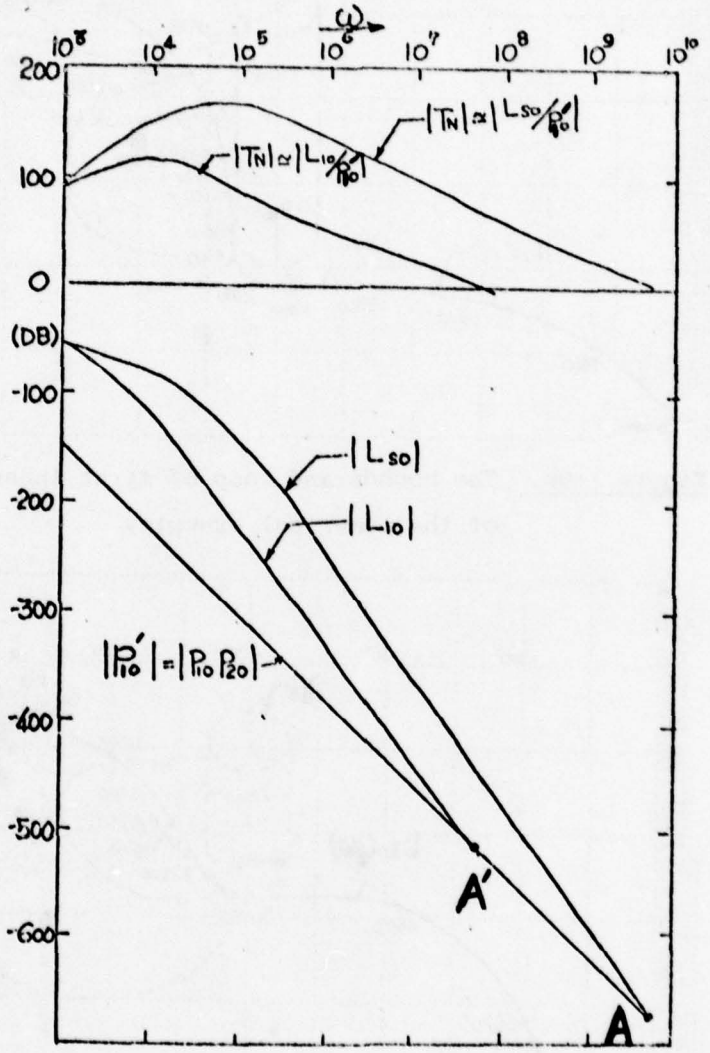

Figure 1-10. Noise responses and $|L_{s0}|$, $|L_{10}|$, $|P'_{10}|$.

Hence, it is desirable to decrease $|L|$ vs ω, as fast as possible in the high frequency range. Even a saving which is small in the logarithmic scale near A in Figure 1-10, can be significant in rms sensor noise effect. Reduction in this 'cost of feedback' is the primary motivation for turning to multiple-loop design.

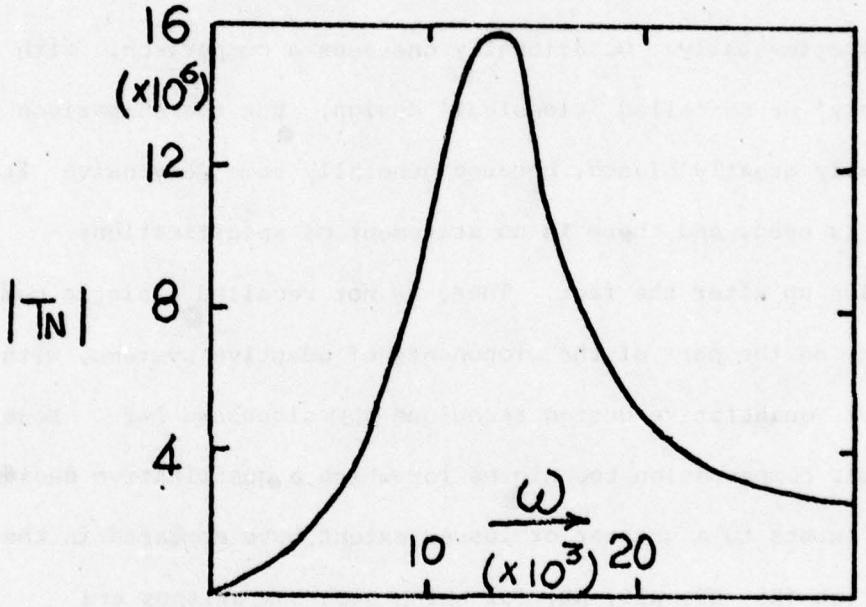

Figure 1-11. Arithmetic plot of $|T_N|$.

1.3.1. Reduction in Cost of Feedback by means of linear time-varying compensation and nonlinear compensation.

To reduce the hf sensor noise effect, one way is by linear time-varying compensation if the problem has time-varying features [R1]. Another is by nonlinear compensation. Actually the so-called "adaptive' system is in the category of nonlinear compensation. They may or may not be better than lti compensation in reducing the 'cost of feedback'. It is noteworthy and scandalous that in

the vast literature on adaptive systems, there is hardly ever any quantitative comparison between the adaptive design promoted and a proper ℓti design accomplishing the same design objectives. One could excuse this not being done in a general manner, because there is hardly any 'adaptive' method permitting quantitative design in the sense here defined. However, it could at least be done experimentally. Occasionally one sees a comparison, with an 'ordinary' or so-called 'classical' design. But the comparison is usually greatly biased, because generally some very naive ℓti design is used, and there is no statement of specifications - even made up after the fact. There is not recalled a single comparison, on the part of the proponents of adaptive systems, with the ℓti quantiative design technique [H3] discussed here. Some nonlinear compensation techniques for which a quantitative design theory exists to a greater or lesser extent have appeared in the literature [H5, H9, H10, K2] for which such comparisons are possible. It is noteworthy that these were expressly motivated by the desire to reduce the 'cost of feedback', so that such comparisons were a natural by-product.

1.3.2. Multiple-loop feedback.

Another method of 'cost of feedback' reduction, in the context of ℓti design, is by means of multiple-loop feedback, restricted to those cases where an additional plant variable (besides the plant output) are available for feedback purposes. Such a multiple loop design technique was first developed [H4] for the cascaded structure of Figure 1-12.

In this thesis, quantitative synthesis is extended as follows:

(a) In Chapter 2, to the 2-branch parallel structure in Figure 13a, in which one branch has n cascaded sections.

(b) In Chapter 3, to the natural generalization of Figure 13a for $n = 2$, into the structure of Figure 13b.

(c) In Chapter 5, to the fairly general structure of Figure 14 of m parallel branches with the i-th branch consisting of a cascade of n_i sections.

1.3.3. Plant Modification.

It is noted that in Figures 1-12 to 1-14, each feedback loop is returned to the plant input X. No feedback is allowed to any internal plant variables e.g. from C to C_2 or more generally from any C_i to C_j, $j > i$ and $j = 2,3,\ldots n-1$. The reason is that any such internal feedback constitutes "plant modification". The plant has been assembled by its specialists to deliver some maximum output C and the permissible levels of $C_2 = C/P_1$, $C_3 = C/P_1P_2,\ldots,C_i = C/P_1\ldots P_{i-1}$ are thereby determined. Suppose there is feedback from C vis H_1 to C_2, as shown in the insert in Figure 1-12. Now $X_2 = \frac{C}{P_1}(1 + P_1H_1)$ with signal level possibly much greater than the previous C/P_1, which the plant may perhaps not be able to handle.

We thus assume that the "feedback specialist" is called in to design the feedback network around the plant, after the latter has been built by the "plant specialist". This is the situation very often in practice. If the feedback specialist does his job properly, i.e. achieves the system response function $T(s)$ within its tolerances $\forall\, P \in \mathcal{P}$, then the signal levels inside the plant will be within the

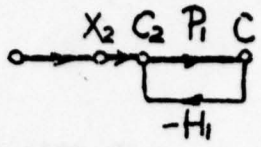

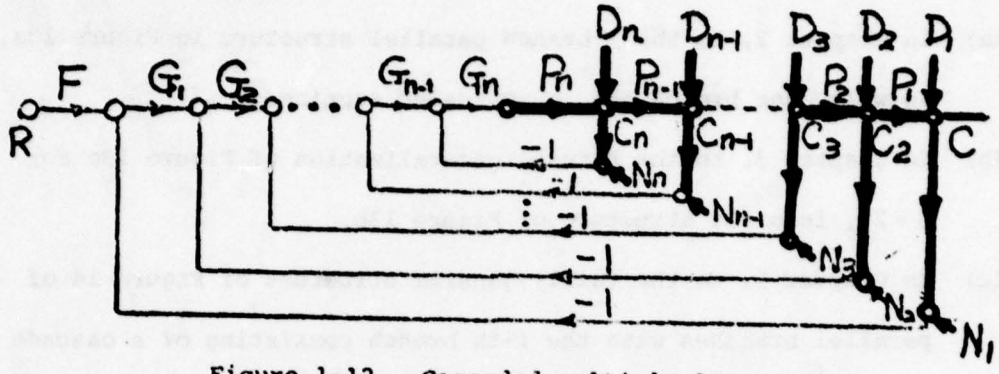

Figure 1-12. Cascaded multiple-loop system with (n+1) D.O.F. structure.

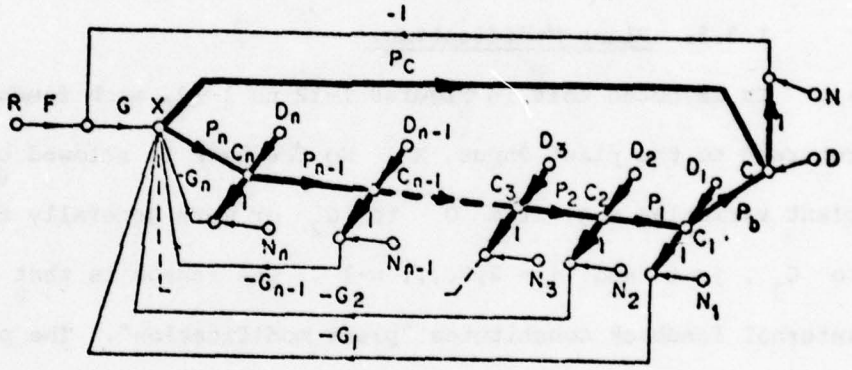

Figure 1-13a. Parallel multiple-loop system with n+2 degree of freedom structure.

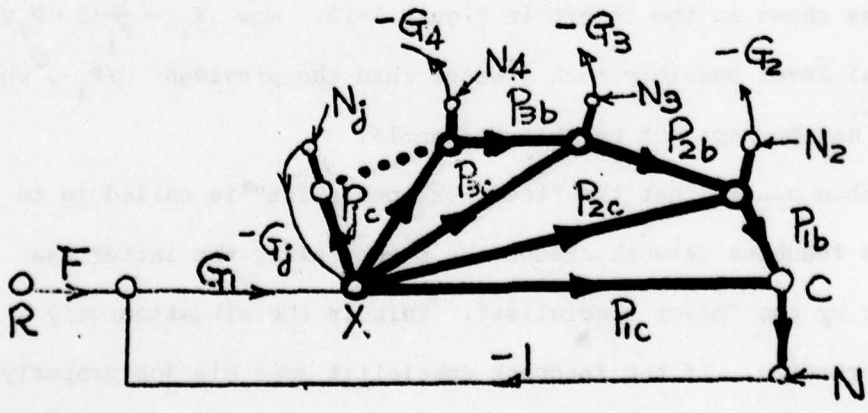

Figure 1-13b. Generalization of structure in Figure 1-13a.

values allowed by the plant specialist, so long as the command input functions r(t) are in the set for which the system was designed.

Recently, quantitative design has been extended for the first time [W1], specifically to the single branch cascade plant, with plant modification allowed. The degree of modification, in a rms sense, of the internal plant variables was added as one more design specification, in addition to those listed here. It was shown that the loop bandwidths can thereby be significantly decreased, beyond that possible in "no plant modification" designs. This indicates that in significant plant uncertainty problems, it is definitely advantageous to have the "feedback specialist" participate with the "plant specialist" in the design of the plant. In this thesis, as previously noted, plant modification is not allowed because this is very often the situation in practice. Also, it is necessary to pose such designs in order to compare the results with plant modification designs.

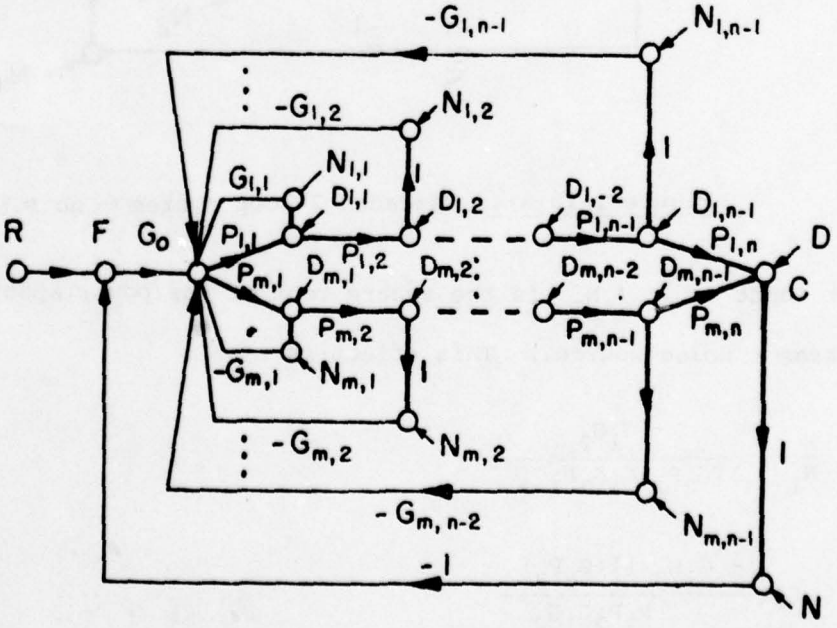

Figure 1-14. Parallel-cascaded multiple-loop structure with m(n-1)+2 D.O.F. structure.

The multiple-loop no plant modification synthesis theory developed here, is based to a large extent on the design theory for the cascaded multiple-loop design theory for Figure 1-12. Hence, it is very important to first thoroughly understand the essentials of the above cascaded design philosophy, which is therefore next presented.

1.4 Review of Cascaded-Loop Design Theory

1.4.1. Cascaded 2-loop design.

The basic idea is to use the inner loop $L_2 = G_2P_2$ in Figure 1-15(a), to minimize the effect of sensor noise N_1 at the

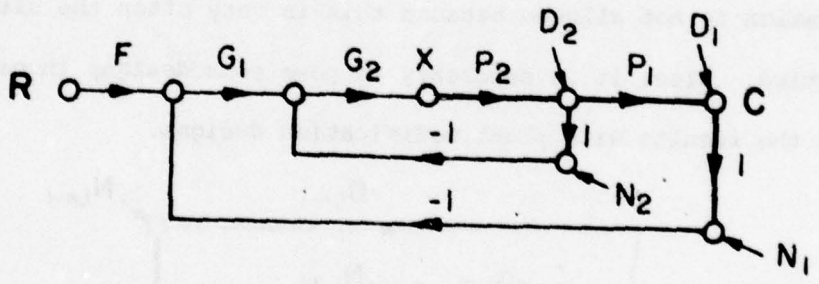

Figure 1-15(a). Cascaded 2-loop system – no P.M.

plant input x . (N_1 is the square root of the power spectrum of the sensor noise source.) This effect is

$$\frac{X}{N_1} = \frac{-G_1G_2}{1+G_2P_2+G_1G_2P_1P_2} \qquad (1.4\text{-}1)$$

$$= \frac{-G_1G_2/(1+G_2P_2)}{1+\frac{P_1P_2G_1G_2}{1+G_2P_2}} \qquad (1.4\text{-}2)$$

$$= \frac{-\frac{G_1}{P_2} \cdot P_{2e}}{1 + P_1 G_1 P_{2e}} \quad \text{where} \quad P_{2e} = \frac{G_2 P_2}{1+G_2 P_2} \tag{1.4-3}$$

$$= -\frac{L_1/(P_1 P_2)}{1 + L_1} \qquad L_1 = P_1 G_1 P_{2e} \tag{1.4-5}$$

$$\approx -\frac{L_1}{P_1 P_2} \quad \text{in the hf range where} \quad |L_1| \ll 1 \ . \tag{1.4-6}$$

Hence to reduce $\frac{X}{N_1}$ in the hf range, one must try to reduce $|L_1|$. But L_1 must cope with the uncertainty in $P_1 P_{2e} = P_1(P_2G_2/1+P_2G_2))$. Assuming the worst case of uncorrelated uncertainties in P_1 and P_2, the best that can be done by the inner loop P_2G_2 is to wipe out the uncertainty of P_{2e}, so that L_1 need only cope with the uncertainty of P_1. Physically, this makes sense - for obviously the inner loop cannot take care of the uncertainty of P_1. There is then left the single-loop system of Figure 1-15(b) and L_1 can be designed to handle the ignorance of P_1 only. The resulting L_1 is therefore more economical in bandwidth than its

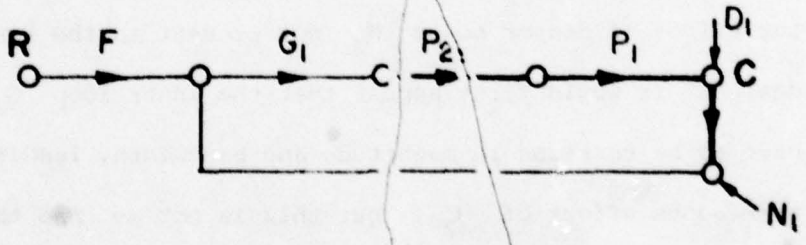

Figure 1-15(b). Equivalent single-loop structure of a cascaded 2-loop system.

counterpart in the single loop system, for the realization of the same C/R specifications. For example, compare the appropriate T_{N_1} in Figure 1-16(a) (logarithmic scale) and in Figure 1-16(b) (arithmetic scale) of the numerical example in Section 1.2-5.

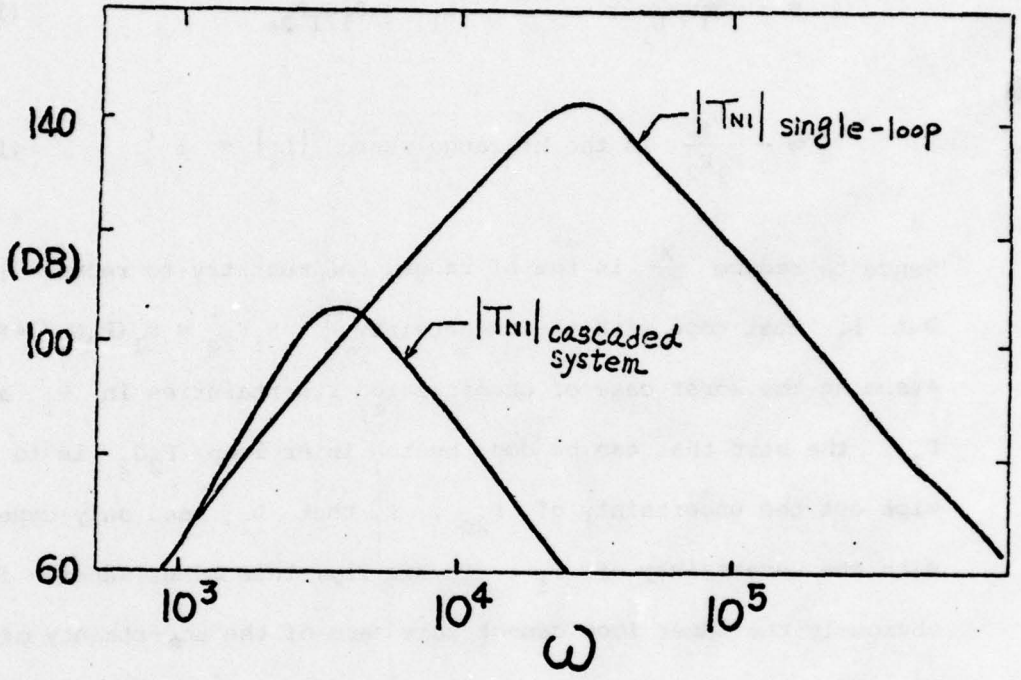

Figure 1-16(a). Comparison of noise response $|T_{N_1}|$ on Bode diagram.

This looks very good, but the obvious question is: What of the effect of sensor noise N_2 not present in the single loop design? It would first appear that the inner loop G_2P_2 would have to be enormous in magnitude and bandwidth, leading to tremendous effect of N_2. But this is not so. And the basic reason is available if one studies the mechanics of sensitivity reduction by frequency response methods. The reason is that the outer loop, even if optimally designed to handle a certain definite amount of uncertainty, is nevertheless able

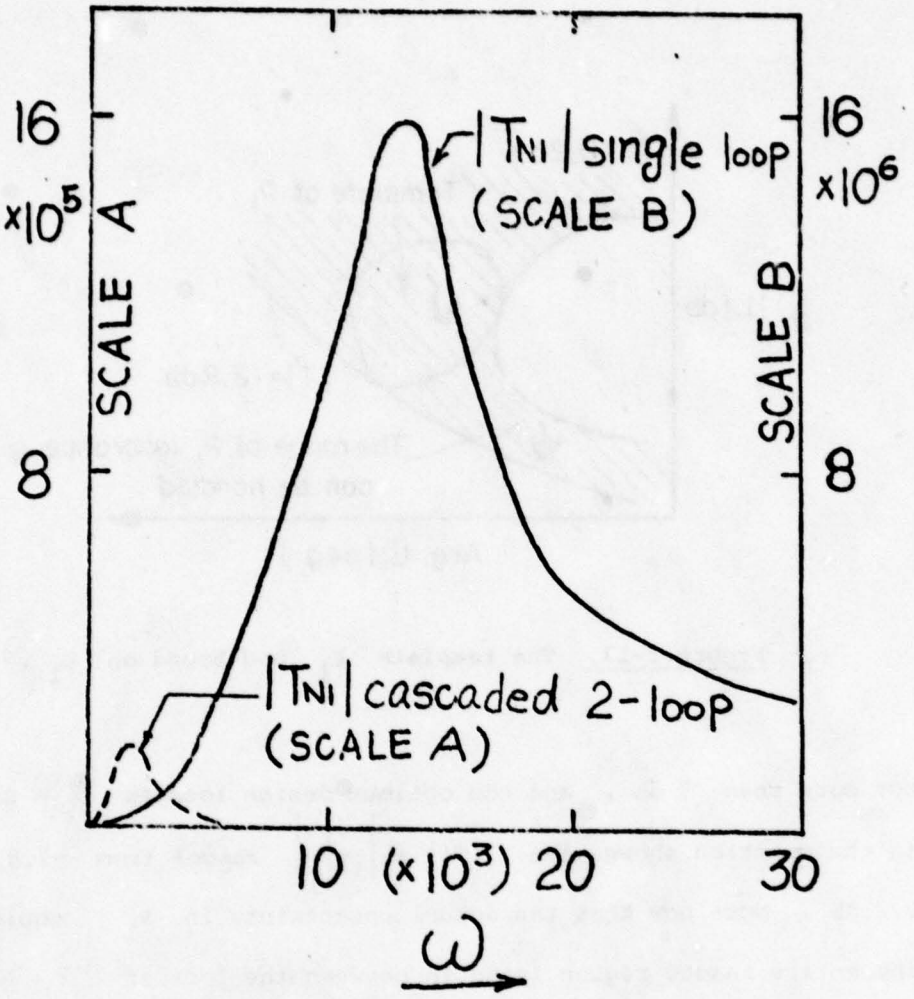

Figure 1-16(b). Comparison of noise response $|T_{N_1}|$ on arithmetical scale plot.

to handle a "much larger" amount of uncertainty. This is nicely seen in the Nichols' chart in Figure 1-17.

Thus, in Figure 1-17, suppose the uncertainty in $P_1(j\omega)$ is given by the template shown of P_1 which is not a point (it would be a point if there was no uncertainty) but a region. Suppose the specifications require the closed loop response uncertainty to be

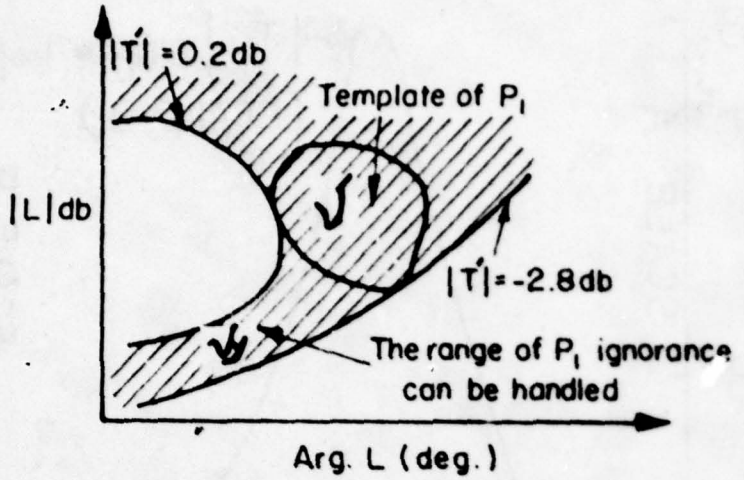

Figure 1-17. The template P_1 and bound on L_1 .

not more than 3 db , and the optimum design locates $L_1 = G_1P_1P_{2e}$ in the position shown, i.e. $|T'| = \left|\frac{L_1}{1+L_1}\right|$ ranges from -2.8 db to 0.2 db . Note now that the actual uncertainty in P_1 , could be the entire shaded region lying in between the loci of $|T'| = .2$ db and $|T'| = -2.8$ db.

Thus P_{2e} can in practice have significant uncertainty, even though the outer loop was designed on the basis of no P_{2e} uncertainty. This is the secret of multiple-loop design – to understand the nature of the "free" uncertainty available in the various frequency ranges.

1.4.2. Nature of "free" uncertainty.

In Figure 1-18, suppose arg $L_o = -130°$, the template of P is a vertical line 20 db in length, $|\Delta T|$ allowed is 8 db, and $|P_o|$ is chosen $|P|_{min}$. It is easily seen that the minimum satisfactory $|L_o| = -7.7$ db . But it is also easily seen that this minimum L_o is satisfactory for any uncertainty (for the vertical line template) $>$ 20 db , even infinite. In fact, the template could even expand to the right significantly, as shown by the dashed lines in Figure 1-18. This kind of situation is true for all $-180° < \text{Arg } L_o < -90°$. It is not true for $\text{Arg } L_o \in [0,-90°]$, but for significant uncertainty it is almost true. Thus, in Figure 1-18, suppose $\text{Arg } L_o = -50°$ with the same plant template and $|\Delta T|$ allowed is 3 db, giving $|L_o|_{min} = 4.8$ db . If 5.3 db is used for $|L_o|$ instead of 4.8 db, then this L_o is satisfactory (for a vertical line template) for any, even infinite uncertainty.

In view of the above phenomenon there is usually little advantage in having the outer loop L_1 ignore the uncertainty in P_2 of Figure 1-15(a) in ω ranges in which L_{10} is in the above regions in the Nichols chart. The exception is when the uncertainty in P_1 is small in the low and intermediate (relative to the overall system bandwidth) ω regions, but the uncertainty in P_2 is large. However, in control systems the power levels, and with them the plant non-linearities (equivalent to uncertainties, see [H11]) and uncertainties, usually increase as one proceeds from plant input to output.

The situation changes radically after L_{10} has "turned the corner", say at point A in Figure 1-19. At point B (with $|P_o| = |P|_{min}$) and a vertical template, it can handle uncertainty

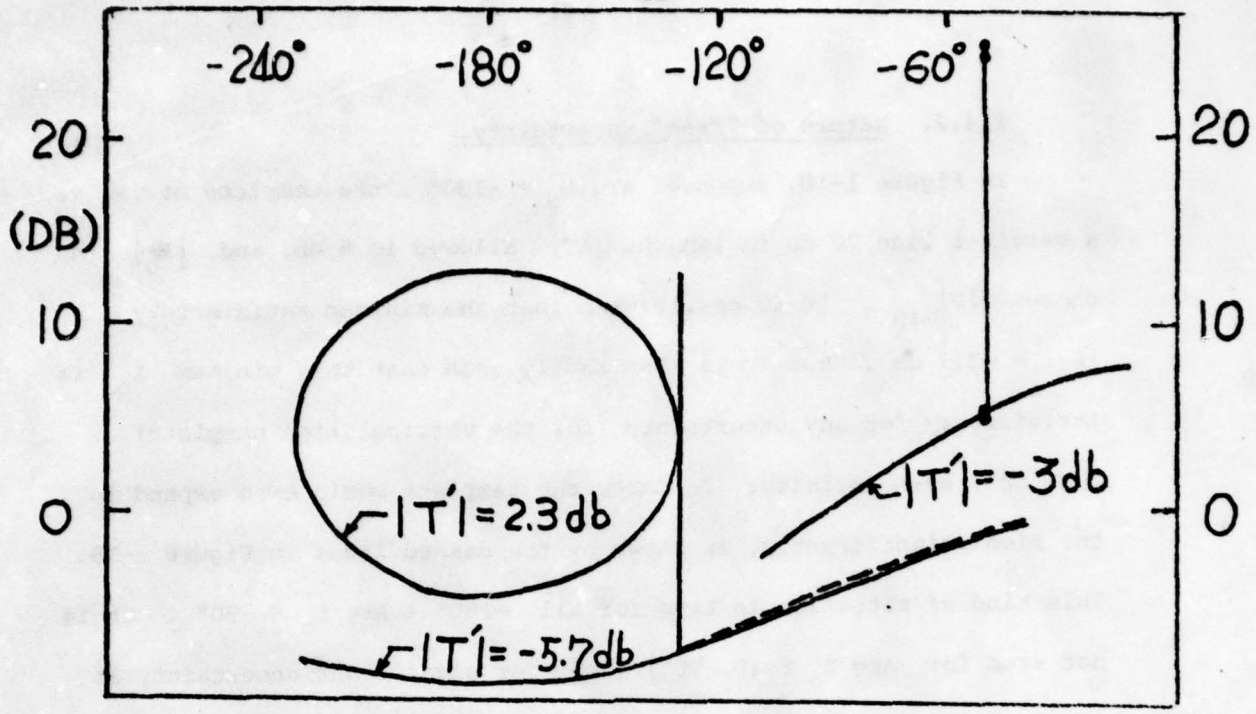

Figure 1-18. The nature of "free" uncertainty for $\omega < \omega_{x1}$.

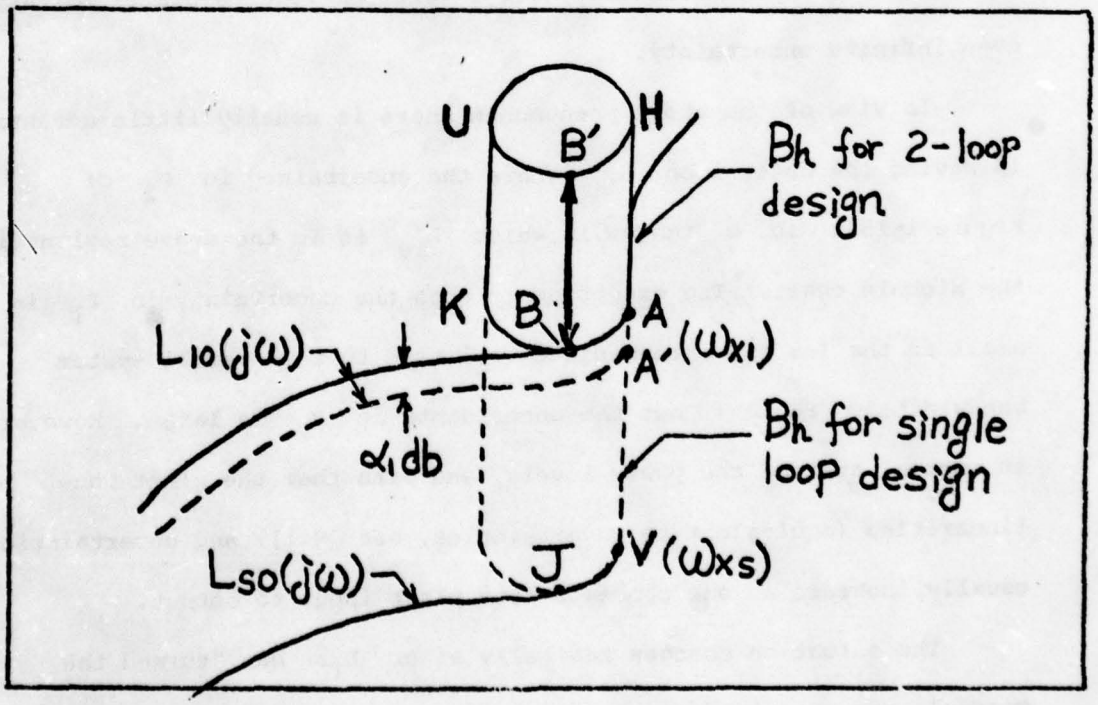

Figure 1-19. The nature of "free" uncertainty for $\omega > \omega_{x1}$.

of BB' only and not any bit more. Hence, in this range it is very advantageous to have the outer loop L_1 handle only the uncertainty in P_1 in Figure 1-15(a). Suppose in this relatively high-frequency region $P_1 \doteq \frac{k_1}{s^{e_1}}$, $P_2 \doteq \frac{k_2}{s^{e_2}}$, $k_1 \in [4,1250]$, $k_2 \in [10{,}000, 312{,}900]$. In a single-loop design the "universal high-frequency" (UHF) boundary of Section 1.2.3 is H AVJ KU in Figure 1-19, with practical optimum L_s shown. The length of B'BJ is $20 \log_{10} 9778.125 \simeq 80$ db. In the 2-loop design, L_1 need handle P_1 uncertainty of 50 db only, giving the UHF boundary HABKU with B'B = 50 db in length, with practical optimum outer loop L_1 in Figure 1-19. In practice, it is best to compromise a little in this range and "overdesign" the outer loop by amount α_1 db, because small overdesign of L_{10} considerably eases the burden on the inner loop L_{20} in this range (see Figure 1-22 for the trade-offs).

1.4.3. Advantage of 2-loop over single-loop design.

The improvement achieved by the above is much better seen in Bode plots of L_{so} and L_{10} . First, it is important to see on the Bode plot, the nature of the "practical optimum" L_{so} of Figure 1-8. This is shown in Figure 1-20. L_{so} is moving down HAV in Figure 1-19 (at maximum premissible phase lag $180-\theta_m$, in order to decrease as fast as possible). Its average slope is approximately $\frac{-(180-\theta_m)}{180} \times 40$ db per decade [H4]. If the shaping of L_{so} is done by hand then such an average slope can be achieved by means of alternating negative real poles and zeros, i.e. over one interval $L_{so}(s)$ has an excess of 2 poles over zeros, followed by one with an

excess of only one. Near the corner at V in Figure 1-19, one arranges for an excess of two, then introduces a zero to provide some extra phase lead, followed by some underdamped complex pole pairs as soon as possible (see [H7, p. 384]). The greater e_L, the excess of poles over zeros of L_S, the further off these complex-pole pairs. If it is done by an automatic computer program, then the pole-zero pattern which emerges depends, of course, on the nature of the program. However, the result in the ω domain obtained by several programs tried, is very similar to that obtained by hand, but the latter is generally more economical in the number of poles and zeros. In any case, in this work we use $e_L = 5$ and the "universal high-frequency cut-off characteristic" (UHFCOC) shown in Figure 1-24a.

The following is very important in revealing the basic simplicity of multiple-loop design. The essential difference between L_{so} and L_{10} is that UHFCOC for L_{10} is introduced $(\Phi-\alpha_1)$ db higher up than for L_{so}, giving BB'B" instead of JJ'J" in Figure 1-20. Hence, if a single-loop design giving L_{so} has been found to solve the problem, it is then very easy to find the outer loop L_{10} for a two (or higher)-loop structure, without a detailed design of L_{10}. One simply translates the UHFCOC portion of L_{so} vertically by $(\Phi-\alpha_1)$ db (and to the left to merge with L_{so} as in Figure 1-20), where Φ is the high-frequency (hf) uncertainty of $P_2P_3\ldots P_n$, on the assumption that in this ω region $P_2P_3\ldots P_n$, is closely equal to its high-frequency asymptote $k_2k_3\ldots k_n/s^{e_1+e_2+\ldots e_n}$ — an assumption made throughout this work.

Improvement in sensor noise effect.

It was shown (Equation 1.3-1) that in the single-loop design $(X/N_1)_s \doteq -L_s/P_1P_2$ in the hf region, whereas (Equation 1.4-6) in the 2-loop structure $(X/N_1)_2 \doteq -L_1/P_1P_2$. It is easy to compare the two noise responses in Figure 1-20. Sketch $P_{10}P_{20}(j\omega)$. Clearly $(X/N_1)_s < (X/N_1)_2$ in the region BB', but $(X/N_1)_2 << (X/N_1)_s$ in much of the region $[\omega_K, \infty]$. In any case, this simple, easy construction permits one to see at once the advantage of the 2-loop design, with respect to effect of sensor noise N_1. Of course, a new sensor with its noise power spectrum N_2^2 has been introduced and its effect at X must be considered. For this purpose, the nature of the inner loop L_2 is next reviewed.

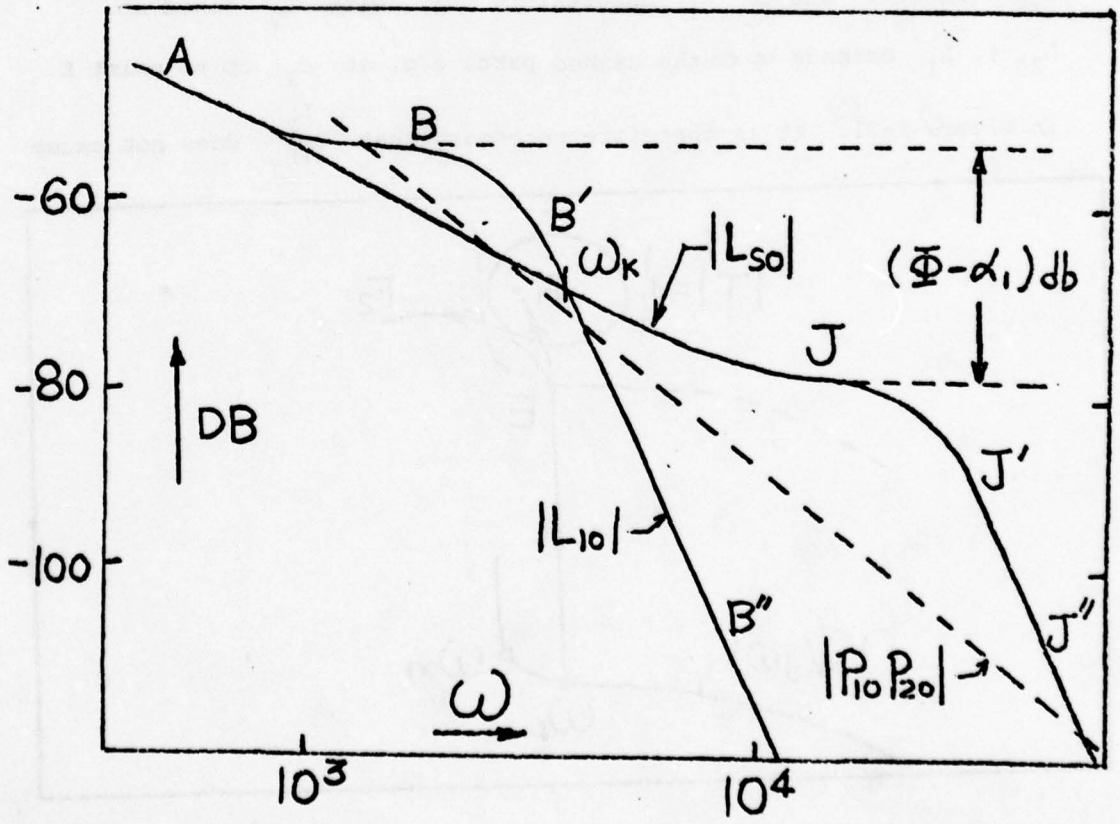

Figure 1-20. Improvement in sensor noise effect.

1.4.4. Design of first inner loop L_2 .

The outer loop L_{10} has been designed to handle all uncertainty in P_1 and P_2 , up to the corner frequency denoted by ω_{x1} in Figure 1-19, at which L_{10} turns the corner of its UHF boundary. Hence, for $\omega < \omega_{x1}$ the demands on L_{20} are very minor (see Figure 1-9b for examples of the bounds $B_2(\omega)$ on $L_{20} = G_2P_{20}$ in Figure 1-15a). But $B_2(\omega)$ are significant for $\omega > \omega_{x1}$, where L_{10} handles the uncertainty only in P_1 . To see this, note that in Figure 1-21, it is required that the actual (due to P_1 and P_2 uncertainties) $\frac{L_1}{1+L_1}$ does not penetrate into the locus γ_1 , where $L_1 = G_1P_1 \frac{L_2}{1+L_2}$, $L_2 = G_2P_2$, with the nominal $L_{10} = G_1P_{10} \frac{L_{20}}{1+L_{20}}$, $L_{20} = G_2P_{20}$. Due to P_1 uncertainty only (with L_2 fixed at L_{20}), L_1 extends up to the dashed part, e.g. at ω_1 up to point E in Figure 1-21. It is therefore necessary that $\frac{L_2}{1+L_2}$ does not cause

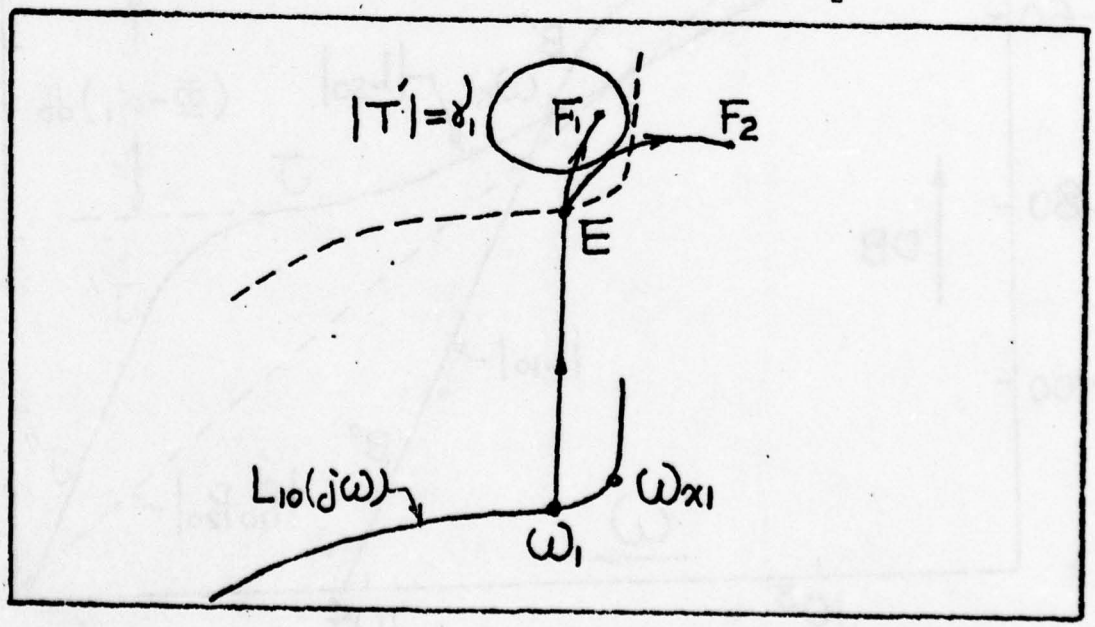

Figure 1-21. Explanation of finding an acceptable region for $\frac{L_2}{1+L_2}$.

further extension into γ_1, e.g. EF_1 is not allowed, but EF_2 is allowed. In this way an acceptable region for $\frac{L_2}{1+L_2}$ at each ω, is found. What are the bounds on L_{20} such that $\frac{L_2}{1+L_2}$ stays in its acceptable region for all P_2? This is almost precisely a repeat of the single-loop problem and is solved in the same manner. It is also necessary to introduce γ_2 (analogous to γ_1 for the single-loop problem) and with it a UHF boundary for L_{20}. The reason is that in Figure 1-15a,

$$\frac{C_2}{D_2} = \frac{1}{(1+L_1)(1+L_2)} \qquad (1.4\text{-}7)$$

Hence, for the same reason as in Section 1.2.3, it is necessary to assign bounds to $\left|\frac{L_2}{1+L_2}\right| \leq \gamma_2$, resulting in the L_{20} UHF boundary, B_{h2}.

Typical bounds $B_2(\omega)$ on L_{20}, which result from the above, are shown in Figure 1-9b. The reason for their nature is discussed in [H4]. The resulting "practical optimum" L_{20} (in the sense previously discussed in 1.4-1 for L_{10}) is also shown in Figure 1-9b. It is useful to note that at some frequency $\omega = \omega_{m2}$ (note its location with respect to B_{h1} in Figure 1-9a), $|L_{20}(j\omega)|$ has a peak value M_2 at which Arg $L_{20}(j\omega_{m2}) \sim -90°$. The value of M_2 is a function of θ_{m1}, the phase-margin of L_{10} (related to γ_1 of Figure 1-9a) and of the overdesign α_1 of L_{10}. Empirically obtained graphs of M_2 vs. these two variables are shown in Figure 1-22, and they will be very useful later. Note also the existence of the "corner" frequency ω_{x2} in Figure 1-9b (analogous to ω_{x1} of Figure 1-9a), at which L_{20} turns the corner at the bottom of B_{h2}.

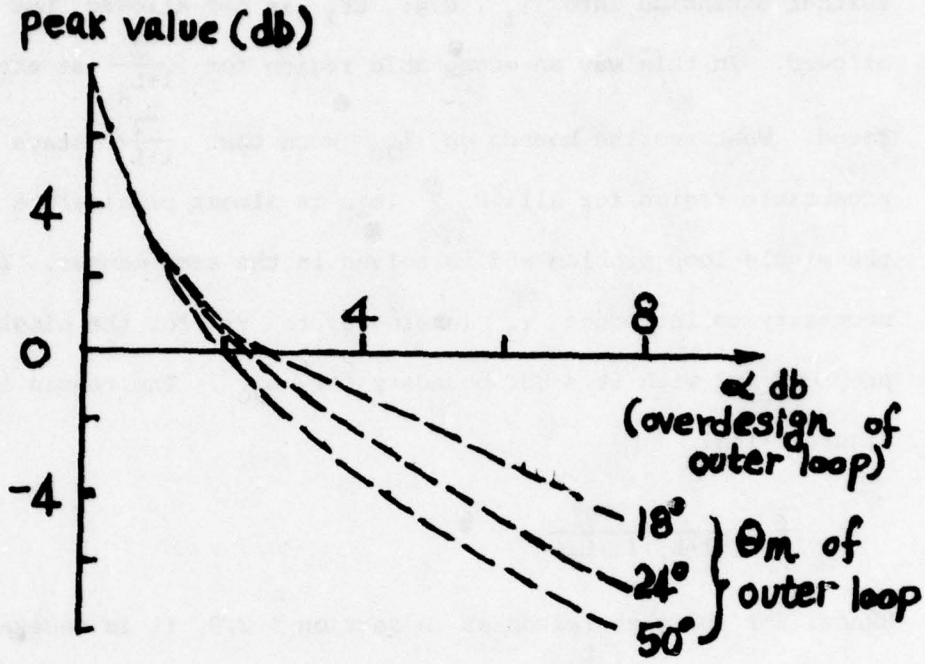

Figure 1-22. Peak value of inner loop as function of θ_m .

Note that for $\omega > \omega_{x2}$, the shape of the practical optimum $L_{20}(j\omega)$ is very similar to that of $L_{10}(j\omega)$ for $\omega > \omega_{x1}$. In these respective ranges the $L_{io}(j\omega)$ assume their respective UHFCOC (recall Section 1.4.3), which are similar functions of the phase margin θ_{mi}, and of e_{Li} the excess of poles over zeros of L_{io} .

Sensor noise effect in first inner loop.

In Figure 1-15a, it is readily found that

$$-\frac{X}{N_2} = \frac{L_2/P_2}{(1+L_1)(1+L_2)} \doteq \frac{L_2}{P_2} \qquad (1.4\text{-}8)$$

in the hf region where $|L_1|, |L_2| << 1$. Hence, on a Bode plot containing $|L_{20}|$, one only needs to sketch $|P_{20}|$, to see $|X/N_2|$.

On the same Bode plot let L_{so} , L_{10} , L_{20} , $P_{10}P_{20}$, P_{20} be sketched. One then sees at a glance the advantage, if any, of a 2-loop design over the single-loop. If the major effect is in the hf region, the effect of N_1 in a single-loop design is the difference between L_{so} and $P_{10}P_{20}$. In a two-loop design it is the difference between L_{10} and $P_{10}P_{20}$ for N_1 , and the difference between L_{20} and P_{20} for N_2 (see Figure 1-23).

1.4.5. Design of second and higher inner loops.

Suppose $n = 3$ in Figure 1-12, so a second inner loop $L_3 = G_3P_3'$ is feasible. If L_3 is not used, then from 1.4.4, the first inner loop L_1 handles the hf ($\omega > \omega_{x1}$) uncertainty of $P_2'P_3'$. If L_3 is used then the relations between L_3 and L_2 are very similar to those between L_2 and L_1 , respectively: L_2 is allowed to handle the uncertainty in $P_2'P_3'$ up to ω_{x2} (of L_{20}). This ω_{x2} is obtained in the same manner as ω_{x1} of L_{10} , i.e. B_{h2} , the UHF boundary for L_{20} is obtained by assigning to L_{20} only the hf uncertainty of P_2' (not of $P_2'P_3'$) and some extra margin α_2 (analogous to α_1 of L_{10}). By definition, L_{20} turns the corner of B_{h2} at ω_{x2} (point in Figure 1-9b).

The bounds on L_{30} are very minor for $\omega < \omega_{x2}$ (just as those on L_{20} were for $\omega < \omega_{x1}$). They become significant for $\omega > \omega_{x2}$ (see Figure 1-9c) and the resulting $|L_{30}|$ reaches a maximum at Arg $L_{30} \sim -90°$ at $\omega = \omega_{m3}$, with $L_{20}(j\omega_{m3})$ located relative to B_{h2} exactly as $L_{10}(j\omega_{m2})$ was relative to B_{h1} (compare points ω_{m2} , ω_{m3} in Figures 1-9a, 9b). The value of $M_3 = |L_{30}(j\omega_{m3})|$ is the same function of θ_{m2} and α_2 as $M_2 = |L_{20}(j\omega_{m2})|$ is of θ_{m1} and α_1 ,

so the graphs in Figure 1-22 may be used. There is needed a B_{h3}, the UHF boundary for L_{30}, exactly like B_{h2} for L_{20}. The shape of L_{30} is therefore very similar to that of L_{20}, except that it unfolds in a higher frequency range. This is called the bandwidth propagation effect. The effect of sensor noise N_3 is found to be

$$-\frac{X}{N_3} = \frac{L_3/P'_3}{(1+L_1)(1+L_2)(1+L_3)} \doteq \frac{L_3}{P'_3} \qquad (1.4\text{-}9)$$

in hf range where each $|L_i| << 1$. Thus one needs only sketch $|L_{30}|$, $|P'_{30}|$ on a Bode plot to see the order of magnitude of $|X/N_3|$ (see Figure 1-23).

1.4.6. Bandwidth propagation effect in cascade design.

It was shown in Section 1.4.3 how the UHFCOC of L_{10} may be obtained from that of L_{so}. The peak point of $|L_{20}|$ at ω_{m2} lies near the end of the almost horizontal part of the UHFCOC of L_{10}. It is then necessary for $|L_{20}(j\omega)|$ to decrease until it reaches the ω_{x2} point of B_{h2} at which its UHFCOC takes place. Near the end of the almost horizontal part of the latter, there is the ω_{m3} value at which $L_{30}(j\omega)$ has its peak. $L_{30}(j\omega)$ must then decrease till it reaches the ω_{x3} point of B_{h3}, and then its UHFCOC takes place, etc. At each step one is pushed to a higher frequency range. But it is interesting to see in Figure 1-23 that the UHFCOC of L_{so} and of the last inner loop $L_{no} = L_{30}$, in Figure 1-23, are not far apart in frequency, with the latter somewhat in a higher range, because there is inevitably some extra frequency range consumed at each inner loop stage.

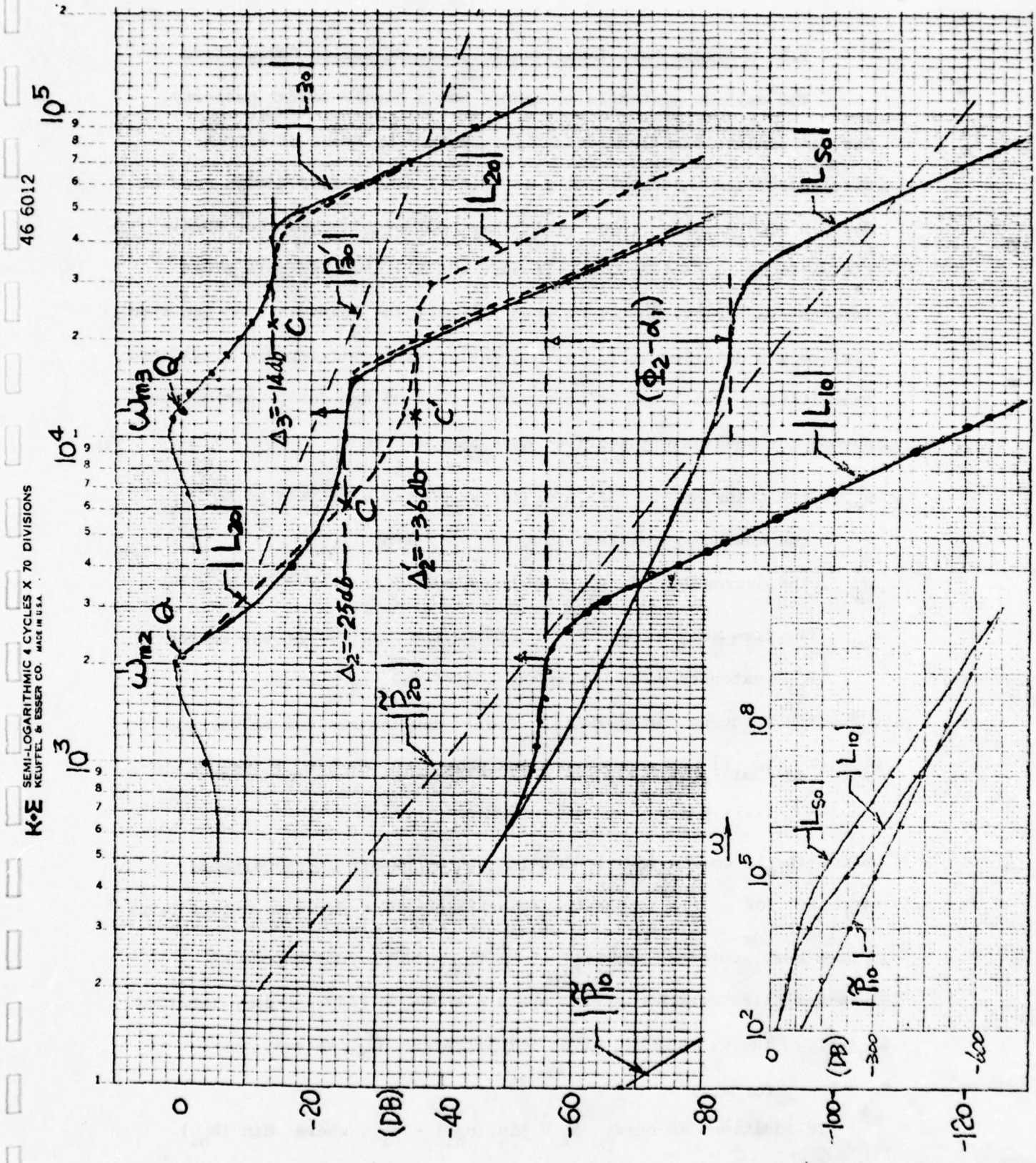

Figure 1-23. Bode plots of detailed design and perspective design.

1.5 A Simple Fast Technique for Cascade Design Perspective

The cascade synthesis procedure has a highly useful property. One can achieve excellent design perspective by means of simple straightforward sketches. Only an initial single-loop design need be done in some detail. These preliminary perspective sketches enable the designer to decide which, if any, and how the available plant internal variables, should be used for feedback purposes. He can then perform his detailed multiple-loop design with considerable confidence that iteration will not be necessary. Most of the design parameters needed for 'design perspective' have been defined:

θ_{mi} , the phase margin for L_{io} (Figures 1-9a,b,c) related to γ_i , the maximum permitted value of $|L_i/(1+L_i)|$.

α_i , the overdesign of L_{io} (Figures 1-9a,b,c).

ω_{xi} , the frequency at which L_{io} turns the "corner" at the bottom of B_{hi} extended downward by the additional α_i value.

ω_{mi} , the frequency at which $|L_{io}(j\omega)|$ has its maximum value, and $M_i = |L_{io}(j\omega_{mi})|$, the corresponding peak value of $|L_{io}|$ for $i = 2,\ldots,n$.

UHFCOC (L_{10}), the universal high-frequency cut off characteristic effective for $\omega > \omega_{x1}$ for the outer loop. That shown in Figure 1-24a is used here, obtained for $e_{L_1} = 5$, $\theta_{m1} = 50°$. Corresponding characteristics for the inner loops are shown in Figure 1-24b, labelled $L_{io}(HF)$. There, they are given for different $\mathcal{O}_m$ values, but $e_{L_i} = 5$ for all.

In addition, we need: $\Delta_i \triangleq \text{Min } (B_{hi}) - \alpha_i$, where Min (B_{hi})

is the point of minimum magnitude of B_{hi} (= -54.5 db in Figure 1-9a for $i = 1$).

Also, we need the value of ω_{mi} and the shape of L_{io} for $\omega \in [\omega_{mi}, \omega_{xi}]$. The latter was obtained by studying numerous designs. It is given in Figure 1-24a, labelled $L_{io}(IF)$, since it applies in the intermediate frequency (IF) region. The arrows in Figures 1-24a,b are used to locate ω_{mi} , as explained below.

1.5.1. Procedure for "design perspective".

1. Make a single-loop design L_{so} to handle the entire problem, e.g. L_{so} in Figure 1-23 for the example of Section 1.2.5. It is assumed that the hf portion of L_{so} is reasonably close to that shown i.e. UHFCOC(L_{10}) in Figure 1-24a.

2. Let Φ_2 be the hf uncertainty of $P_2P_3...P_n$, and allow α_1 an overdesign margin for L_{10} . Obtain L_{10} by shifting the UHFCOC portion upwards by $(\Phi_2 - \alpha_1)$ db as shown in Figures 1-20, 1-23.

3. The value of ω_{m2} is at the arrow on UHFCOC(L_{10}) in Figure 1-24a. The value of $M_2 = |L_{20}(j\omega_{m2})|$ is available from the graphs in Figure 1-22. Locate M_2 at $\omega = \omega_{m2}$ and let this be point Q in Figure 1-23. Point Q is $|L_{20}(j\omega_{m2})|$. Draw a horizontal line in Figure 1-23 at Δ_2 magnitude (= -25 db for above example). Transparencies of Figures 1-24a,b are assumed available. Place $L_{io}(IF)$ of Figure 1-24a on Figure 1-23 so that the two Q points coincide. Find where $L_{io}(IF)$ of Figure 1-24a intersects the Δ_2 line of Figure 1-23 and label this point of intersection as point C in Figure 1-23.

4. Pick the $L_{io}(HF)$ curve in Figure 1-24b, according to the

θ_{m2} value being used for L_{20} . Lay L_{io}(HF) on Figure 1-23, such that the two C points (of L_{io}(HF) and that obtained in Step 3) coincide. L_{20} consists of L_{io}(IF) of Figure 1-24a in the intermediate ω range and of L_{io}(HF) of Figure 1-24b in the high-frequency range. Use the portion of L_{io}(HF) to the left of C to obtain a smooth continuous curve for L_{20} .

5. Steps 3, 4 are repeated in order to determine L_{30} . Use the arrow on L_{io}(HF) of Figure 1-24b, to locate ω_{m3} . Use Figure 1-22 to obtain M_3 , giving a new point Q in Figure 1-23. Then lay L_{io}(IF) of Figure 1-24a on Figure 1-23, so that the Q's coincide, etc. A horizontal line of value Δ_3 is drawn, etc. The entire process is repeated until all the loops are exhausted.

The results in Figures 1-23,25 are examples of the excellent agreement obtained in practice between these quick estimates and the actual final detailed designs.

6. After each L_{io} is obtained, it is a good idea to sketch the effective P values to use for the sensor noise effect. Thus after L_{so} is obtained, sketch $|\tilde{P}_{io}| = |P_{10}P_{20}\cdots P_{no}|$ in Figure 1-23. If there is little sensor noise amplification ($|L_{so}/\tilde{P}_{io}|$ not large over a large ω range), there may be no point in using more feedback loops. After L_{10} has been obtained, it is easy to see the saving in sensor N_1 noise effect, by using L_2 . Sketch $|\tilde{P}_{20}| = |P_{20}\cdots P_{no}|$ to see the hf N_2 sensor noise effect ($\approx |L_{20}/\tilde{P}_{20}|$). Similarly $|L_{io}/\tilde{P}_{io}|$, $|\tilde{P}_{io}| = |P_{io}\cdots P_{no}|$, gives the hf N_i sensor noise effect.

The designer has to decide which sensor points to use and the corresponding α_i trade-off values. It is emphasized that this design

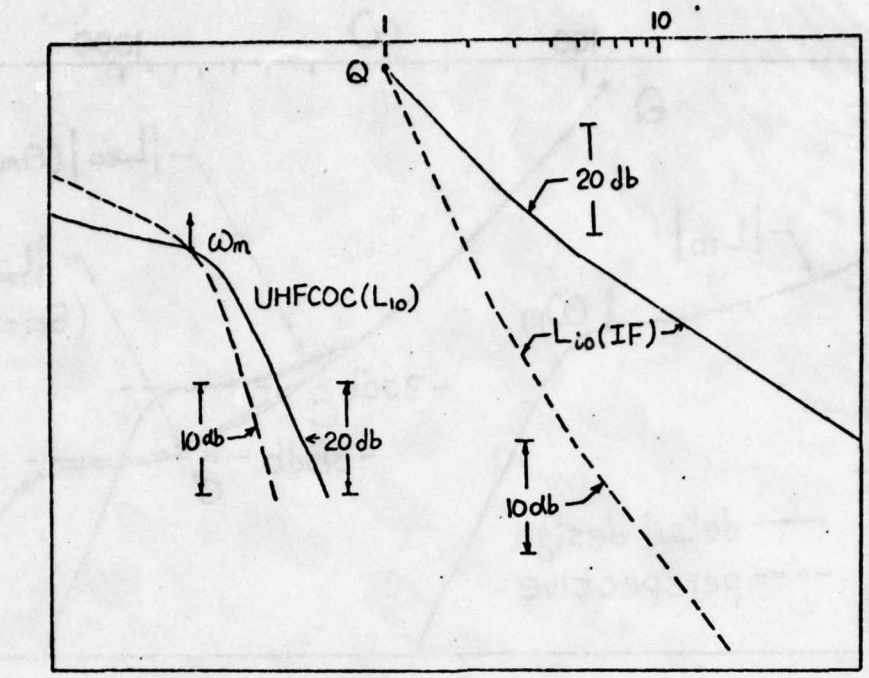

(a)

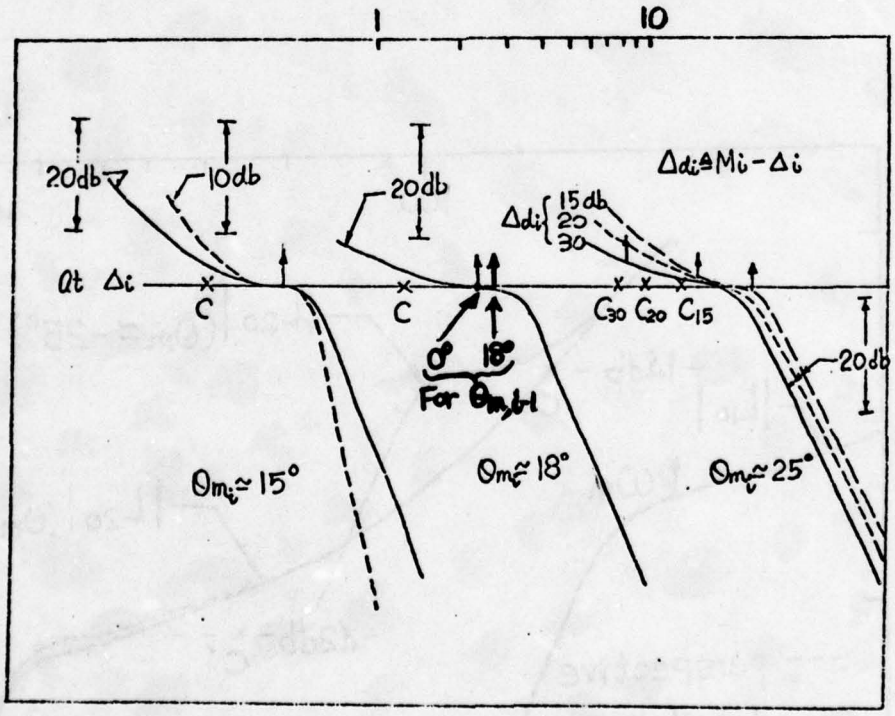

(b)

Figure 1-24a. The universal HF and IF characteristics for the outer loop.

Figure 1-24b. The corresponding L_{io}(HF) characteristics for the inner loop.

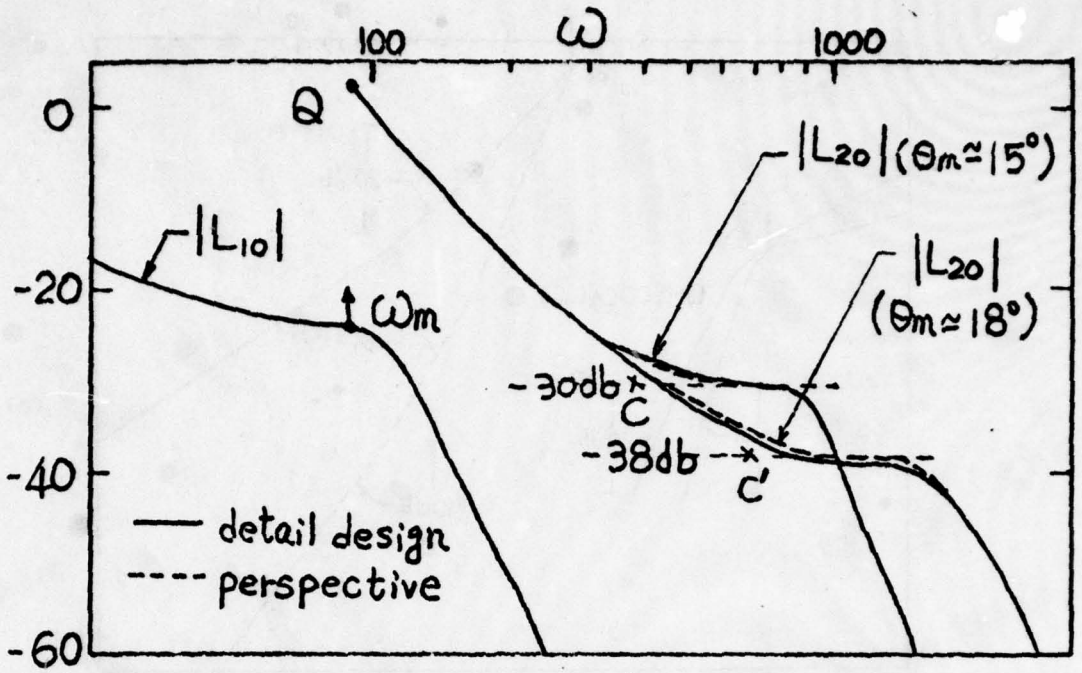

(a)

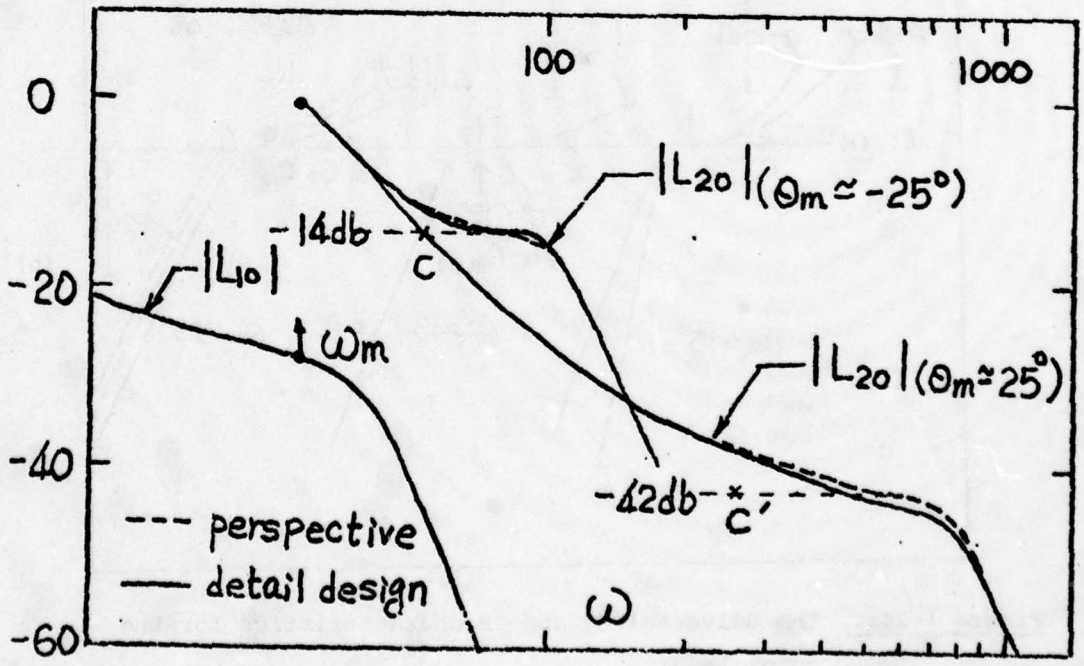

(b)

Figures 1-25a,b. Demonstration of design perspective.

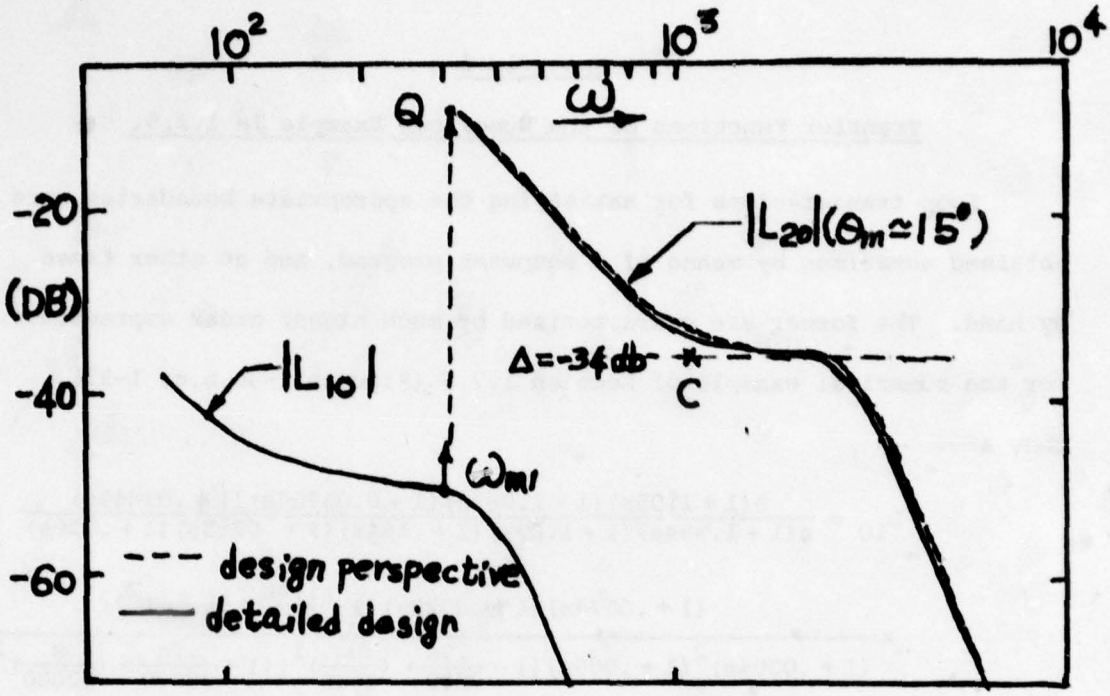

(c)

Figure 1-25c. Demonstration of design perspective.

perspective approach does not give him this information immediately. Design perspective is, however, a very useful, fast, simple, tool for making his choice. It makes it easy for him to try different combinations. For example, he may find it questionable to use a sensor at C_2 perhaps because N_2 is very large. He can then consider using a larger value of α_1, thereby throwing more burden on L_{10} and less on L_{20}. He need not execute a detailed design. The above design perspective gives him the answer in a few minutes. He may decide to forego the sensor at C_2. If so, in our terminology the new P_1 = the old P_1P_2, i.e. the outer loop must now handle $\forall\ \omega$ the uncertainty in the former P_1P_2.

Our objective is to develop similar design perspectives for the more complex structures of Figures 13a, 13b, 14.

Appendix 1

Transfer Functions of the Numerical Example in 1.2.5.

Loop transmissions for satisfying the appropriate boundaries were obtained sometimes by means of a computer program, and at other times by hand. The former are characterized by much higher order expressions. For the numerical example of Section 1.2.5 (Figures 1-9a,b,c, 1-23), they are:

$$L_{10} = \frac{5(1+1.05s)(1+1.087s)(1+0.05764s)(1+.03845s)}{s(1+1.954s)(1+1.89s)(1+.164s)(1+.0265s)(1+.026s)}$$

$$\times \frac{(1+.0074s)(1+.0028s)\left[1+\frac{1.4s}{2200}+\left(\frac{s}{2200}\right)^2\right]}{(1+.0004s)^2(1+.005s)\left[1+\frac{.7s}{2600}+\left(\frac{s}{2600}\right)^2\right]\left[1+\frac{.7s}{22000}+\left(\frac{s}{22000}\right)^2\right]^2}$$

$$L_{20} = \frac{0.5}{\left[1+\frac{0.4s}{1920}+\left(\frac{s}{1920}\right)^2\right]} \times \frac{1+\frac{s}{13800}}{\left[1+\frac{0.6s}{16000}+\left(\frac{s}{16000}\right)^2\right]^2}$$

$$\times \left(\frac{1+\frac{s}{1080}}{1+\frac{s}{900}}\right) \times \left(\frac{1+\frac{s}{8640}}{1+\frac{s}{19200}}\right)$$

$$L_{30} = \frac{0.645}{\left[1+\frac{0.6s}{11250}+\left(\frac{s}{11250}\right)^2\right]} \times \frac{1+\frac{s}{45000}}{\left[1+\frac{0.3s}{45000}+\left(\frac{s}{45000}\right)^2\right]}$$

$$\times \frac{1}{\left[1+\frac{2s}{180000}+\left(\frac{s}{180000}\right)^2\right]}$$

CHAPTER 2

THE CASCADE STRUCTURE IN PARALLEL WITH ONE BRANCH

2.1 Introduction

Quantitative feedback design theory was defined in Section 1.1. Prior to this work it was confined to the cascaded plant structure of Figure 1-12. This chapter extends quantitative synthesis to the plant structure (heavy lines) of Figure 2-1, consisting of two parallel branches, one of which has n internal sensing points $C_1, C_2, \ldots C_n$. It is assumed the system input r and output c can also be sensed, giving $n+2$ degrees of freedom, in the form of $n+2$ independent data processing of these measurements. Figure 2-1 shows one canonic structure which exploits this freedom, but there is an infinitude of others — see Section 2.4.

It is assumed each plant section has independently uncertain parameters giving for each, a set $\{P_i\} \in \mathcal{P}_i$, and the objective, as in

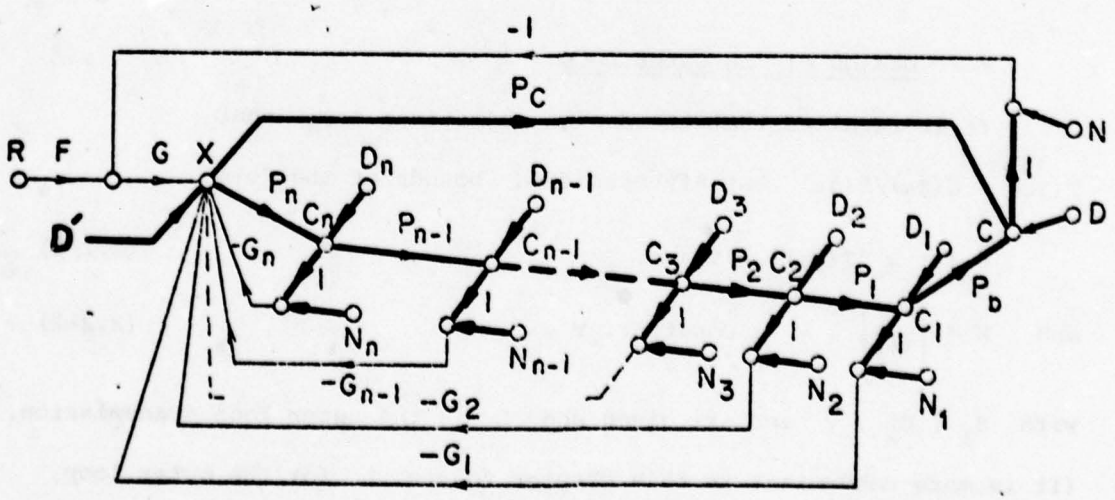

Figure 2-1. System structure (Heavier lines indicate plant with sensor noise sources).

Section 1.1, is to guarantee that these objectives are satisfied $\forall P_i \in \mathcal{P}_i$. Just as in the cascade case, no analytic theory is available but an engineering design theory is developed for a large class of practical plants. The emphasis is on the minimization of net sensor noise effect at the plant input X. A transparent design theory is developed which is very similar in its results, to that of the cascade system, although its development is more difficult. There is the same 'bandwidth propagation' phenomenon as in Section 1.4.6. Also, "design perspective" (Section 2.5) is possible by relatively simple, fast sketches, based on only a preliminary single-loop design for the problem. This enables the designer to decide which loops to use and how, and gives him a very good idea of the final design — without a detailed design. Such rapid perspective design (Section 2.5) is compared with detailed design for a specific 3-loop numerical example with large uncertainty. The agreement is excellent (Figure 2-5). The treatment is devoted entirely to minimum-phase systems.

2.2 Design of the Outer Loop

It is recalled that the design objectives are: that $T(j\omega) = C(j\omega)/R(j\omega)$ satisfy specified bounds of the form

$$B_2(\omega) \leq |T(j\omega)| \leq B_1(\omega) \tag{2.2-1}$$

and $$M \triangleq \left|\frac{L}{1+L}\right| \leq \gamma \text{ a constant, } \forall \omega \tag{2.2-2}$$

with B_1, B_2, γ apriori given and L is the outer loop transmission. (It is more convenient in this chapter to use L for the outer loop, L_1 for the first inner, etc., unlike the notation in Chapter 1.) Just

as in the cascade case, (2.2-1, 2) are achievable [H3] with a single loop $G_i = 0$, $i = 1,\ldots,n$, $G = G_S \neq 0$ in Figure 2-1. But the resulting $L_S = G_S P$ may then require very large bandwidth, causing great amplification of the sensor noise N , as in a later example — Figure 2-6a,b. The simplistic approach, later justified, is to design the outer loop L from C to cope only with the uncertainty in P_b , P_c which can give an L much more economical than in a single-loop design in which L must cope with all P . The first inner loop L_1 from C_1 may be designed to cope only with P_1 , with possible great saving compared to an L_1 which copes with $P_1 P_2 \ldots P_n$. Similarly the second inner loop need cope only with P_2 , etc. The result has considerable transparency and insight, giving the designer a good perspective of the optimum division of the feedback burden among the loops, even before execution of the design details (Section 2.5). Simplifications initially made in order to concentrate on the essentials, are covered in Section 2.6. In Figure 2-1, let

$$P_a \triangleq P_n P_{n-1} \ldots P_2 P_1 \quad , \quad P \triangleq P_a P_b + P_c \quad ,$$

$$\mathcal{D} \triangleq (1 + P_n G_n + P_n P_{n-1} G_{n-1} + \ldots + P_n \ldots P_1 G_1) + PG$$

$$\triangleq \mathcal{D}_1 + PG \triangleq \mathcal{D}_1 (1+L) \quad , \quad L = \frac{PG}{\mathcal{D}_1} \triangleq P_e G \quad . \qquad (2.2\text{-}3a\text{-}f)$$

$$T(s) = \frac{C(s)}{R(s)} = \frac{FGP}{\mathcal{D}} = \frac{FGP/\mathcal{D}_1}{1 + (GP/\mathcal{D}_1)} = F \frac{L}{1+L} \quad .$$

$$-\frac{X}{N} = \frac{G}{\mathcal{D}} = \frac{G}{\mathcal{D}_1 (1+L)} = \frac{L/P}{1+L} \quad .$$

In (2.2-3f) the sensor noise effect is examined at the plant input X where it tends to be large (Figure 2-6), causing plant saturation. In the high frequency range (denoted as hf), (2.2-3f) $\rightarrow L/P$

where $|L(j\omega)| << 1$ but $|L/P|$ can be very large (Figure 2-5) — the hf range is the major trouble source. For example, in Figure 2-6b, the lowest ω range with large and sharp peaking of $|X/N|$ is 300 rps at which, from Figure 2-5, the nominal $|L| \sim -48$ db but $|P| \sim -83$ db. Hence, the major effort in sensor noise effect minimization will be made in hf. This highly justified fact is very helpful in simplifying the problem. Since P is contrained in (2.2-3b), such minimization requires $|L|$ minimization. But from (2.2-3d), L must cope with $P_e = P/\mathcal{D}_1$ uncertainty. Therefore, for maximum economy of L, choose the G_i, $i = 1,\ldots,n$ in $\mathcal{D}_1$ of (2.2-3c) to minimize the uncertainty in $P_e = P/\mathcal{D}_1$.

Consider accordingly the uncertainty in

$$P_e = \frac{P_1P_2\ldots P_nP_b + P_c}{1 + P_nG_n + \ldots + P_n\ldots P_2P_1G_1}$$ in hf, where each $P_i \to k_i/s^{e_i}$, e_i the excess of poles over zeros of P_i. Since $P_1P_2\ldots P_nP_b$ parallels P_c in Figure 2-1, it is assumed in the meantime (see Section 2.6) that $(e_1 + e_2 + \ldots + e_n)$ $e_b \triangleq e_a + e_b = e_c$. Hence, at hf

$$P_e = \frac{P}{\mathcal{D}_1} \to \frac{k_ak_b+k_c}{s^{e_c}[1+k_ng_n+\cdots+k_ag_1]} = \frac{k_e}{s^{e_c}}, \quad \text{where} \tag{2.2-4a,b}$$

$$G_n \triangleq g_ns^{e_n}, \; G_{n-1} \triangleq g_{n-1}s^{e_n+e_{n-1}}, \; \ldots, \; G_1 \triangleq g_1s^{e_a}.$$

The notation in (2.2-4b) is used to simplify the expressions. The resulting G_i do not necessarily have zeros at the origin — see Section 2.3.

The range of k_i is taken as $[a_i,b_i]$, $b_i > a_i > 0$. In the logarithmic complex plant (Nichols chart), P_e is not a point but a

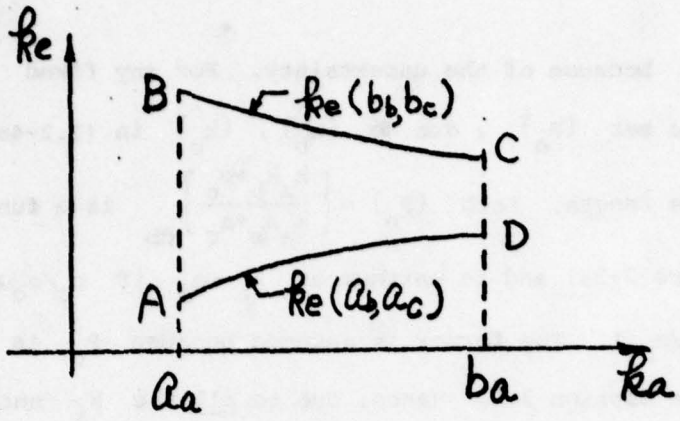

Figure 2-2a. Desired dependence of k_e on k_a if $b_c/a_c \geq b_b/a_b$.

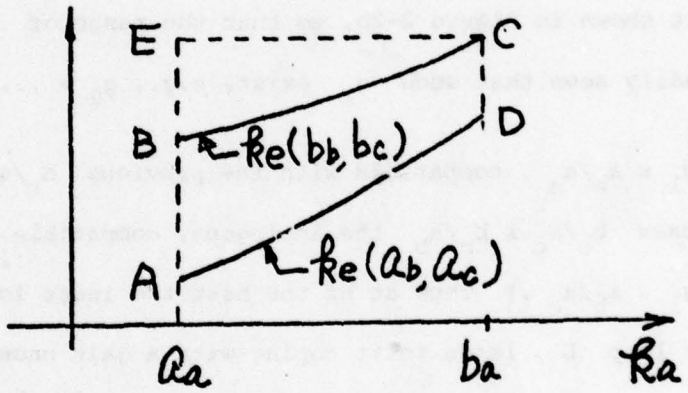

Figure 2-2b. An example of undesirable dependence of k_e on k_a if $b_c/a_c \geq b_b/a_b$.

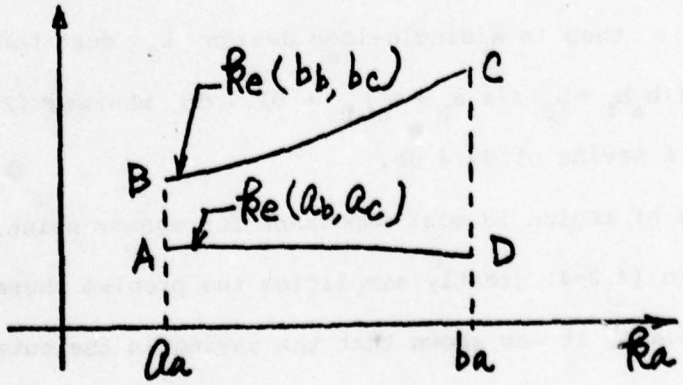

Figure 2-2c. Desired dependence of k_e on k_a if $b_c/a_c < b_b/a_b$.

set $\{P_e\}$ because of the uncertainty. For any fixed $k_1,\cdots,k_n$ values the set $\{P_e\}$, due to $\{k_b\}$, $\{k_c\}$ in (2.2-4a), is a vertical line whose length, Lgth $\{P_e\} = \left[\frac{k_a k_b + b_c}{k_a a_b + a_c}\right]_{db}$ is a function of k_a, (see Figure 2-2a) and is maximum at $k_a = a_a$ if $b_c/a_c \geq b_b/a_b$ (at b_a if $b_c/a_c \leq b_b/a_b$). The former is assumed because P_c is in parallel with $P_a P_b$ — see Section 2.6. Hence, due to <u>all</u> the k_i uncertainty sets Lgth$\{P_e\} \geq (a_a b_b + b_c)/(a_a a_b + a_c)$, with equality iff $\exists\, g_i$ such that sets $\{k_e(k_a,k_b,k_c)\}$ of (2.2-4a) $\subseteq \{k_e(a_a,k_b,k_c)\}$ as the k_i independently range over $[a_i,b_i]$. For example, $g_1 = 1/2\ b_b/b_c$ has the effect shown in Figure 2-2b, so that the range of k_e is AE > AB. It is readily seen that such g_i exist, e.g., $g_2 = \ldots = g_n = 0$, $b_b/b_c \leq g_1 \leq a_b/a_c$, compatible with the previous $b_c/a_c \geq b_b/a_b$. (In the case $b_c/a_c \leq b_b/a_b$ the analogous, compatible condition is $b_b/b_c \geq g_1 \geq a_b/a_c$.) Thus at hf the best the inner loops can do for the outer loop L, leads to it coping with a gain uncertainty set.

$$\{a_a k_b + k_c\} \triangleq \mathcal{V}^{\circ}\{P_e^{\circ}\}, \text{ of Lgth } \mathcal{V}^{\circ} = \frac{a_a b_b + b_c}{a_a a_b + a_c}. \qquad (2.2\text{-}5a,b)$$

For example, if $n = 2$, all $a_i = 1$, $b_i = 40, 10, 60, 200$ for $i = 1,2,b,c$ then in a single-loop design L_S must handle hf $\{P\}$ of length $[(b_a b_b + b_c)/(a_a a_b + a_c)]_{db} = 81.7$ db whereas (2.2-5b) gives 42,3 db, a saving of 39.4 db.

The hf region is most important for sensor noise, and the hf form of P_i in (2.2-4) greatly simplifies the problem there. In Chapter 1, Section 1.4.4, it was shown that the saving in the outer loop is very minor for $\omega < \omega_x$ (the frequency at which L turns the corner —

Figure 1-9a). Therefore, just as in the cascade case, let L handle the entire plant uncertainty problem up to ω_x. The value of ω_x is obtained by having L handle the smaller hf uncertainty of (2.2-5b). The region of concern for the inner loops is thus at hf, where each $P_j \doteq k_j/s^{e_j}$. Therefore, to simplify the presentation and notation we write $P_j = k_j/s^{e_j}$, $j = a,b,c$ as if (2.2-4,5) apply for all ω. Outer-loop design is now a single-loop problem with the equivalent plant P_e of (2.2-4a) denoted by

$$P_e^o \triangleq \frac{P_{a0}P_b+P_c}{1+P_{n0}G_n+\cdots+P_{n0}\cdots P_{20}P_{10}G_1} = \frac{a_a k_b+k_c}{(1+a_n g_n+\cdots+a_a g_1)s^{e_c}} \triangleq \frac{k_e^o}{s^{e_c}} \quad \text{and} \quad L^o = P_e^o G \,. \tag{2.2-6a,b}$$

The super-oh on P_e, k_e, L indicates P, k_e, L with $P_1, P_2, \ldots, P_n$ at their nominal values. The problem is to find G or equivalently a <u>nominal</u> (the sub-oh indicates nominal values) $L_0^o = P_{e0}^o G$ so that (2.2-2) and $\Delta\ell_n|T(j\omega)| \leq \ell_n \frac{A_2(\omega)}{A_1(\omega)}$ of (2.2-1), are satisfied. The optimum design for this single-loop problem [H3] was reviewed in Section 1.2, so we proceed directly with an example which is very helpful in explaining the multiple-loop design theory.

2.2.1. Design example.

In Figure 2-1 let $n = 2$, $P_j = k_j/s$, $j = 1,2,b$; $P_c = k_c/s^3$; $a_1 = 20$, $a_2 = 50$, $a_b = 1$, $a_c = 1000$, $b_1 = 800$, $b_2 = 500$, $b_b = 60$, $b_c = 200{,}000$. Time-domain bounds on the acceptable step response are shown in Figure 2-3a, and their translation into bounds on $|T(j\omega)|$ are shown in Figure 2-3b. Such translation is somewhat of an engineering art, but in practice good results have been obtained with moderate effort [H3, K1, S1]. Also, $\gamma = 2.3$ db in (2.2-2), corresponding to $\sim 23.5\%$ overshoot for the second order model. The nominal plant values are taken as a_i (with no loss in generality). Note: The specifications must be consistent with physical reality, i.e., it is crucial [H8] that $\exists\ \omega_0$, such that for $\omega > \omega_0$, the largest variation $P_e < \ell_n \frac{A_2(\omega)}{A_1(\omega)}$, in order that no sensitivity reduction be needed at large enough ω , permitting $L(j\omega) \to 0$ as $\omega \to \infty$. From Figure 2-3, $\omega_0 \approx 55$ for a multiple-loop design, 280 for a single-loop design, revealing the advantage of the former with respect to the outer loop.

Single-loop design theory was reviewed in Section 1.2. The bounds and the resulting loop transmission on $L_0^o(j\omega)$ are shown in Figure 2-4 and its Bode plot in Figure 2-5.

It is easy to derive the single-loop $L_s(j\omega)$ which would be necessary for the same problem and this is included in Figure 2-5, to emphasize the saving in bandwidth and sensor noise effect.

Returning to the multiple loop design, note that the nominal L of (2.2-3d), denoted by L_0 is identical to L_0^o and the nominal P_{e0} of (2.2-3d) to P_{e0}^o , justifying $G = L_0/P_{e0} = L_0^o/P_{e0}^o$. Here,

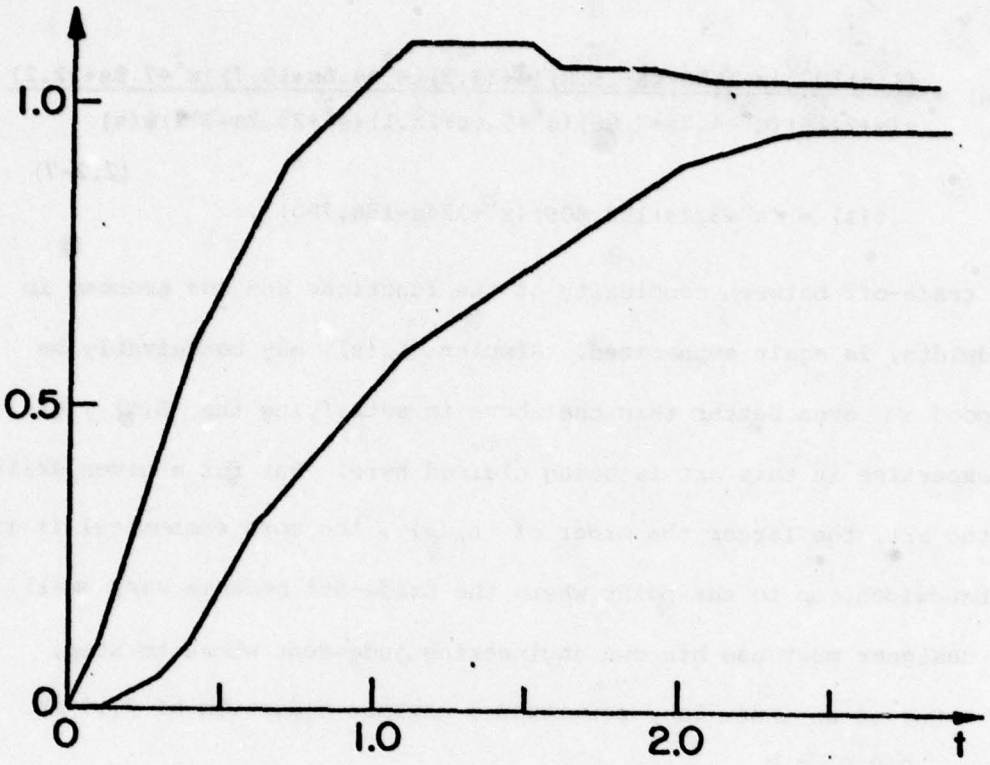

Figure 2-3a. Specified time-domain bounds on step response.

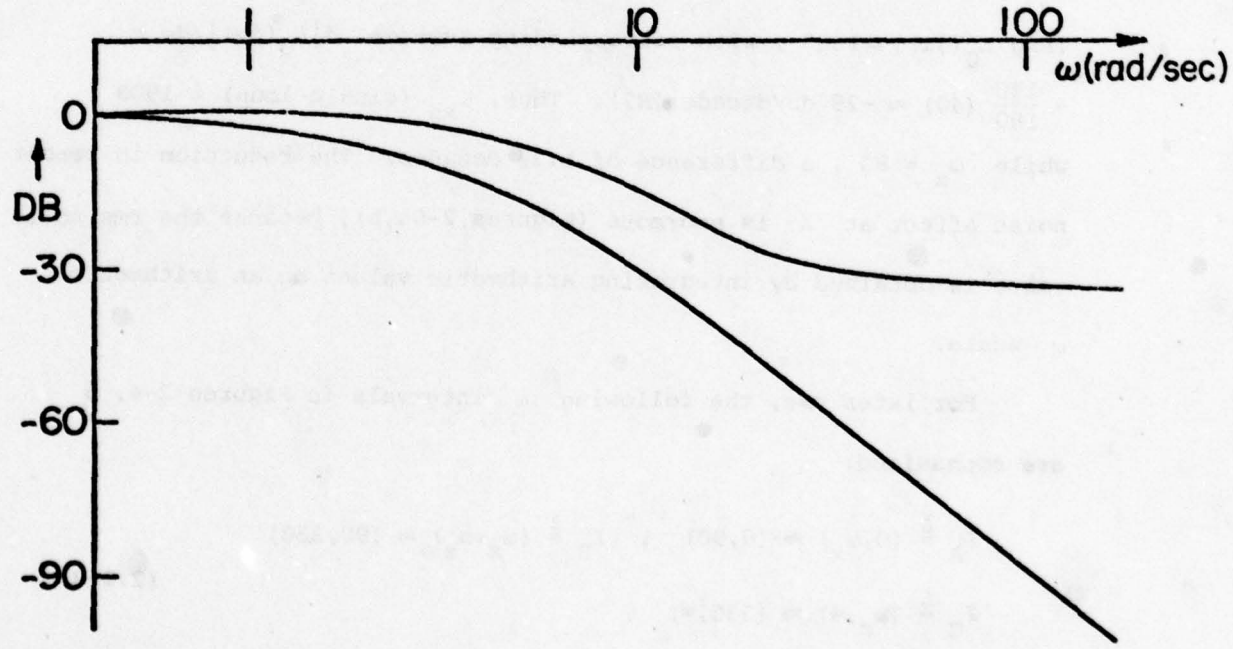

Figure 2-3b. "Equivalent" frequency-domain bounds.

$$L_0(s) = \frac{(1.6)10^{10}(s+1.96)(s+15.8)(s+39.5)(s^2+4.6s+10.7)(s^2+7.8s+22.2)}{s(s+2.16)(s^2+4.7s+7.86)(s^2+5.6s+25.1)(s^2+25.2s+371)\psi(s)}$$

$$\psi(s) = (s^2+324s+153{,}800)(s^2+324s+158{,}700) \quad . \tag{2.2-7}$$

The trade-off between complexity of the functions and the economy in bandwidth, is again emphasized. Simpler $L_0(s)$ may conceivably be as good or even better than the above in satisfying the $B(\omega)$, as no expertise in this art is being claimed here. But for a given skill in the art, the larger the order of $L_0(s)$, the more economical it is in bandwidth, up to the point where the trade-off becomes very small. The designer must use his own engineering judgement where to stop.

Use of an inner loop permitted a maximum reduction of 39.4 db ($20 \log \frac{b_2 b_1 b_b + b_c}{a_2 a_1 b_b + b_c} = 20 \log 93.7$) here, giving a saving in bandwidth of $\sim 40/29$ decades, because along B_h in Figure 2-4, $[\text{Arg } L_0(j\omega)] \simeq 130°$, with corresponding average $d|L_0(j\omega)|/d\omega = -\frac{130}{180}(40) \approx -29$ db/decade [H7]. Thus, ω_{xs} (single-loop) $\doteq 1900$, while $\omega_x = 80$, a difference of 1.38 decades. The reduction in sensor noise effect at X is enormous (Figures 2-6a,b), because the rms noise value is obtained by integrating arithmetic values on an arithmetic ω scale.

For later use, the following ω intervals in Figures 2-4, 5 are emphasized:

$$I_A \triangleq [0,\omega_x) \approx [0,90) \quad , \quad I_B \triangleq [\omega_x,\omega_z) \approx [90,330)$$
$$I_C \triangleq [\omega_z,\infty) \approx [330,\infty) \quad . \tag{2.2-8}$$

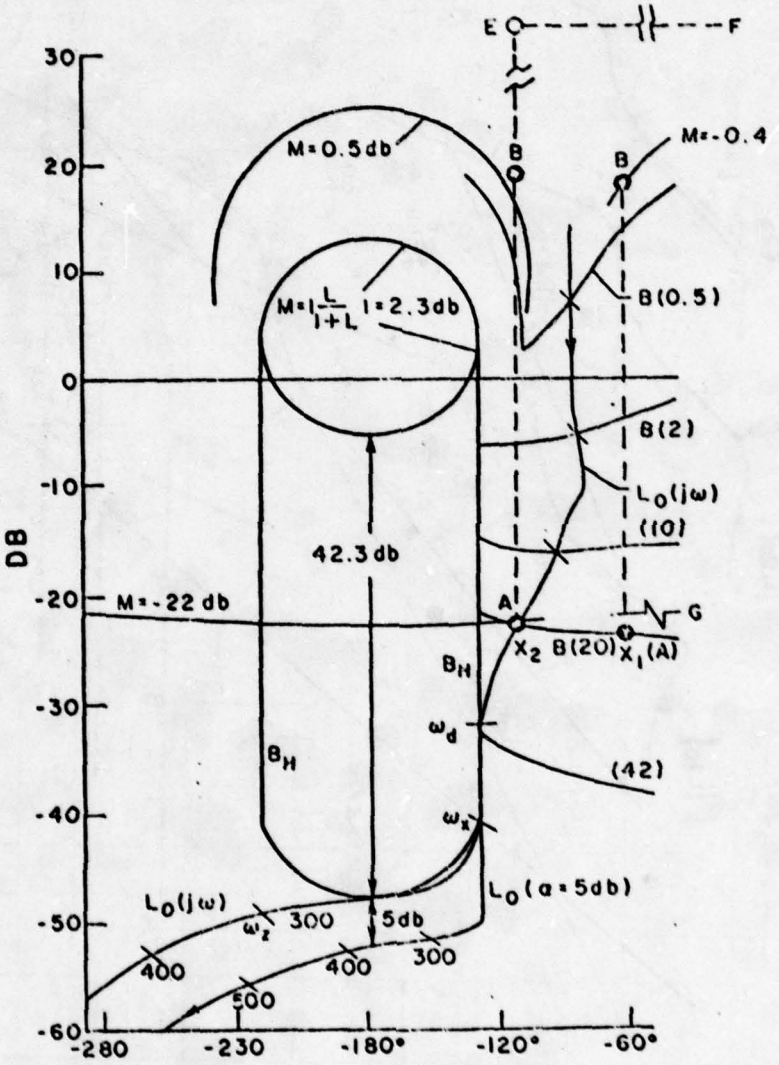

Figure 2-4. Bounds $B(\omega)$ on nominal outer loop transmission $L_0(\omega)$ in Nichols chart.

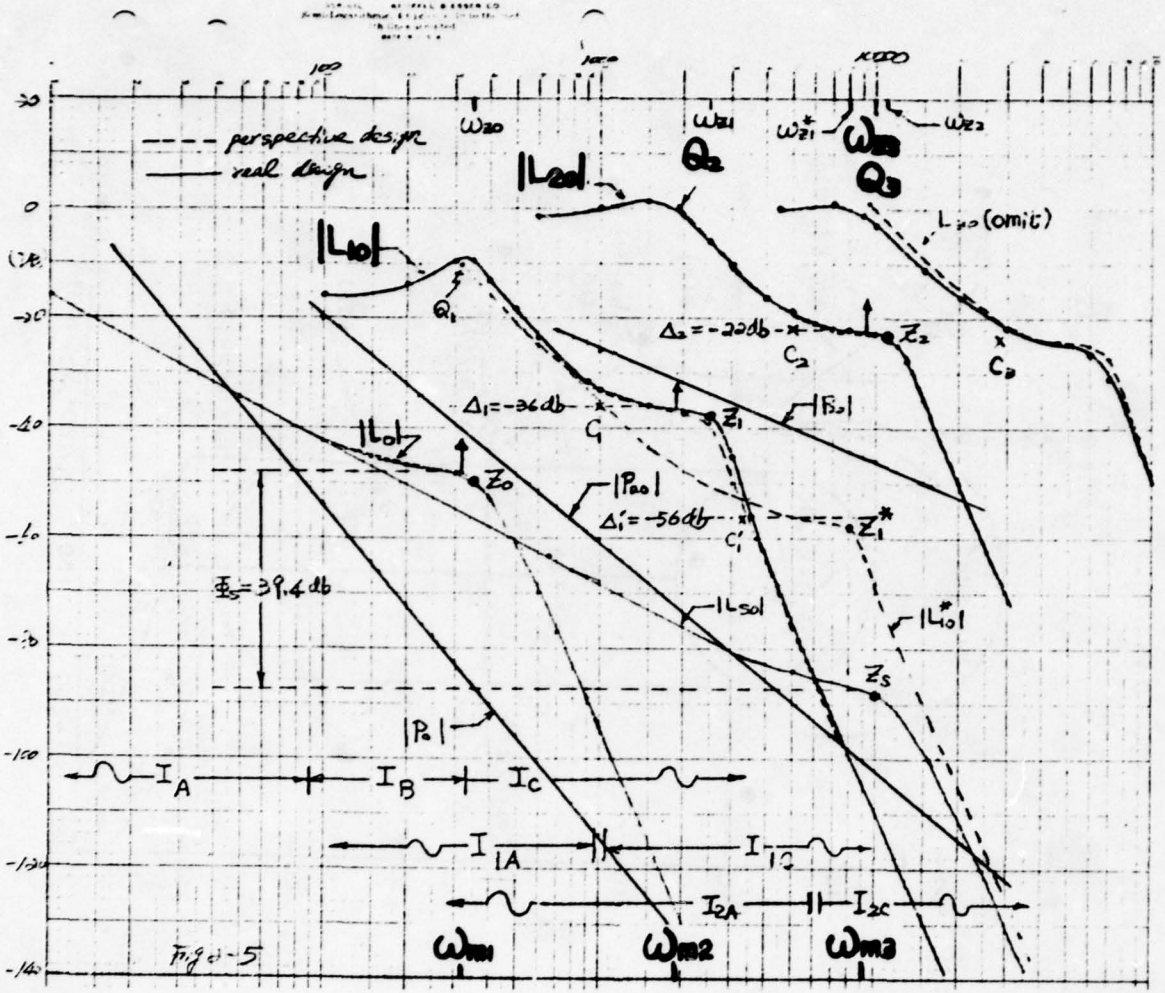

Figure 2-5. Bode plots of detailed design and perspective design.

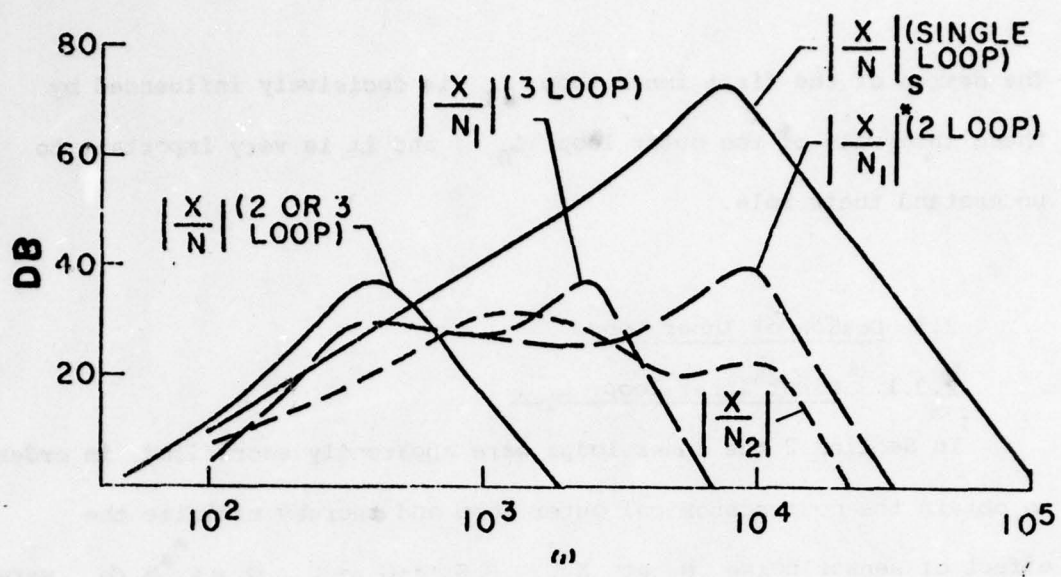

Figure 2-6a. Sensor noise effects at X — in decibels.

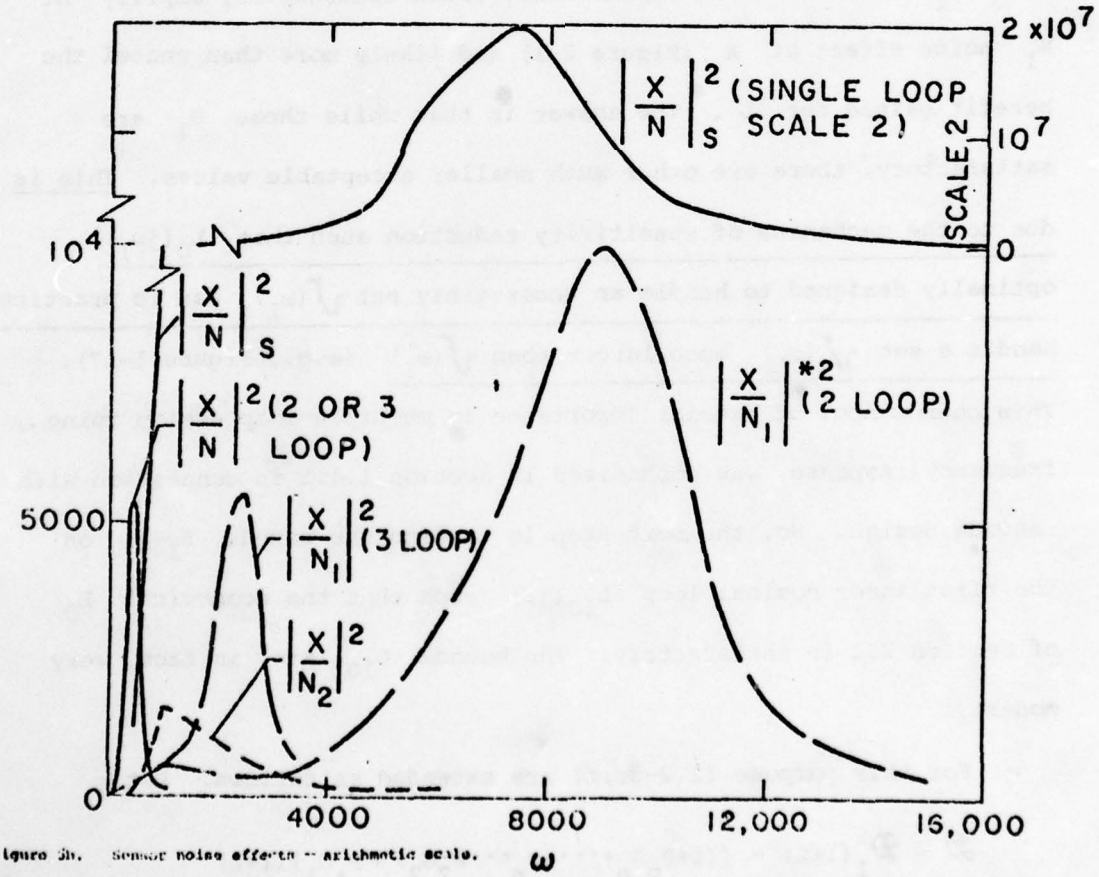

Figure 2-6b. Sensor noise effects at X — arithmetic scale.

The design of the first inner loop L_1 is decisively influenced by these intervals of the outer loop L_0, and it is very important to understand their role.

2.3 Design of Inner Loops

2.3.1. First inner loop L_1.

In Section 2 the inner loops were apparently sacrificed, in order to obtain the most economical outer loop and thereby minimize the effect of sensor noise N at X. $G_2G_3\cdots G_n = 0$, $G_1 = s^{e_a}b_b/b_c$ were found satisfactory for this purpose. The obvious criticism is that this G_1, besides being impractical, would tremendously amplify hf N_1 noise effect at X (Figure 2-1) and likely more than cancel the benefit gained for L. The answer is that while these G_i are satisfactory, there are other much smaller acceptable values. This is due to the mechanics of sensitivity reduction such that $L_0(j\omega_1)$ optimally designed to handle an uncertainty set $\sqrt{}(\omega_1)$ can in practice handle a set $\sqrt{}_y(\omega_1)$ much larger than $\sqrt{}(\omega_1)$ (e.g., Figure 1-17). This phenomenon, of crucial importance in multiple-loop design using frequency response, was emphasized in Section 1.4.1 in connection with cascade design. So, the next step is to find the bounds $B_1(\omega)$ on the first inner nominal loop $L_{10}(j\omega)$ such that the economical L_0 of Section 2.2 is satisfactory. The bounds L_{10} are, in fact, very modest.

For this purpose (2.2-3c,f) are extended as follows. Let

$$\mathcal{D} = \mathcal{D}_1(1+L) = [(1+P_nG_n+\cdots+P_n\cdots P_2G_2) + P_aG_1](1+L)$$

$$\triangleq (\mathcal{D}_2+P_aG_1)(1+L) = \mathcal{D}_2(1+L_1)(1+L) \quad , \qquad (2.3\text{-}1a,b)$$

$$L_1 = \frac{P_a G_1}{\mathcal{D}_2} \quad , \quad \frac{X}{N_1} = \frac{G_1}{\mathcal{D}} = \frac{G_1}{\mathcal{D}_2(1+L_1)(1+L)} = \frac{L_1/P_a}{(1+L_1)(1+L)} \quad . \quad (2.3\text{-}1c)$$

$\doteq L_1/P_a$ in the crucial hf . Hence to minimize $|X/N_1|$ at fixed L , minimize $|L_1|$. But L_1 must cope with the uncertainty in $P_1, P_2, \cdots, P_n$ ignored by L^o . However, if G_2 can cope with $P_2, \cdots, P_n$ then L_1 need only cope with P_1 . L_1 is designed accordingly and denoted by L_1^o to indicate its neglect of $P_2, \cdots, P_n$ uncertainty. So now, P_e^o of (2.2-6) is replaced by

$$P_e^1 \triangleq \frac{P_1 P_{20} \cdots P_{n0} P_b + P_c}{1 + P_{n0} G_n + \cdots + P_{n0} \cdots P_{20} P_1 G_1} = \frac{\lambda_1 P_{a0} P_b + P_c}{\mathcal{D}_{20}(1+\lambda_1 L_{10})} \quad ,$$

$$\lambda_1 \triangleq \frac{P_1}{P_{10}} \qquad (2.3\text{-}2a,b,c)$$

$$\text{with } \mathcal{V}^1 = \mathcal{V}\{P_e^1\} = \left\{ \frac{\lambda_1 a_a k_b + k_c}{1+\lambda_1 L_{10}} \right\}$$

instead of $\mathcal{V}^o = \{a_a k_b + k_c\}$ of (2.2-5a). In (2.3-2) L_{10} is the nominal $L_{10}^o \equiv L_{10}$ (cf $L_0^o \equiv L_0$) and $\mathcal{D}_{20} = \mathcal{D}_2$ at nominal P_{i0} , for $i = 1, \ldots, n$.

L_0 was designed to handle P_e^o with its $\mathcal{V}^o$, but now it must handle P_e^1 with its $\mathcal{V}^1 \supset \mathcal{V}^0$. What are the bounds $B_1(\omega)$ on $L_{10}(j\omega)$ so that the original L_0 remains satisfactory? This question may be answered by simply trying L_{10} values and checking if (2.2-1,2) are satisfied. It is found that the $B_1(\omega)$ are decisively influenced by the intervals I_A , I_B , I_C of L_0 in (2.2-8). The results are stated here and their explanation in Appendix 1, at the end of this chapter. Note the similarity of these bounds to those on the first inner loop in cascade design — Chapter 1, Figure 1-9.

Nature of $B_1(\omega)$ bounds on L_{10} .

(1) For $\omega \in I_A = [0,90]$, $B_1(\omega)$ are upper bounds, i.e., $|L_{10}(j\omega)|$ must be < some value, which is a function of $\text{Arg}L_{10}(j\omega)$ — Figure 2-7a.

(2) For $\omega \in I_B = [90,330]$, $B_1(\omega)$ are lower ones precluding $L_{10} \equiv 0$ (Figure 2-7b).

(3) For $\omega \in I_C = [330,\infty]$, $B_1(\omega)$ in Figure 2-7b are closed curves in the Nichols Chart which tend to a vertical line B_{1H} of length $\left(\frac{b_1}{a_1}\right)$ at $\text{Arg}L_{10} = -\pi$.

Just as in the design of L_0 , so the optimum L_{10} would lie on $B_1(\omega)$ at all ω but is in practive approximated by a rational function — Figures 2-4, 2-7. One may define intervals of L_{10} similar to I_A , I_B , I_C of L_0 , i.e., in Figures 2-4,7: $I_{1A} = [0,\omega_{1x}^-)$; $I_{1B} = [\omega_{1x}^-,\omega_{1x}^+)$; $I_{1C} = [\omega_{1x}^+,\infty)$. Here $I_{1B} \doteq 0$ because B_{1H} has zero width. In practice, one would likely (in addition to (2.2-2), assign bounds in Figure 2-1, on

$$\frac{C_i}{D_i} = \frac{1}{(1+L)(1+L_1)\cdots\ 1+L_n} \qquad (2.3\text{-}3)$$

leading to θ_{mi} values and finite width B_{iH} and larger I_{iB} . Such finite B_{iH} are easily added in Figures 2-7,8, but are omitted here for simplicity.* $L_{10}(j\omega)$ is sketched in Figure 2-7b and is

$$L_{10} = \frac{0.14\,(1+\frac{s}{800})(1+\frac{s}{2000})}{(1+\frac{s}{600})\,[1+\frac{.4}{340}\,s+(\frac{s}{340})^2\,][\,1+\frac{.5s}{2500}\,+(\frac{s}{2500})^2\,]^2}$$

---

* The constraints on the inner loops, due to 2.3-3, are considered in detail in Chapter 3, Section 4.

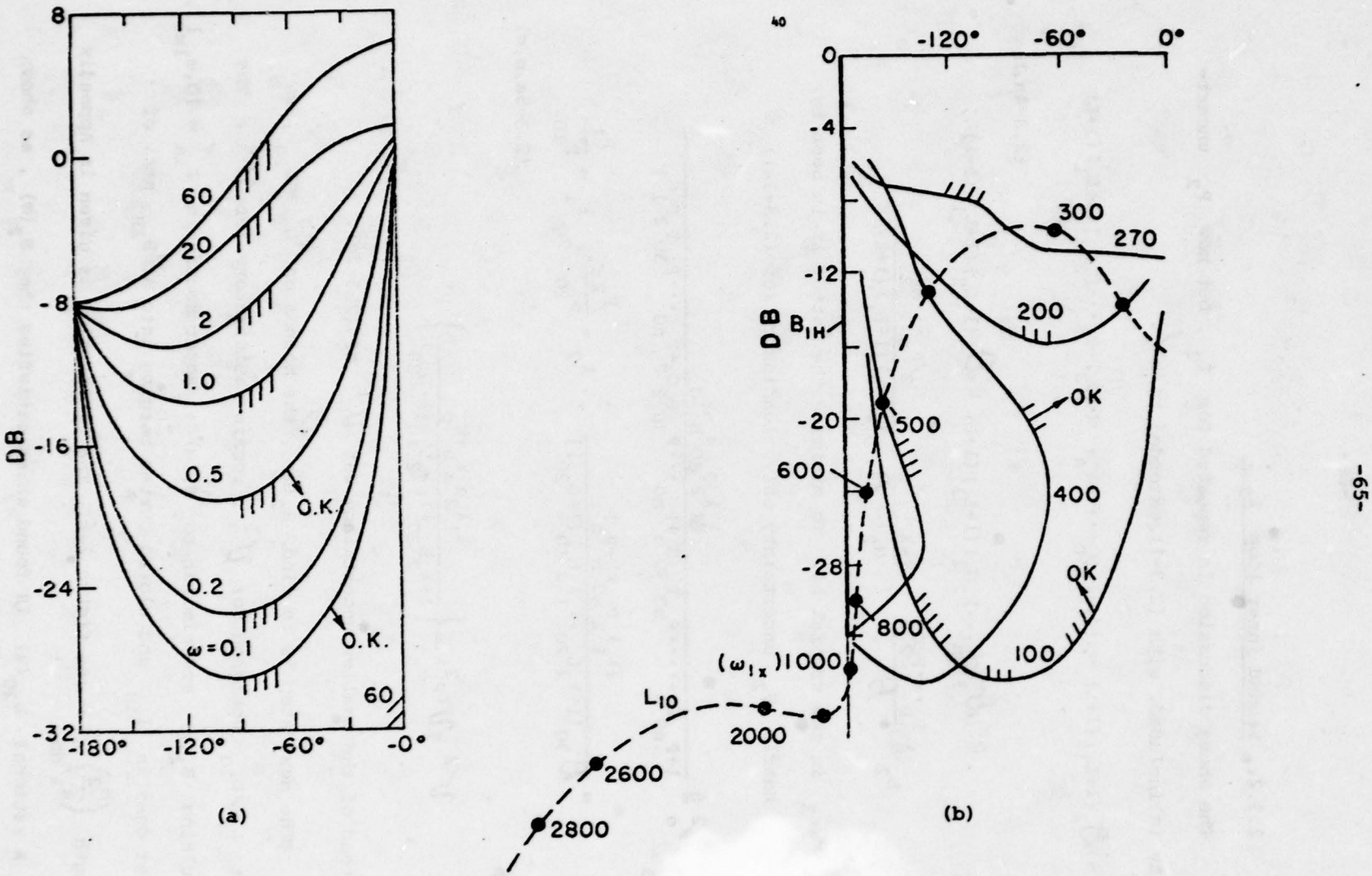

Figure 2-7. Bounds $B_1(\omega)$ on $L_{10}(j\omega)$ — upper bounds in I_A, lower ones in I_B.

2.3.2. Second inner loop L_2 .

The above discussion is repeated for L_2 , but now P_2 uncertainty is included, with (2.3-1) extended to

$$\mathcal{D} = \mathcal{D}_2(1+L_1)(1+L) = [(1+P_nG_n+\cdots+P_n\cdots P_3G_3)+P_n\cdots P_2G_2](1+L_1)(1+L)$$

(2.3-4a,b,c)

$$\triangleq (\mathcal{D}_3+P_n\cdots P_2G_2)(1+L_1)(1+L) \triangleq \mathcal{D}_3(1+L_2)(1+L_1)(1+L) ,$$

$$L_2 \triangleq \frac{P_n\cdots P_2G_2}{\mathcal{D}_3} \quad , \quad \frac{-X}{N_2} = \frac{G_2}{\mathcal{D}} = \frac{L_2/P_n\cdots P_2}{(1+L_2)(1+L_1)(1+L)}$$

$\doteq L_2/P_2P_3$ in the crucial hf. To minimize the latter it is best to let L_2 handle P_2 uncertainty only, leading to (cf (2.3-2a))

$$P_e^2 \triangleq \frac{\lambda_1\lambda_2P_{a0}P_b+P_c}{1+P_{n0}G_n+\cdots+P_{n0}P_{30}G_3+P_{n0}\cdots P_{30}P_2G_2+P_{n0}\cdots P_{30}P_2P_1G_1}$$

$$= \frac{(\lambda_1\lambda_2P_{a0}P_b+P_c)}{\mathcal{D}_{30}[1+\lambda_2L_{20}+\lambda_1\lambda_2L_{10}(1+L_{20})]} \quad , \quad \lambda_2 = \frac{P_2}{P_{20}} \quad , \quad \lambda_1 = \frac{P_1}{P_{10}}$$

(2.3-5a,b,c)

with

$$\mathcal{V}^2 = \mathcal{V}\{P_e^2\} = \left\{\frac{\lambda_1\lambda_2a_ak_b+k_c}{1+\lambda_2L_{20}+\lambda_1\lambda_2L_{10}(1+L_{20})}\right\}$$

instead of the smaller uncertainty set $\mathcal{V}^1$ of (2.3-2c).

The next step is to find $B_2(\omega)$, the bounds on $L_{20}^0 \equiv L_{20}$, so that L_0 , L_{10} designed for $\mathcal{V}^1$, remain satisfactory for $\mathcal{V}^2$. The resulting $B_2(\omega)$ are similar to $B_1(\omega)$: upper bounds in $I_{1A} = [0,\omega_{1x})$, lower ones in I_{1B} and closed curves merging into a B_{2H} etc. of length $\left(\frac{b_2}{a_2}\right)_{db}$ — see Figure 2-8. The explanation is given in Appendix 2. A rational $L_{20}(s)$ is found which satisfies the $B_2(\omega)$, as shown in Figures 2-8, 2-5 with

$$L_{20}(s) = \frac{0.63\left(1+\frac{s}{6000}\right)}{\left[1+\frac{0.6s}{1750}+\left(\frac{s}{1750}\right)^2\right]\left[1+\frac{0.6s}{15000}+\left(\frac{s}{15000}\right)^2\right]^2}$$

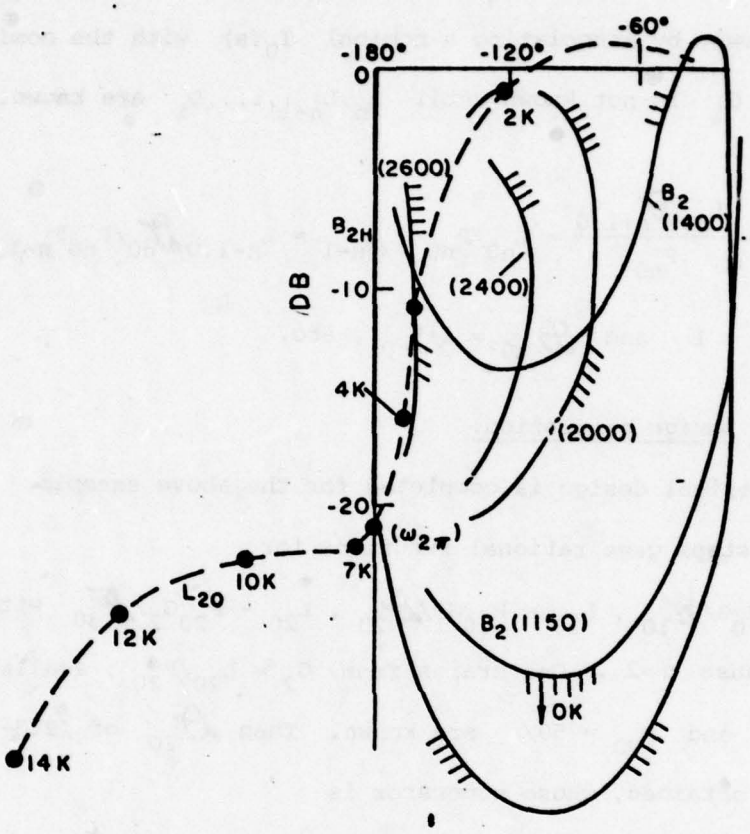

Figure 2-8. Bounds $B_2(\omega)$ on $L_{20}(j\omega)$ — upper in I_{1A}.

2.3.3. Third and higher inner loops.

One can continue indefinitely in this manner. The resulting L_{20} (Figures 2-5,8) has three intervals I_{2A}, I_{2B}, I_{2C} which decisively influence the bounds on a L_{30} designed to handle P_3 uncertainty, etc. The general forms for the $\mathcal{D}_i$, L_i etc. are for $i = 1,\cdots,n$.

$$\mathcal{D}_i = \mathcal{D}_{i+1}(i+L_i) \quad , \quad L_i = \frac{P_n\cdots P_i G_i}{\mathcal{D}_{i+1}}$$

$$\frac{-X}{N_i} = \frac{L_i/P_n\cdots P_i}{(1+L_i)(1+L_{i-1})\cdots(1+L)} \qquad (2.3\text{-}6a\text{-}d)$$

$$P_e^i = \frac{(\lambda_1\lambda_2\cdots\lambda_i P_{a0}P_b+P_c)}{\mathcal{D}_{i+1,0}[1+\lambda_i L_{i0}+\lambda_i\lambda_{i-1}L_{i-1,0}(1+L_{i0})+\cdots+\lambda_i\cdots\lambda_1 L_{10}(1+L_{20})\cdots(1+L_{i0})]}$$

Note that F in Figure 2-1 is available from Equation (2.2-3e) as soon as L_0 is known, by associating a nominal $T_0(s)$ with the nominal $L_0(s)$. But G_i is not known until $L_n, L_{n-1}, \ldots, L_i$ are known. Thus from (2.3-6b)

$$G_n = \frac{L_{n0}\mathcal{D}_{n+1,0}}{P_{n0}} = L_{n0}/P_{n0} \ , \ G_{n-1} = L_{n-1,0}\mathcal{D}_{n0}/P_{n0}P_{n-1,0}$$

with $\mathcal{D}_{n+1,0} = 1$ and $\mathcal{D}_{n0} = 1+L_{n0}$, etc.

2.3.4. Design completion.

The numerical design is completed for the above example. The previous steps gave rational functions for $L_0 = GP_{e0} = P_0G/\mathcal{D}_{10}$, $L_{10} = P_{a0}G_1/\mathcal{D}_{20}$, $L_{20} = P_{20}G_2/\mathcal{D}_{30}$ with $\mathcal{D}_{30} = 1$ because $n=2$. One starts from $G_2 = L_{20}/P_{20}$, available because L_{20} and $P_{20} = 50/s$ are known. Then $\mathcal{D}_{20}$ of (2.3-1a) = $1 + P_{20}G_2$ is obtained, whose numerator is

$$[s^2+1260s+(5.14)10^6][s^2+7860s+(1.90)10^8][s^2+9930s+(2.58)10^8] \ .$$

The denominator is known from that of L_{20}.

The next step is to evaluate $G_1 = L_{10}\mathcal{D}_{20}/P_{a0}$, $L_{10}, \mathcal{D}_{20}$ known and $P_{a0} = 1000/s^2$. This gives $\mathcal{D}_{10} = 1 + P_{20}G_2 + P_{20}P_{10}G_1$, whose numerator is

$$(s+605)[s^2+132s+(1.32)10^5][s^2+1260s+(5.10)10^6][s^2+1200s+(6.05)10^6]$$

$$[s^2+1300s+(6.50)10^6][s^2+7860s+(1.90)10^8][s^2+9930s+(2.58)10^8] \ .$$

Next find $G = L_0\mathcal{D}_{10}/P_0$, with $P_0 = 2000/s^3$. F in Figure 2-1 is obtained precisely as in single-loop design ([H3]). Here it was chosen [with $F(0) = 1$],

$$F(s) = \frac{(1.59)10^5(s+5.05)}{(s^2+289s+103000)(s^2+3.67s+7.80)} \quad .$$

The system was simulated on the digital computer with the results shown in Figures 2-9a,b. Runs with very similar outputs are shown by a single curve labelled S . There is a slight excursion beyond the upper bound in Figure 2-9a for some parameter combinations, and for small t of the lower bound. But this is due to inexact translation of time-domain bounds into equivalent ω-domain bounds, because the ω-domain specifications are all satisfied by the design. The slight violations in Figure 2-9a are not atypical in the experience of the authors. As previously emphasized, such translation is only an art as yet. With a little more effort it is possible to precisely satisfy the time-domain bounds — this has been proven ([H11]). But generally such slight violations are acceptable. The maximum overshoot in the disturbance response in Figure 2-9b, is 25% which is very well correlated with γ of 2.3 db specified, which gives 23.5% overshoot for a second order system. The extent to which the design results fill up the bounds, indicates a design very close to optimum.

2.4 Generality of Structure

In the system considered, input R in Figure 2-1 and $n+1$ plant outputs are available for processing, permitting an infinitude of $n+2$ degree-of-freedom structures. The $n+2$ fundamental system functions are the system transfer function $T(s) = C/R$ and the $n+1$ loops $L, L_1, \cdots, L_n$. In any acceptable structure, L is gotten by cutting the outer loop just after the C sensor, giving in Figure 2-10, $L = PQHH_1H_2\Delta_1$, $\Delta_1 = 1 + P_2H_2 + P_1P_2H_1H_2$. Keeping the first cut

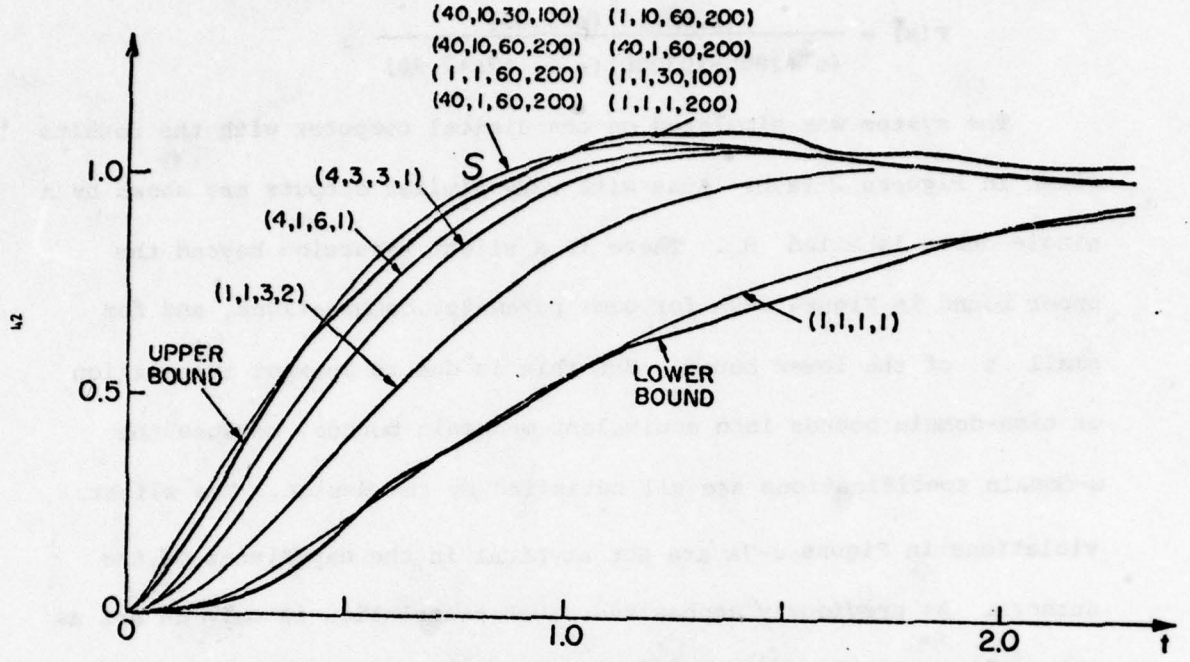

Figure 2-9a. Comparisons of time-response bounds with simulation results.

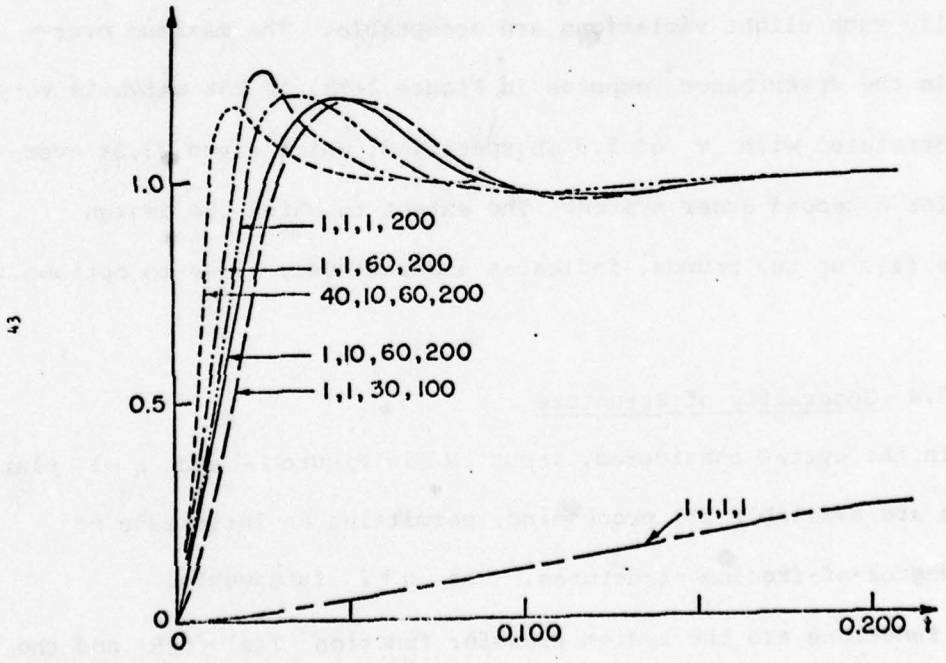

Figure 2-9b. Disturbance response.

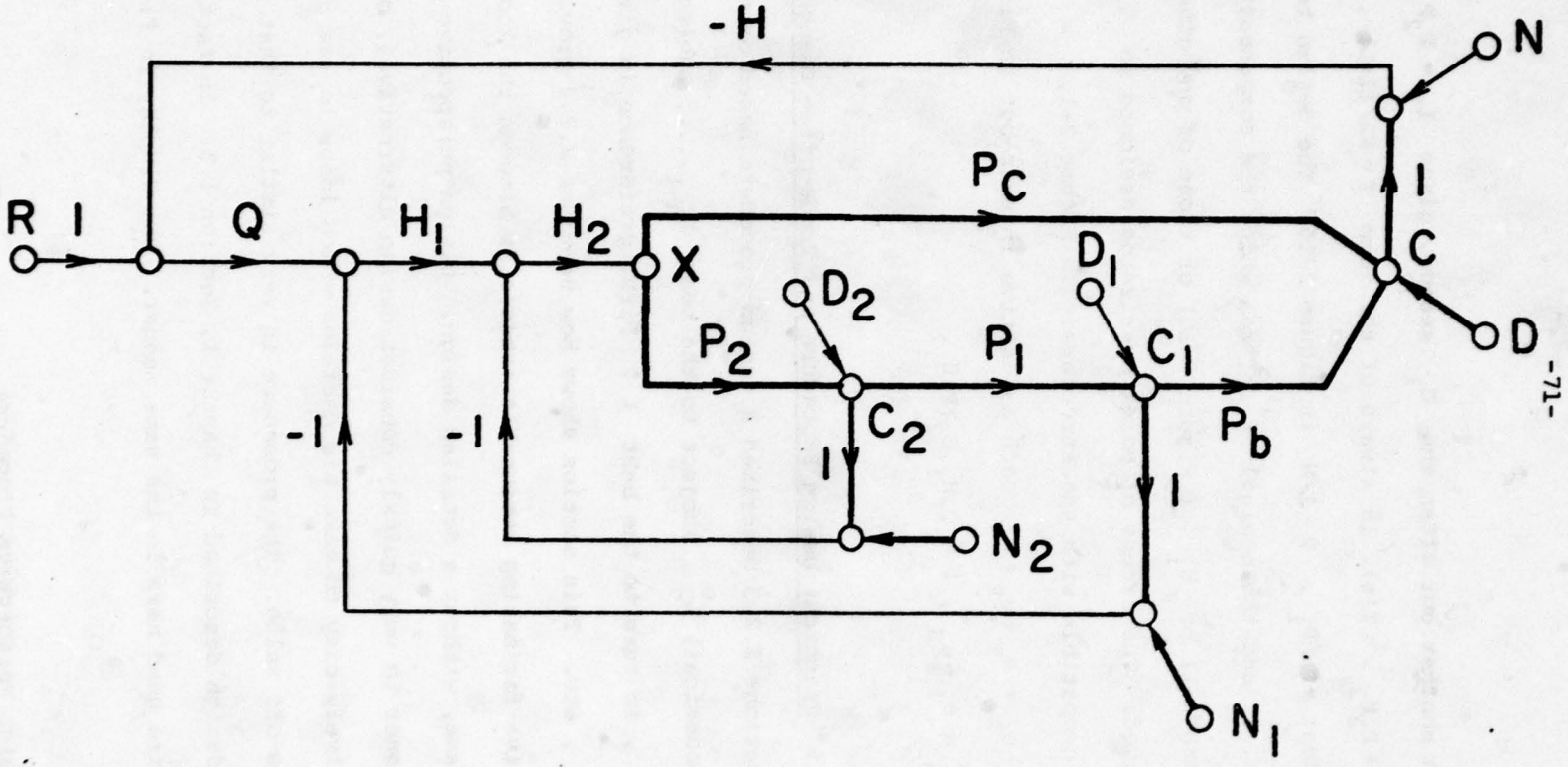

Figure 2-10. Multiple-loop system for n=2 , with a different 4 degree of freedom structure.

$P_a = P_1 P_2$, $P = P_a P_b + P_c$.

and with another cut after the C_1 sensor, gives $L_1 = P_2P_1H_1H_2/\Theta_2$, $\Theta_2 = 1 + P_2H_2$. $T(s)$ is always of the form $T = \psi L/(1+L)$, ψ independent of P_i, $\psi = 1/H$ in Figure 2-10. The design technique provides T and the nominal L_{i0} from which the compensations G_i (of Figure 2-1) or H_i (of Figure 2-10) or those of any other structure are derived. The excess of poles over zeros assigned to $T(s)$, e_T, must be compatible with the structure. In Figure 2-1, $e_T = e_F + e_L = e_F + e_P + e_G$ each a positive integer but in Figure 2-10, $e_L = \Sigma e_i = e_T + e_H$, $i = Q, H_1, H_2, P, H$.

2.5 Practical Design Procedure and Trade-off — Design Perspective

Sections 2.2,3 described a design procedure based on the best (most economical) L_n, subject to the best L_{n-1},..., subject to the best L_1, in turn to the best L. First preference is given to L, then L_1, etc. This section shows how Sections 2.2,3 provide the perspective for making reasonable trade-offs between the loops early in the game, without a detailed design. Design perspective enables the designer to very quickly consider design alternatives, making it comparatively easy to make his decision which loops to use and the α_i trade-off value. The procedure is very similar to that for the cascade design described in Chapter 1, Section 1.5. In fact, Figures 1-24a,b are used here in the same manner. The display in Figure 2-5 is used.

Design Perspective Procedure.

1. The first step is to design the single-loop L_{s0} to hadle the entire uncertainty of P in (2.2-3b). Let α_0 be the overdesign

margin of L_0 , then the outer loop L_0 of a multiple-loop design, is obtained by shifting the UHF characteristic of L_{s0} upward by ϕ_s , the net saving due to the multiple-loop design, here 39.4 db - α_0 ($\alpha_0 = 0$ was used in our example). $\phi_s = 20 \log \left[\frac{\lambda_{1x} a_a b_b + b_c}{a_a b_b + b_c} \right] - \alpha_0$ db — see Figure 2.2-5.

2. Find ω_{m1} (at which L_{10} has its peak value) by placing a transparency of L_{outer} (of Figure 1-24a) over L_0 of Figure 2-5 and noting the arrow.

3. Locate Q_1 (the peak position of L_{10}) at ω_{m1} , with value of M_1 ($\simeq$ -10 db) obtained from Appendix 3 of this chapter. Point Q_1 is $|L_{10}(j\omega_{m1})|$. Draw a horizontal line in Figure 2-5 at Δ_1 magnitude with $\Delta_1 = \min (B_{h1}) - \alpha_1$ ($\simeq$ -36 or -56 db for the example), where $\min (B_{h1})$ is the point of minimum value of B_{h1} . Lay $L_{i0}(IF)$ of Figure 1-24a over Figure 2-5, so that Q coincides with Q_1 . Find the intersection point C_1 (or C_1') of this $L_{i0}(IF)$ with Δ_1 (or Δ_1') horizontal line in Figure 2-5.

4. Pick the $L_{i0}(HF)$ curve in Figure 1-24b, according to the θ_{m1} value being used for L_{10} . Lay $L_{i0}(HF)$ on Figure 2-5, such that C coincides with C_1 (or C_1'). L_{10} consists of $L_{i0}(IF)$ of Figure 1-24a in the intermediate ω range and of $L_{i0}(HF)$ of Figure 1-24b in the high frequency range. Use the pattern of $L_{i0}(HF)$ to the left of C to obtain a smooth continuous curve for L_{10} .

5. Steps 3,4 are repeated in order to determine L_{20} . Use the arrow on $L_{i0}(HF)$ of Figure 1-24b, to locate ω_{m2} . Use (2.A3-6) to obtain M_2 , giving a new point Q_2 in Figure 2-5. Then lay $L_{i0}(IF)$

of Figure 1-24a on Figure 2-5, so that $Q_2 = Q$. A horizontal line of value $\Delta_2 = \text{Min}\ (B_{h2}) - \alpha_2$ ($\simeq$ -22 db in the example) is drawn, etc., where $\text{Min}\ (B_{h2})$ is the point of minimum value of B_{h2} . The entire process is repeated until all the loops are exhausted. The dashed lines in Figure 2-5 are the results of using this perspective technique. They are in excellent agreement with the actual detailed design (solid lines in Figure 2-5) obtained by using the computer to obtain the inner loop bounds, finding a rational $L_{i0}(s)$ to satisfy these bounds, etc.

6. After each L_{i0} is obtained, it is a good idea to sketch the effective P values to use for the sensor noise effect. Thus after L_{s0} is obtained, sketch $|P_0| = |P_{a0}P_{b0} + P_{c0}|$ in Figure 2-5. If there is little sensor noise amplification ($|L_{s0}/P_0|$ not large over a large ω range), there may be no point in using more feedback loops. After L_0 has been obtained, it is easy to see the saving in sensor N noise effect, by using L_1 . Sketch $|P_{a0}|$ to see the hf N_1 sensor noise effect ($\simeq |L_{10}/P_{a0}|$). Similarly $|L_{20}/P_{20}|$, gives the hf N_2 sensor noise effect.

The designer has to decide which sensor points to use and the corresponding α_i trade-off values. Design perspective enables him to try out various designs very quickly and easily, and thus arrive at a suitable trade-off, after which he can proceed with a careful detailed design.

2.5.1. Bandwidth propagation and similarity with the cascade plant structure.

Let the bandwidth $BW(L_i)$ be arbitrarily defined as that at which L_{i0} achieves its final asymptotic slope: ω_{z0} for L_0 , ω_{z1} for

L_{10} , ω_{z2} for L_{20} in Figure 2-5. $BW(L_i)$ increases with i . This phenomenon occurs in precisely the same manner in the cascade-system (Chapter 1, Figure 1-23). The relations between the L_{i0} , the role of b_i/a_i , the sensor noise effects and trade-offs, etc. are very similar in the two structures. However, the values of $|L_{i0}|_{max}$ are different and the derivation is more difficult here. Here, at each new L_i stage, one must use a more complex form of P_e . In the cascade system, the step from i to $i+1$ is identical to that from $i-1$ to i . But the final results are remarkably similar.

In Figure 2-5, $BW(L_{n0}) = \omega_{z2}$ is comparable with $BW(L_{S0})$ at ω_{zs} , a little larger due to the extra few db of gain margin needed per section. Thus, the final cut-off frequency for a single-loop design is comparable to that for a multiple-loop design, but they are associated with different loops so there can be a great improvement in sensor noise effect. Thus, in Figure 2-5, $(Z_2-Z_s)db = -22+89 = 67$ db , while $|P_{20}|_{db} - |P_0|_{db} = 127$ db, an improvement if $|N_2/N| < 127 - 67 = 60$ db. In practice it is reasonable to assume that the plant power levels and with them the sensor noise levels increase in proceeding from input to output. The design procedure is highly transparent permitting a good estimate of the optimum division between the feedback loops, without a detailed design.

2.5.2. <u>High-frequency uncertainty.</u>

Clearly, multiple-loop design can be highly superior to single-loop, for large hf plant uncertainty. The linearized plant model is usually due to linearization of a nonlinear plant about an operating point or trajectory. Large variations can exist due to different

operating points, e.g., in flight control ([O1]) where values > 1000 have been reported.

It has been proven that in a large class of linear and nonlinear time-varying uncertain plants the latter can be represented for synthesis purposes by an equivalent linear time-invariant uncertain plant set $P_{eq}[s]$ ([H1, H11]). The set equivalence is exact with respect to a prescribed acceptable plant output set. Linear time invariant design applied to the $P_{eq}[s]$ problem is guaranteed to work for the original nonlinear problem. A nonlinear plant <u>with no uncertainty</u> can thus generate large hf uncertainty in $P_{eq}[s]$, e.g., consider $y = k^3x^3$, x the input and y the output. Suppose a fairly linear response is desired for $y = A^3(1-e^{-t})^3$, $A \in [0.5,5]$. To find $P_{eq}[s]$, evaluate $\frac{Y(s)}{X(s)} = P_{eq} = \frac{6kA^2}{(s+2)(s+3)}$ in this case. Since $A \in [0.5,5]$, the hf gain of P_{eq} varies by a factor of 100, due to A^2. For a simple dynamic example, consider $\dot{y} + By^{1/3}\text{sgn } y = kx$, giving $P_{eq} = \frac{6kA^3}{(s+3)[BAs+6A^3+2BA]} \to 6kA^2/Bs^2$ at hf, with uncertainty factor of 100.

2.6 Justification of Assumptions

<u>General Plants</u>. This section is devoted to the justification of simplifying assumptions in 2.2,3. One was use of $P_i = k_i/s^{e_i}$ for all ω, not just in hf where it is applicable. Recall in Section 2.2, the first step was to find the smallest $\{P_e^o\}$ of (2.2-6a), by minimizing over $G_1,\cdots,G_n$ and the values of $P_{10},\cdots,P_{n0}$. Suppose $P_j = k_j/(s+q_j)$ with k_j, q_j uncertain. This minimization problem is extremely difficult at medium ω. Fortunately, it makes little

difference if it is not done at all. The reason is that which made the inner loops unnecessary for $\omega < \omega_x$, in cascade design (Section 1.4.4), and in this chapter L_{10} unnecessary in I_A, L_{20} in I_{1A}, etc., i.e., under certain conditions there is little difference in $|L_0 = GP_0|_{min}$ needed, whether $\{P\}$ = set S_1 or set $S_2 << S_1$. In Figure 2-4, suppose that instead of AB (A at X_2), the much larger uncertainty set is ABEFG with E,F extending even to ∞. L_0 at X_2 results in almost the same $\Delta \ell n|T|$ for both (23.85 db instead of 23.5 db).

It is therefore concluded that for $\omega < \omega_x$, $\{P\}$ of (2.2-3b) be used for L_0 design, just as in L_S design. P_e^o is used only for $\omega > \omega_x$ and it is assumed that in this hf range P_j is well approximated by k_j/e^{s_j}. This has been verified for several numerical examples, e.g., for n=1 with $P_a = k_a/(s+q_a)$, $P_b = k_b/s$, $P_c = k_c/s(s+q_c)$, $k_a \in [1,400]$, $k_b \in [1,60]$, $k_c \in [1,200]$, $q_i \in [0,5.2]$, all independently uncertain. The maximum difference in the two $B(\omega)$ is only three db even though the difference between $\{P\}$ and $\{P_e^o\}$ is $\approx$40 db. If this conclusion is incorrect for an unusual case, then it is also likely that the obligation on L_{10} and I_A will be greater too. By using $\{P\}$ in medium ω, one is certain that the obligations on L_{10} in I_A will be negligible, as in Section 2.2. The simple and transparent forecasting of Section 2.5 may then be used. If these indicate less than desired saving in sensor noise effect, then one can return to check if greater saving is possible with P_e^o in I_A.

Another assumption in Section 2.2 was $b_c/a_c > b_b/a_b$. If the opposite is true then minimum Lgth $\{P_e^o\}$ is at $k_a = b_a$ of value $(b_a/b_b+b_c)/(b_a a_b+a_c)$ because $d\left[\frac{k_a b_b + b_c}{k_a a_b + a_c}\right] / dk_a < 0$ as shown in Figure 2-2c. There exist a set of g_i , e.g., $g_2 = \ldots = g_n = 0$, $\frac{a_b}{a_c} \leq g_1 \leq \frac{b_b}{b_c}$, which achieve this and the procedure is precisely the same as before. A third assumption is that $e_a+e_b = e_c$ giving (2.2-4) with $\{P_e\}$ in hf a vertical line in the Nichols chart. Suppose, however, $e_a+e_b = e_c+\psi$, ψ an integer. Then in (2.2-5b), after proper factoring out, b_c is replaced by $b_c(j\omega)^\psi$, a_c is replaced by $a_c(j\omega)^\psi$. The template $\sqrt{}^o$ is no longer a constant, but a function of ω . However, if ψ is even it is still a vertical line, so the simplicity and transparency of the design procedure is retained. The design of the outer loop is only slightly affected. One proceeds precisely as before and obtains the bounds $B(\omega)$ on L_0^o , etc. It is conceivable that $P(j\omega) = 0$ at some discrete finite ω values at some plant parameter combinations, if $\psi = 2$ for example. Of course, this means that over some intervals in the hf region, the two parallel paths are basically working against each other — which is probably unlikely in a well designed plant. But if this is so, the specifications on $T(j\omega)$ and $C/D(j\omega)$ must allow for it. Of course, the modification of b_c , a_c by $(j\omega)^\psi$ persists in the inner loop design considerations (2.3-2c, 2.3-5c, etc.). However, for ψ even, the design transparency is not affected. The arguments given in Appendices 1, 2 are applicable as before, inasmuch as they apply at each ω and are based on the two terms in the numerators of $\sqrt{}^i$ in (2.3-2c, 2.3-5c, etc.) being real. Separate treatment is required for ψ odd as it is a much lengthier problem.

Another assumption was that the disturbance attenuation was a minor problem, dealt with by (2.2-2, 2.3-3). The procedure is basically the same if it is a major problem, for then $C_D = C/D$ must satisfy $|C_D(j\omega)| \leq \gamma(\omega)$ no longer a constant, over $\{P\}$. This can be translated into bounds $B_D(\omega)$ on $L_0(j\omega)$. The more stringent of $B_D(\omega)$ and of $B(\omega)$ due to (2.2-1), is used but thereafter the design procedure is the same.

2.6.1. Unstable and nonminimum-phase plants.

Minimum-phase plants were assumed in Sections 2.2, 2.3 for simplicity. But clearly the design procedure applies so long as the L_{i0} exist which satisfy the $B_i(\omega)$. Consider L_0 first. It must handle $\{P_e^o\}$ giving (Section 2.2) a single-loop problem. The latter is solvable if $\{P_e^o\}$ contains open-loop poles whose range of uncertainty includes part of the right-half as well as the left-half plane [H3, H6]. If however, $\{P_e^o\}$ includes nonminimum-phase elements then L_0 exists only if the performance specifications are compatible with the now limited bandwidth of L_0. The same conclusions apply to the inner loops. Again, right half-plane P_i poles pose no problem, but such zeros impose limitations on L_{i0}.

2.7 Summary

For a class of feedback systems with large uncertainty, a multiple-loop design can result in sensor noise sensitivity much smaller than in a single-loop design satisfying the same specifications. The designer can divide up the feedback burden among the loops in a sensibly optimum manner, wherein the uncertainties of the plant

sections, their levels and associated sensor noise sources play important roles, An important feature of the design techniques is its transparency. In return for learning the mechanics of sensitivity reduction in the language of frequency response, there is gained excellent insight into the trade-offs between loops and the overall cost of design in terms of bandwidth and noise sensitivity — even without performing the detailed design. It is interesting that although the derivation in this chapter is much more difficult than for the cascade system, the results are remarkably similar. This is revealed by the great similarity of the Design Perspective procedure of Section 2.5, to that for the cascade structure, of Chapter 1, Section 1.5.

Chapter 2, Appendix 1 — Bounds $B_1(\omega)$ on First Inner Loop

Section 2.3 presented without explanation the bounds $B_1(\omega)$ in terms of the intervals I_A, I_B, I_C of $L_0(j\omega)$. The explanation is available by considering the uncertainty of variation set (2.3-2c).

$$\mathcal{V}^1 = \left\{ \frac{\lambda_1 a_a k_b + k_c}{1+\lambda_1 L_{10}} \right\} \supset \mathcal{V}^0 = \{a_a k_b + k_c\} \quad \text{of (2.2-5c).}$$

$\mathcal{V}^0$ is the line AB in Figures 2-Ala,b,c, whereas $\mathcal{V}^1$ is the larger set ABC_jD_j, a function of L_{10} and λ_{1max}. The point A is always the nominal L_0, $\lambda_1 = 1$, $k_b = a_b$, $k_c = a_c$ irrespective of the value of L_{10}, because that is the objective of the $B_1(\omega)$. Attention is focused on the range $-\pi < \text{Arg}L_{10} < 0$. The following properties of $\mathcal{V}^1$ are important.

(P1) In Figure 2-Ala, as $|L_{10}|$ is increased at fixed Arg L_{10}, boundaries BC_i, AD_i shift downward — compare BC_3C_3' at 0 db with BC_2C_2' at -20 db and BC_1C_1' at -40 db; and similarly the AD_iD_i'.

(P2) For fixed L_{10}, the effect of increase in λ_1 is extension of the BC_i, AD_i, i.e., widening of the regions by decreasing amounts, to a maximum of

$$\Delta\theta = \left|\theta - \tan^{-1} \frac{m \sin\theta}{1 + m\cos\theta}\right|$$

as $\lambda_{1x} = \infty$, where $L_{10} = m \angle\theta$. This can be seen as follows from Figure 2-Ald.

$$\Delta\theta = \tan^{-1} \frac{\lambda_{1x} m \sin\theta}{1 + \lambda_{1x} m\cos\theta} - \tan^{-1} \frac{m\sin\theta}{1+m\cos\theta}$$

$$\to \theta - \tan^{-1} \frac{m\sin\theta}{1+m\cos\theta}$$

This effect of large λ_1 is important in explaining the nature of $B_2(\omega)$.

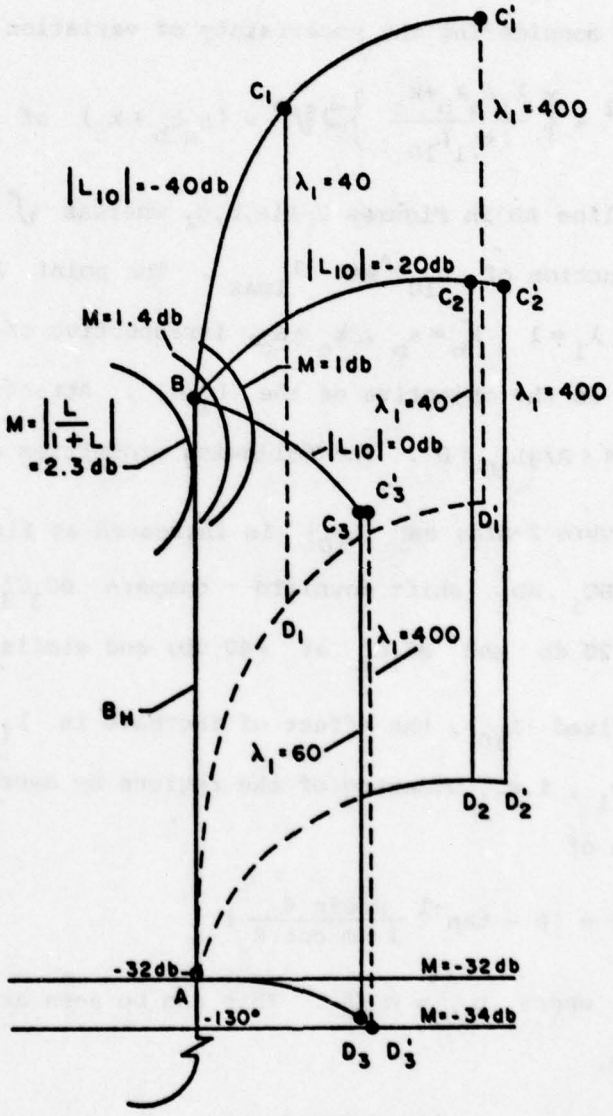

Figure 2-A1a. Explanation of nature of $B_1(\omega)$ in I_A — family of $\sqrt{1}$ at fixed $\text{Arg}L_{10} = -90°$, for various $|L_{10}|$ and λ_1.

(P3) For given λ_{1max} and $|L_{10}|$, $\mathcal{V}^1$ at $\angle L_{10} = \theta$ is the mirror image (about AB) of $\mathcal{V}^1$ at $\angle L_{10} = -\theta$.

The upper bounds of $B_1(\omega)$ in I_A are explained by property (P1) in Figure 2-Ala. A family of $\mathcal{V}^1$ at fixed $\angle L_{10} = -90°$ is tried at $\omega = 40 \in I_A$, i.e., point A of $\mathcal{V}^1$ is set at $L_0(j40) \doteq$ -32 db $\angle -130°$ (from Figure 2-4) at which Figure 2-1 requires

$$\Delta \left| \frac{T_{max}}{T_{min}} \right| \leq 34.3 \text{ db} .$$

At $\omega = 40$ (2.2-1,2) are precisely satisfied. It is seen in Figure 2-Ala that at $\text{Arg}L_{10} = -90°$, $|L_{10}| < -20$ db is OK while $|L_{10}| \geq 0$ db is not because $\Delta|T| = |-34-2.3| = 36.3$ db and larger $|L_{10}|$ gives larger $\Delta|T|$. The upper bound here is between 0 db and -20 db. From a study of the shape of constant $|L/1+L|$ loci on the Nichols chart, it is seen that this result applies for all $\omega \in I_A$ at which $\text{Arg}L_0 \leq -90°$. In Figure 2-4, there is a small interval in which $\text{Arg}L_0 > -90°$ and in general there may be a low frequency region where $\text{Arg}L_0 > -90°$. However, the final result is basically the same, because of the very small sensitivity of the loci of constant $|L/1+L|$ on the Nichols chart at $|L| >> 1$.

It is worth noting that in I_A, if L_{10} did not exist at all, then $\mathcal{V}^i$, $i = 1,\ldots,n$ would only be a much longer vertical line with lowest point at A. From Figure 2-Ala, both (2.2-1) and (2.2-2) would still be satisfied. Thus for $\omega \in I_A$, L_0 designed for P_B, P_C uncertainty only, automatically handles $P_1 \cdots P_n$ uncertainty as well. However, L_1 is needed in I_B, precluding $L_{10} \equiv 0$ in I_A and giving there upper bounds as in Figure 2-Ala. Similarly note that in I_A, $B_1(\omega)$ are

hardly affected by large increase of λ_1 — see Figure 2-Ala. Therefore, L_{10} could handle the entire uncertainty of P_a, i.e., λ_a in place of λ_1 if $G_2 = G_3 = \ldots G_n = 0$.

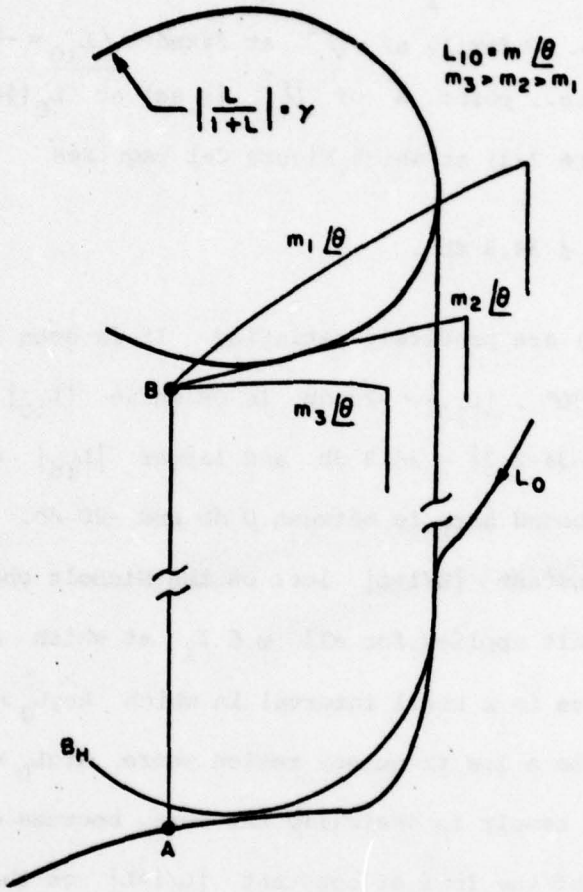

Figure 2-Alb. Explanation of nature $B_1(\omega)$ in I_B — family of $\sqrt{1}$ at fixed $\text{Arg}L_{10} = \theta$.

Property (P1) also explains in Figure 2-Alb the lower bounds in I_B. At $|L_{10}| = m_1$, $\sqrt{1}$ penetrates into $M < 2.3$ db, violating (2.2-2). Thus in Figure 2-Alb, at $\text{Arg}L_{10} = \theta$, $|L_{10}|_{min} = m_2$. In this range, (2.2-2) easily dominates so there is no danger of violating (2.2-1) (cf Figure 2-Ala) except possibly at very large $|L_{10}|$, which

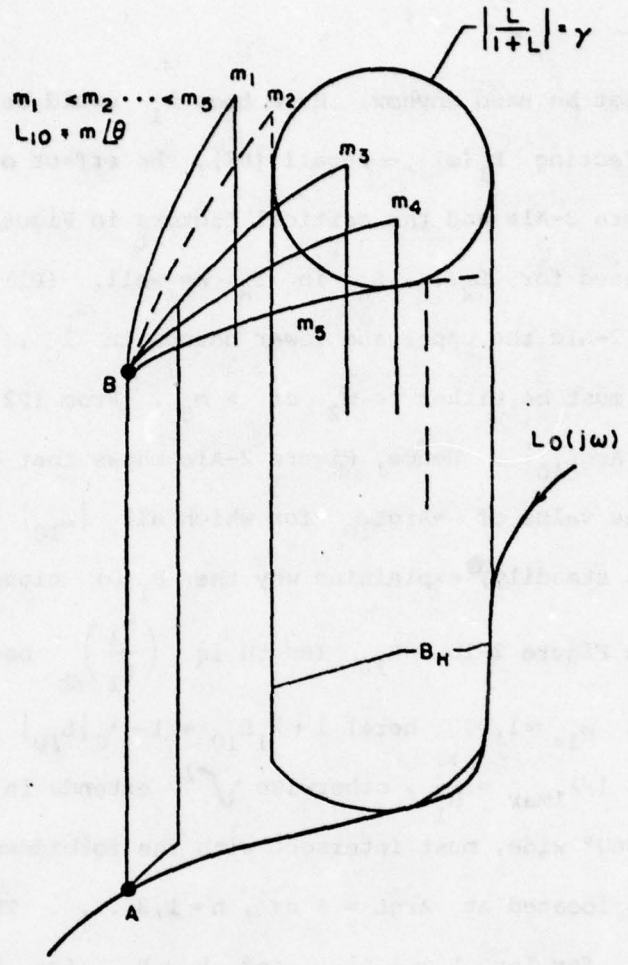

Figure 2-Alc. Explanation of nature of $B_1(\omega)$ in I_C ; At $\text{Arg}L_{10} = \theta$, $m_2 > |L_{10}|_{0k} > m_5$.

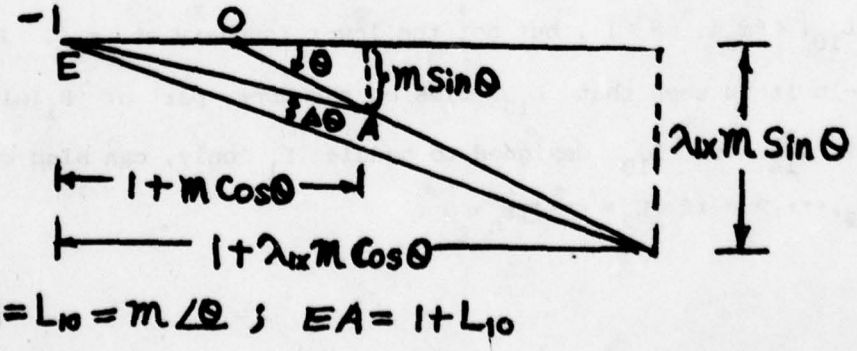

Figure 2-Ald. Derivation of $(\Delta\theta)_{max}$.

would not be used anyhow. Here too, λ_1 could be increased to ∞ without affecting $B_1(\omega)$ — recall (P2), the effect of large λ_1 on $\sqrt{}^1$ in Figure 2-Ala and the critical factors in Figure 2-Alb. Thus there is no need for $L_2,\ldots,L_n$ in I_B as well. (P1) also explains in Figure 2-Alc the upper and lower bounds in I_C. Thus at $\underline{/L_{10}} = \theta$, $|L_{10}|$ must be either $< m_2$ or $> m_5$. From (P2) the width of $\sqrt{}^1$ is $< |\text{Arg}L_{10}|$. Hence, Figure 2-Alc shows that as ω increases in I_C, the value of $-\text{Arg}L_{10}$ for which all $|L_{10}|$ are acceptable, increases steadily, explaining why the $B_1(\omega)$ closed curves shrink to B_{1H} in Figure 2-1b. B_{1H} length is $\left(\frac{b_1}{a_1}\right)_{db}$ because at $\text{Arg}L_{10} = -\pi$ (say at $\omega_{1\pi} \propto 1{,}000$ here) $1 + \lambda_1 L_{10} = 1 - \lambda_1 |L_{10}|$ with $|L_{10}| < 1/\lambda_{1max} = \frac{a_1}{b_1}$, otherwise $\sqrt{}^1$ extends in length to ∞ and being 360° wide, must intersect with the forbidden $\left|\frac{L}{1+L}\right| < \gamma = 2.3$ db regions located at $\text{Arg}L = \pm n\pi$, $n = 1,3,\ldots$. This is also seen from (2.3-3), for let $L_i = \lambda_i L_{i0}$, and $P_\alpha = P_{a0}$ for $a \neq i$. Then at $\text{Arg}L_{i0} = -\pi$, $|L_{i0}| < 1/\lambda_{imax}$ is essential, otherwise $|C_i/D_i|$ is infinite at λ_{imax}.

Increase of λ_1 affects the bounds at m_2, requiring $|L_{10}| < \beta m_2$, $\beta < 1$, but not the lower boundary at m_5. In Figure 2-1b it is seen that L_{10} lies on the upper part of $B_1(\omega)$ for most of I_{1A}, so L_{10} designed to handle P_1 only, can also cope with $P_2,\cdots,P_n$ if $L_2 = \cdots = L_n = 0$.

Chapter 2, Appendix 2 — Bounds on Second and Higher Inner Loops

The function of L_{20} is to guarantee that L_{10} is satisfactory despite its design on the basis of P_e^1 of (2.3-2a). It was seen in Appendix 1 that for $\omega \in I_A, I_B$ and part of I_C, L_{10} suffices, i.e., L_{20} may be zero. This is so only for $\omega < \omega_{x1}$ at which $\angle L_{10} = -\pi$. In this case $\theta_{m1} = 0$, so ω_{x1} is denoted by $\omega_{1\pi}$. It was noted also that $|L_{10}(j\omega_{1\pi})| < \frac{1}{\lambda_{1max}}$, so L_2 is needed for $\omega = \omega_{1\pi}$. Hence, $L_{20} \equiv 0$ is impossible in I_{1A} and it is not surprising that the $B_2(\omega)$ there are upper bounds (recall in Appendix 1 precisely the same situation for $L_{10}(j\omega)$ in I_A). At $\omega = \omega_{1\pi} \in I_{1B}$, $1 + \lambda_{1max} L_{10} = \varepsilon > 0$ (.38 in the example), so the denominator (2.3-5a) of P_e^2 is $\mathcal{D}_{30}(1-\lambda_2+\varepsilon\lambda_2+\varepsilon\lambda_2 L_{20})$, and for it $\neq 0$ at $\text{Arg}L_{20} = 0$, $|L_{20}| > \frac{1-\varepsilon}{\varepsilon} - \frac{1}{\varepsilon\lambda_{2max}} = 1.4$ here. So there is a lower bound on $|L_{20}(j\omega_{1\pi})|$ which is a function of $\text{Arg}L_{20}$.

To find $B_2(\omega)$ in I_{1C} it is necessary to use P_e^2 of (2.3-5a) in place of P_e^1 of (2.3-2a). It is convenient, however, to express P_e^2 in terms of P_e^{1*}, defined as P_e^1 with $\lambda_1\lambda_2$ replacing λ_1, because $\mathcal{V}\{P_e^2\}$ is easier expressed in terms of $\mathcal{V}\{P_e^{1*}\}$, while $\mathcal{V}\{P_e^{1*}\}$ is easily gotten from $\mathcal{V}\{P_e^1\}$ shown in Figure 2-Ala by letting $\lambda_1 > \lambda_{1max}$. From (2.3-5a) and replacing λ_1 in (2.3-2a) by $\lambda_1\lambda_2$,

$$\frac{P_e^2}{P_e^{1*}} = \frac{(1+\lambda_1\lambda_2 L_{10})}{\left(\frac{1+\lambda_2 L_{20}}{1+L_{20}}\right) + \lambda_1\lambda_2 L_{10}} = \frac{OV}{OC_i} \qquad (2.A2\text{-}1)$$

in Figure 2-A2, as follows. Let $OQ = \lambda_1\lambda_2 L_{10}$ ($\text{Arg}L_{10} < -\pi$ in I_{B1}, I_{C1}), $QV = 1$, $QD_i = a$, $|D_iV| = |aL_{20}|$, $\text{Arg}E_iD_iV = \text{Arg}E_iD_iC_i = \text{Arg}L_{20}$,

$D_iC_i = \lambda_2 D_iV = \lambda_2 aL_{20}$, so $0V = 0Q + QV = \lambda_1\lambda_2 L_{10} + 1$,

$$QC_i = \frac{QC_i}{1} = \frac{QC_i + D_iC_i}{QD_i + D_iV} = \frac{a + a\lambda_2 L_{20}}{a + aL_{20}} = \frac{1 + \lambda_2 L_{20}}{1 + L_{20}} \quad \text{and}$$

$$0C_i = 0Q + QC_i = \lambda_1\lambda_2 L_{10} + \frac{1 + \lambda_2 L_{20}}{1 + L_{20}} \quad , \text{ giving (2.A2-1).}$$

Figure 2-A2 was sketched for $\omega = 2000$, $\lambda_1 = 40$, $\lambda_2 = 10$, at which (Figure 2-7b) $L_{10} = .0158\ \underline{/-230°}$, $L_0 = -127$ db $\underline{/-430°}$, for assumed $\text{Arg}L_{20} = -117°$ constant. The D_i describe an arc of a circle as $|L_{20}|$ is varied, as do the C_i drawn for $\lambda_2 = 10 = \lambda_2 \text{max}$, i.e., $D_iC_i = 10\ D_iV$. Clearly for $|L_{20}| << 1$, $0V/0C \to 1$ and for $|L_{20}| >> 1$, $|0V/0C| < 1$, so such $|L_{20}|$ are acceptable. Obviously $\exists\ \lambda_2 < \lambda_{2\text{max}}$, $\exists$ resulting C_i circle passes through 0, giving infinite $0V/0C_i$ and the resulting $\mathcal{U}\{P_e^2\}$ passes through $M = 2.3$ db. Thus, $\exists$ upper and lower bounds in this ω range. As ω increases, $|L_{10}|$ and its angle decrease, so the arc $C_iC_j\cdots$ does not extend to 0 in Figure 2-A2 and any $|L_{20}|$ is acceptable. Hence, the $B_2(\omega)$ tend to a line B_{2H} at $-\pi$, from 0 to $(a_2/b_2)_{db}$. $B_2(\omega)$ are shown in Figure 2-8, including a sensibly optimum $L_{20}(j\omega)$ with its intervals I_{2A} , I_{2B} , I_{2C} .

For the third inner loop (if $n > 2$), P_e^3 is needed and there is an analogous situation with respect to I_{2A} . At I_{2B} , $\omega_{2\pi}$ (at which $\text{Arg}L_{20} = -\pi$) is very large (~ 6500) and as before, there is a lower bound on L_{30} at $\omega_{2\pi}$. For $\omega \gtrsim \omega_{2\pi}$, $|L_0|$, $|L_{10}| << 1$, so in (2.3-6d), Denom. $(P_e^3) = 1 + \lambda_3 L_{30} + \lambda_3\lambda_2 L_{20}(1 + L_{30})$, similar to Denom. (P_e^2) if i is replaced by $i - 1$. P_e^3/P_e^{2*} similar to (2.A2-1) is

AD-A072 644 COLORADO UNIV BOULDER DEPT OF ELECTRICAL ENGINEERING F/G 13/8
QUANTITATIVE SYNTHESIS OF MULTIPLE LOOP FEEDBACK SYSTEMS WITH L--ETC(U)
JUN 79 T WANG, I HOROWITZ AFOSR-76-2946
UNCLASSIFIED AFOSR-TR-79-0880 NL

2 OF 3
AD A072644

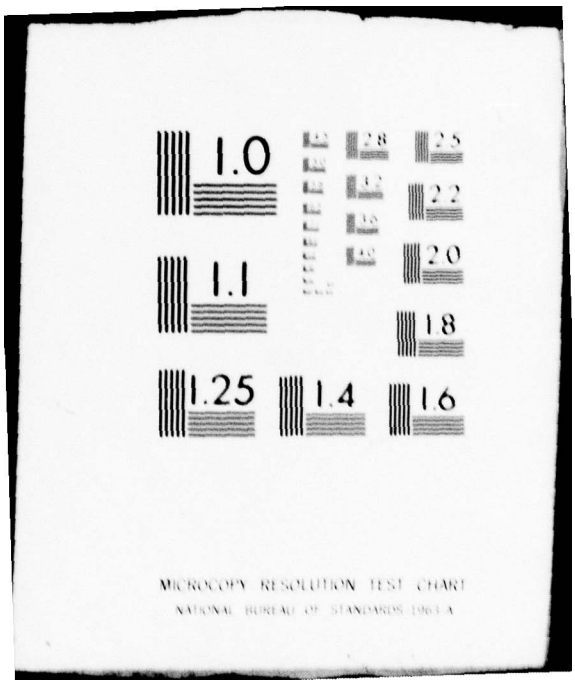
1.0
1.1
1.25
1.4
1.6
2.8
2.5
2.2
2.0
1.8
MICROCOPY RESOLUTION TEST CHART
NATIONAL BUREAU OF STANDARDS 1963-A

obtained giving a figure similar to Figure 2-A2 and analogous $B_3(\omega)$. The process is continued to $B_4(\omega),\ldots,B_n(\omega)$.

Case $\theta_{mi} \neq 0$.

The above is all based on $\theta_{mi} = 0$, $i \geq 1$. For then $\omega_{xi} = \omega_{i\pi}$. But if $\theta_{mi} \neq 0$, there are demands on L_{i0} for $\omega > \omega_{x,i-1}$.

For $\omega > \omega_{x1}$, the constraint on L_{20} is that due to $\lambda_2 \in [1,\lambda_{2x}]$, the outer loop does not cross the γ_0 locus. Or, alternatively, the inner loop does not cross the γ_1 locus. For $\theta_{m1} = 0$, the γ_1 locus is merely the single point -1. From Equation (2.3-1b)

$$L_1 = \frac{P_1 P_2 G_1}{1 + P_2 G_2} \qquad \text{(case } n=2\text{)}$$

$$= \frac{P_1 G_1 L_2}{G_2 (1 + L_2)} \quad ,$$

which is of the same form as in the cascade problem. Therefore, the constraint on L_2 here is similar to that on L_2 in the cascade case. The formula for the peak value of $|L_2|$, i.e. $|L_2(j\omega_{m2})|$ used in Design Perspective is that used in the cascade problem (Figure 1-2.2). This is so for the other inner loops also.

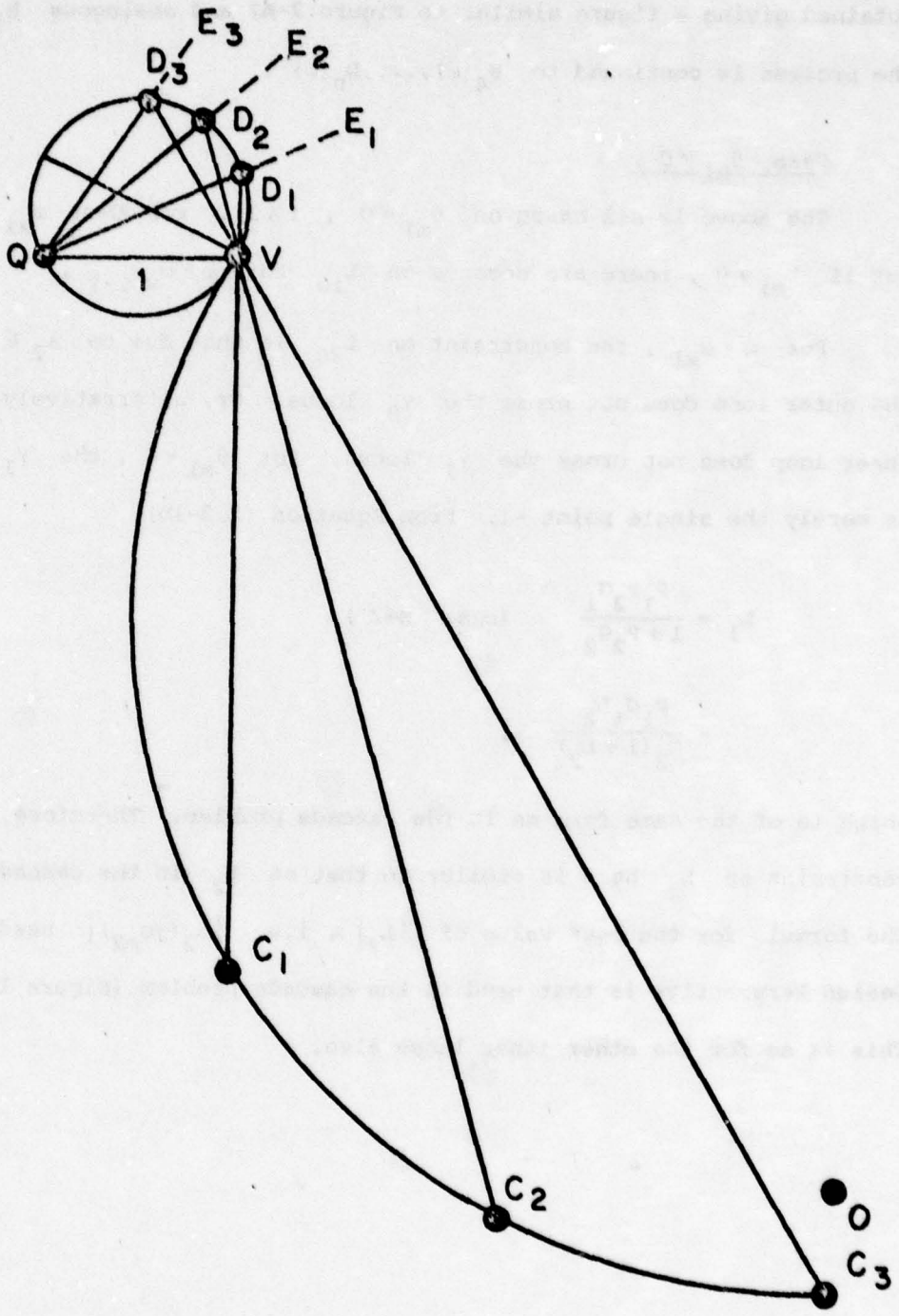

Figure A2. Explanation of nature of $B_2(\omega)$ in I_{1C}.

Chapter 2, Appendix 3 — Estimates of the Peak Values of the Inner Loops

2.A3-1 — The first inner loop L_{10}.

In Figure 2-A3a, the frequency ω_{m1} is approximately at point A with $\angle L_0(\omega_{m1}) \simeq -225°$, also $\text{Arg}L_{10}(j\omega_{m1}) \approx -90°$, and the bound on $L_{10}(j\omega_{m1})$ corresponds to the template tangent to the γ locus, say at point E. BEC is the locus of point B at $k_b = b_b$, $k_c = b_c$, due to the uncertainty of $\lambda_1 \in [1, \lambda_{1x}]$. The difference between any point on BEC and point B can be written, from (2.3-2c), as

$$\left(\frac{\lambda_1 a_a b_b + b_c}{1 + \lambda_1 L_{10}}\right) \Big/ \left(\frac{a_a b_b + b_c}{1 + L_{10}}\right) \triangleq f(\lambda_1) \quad . \tag{2.A3-1}$$

Let $\lambda_1 = \lambda_1^*$ at point E, the vertical difference between E and B is $|f(\lambda_1^*)| = (\alpha_0 + \beta_0)$ db. Both λ_1^* and L_{10} are not known, but we have found that using $\lambda_1^* = \lambda_{1x}$ partly offsets neglect of β_0. With these approximations, Equation (2.A3-1) can be solved for $|L_{10}(\omega_{m1})|$, giving (for α_0 in db),

$$\left(\frac{\lambda_{1x} a_a b_b + b_c}{a_a b_b + b_c}\right)^2 \cdot \frac{1 + |L_{10}|^2}{1 + \lambda_{1x}^2 |L_{10}|^2} = \delta_{\alpha_0}^2 \triangleq \left[10^{(\alpha_0/20)}\right]^2 \tag{2.A3-2}$$

Define $\delta_s \triangleq \dfrac{\lambda_{1x} a_a b_b + b_c}{a_a b_b + b_c}$ and $\delta_{\alpha s} \triangleq \delta_\alpha / \delta_s$, then Equation (2.A3-2) becomes

$$M_1 \triangleq |L_{10}(\omega_{m1})| = \sqrt{\frac{1 - (\delta_{\alpha s})^2}{(\delta_{\alpha s} \lambda_{1x})^2 - 1}} \quad . \tag{2.A3-3}$$

Due to the shapes of the inner loops (see Figures 2-7b,c), it is found that better results are achieved by adding a few db (e.g. 1.5 db) to

the value obtained from (2.A3-3). In the design example of Section 2.2.1, $\lambda_{1x} = 40$, $\delta_{\alpha 0} = 1$, $\delta_s = 10$, gives $\delta_{\alpha s} = 0.1$ and $|L_{10}(\omega_{m1})| = 0.26$. Adding 1.5 db, gives $|L_{10}(\omega_{m1})| \simeq$ 20 log (0.26) + 1.5 $\simeq$ -10 db . The above calculation was used to find $|L_{10}(j\omega_{m1})|$ in the design perspective sketches of Figure 2-5.

2.A3-2 — Second and higher inner loops.

The case $\theta_{m1} = 0$ is considered here ($\theta_{m1} \neq 0$ was treated in Appendix 2). The peak value of $|L_{20}|$ occurs at $\omega \triangleq \omega_{m2}$ at which we have found approximately $\angle L_{10} \simeq -225°$. The constraining condition is that the template of the outer loop (due to $\lambda_i \in [1, \lambda_{ix}]$, $i = 1,2$) does not cross the locus of γ .

The nominal $L_0(j\omega_{m2})$ is at point A_1 on Figure 2-A3a, which is so far down that the determining condition essentially is that the denominator of $L_0(\lambda_1, \lambda_2) \neq 0$. This condition can be written (see 2.3-5a)

$$(1 + \lambda_2 L_{20}) + (\lambda_1 \lambda_2 L_{10}) \cdot (1 + L_{20}) \neq 0 \quad . \tag{2.A3-4}$$

At $\omega = \omega_{m2}$, the nominal $|L_{10}| \simeq -(\lambda_{1x} + \alpha_1 + \beta_1)$db (see Figure 2-A3b) where α_1 db is the overdesign margin of L_{10} , so (we drop β_1 for the same reason β_0 was dropped previously) $\lambda_{1x} L_{10} = -(\alpha_1)$db $\angle -225°$, $\delta_{\alpha 1} \triangleq 10^{(\alpha_1/20)}$, and (2.A3-4) becomes

$$L_{20} \neq -\left\{ \frac{(\sqrt{2}\, \delta_{\alpha 1}/\lambda_2 - 1) + j1}{(\sqrt{2}\, \delta_{\alpha 1} - 1) + j1} \right\}$$

with $\neq$ replaced by $=$ the limiting case, giving

$$|L_{20}(\omega_{m2})| = \sqrt{\frac{(\sqrt{2}\, \delta_{\alpha 1}/\lambda_0 - 1)^2 + 1}{(\sqrt{2}\, \delta_{\alpha 1} - 1)^2 + 1}} \quad . \tag{2.A3-5}$$

Since $\frac{d|L_{20}|^2}{d\lambda_2} \geq 0$, we use $\lambda_2 = \lambda_{2x}$, giving

$$M_2 \triangleq |L_2(\omega_{m2})| = \sqrt{\frac{(\sqrt{2}\,\delta_{\alpha 1}/\lambda_{2x} - 1)^2 + 1}{(\sqrt{2}\,\delta_{\alpha 1} - 1)^2 + 1}} \quad . \qquad (2.A3\text{-}6)$$

In the example of Section 2.2.1, $\lambda_{2x} = 10$, $\alpha_1 = 2$ db $(\delta_{\alpha 1} = 1.26)$, $M_2 \simeq 0.18$ db , used in the design perspective in Figure 2-5.

For $n = 3$, the first part of the previous is the same, but the denominator of $L(\lambda_1,\lambda_2,\lambda_3)$ is now (from Equation 2.3-6d)

$$1 + \lambda_3 L_{30} + \lambda_3\lambda_2 L_{20}(1 + L_{30}) + \lambda_3\lambda_2\lambda_1 L_{10}(1 + L_{20})(1 + L_{30}) \quad .$$

However, at ω_{m3} , $\lambda_{1x}|L_{10}| << |L_{20}|, |L_{30}|$, so the above is closely

$$1 + \lambda_3 L_{30} + \lambda_3\lambda_2 L_{20}(1 + L_{30}) \quad ,$$

which is the same as (2.A3-4) if L_i is replaced by L_{i+1} , for $i = 1,2$. Hence, in (2.A3-6) replace i by $i+1$ for $i = 1,2$, giving

$$M_3 = \sqrt{\frac{(\sqrt{2}\,\delta_{\alpha 2}/\lambda_{3x} - 1)^2 + 1}{(\sqrt{2}\,\delta_{\alpha 2} - 1)^2 + 1}} \qquad (2.A3\text{-}7)$$

and in general

$$M_{i+1} = \sqrt{\frac{(\sqrt{2}\,\delta_{\alpha i}/\lambda_{i+1,x} - 1)^2 + 1}{(\sqrt{2}\,\delta_{\alpha i} - 1)^2 + 1}} \quad \text{for } i \geq 2 \quad ,$$

where $\delta_{\alpha i}$ is the overdesign margin of L_i in arithmetic value.

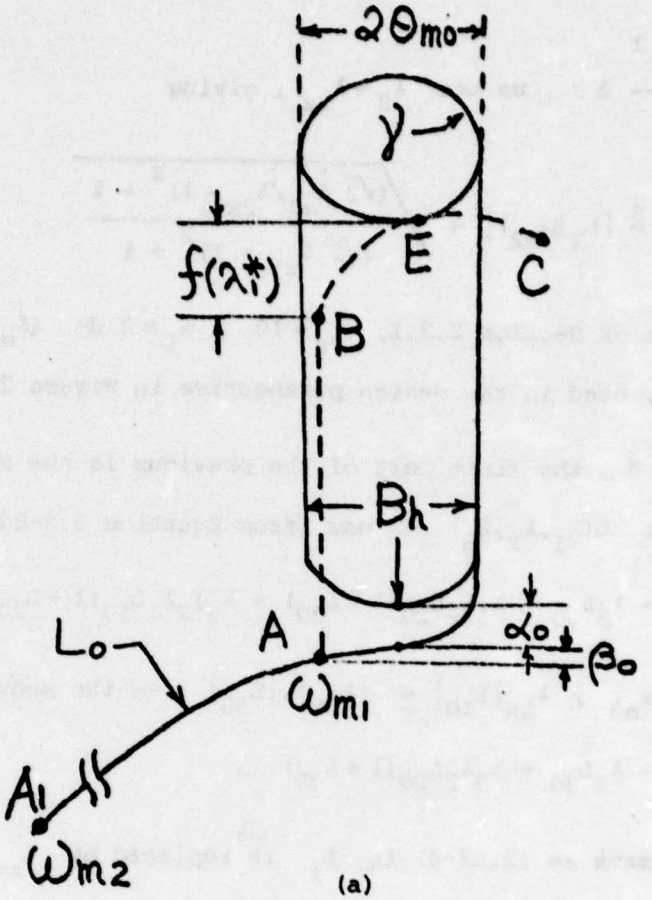

(a)

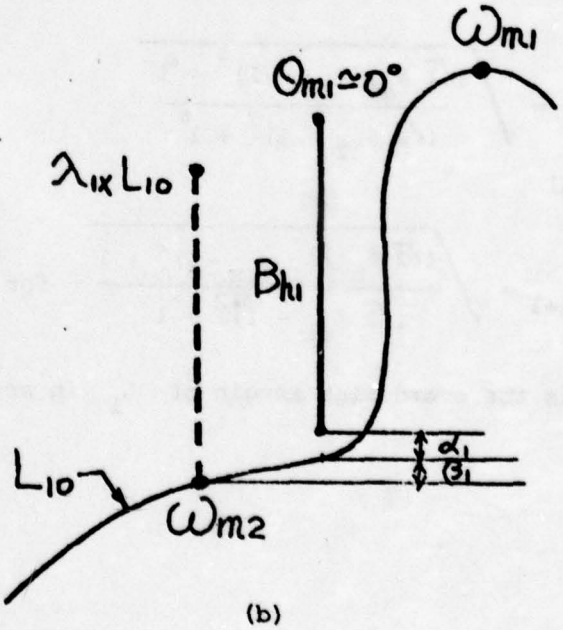

(b)

Figure 2-A3. Explanations for estimating the peak values of the inner loops.

CHAPTER 3

THE TRIANGULAR MULTIPLE-LOOP PLANT

3.1 Introduction

This chapter extends quantitative synthesis to the plant structure of Figure 3-1, denoted as the "triangular multiple-loop plant", again with no "plant modification" (Section 1.3.3). This plant can be considered as one form of generalization of the cascade-parallel plant of Figure 2-1, in which the cascade branch has only two sections. Chapter 5 presents another generalization. It is not surprising that quantitative synthesis for Figure 3-1 contains elements of cascade synthesis (Chapter 1) and of cascade-parallel synthesis (Chapter 2). The objectives are, as before, to satisfy specifications of the form (2.2-1,2), with minimum net sensor noise effects at the plant input. And, as before, "design perspective" is sought which permits the designer, with relatively little effort, to see the important trade-offs and enables him to decide which of the available sensing points to use.

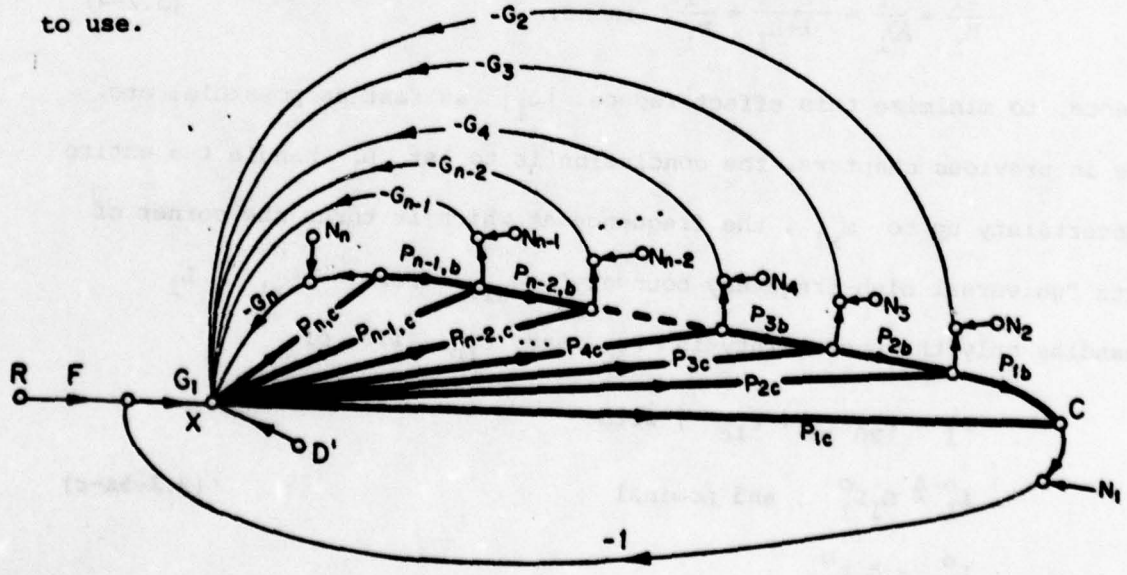

Figure 3-1. Triangular system structure of multiple-loop plant.

The following notation is used:

$$P_n = P_{nc} \quad , \quad P_{n-1} = P_n P_{n-1,b} + P_{n-1,c} \quad ,$$

$$P_{n-2} = P_{n-1} P_{n-2,b} + P_{n-2,c} \quad , \quad P_{n-3} = P_{n-2} P_{n-3,b} + P_{n-3,c}$$

$$\ldots \quad P_3 = P_4 P_{3b} + P_{3c} \quad , \quad P_2 = P_3 P_{2b} + P_{2c} \qquad (3.1\text{-}1a\text{-}c)$$

$$P_1 = P_2 P_{1b} + P_{1c} \quad .$$

3.2 Design of the Outer Loop

In Figure 3-1, with the notation of 3.1-1, the system transfer function is

$$\frac{C}{R} = T = F \frac{P_1 G_1}{\Omega_1} = F \frac{L_1}{1+L_1} \quad , \text{ where} \qquad (3.2\text{-}1)$$

$$\Omega_1 \triangleq (1 + P_n G_n + P_{n-1} G_{n-1} + \ldots + P_3 G_3 + P_2 G_2) + P_1 G_1 \triangleq$$

$$\Omega_2 + P_1 G_1 \qquad (3.2\text{-}2)$$

$$L_1 = P_1 G_1 \Omega_2 \quad . \qquad (3.2\text{-}3)$$

The effect of sensor noise N_1 at the plant input X, is

$$\frac{-X}{N_1} = \frac{G_1}{\Omega_1} = \frac{L_1/P_1}{1+L_1} \doteq \frac{L_1}{P_1} \quad \text{in hf.} \qquad (3.2\text{-}4)$$

Hence, to minimize this effect reduce $|L_1|$ as fast as possible, etc. As in previous chapters, the conclusion is to let L_1 handle the entire uncertainty up to ω_{x1}, the frequency at which it turns the corner of its "universal high-frequency boundary" B_{h1}. For $\omega > \omega_{x1}$, L_1 handles only the uncertainty in P_{1c} and P_{1b}, i.e. of

$$P_1^o = P_{20} P_{1b} + P_{1c} \quad , \text{ with}$$

$$L_1^o \triangleq G_1 P_1^o \quad , \text{ and nominal} \qquad (3.2\text{-}5a\text{-}c)$$

$$L_{10}^o = G_1 P_{10}^o \quad .$$

Note the similarity of this notation to that in Chapter 2 (Equations 2.2-6a,b).

P_2 here replaces $P_a = P_1P_2\ldots P_n$ of Figure 2-1. It is again assumed that in $\omega > \omega_{x1}$, each P_{ij} is closely equal to its hf asymptote $k_{ij}/s^{e_{ij}}$. The value of k_2 ($P_2 \to k_2/s^{e_2}$) to be used as nominal in order to minimize the template of P_1^o, and the resulting requirement on G_1, are deduced exactly as in Chapter 2, Section 2, so the discussion is not repeated here. Thus, the design of the outer loop L_{10}^o is exactly as in Chapter 2, if P_a there is replaced by P_2 here.

3.3 Design of First Inner Loop L_2

The obvious step now is to allow for the uncertainty in P_{2b}, P_{2c} to be handled by the loop via G_2. For this purpose, let

$$P_2^o = P_{30}P_{2b} + P_{2c} \triangleq \lambda_2^1(P_{30}P_{2b0} + P_{2c0}) = \lambda_2^1 P_{20} \qquad (3.3\text{-}1)$$

$$L_1^1 = \frac{(P_2^oP_{1b} + P_{1c})G_1}{(1 + P_{n0}G_n + \ldots + P_{30}G_3) + P_2^oG_2} = \frac{(\lambda_2^1P_{20}P_{1b} + P_{1c})G_1}{\Omega_{30} + \lambda_2^1P_{20}G_2}$$

$$= \frac{(\lambda_2^1P_{20}P_{1b} + P_{1c})G_1}{\Omega_{30}(1 + \lambda_2^1L_{20})} \quad , \quad L_{20} = \frac{P_{20}G_2}{\Omega_{30}} \qquad (3.3\text{-}2a\text{-}c)$$

with $$\Omega_{30} = 1 + P_{n0}G_n + \ldots + P_{30}G_3 \quad . \qquad (3.3\text{-}4)$$

Equation (3.3-2c) should be compared with (2.3-2b). Except for the slight difference in notation, the problems are identical. L_{10}^o was designed to handle uncertainties of P_{1b}, P_{1c} only (in Chapter 2 P_b, P_c only), but L_{10}^1 must handle the uncertainty of

$$P_1^1 \triangleq \frac{\lambda_2^1P_{20}P_{1b} + P_{1c}}{\Omega_{30}(1 + \lambda_2^1L_{20})} \quad , \qquad (3.3\text{-}5)$$

which is analogous to P_c^1 of (2.3-2), with L_{20} here analogous to L_{10} of (2.3-2), λ_2^1 here to λ_1 there. The design procedure for L_{20} (first inner loop here) is therefore identical to that of the first inner loop in Chapter 2 (denoted there by L_{10}), and requires no further discussion.

3.4 The Two Constraints on Second Inner Loop

At this point, we distinguish between two cases. The first is that treated in Chapter 2, where the only specifications are those in (2.2-1,2). There are none on X/D^1 of (2.3-3), and therefore no phase margins in the universal hf bounds B_{hi}. In this case, the latter are vertical lines in Figures 2-7b,8. The inner loop designs in Chapter 2 were all done on this basis. In the second case, there is also the specification (2.3-3) and similarly in Figure 3-1, on

$$\frac{X}{D^1} = \frac{1}{(1+L_1)(1+L_2)\ldots(1+L_n)} \qquad (3.4\text{-}1)$$

with $L_2, L_3, \ldots L_n$ defined later.

Due to the bandwidth propagation effect, the peak of each $|1+L_i|^{-1}$ occurs in a different ω range, so each factor can be considered separately. A maximum γ_i (analogous to γ of 2.2-2) is assigned to each $\left|\frac{L_i}{1+L_i}\right|$, which is reflected by a phase-margin θ_{mi} analogous to θ_m of the outer loop in Chapter 2, and a finite width B_{hi}. The specifications on each can be different, because larger peak values may be tolerable at higher frequencies. In this second case, when designing L_3, one must take care that both the B_{h1} of L_1 and B_{h2} of L_2 are not violated. The latter constraint dominates.

Similarly, when designing any L_j one must consider the B_{hi} of L_i for $i = 1,2,3,\ldots,j-1$. The last constraint (on L_{j-1}) dominates.

The reason for the above domination is demonstrated for the cascade-parallel problem of Chapter 2, by means of Figure 3-2, where the values of the ω_{xi} , ω_{mi} relative to the $B_{h,i-1}$ are shown. The obligations on the second inner loop (of Chapter 2) L_2 due to the outer loop L begin at ω_{x1} . But $|L_{10}(j\omega_{x1})|$ is very small (e.g. in Chapter 2, Figure 2-7b, $\omega_{x1} \approx 1000$), with ω_{x1} located a good ways down the hf asymptote of L_0 . The only danger to L (due to L_2) is that $1+L \doteq 0$. The resulting bound on L_{20} in the Nichols chart is the vertical line at $-180°$ from 0 db to $-(\lambda_{2x})$ in db . The limitation at ω_{x1} imposed on L_2 (due to B_{h1}) is much more serious as it is similar to the one imposed at ω_x (of the outer loop) in a cascade design, on the first inner loop, due to the bound B_h on the outer loop. This is seen as follows.

From (2.3-1c) when uncertainty in both P_1 and P_2 is considered, the first inner loop is

$$L_1 = \frac{P_a G_1}{\Delta_2} = \frac{P_{n0}\cdots P_{30}P_2P_1G_1}{1 + P_{n0}G_n + \ldots + P_{n0}\cdots P_{30}G_3 + P_{n0}\cdots P_{30}P_2G_2}$$

$$= \frac{P_{n0}\cdots P_{30}P_2P_1G_1}{(1 + P_{n0}G_n + \ldots + P_{n0}\cdots P_{30}G_3)\left[1 + \dfrac{P_{n0}\cdots P_{30}P_2G_2}{1 + P_{n0}G_n + \ldots + P_{n0}\cdots P_{30}G_3}\right]}$$

$$\triangleq \frac{L_2P_1G_1}{G_2(1+L_2)} \quad . \tag{3.4-2}$$

Consider a cascade design of 2 sections in Figure 3-3. The outer loop is

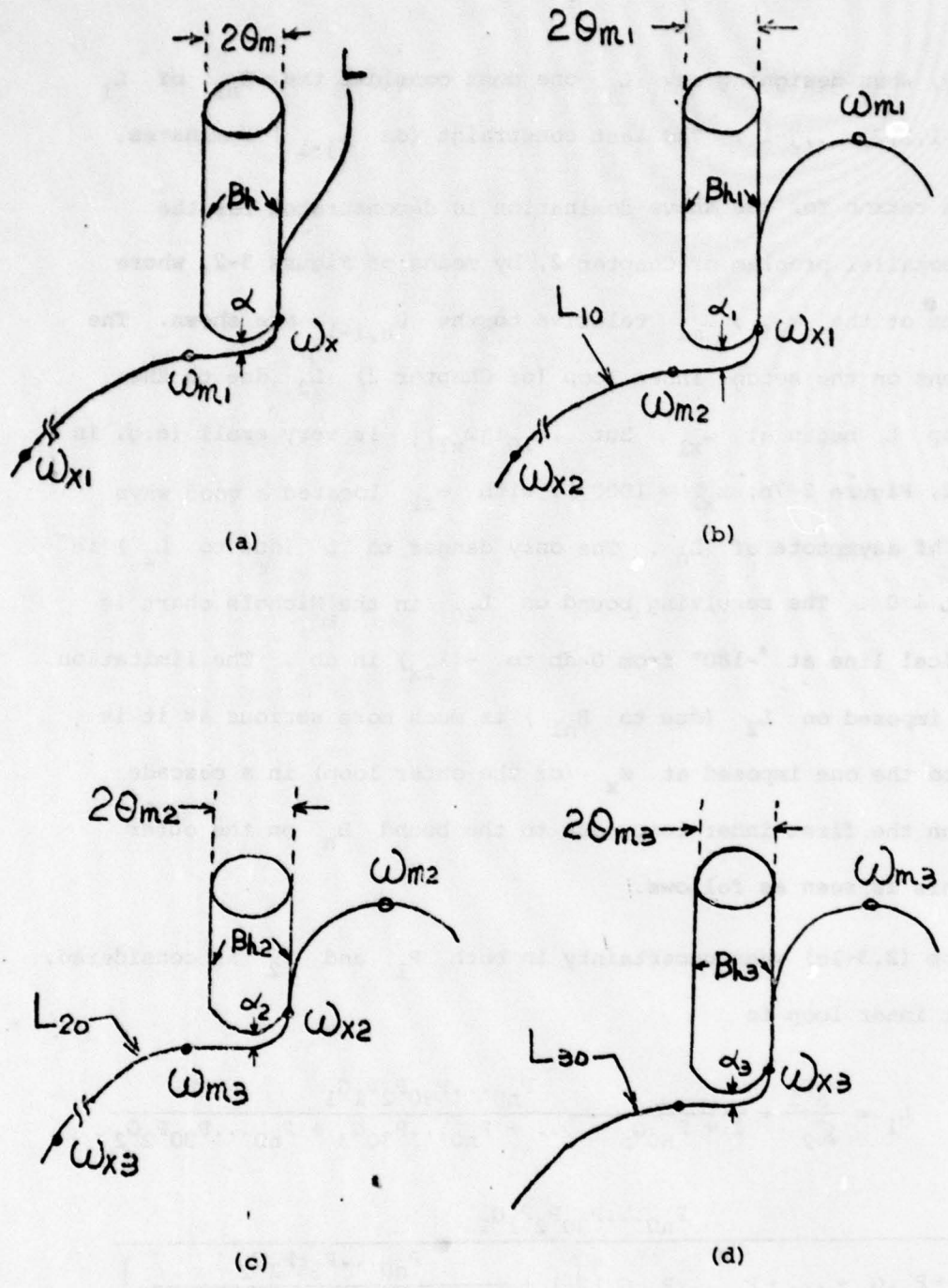

Figure 3-2. Some typical values of ω_{xi} , ω_{mi} relative to the $B_{h,i-1}$.

$$L_0 = \frac{P_B P_A G_A}{1 + P_B G_B} \quad , \qquad (3.4\text{-}3)$$

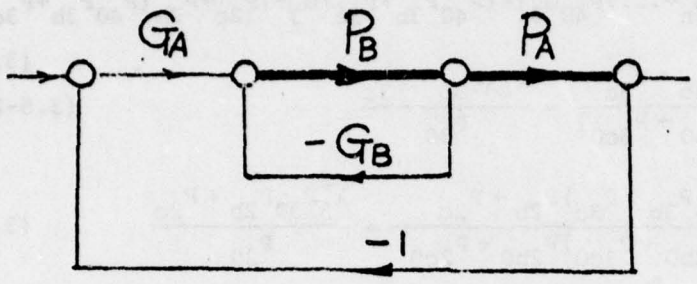

Figure 3-3. A cascade system of 2 sections.

which is analogous to (2.4-2) with

$$G_B = G_2 \quad , \quad P_1 = P_A \quad , \quad P_B = \frac{P_{n0} \cdots P_{30} P_2}{1 + P_{n0} G_n + \cdots + P_{n0} \cdots P_{30} G_3} \qquad (3.4\text{-}4a\text{-}c)$$

Hence, the bounds on the second inner loop,

$L_{20} = \dfrac{P_{n0} \cdots P_{20} G_2}{1 + P_{n0} G_n + \cdots + P_{n0} \cdots P_{30} G_3}$ in (3.4-2), such that those on L_1 are satisfied, are precisely of the same type as those on $L_{B0} = P_{B0} G_B$, in (3.4-3), so that those on L_0 are satisfied.

In the case of the third inner loop (L_4 in the notation of Chapter 3), the bounds on L_3 , L_2 , L_1 must all be considered. For the same reason as in the above, those on L_3 dominate.

3.5 Design of Second Inner Loop L_3

Suppose $\theta_{m2} = 0$, so the universal hf boundary of L_{20} is a vertical line. Only the constraint on L_3 due to the bound on L_1 need be considered. The uncertainties in P_{3b} , P_{3c} previously

omitted, are now included, giving

$$L_1^2 = \frac{\{P_{1b}[P_{2c}+P_{2b}(P_{3c}+P_{3b}P_{40})]+P_{1c}\}G_1}{[1+P_{n0}G_n+\ldots+P_{40}G_4]+(P_{40}P_{3b}+P_{3c})G_3+[P_{2c}+P_{2b}(P_{40}P_{3b}+P_{3c})]G_2} \tag{3.5-1}$$

Let $$\lambda_3^2 = \frac{P_{40}P_{3b}+P_{3c}}{[P_{40}P_{3b0}+P_{3c0}]} = \frac{P_{40}P_{3b}+P_{3c}}{P_{30}} \tag{3.5-2a,b}$$

$$\lambda_2^2 = \frac{(P_{40}P_{3b}+P_{3c})P_{2b}+P_{2c}}{\{(P_{40}P_{3b0}+P_{3c0})P_{2b0}+P_{2c0}\}} = \frac{\lambda_3^2 P_{30}P_{2b}+P_{2c}}{P_{20}} \tag{3.5-3}$$

$$L_{30} = \frac{P_{30}G_3}{(1+P_{n0}G_n+\ldots+P_{40}G_4)} = \frac{P_{30}G_3}{\mathcal{D}_{40}} \tag{3.5-4a,b}$$

so $$L_1^2 = \frac{(P_{1b}P_{20}\lambda_2^2+P_{1c})G_1}{\mathcal{D}_{40}[1+\lambda_3^2 L_{30}+\lambda_2^2 L_{20}(1+L_{30})]} \; . \tag{3.5-5}$$

The effective plant is

$$P_1^2 = \frac{\lambda_2^2 P_{1b}P_{20}+P_{1c}}{1+\lambda_3^2 L_{30}+\lambda_2^2 L_{20}(1+L_{30})} \tag{3.5-6}$$

which is comparable with P_e^2 of (2.3-5b), if λ_2^2 (here) is set equal to $\lambda_1\lambda_2$ (there), λ_3^2 (here) to λ_2 (there). Thus, if $\theta_{m2}=0$, the design of the second inner loop here is similar to that of the second inner loop in Chapter 2.

However, in the case of θ_{m2} constraints on L_2, these dominate the design of L_{30}, whose design is then comparable to that of the first inner loop in the parallel-cascade design of Chapter 2. This is seen by exhibiting the first inner loop L_2 in terms of the uncertainties in P_{3b}, P_{3c}. Let

$$P_3^o = P_{3c}+P_{3b}P_{40} \; , \tag{3.5-7}$$

and then

$$L_2^1 = \frac{(P_{2c} + P_3^o P_{2b})G_2}{\mathcal{D}_{40}\left(1 + \frac{P_3^o G_3}{\mathcal{D}_{40}}\right)} \qquad (3.5\text{-}8)$$

Compare L_2^1 to the first inner loop of Chapter 2, whose effective plant in (2.3-2a) is

$$P_e^1 = \frac{P_c + (P_1 P_{20} \cdots P_{n0})P_b}{\mathcal{D}_{20}\left[1 + \frac{(P_1 P_{20} \cdots P_{n0})}{\mathcal{D}_{20}} G_1\right]} \quad . \qquad (3.5\text{-}9)$$

Thus, the design of $L_{30} = P_{30}G_3\mathcal{D}_{40}$ to satisfy the bounds on L_2, is analogous to the design of the first inner loop in Chapter 2, to satisfy the bounds on the outer loop.

Higher Inner Loops

For the case of i-th inner loop design, if $\theta_{mj} = 0$ for $2 \leq j \leq i-1$, then the effective plant P_1^i can be written as

$$P_1^i = \frac{(\lambda_i^i P_{i0} P_{1b} + P_{1c})}{1 + \lambda_{i+1}^i L_{i+1,0} + \lambda_i^i L_{i,0}(1+L_{i+1,0}) + \ldots + \lambda_2^i L_{20}(1+L_{30})(1+L_{40})\ldots(1+L_{i+1,0})} \qquad (3.5\text{-}10)$$

with $$\lambda_{i+1}^i = \frac{P_{i+1}}{P_{i+1,0}} \quad , \quad \lambda_j^i = \frac{(\lambda_{j+1}^i P_{j+1,0} P_{jb} + P_{jc})}{P_{j0}} \quad , \quad j = 2,3,\ldots i \qquad (3.5\text{-}11a,b)$$

and $$L_1^i = \frac{P_1^i G_1}{\mathcal{D}_{i+2,0}} \quad , \quad L_{j0} = \frac{P_{j0} G_j}{\mathcal{D}_{j+1,0}} \quad , \quad j = 2,3,\ldots i \quad . \qquad (3.5\text{-}12a,b)$$

In the case the $\theta_{mi} \neq 0$, the design of L_{40} is dominated by the need to satisfy the B_{h3} bound on L_3. Write

$$L_3^1 = \frac{[P_{3c} + P_{3b}(P_{4c} + P_{4b}P_{50})]G_3}{\mathcal{D}_{50}\left[1 + \frac{(P_{4c} + P_{4b}P_{50})G_4}{\mathcal{D}_{50}}\right]}$$

$$\triangleq \frac{(P_{3c} + P_{3b}P_4^o)G_3}{\mathcal{D}_{50}\left(1 + \frac{P_4^o G_4}{\mathcal{D}_{50}}\right)} \quad . \tag{3.5-13}$$

Compare this to (3.5-8), and it is seen that the design of the third inner loop to satisfy the bounds on the second inner loop, is analogous to the design of the first inner loop in Chapter 2, to satisfy the bounds on the outer loop. The extension to higher inner loops is obvious.

3.6 Sensor Noise Effects at Plant Input

These effects are found here as the nominal plant values. The effect of N_1 was given in (3.2-4), repeated here

$$\frac{-X}{N_1} = \frac{L_{10}/P_{10}}{1 + L_{10}} \quad . \tag{3.6-1}$$

The effect of N_2 is given by

$$\frac{-X}{N_2} = \frac{G_2}{\mathcal{D}_{10}} = \frac{G_2}{\mathcal{D}_{20}(1+L_{10})} = \frac{G_2}{\mathcal{D}_{30}(1+L_{20})(1+L_{10})} = \frac{L_{20}/P_{20}}{(1+L_{20})(1+L_{10})} \tag{3.6-2}$$

In general,

$$\frac{-X}{N_i} = \frac{G_i}{\mathcal{D}_{10}} = \frac{L_{i0}/P_{i0}}{(1+L_{i0})\ldots(1+L_{10})} \quad . \tag{3.6-3}$$

3.7 Design Example

The procedure for quickly achieving approximate designs is fairly obvious, in view of the above noted similarities of the present design problem with that in Chapter 2. The explanation is presented by means of the following example. The detailed design will be presented first, followed by Design Perspective in Section 3.8.

3.7.1. Problem Statement.

The structure is shown in Figure 3-4a with

$$P_{4c} = \frac{[1,40]10^3}{s} \quad , \quad P_{3b} = \frac{[1,18]100}{s} \quad , \quad P_{3c} = \frac{[1,60]10^5}{s^2}$$

$$P_{2b} = \frac{[1,18]10}{s} \quad , \quad P_{2c} = \frac{[2,120]10^6}{s^3} \qquad (3.7\text{-}1)$$

$$P_{1b} = \frac{[1,60]}{s} \quad , \quad P_{1c} = \frac{[4,800]10^6}{s^4} \quad .$$

The numbers were deliberately chosen so that the outer loop and first inner loop designs here are identical to those of the design example in Chapter 2, Section 2.2.1. Time-domain bounds on the acceptable step response and its translation into bounds on $|T(j\omega)|$ are the same as Figure 2-3a,b of Chapter 2. In the notation of (3.1-1)

$$P_4 = P_{4c} = [1,40]10^3/s \text{ with uncertainty } U_4 = 40$$

$$P_3 = P_4P_{3b} + P_{3c} = [2,780]10^5/s^2 \quad , \quad U_3 = 390$$

$$P_3^o = P_{40}P_{3b} + P_{3c} = [2,78]10^5/s^2 \quad , \quad U_3^o = 39$$

$$P_2 = P_3P_{2b} + P_{2c} = [4,14160]10^6/s^3 \quad , \quad U_2 = 3540 \qquad (3.7\text{-}2)$$

$$P_2^o = P_{30}P_{2b} + P_{2c} = [4,156]10^6/s^3 \quad , \quad U_2^o = 39$$

$$P_1 = P_2P_{1b} + P_{1c} = [8,850400]10^6/s^4 \quad , \quad U_1 = 106,300$$

$$P_1^o = P_{20}P_{1b} + P_{1c} = [8,1040]10^6/s^4 \quad , \quad U_1^o = 130 \quad .$$

In decibels, $U_3 = 51.8$ db , $U_2 = 71$ db , $U_1 = 100.5$ db .

This example is used for two cases that were discussed in Section 3.4. For the first case (case A), there are none on X/D' of (2.3-3), and therefore $\theta_{mi} \doteq 0°$. In the second case (case B), there is also the specification of (3.4-1), i.e. $\theta_{mi} \neq 0°$. However, the

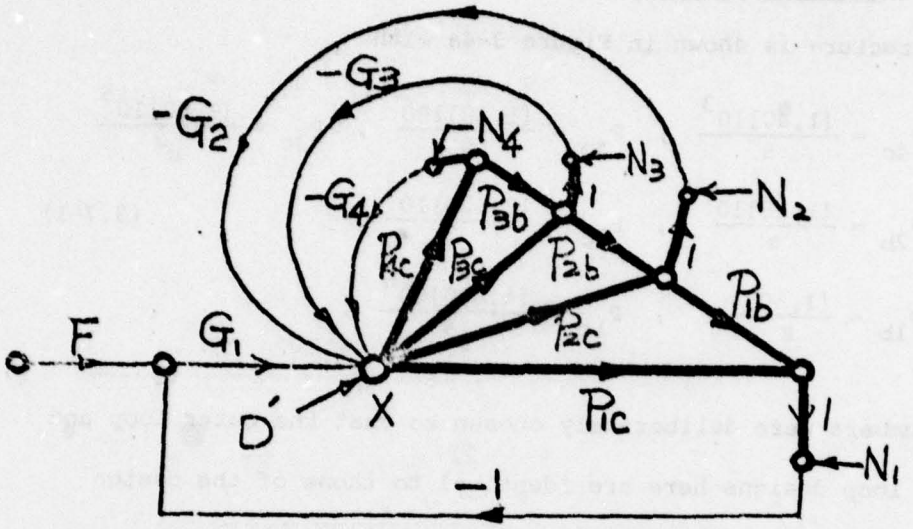

Figure 3-4a. System structure of the design example.

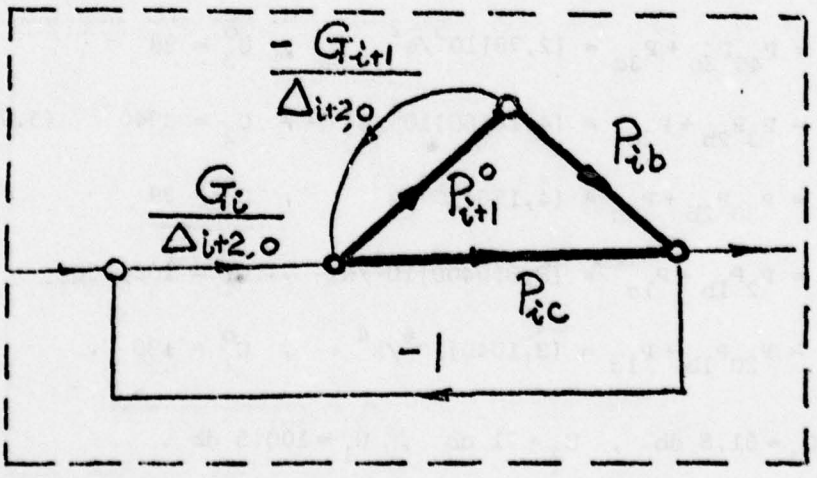

Figure 3-4b. An equivalent system in numerical example.

design of the outer loop (L_{10}) is the same, because the design of the outer loop does not need to refer to the constraints of inner loops.

3.7.2. Outer Loop Design.

As discussed in Section 3.2, let L_1 handle the entire uncertainty up to ω_{x1}. But for $\omega > \omega_{x1}$, L_1 handles only the uncertainty in P_{1c} and P_{1b} with all the other plants at their nominal values. From (3.7-2), $U_1^o = 130$ = the outer loop uncertainty of the design example in Chapter 2 given from (2.2-5b). The condition in Section 2.2 (following 2.2-4a,b) $b_c/a_c \geq b_b/a_b$ becomes here $b_{1c}/a_{1c} = 800/4 > b_{1b}/a_{1b} = 60/1$, so the outer loop of the design example in 2.2.1 can be used here as L_{10}. L_{10} on Nichols chart is shown repeatedly in Figure 3-5a.

3.7.3. Inner Loop Design.

First Inner Loop.

For the first inner loop design, L_1^1 should handle the uncertainty in effective plant P_1^1 of (3.3-4), with

$$\lambda_2^1 = \frac{P_{30}P_{2b} + P_{2c}}{P_{30}P_{2b0} + P_{2c0}} = \frac{2\times 18 + 120}{2\times 1 + 2} = 39 \simeq \lambda_1 = 40 \quad \text{of (2.3-2b).}$$

Again, in case of $\theta_{m2} \simeq 0°$, the designed first inner loop L_{10} of 2.3.1 can be used as the first inner loop L_{20} here. However, a small phase margin of 18° was actually used, as shown in Figures 3-5b,7,10 for both cases A and B, with

$$L_{20} = \frac{0.168(1 + \frac{s}{2286})(1 + \frac{s}{180})(1 + \frac{s}{1440})}{[1 + \frac{0.4s}{320} + (\frac{s}{320})^2][1 + \frac{0.6s}{2680} + (\frac{s}{2680})^2]^2(1 + \frac{s}{150})(1 + \frac{s}{3200})} \qquad (3.7\text{-}3)$$

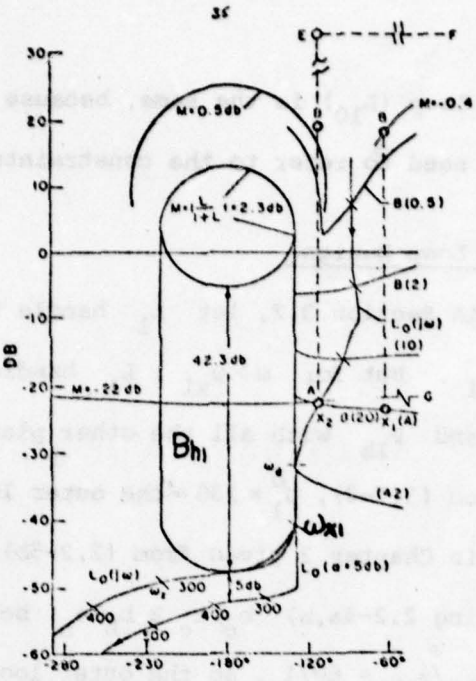

Figure 3-5a. Bounds and loop of L_{10} on Nichols chart.

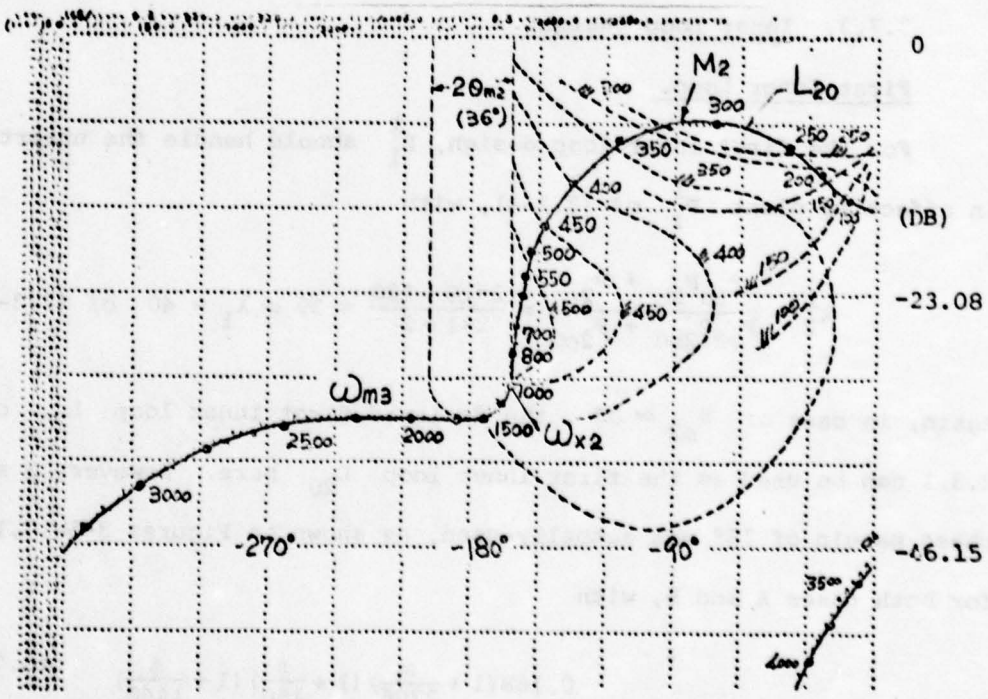

Figure 3-5b. Bounds and loop of L_{20} .

3.7.4. Second and Higher Inner Loop (Case A).

The second inner loop L_{30} for handling the effective plant P_1^2 of (3.5-6) is analogously derived as in Chapter 2 for $\theta_{m2} = 0$ to satisfy the B_{h1} constraint on the outer loop. The values of λ_2^2, λ_3^2 of P_1^2 in (3.5-6) are now

$$\lambda_3^2 = \frac{P_{40}P_{3b} + P_{3c}}{P_{30}} = \frac{1\times 18 + 60}{2} = 39$$

$$\lambda_2^2 = \frac{\lambda_3^2 P_{30}P_{2b} + P_{2c}}{P_{20}} = \frac{39\times 2\times 18 + 120}{2} = 381 \quad . \tag{3.7-4a,b}$$

The bounds on L_{30} and the designed L_{30} (also allowing 18° phase margin) are shown in Figure 3-6a, with

$$L_{30} = \frac{0.068\left(1 + \frac{s}{14400}\right)\left[1 + \frac{0.8s}{2250} + \left(\frac{s}{2250}\right)^2\right]\left(1 + \frac{s}{7000}\right)}{\left[1 + \frac{0.4s}{2300} + \left(\frac{s}{2300}\right)^2\right]\left[1 + \frac{0.6s}{2250} + \left(\frac{s}{2250}\right)^2\right]\left[1 + \frac{0.6s}{14000} + \left(\frac{s}{14000}\right)^2\right]^2}$$

$$\times \frac{1}{(1 + s/23000)} \tag{3.7-5}$$

Similarly, the bounds and loop transmission of the 3rd inner loop (i.e. i=3) L_{40} are shown in Figure 3-6b with

$$L_{40} = \frac{0.068\left(1 + \frac{s}{75200}\right)\left[1 + \frac{0.8s}{11745} + \left(\frac{s}{11745}\right)^2\right]\left(1 + \frac{s}{36540}\right)}{\left[1 + \frac{0.4s}{12000} + \left(\frac{s}{12000}\right)^2\right]\left(1 + \frac{s}{120000}\right)\left[1 + \frac{0.6s}{11745} + \left(\frac{s}{11745}\right)^2\right]\left[1 + \frac{0.6s}{73000} + \left(\frac{s}{73000}\right)^2\right]^2} \tag{3.7-6}$$

L_{40} is designed to handle the uncertainty of the effective plant P_1^3 in (3.5-10) with $\lambda_4^3 = 40$, $\lambda_3^3 = 390$, $\lambda_2^3 = 3540$, L_{j0} , L_1^3 obtained from (3.5-11,12) for $i = 3$, $2 \leq j \leq i$.

The Bode plots of all the loop transmissions for both the detailed design and the perspective design (explained later) of case A are shown

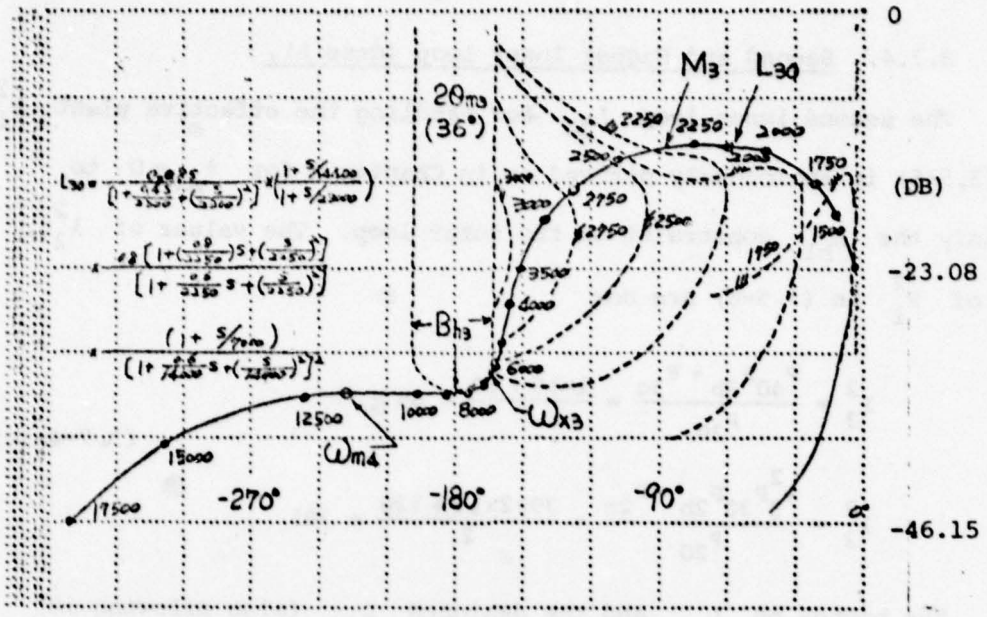

Figure 3-6a. Bounds and loop of L_{30} .

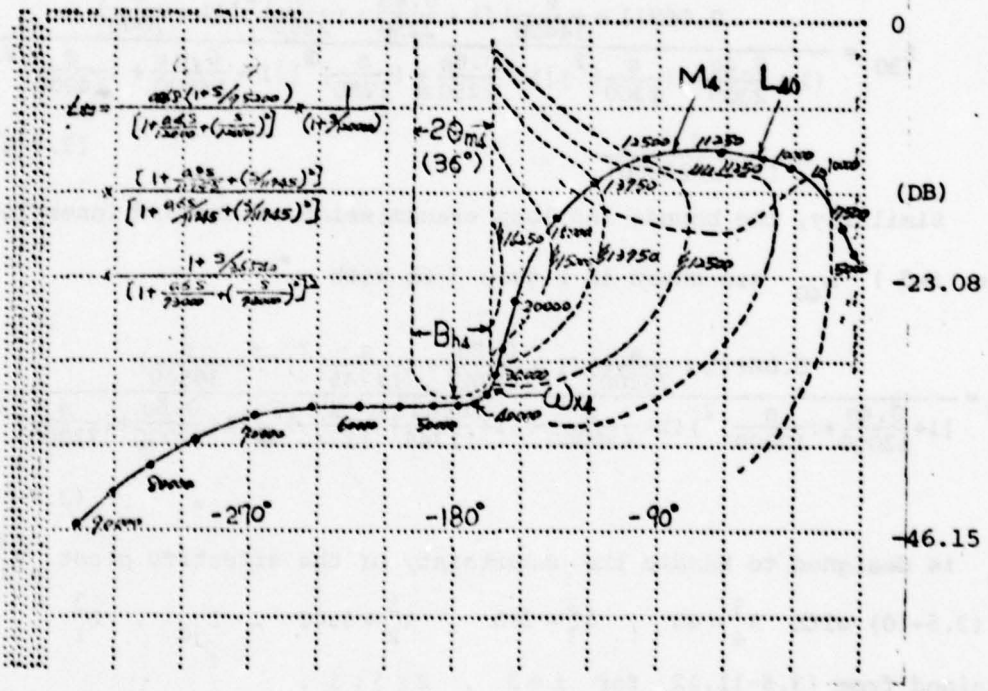

Figure 3-6b. Bounds and loop of L_{40} .

in Figure 3-7. Figures 3-8a,b show the sensor noise effects of the different designs in logarithmic and arithmetic scales respectively.

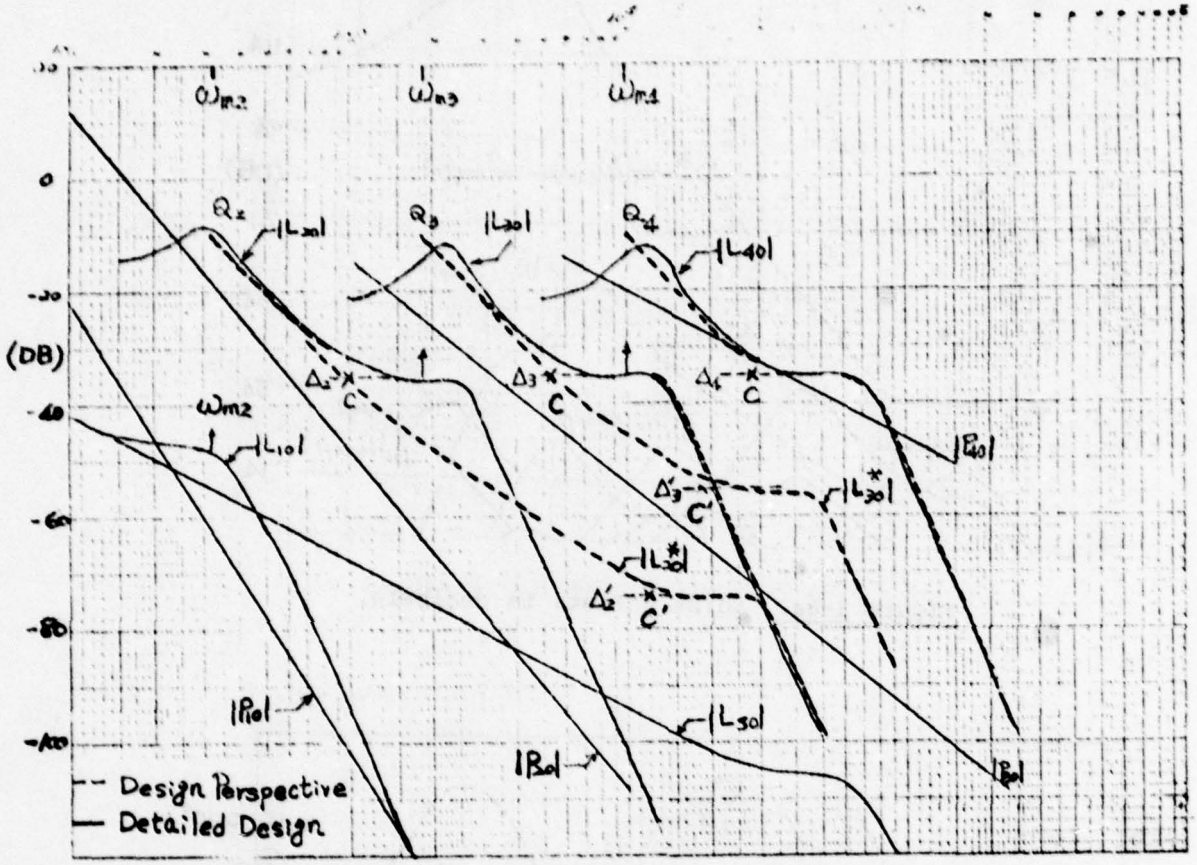

Figure 3-7. Bode plots of loop transmissions for perspective and detailed design.

3.7.5. Second and Higher Inner Loop (Case B).

In this case, $\theta_{m1} = 50°$, $\theta_{m2} = \theta_{m3} = 18°$ are used. It was shown in Section 3.5 that if there exists the constraint of maintaining some $\theta_{m,i-1}$ value, then if $\theta_{mi} \neq 0$, the design of the i-th inner loop to satisfy this $\theta_{m,i-1}$ constraint, is analogous to the design of the first inner loop in Chapter 2 to satisfy the bounds on the outer loop. The first inner loop L_{20} (i.e. i=1) of case A was purposely designed with $\theta_{m2} = 18°$ so it could be used here (however, in case A, there was

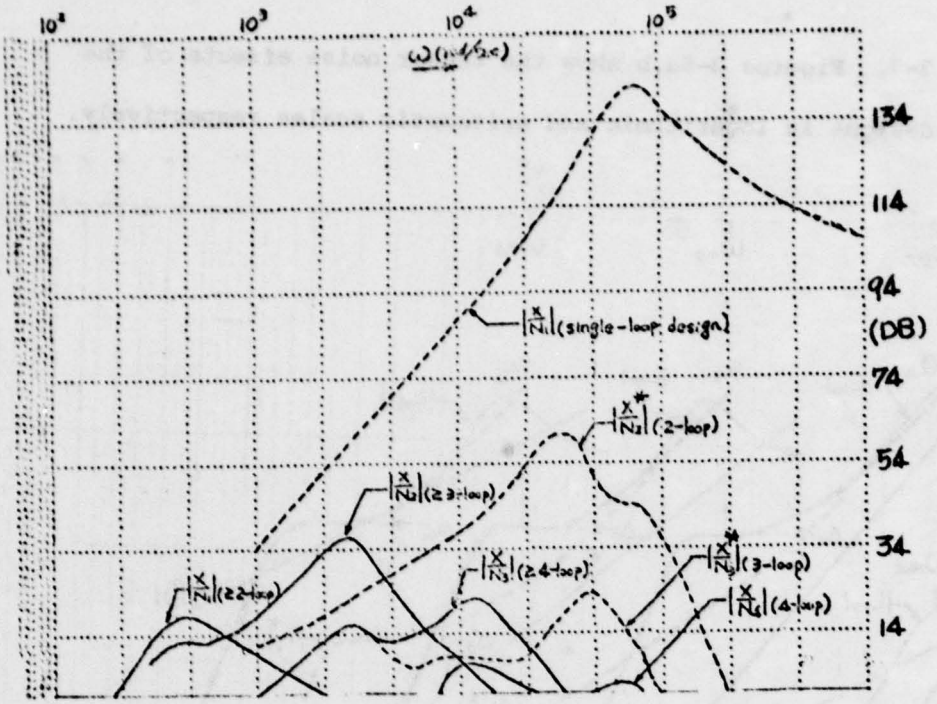

Figure 3-8a. Noise effects in decibels.

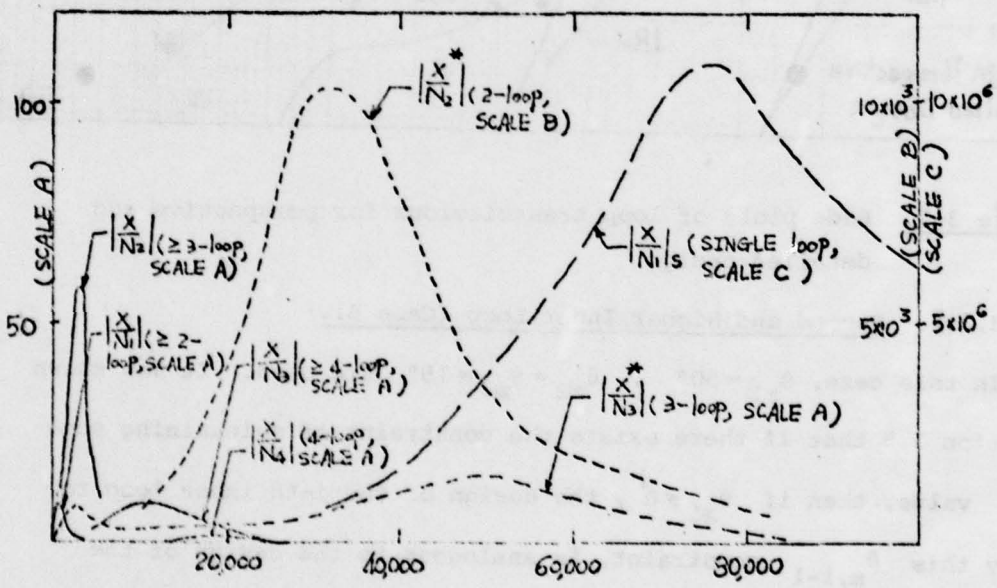

Figure 3-8b. Noise effects in arithmetic scale.

no consideration of θ_{m2} in designing L_{30}). Actually, for $i = 1,2,3$, $U_4 = 40 \doteq U_3^o = U_2^o = 39$, the problem becomes that of Figure 3-4b from Equations (3.3-2), (3.5-8), (3.5-13) for each i . The bounds obtained on L_{30} , L_{40} and the loop transmissions are shown in Figure 3-9a,b respectively, with

$$L_{30} = \frac{0.168(1 + \frac{s}{16000})(1 + \frac{s}{10000})(1 + \frac{s}{1260})}{[1 + \frac{0.4s}{2240} + (\frac{s}{2240})^2](1 + \frac{s}{22400})(1 + \frac{s}{1050})[1 + \frac{0.6s}{18760} + (\frac{s}{18760})^2]^2} \qquad (3.7\text{-}7a,b)$$

$$L_{40} = \frac{0.168(1 + \frac{s}{112000})(1 + \frac{s}{70000})(1 + \frac{s}{8820})}{[1 + \frac{0.4s}{15680} + (\frac{s}{15680})^2](1 + \frac{s}{156800})[1 + \frac{0.6s}{130900} + (\frac{s}{130900})^2]^2(1 + \frac{s}{7350})}$$

The Bode plots for both the detailed and perspective designs are shown in Figure 3-10. Figures 3-11a,b show the sensor noise effects for these designs in logarithmic and arithmetic scales respectively.

3.8 Design Perspective Procedure

As in Chapters 1,2 Design Perspective enables the designer after picking a specific structure and specific trade-off values, to very rapidly obtain a good approximation to the actual final detailed design for that specific structure and trade-off values.

1) The first step is to design the single-loop L_{s0} to handle the entire uncertainty of P_1 (= 100.5 db) in (3.2-5a). Let α_0 be the trade-off (overdesign) margin of L_0 . Then the outer loop L_{10} of a multiple-loop design is obtained by shifting the UHF characteristic of L_{s0} upward by Φ_s , the net saving due to the multiple-loop design. In our example, $\alpha_0 = 0$, so $\Phi_s = (U_1 - U_1^o)$ db $\simeq 58$ db . Here, the L_{10} used

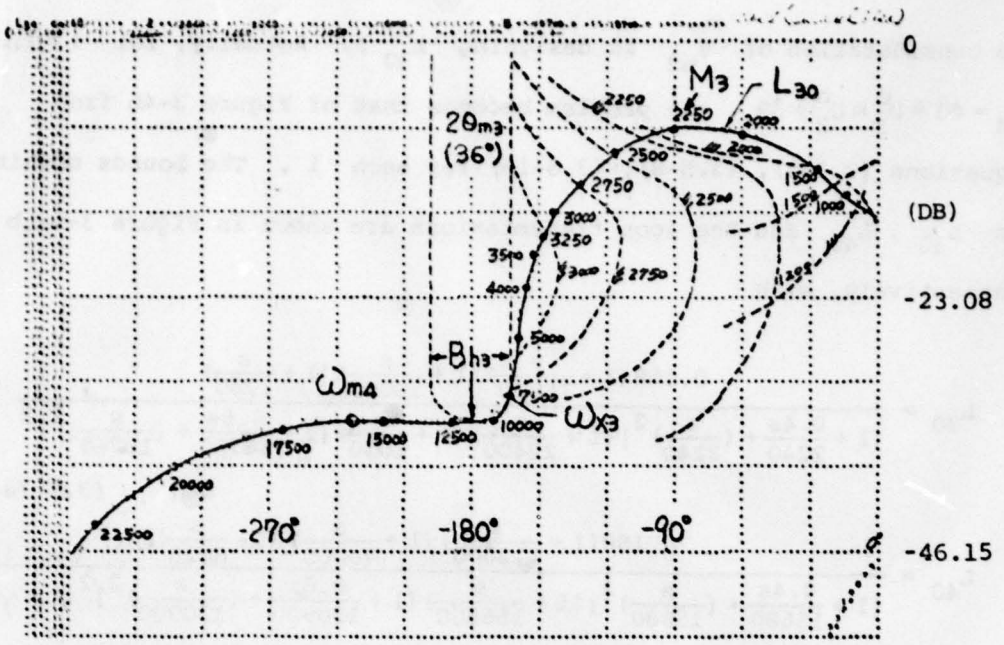

Figure 3-9a. Bounds and loop of L_{30} .

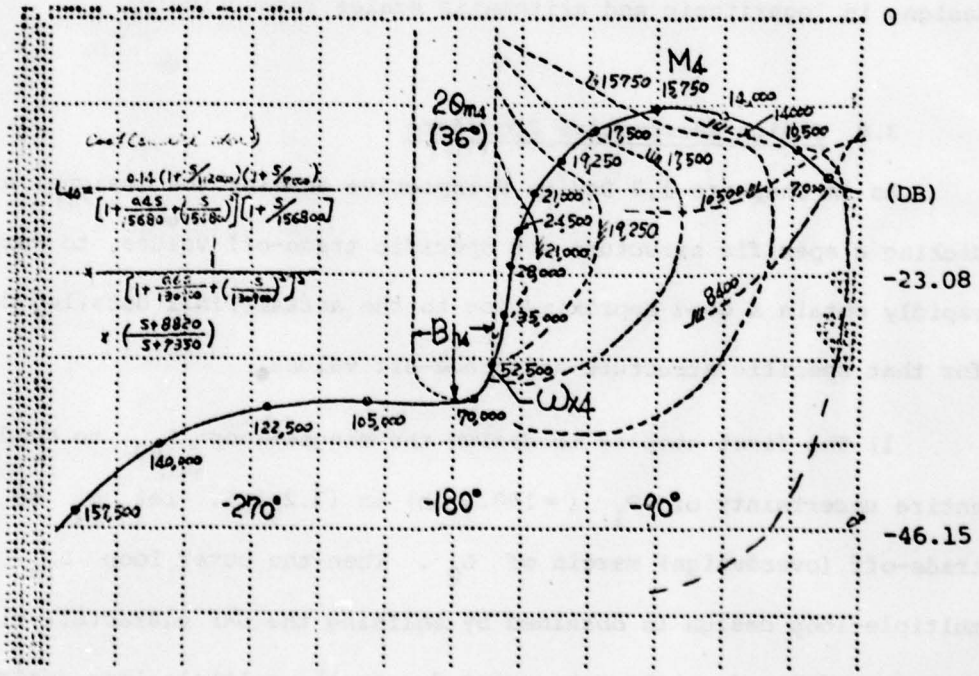

Figure 3-9b. Bounds and loop of L_{40} .

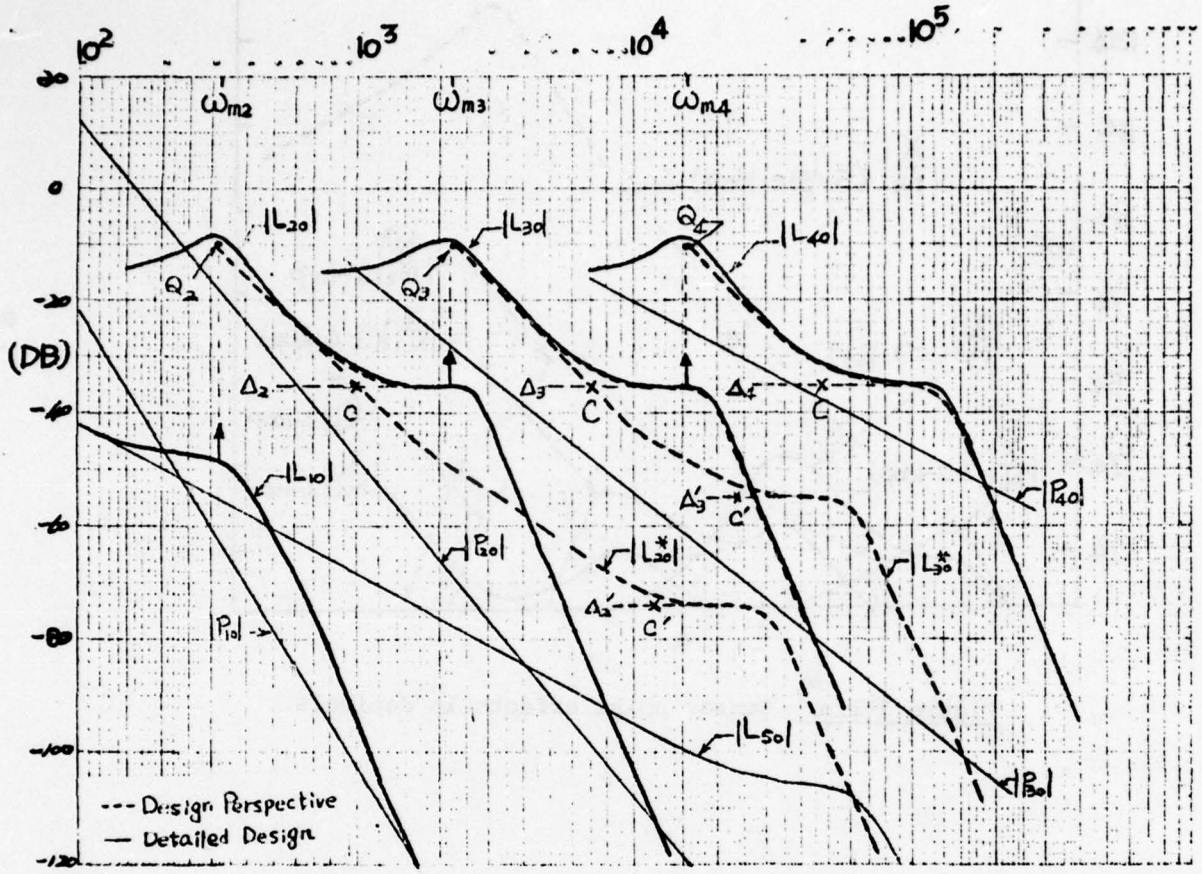

Figure 3-10. Bode plots of perspective and detailed design.

was obtained in Chapter 2, so the L_{10} (perspective) is obtained in exactly the same manner as in Section 2.5.

2) Find ω_{m2} (at which $|L_{20}|$ has its peak value) by placing a transparency of L_{outer} of Figure 1-24a over L_{10} of Figure 3-7,10 and noting the arrow.

3) Locate Q_2 (the peak position of $|L_{20}|$) at ω_{m2}, with value of M_2 ($\simeq$-10 db) obtained from Appendix 3 of Chapter 2. Point Q_2 is $|L_{20}(j\omega_{m2})|$. Draw a horizontal line in Figure 3-7,10 at Δ_2

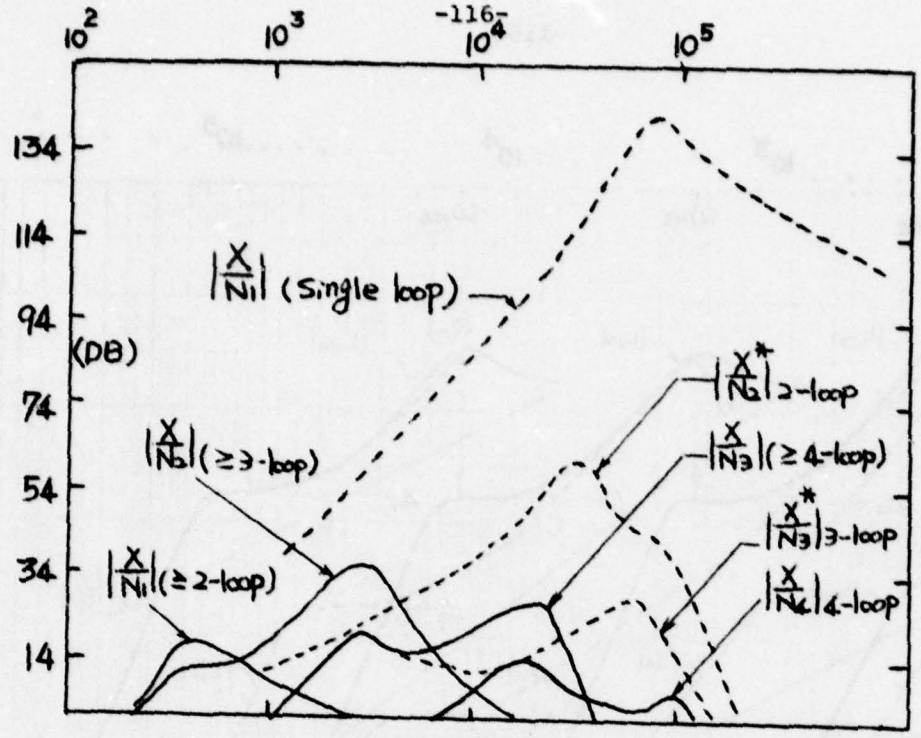

Figure 3-11a. Sensor noise effects in decibels.

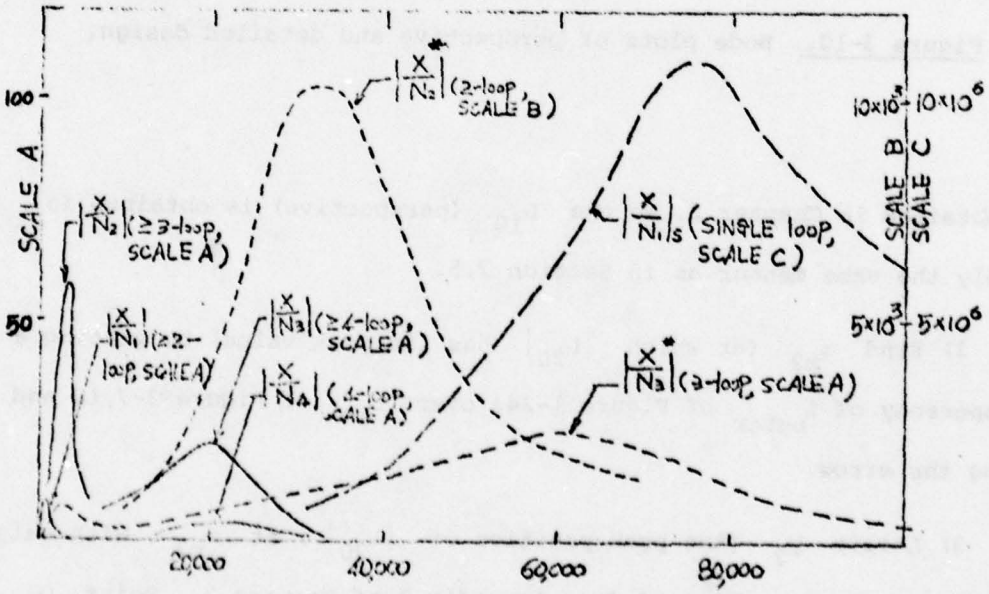

Figure 3-11b. Sensor noise effects in arithmetic scale.

magnitude, with $\Delta_2 = \text{Min}(B_{h2}) - \alpha_1 \simeq -35$ db for the example, where $\text{Min}(B_{h2})$ is the point of minimum value of B_{h2}. Here $\Delta_2' \simeq -74$ db for $|L_{20}^*|$ is also done, because $L_{i0} = 0$ for $i \geq 3$. Lay $L_{i0}(IF)$ of Figure 1-24a over Figures 3-7,10, so that Q coincides with Q_2. Find the intersection point C_2 (or C_2') of this $L_{i0}(IF)$ with the Δ_2 (or Δ_2') horizontal line in Figures 3-7,10.

4) Pick the $L_{i0}(HF)$ curve in Figure 1-24b, according to the θ_{m2} value ($\simeq 18°$ here) being used for L_{20}. Lay $L_{i0}(HF)$ on Figures 3-7,10, such that C coincides with C_2 (or C_2'). L_{20} consists of $L_{i0}(HF)$ of Figure 1-24a in the intermediate ω range and of $L_{i0}(HF)$ of Figure 1-24b in the high frequency range. Use the pattern of $L_{i0}(HF)$ to the left of C to obtain a smooth continuous curve for L_{20}.

5) Steps 3,4 are repeated in order to determine L_{30}. Use the arrow on $L_{i0}(HF)$ of Figure 1-24b to locate ω_{m3}, according to the θ_{m2} value being used ($\theta_{m2} = 0°$ for case A, 18° for case B). Use (2.A.3-6) to obtain M_3, giving a new point Q_3 in Figure 3-7,10. Then lay $L_{i0}(IF)$ of Figure 1-24a on Figures 3-7,10, so that $Q_3 = Q$. A horizontal line of value $\Delta_3 = \text{Min}(B_{h3}) - \alpha_3$ is drawn, etc. In the example, $\Delta_3 \simeq -35$ db for $|L_{30}|$ and $\Delta_3' \simeq -55$ db for $|L_{30}^*|$. $\text{Min}(B_{h3})$ is the point of minimum value of B_{h3}. The entire process is repeated until all the loops are exhausted. The dashed curves in Figures 3-7,10 are the results of using this perspective technique. They are in excellent agreement with the actual detailed design (solid lines in Figures 3-7,10), obtained by using the computer to obtain the inner loop bounds, finding a rational $L_{i0}(s)$ to satisfy these bounds, etc.

6) After each L_{i0} is obtained, it is a good idea to sketch the effective P values to use for the sensor noise effect. Thus, after L_{s0} is obtained, sketch P_{10} of (3.2-5) in Figures 3-7,10. If there is little sensor noise amplification ($|L_{s0}/P_{10}|$ not large over a large ω range), there may be no point in using more feedback loops. It is also easy to see the saving in sensor N_1 noise effect, by using $|L_{10}/P_{10}|$. Sketch $|P_{20}|$ to see the hf N_2 sensor noise effect ($\propto |L_{20}/P_{20}|$). Similarly $|L_{30}/P_{30}|$ gives the hf N_3 sensor noise effect.

The designer has to decide which sensor points to use and the corresponding α_i trade-off values. Design perspective anables him to try out various designs very quickly and easily, and thus arrive at a suitable trade-off, after which he can proceed with a careful detailed design.

CHAPTER 4

THE BASIC PARALLEL-CASCADE STRUCTURE

4.1 Introduction

This chapter extends "quantitative synthesis" to the plant structure (heavy line) of Figure 4-1a, consisting of two parallel branches, each with one internal sensing point C_{i2} $(i = 1,2)$. The system input r and output C can be sensed, giving 4 degrees of freedom, in the form of 4 independent data processing of these measurements. It is assumed, as in previous chapters, that each plant section has independently uncertain parameters, with known ranges. The tolerances 2.2-1,2 are to be satisfied $\forall P_{ij} \in \mathcal{P}_{ij}$. Emphasis is on the minimization of net sensor noise effects at the plant input x. Again, this problem obviously does not lend itself to a rigourous mathematical theorem-proving treatment. So again, the approach taken is to find the principal design factors and trade-offs. Several design philosophies are presented, and except for one of these, "Design Perspective" (Section 4.5) is provided by relatively simple fast sketches, based on only a preliminary single-loop design for the problem. This enables the designer to decide early in the game, which loops to use and how, and gives him even then a very good idea of the final design. This chapter paves the way for the much more complex plant structure of Chapter 5.

4.2 Design of the Outer Loop

The objectives of the problem are the same as Equations (2.2-1), (2.2-2). They are also achievable [H3] with a single loop $G_1 = G_s$, $G_{12} = 0$, $G_{22} = 0$ in Figure 4-1. But the resulting $L_s = G_s P$ may then require very large bandwidth, causing great amplification of sensor noise N_1, as in the previous chapters. In Figure 4-1a, let

$$P \triangleq P_{12}P_{11} + P_{22}P_{21} \quad , \quad T(S) = \frac{C(s)}{R(s)} = F(s)\,\frac{L_1(s)}{1+L_1(s)}$$

$$L_1(s) \triangleq \frac{PG_1}{1 + P_{12}G_{12} + P_{22}G_{22}} \triangleq P_e G_1 \qquad (4.2\text{-}1a\text{-}d)$$

$$\frac{-X}{N_1} = \frac{G_1}{1 + P_{12}G_{12} + P_{22}G_{22} + PG} = \frac{L_1/P}{1+L_1} \quad .$$

In (4.2-1d) the sensor noise effect is examined at the plant input X where it tends to be large (see Figure 4-8), causing plant saturation. As shown in Chapters 1,2, the hf range is the major trouble source, so the major effort in sensor noise effect reduction will be made in hf. It was also shown in Section 1.4.4 that the saving in the outer loop L_1 (by using the inner loops) is very minor for $\omega < \omega_{x1}$, so the same design philosophy of Chapters 1 and 2 is used here: Let the outer loop L_1 from C (of Figure 4-1a) cope with the uncertainty of the entire plant P up to ω_{x1}, but handle only the uncertainty in P_{11}, P_{21} for $\omega \geq \omega_{x1}$. This gives an L_1 much more economical than in a single-loop design in which $L_1 = L_s$ must cope with the entire P for all ω. Outer loop design in the hf range, is now a single-loop problem with the equivalent plant P_c of (4.2-1c), denoted by

$$P_e^1 \triangleq \frac{(P_{120}P_{11} + P_{220}P_{21})}{1 + P_{120}G_{12} + P_{220}G_{22}} \quad , \quad L_1 \triangleq P_e^1 \cdot G_1 \quad , \quad L_{10} = P_{e0}^1 \cdot G_1$$

(4.2-2a-c)

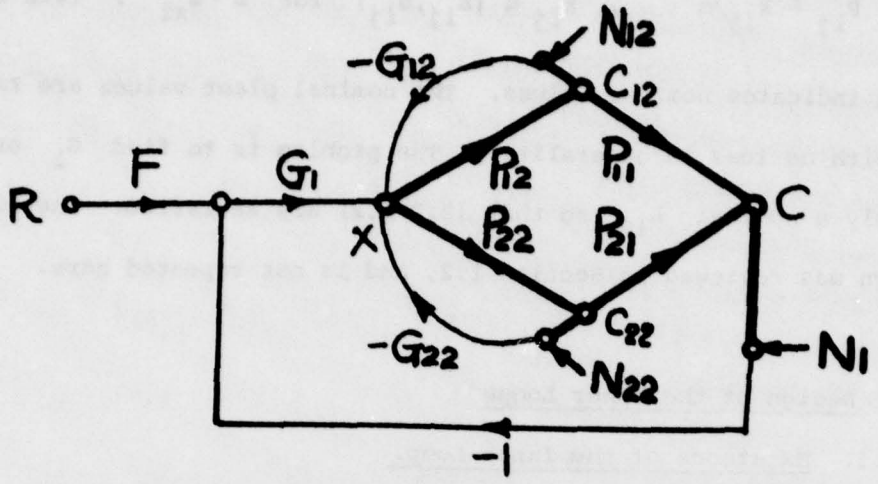

Figure 4-1a. The basic parallel-cascaded structure.

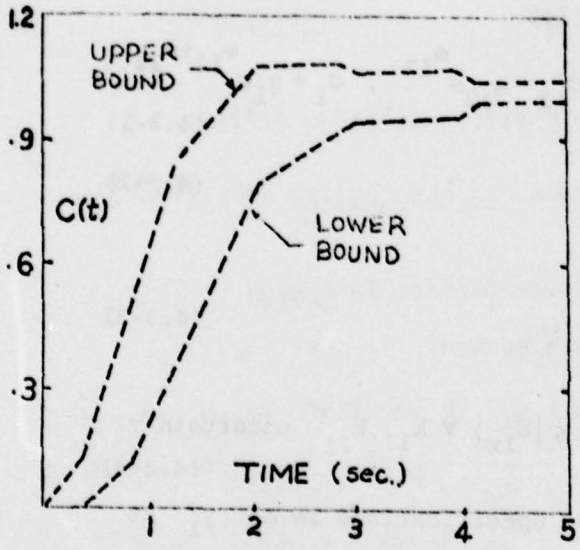

Figure 4-1b. Specified time-domain bounds on step response.

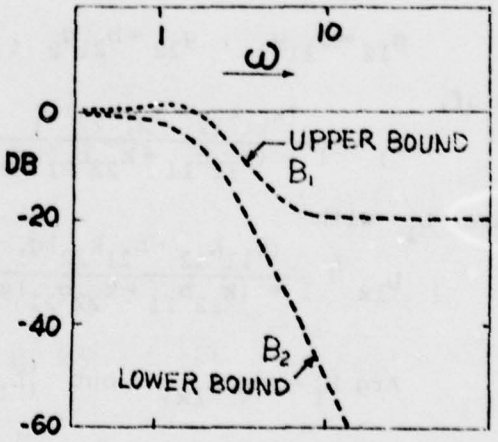

Figure 4-1c. "Equivalent" frequency-domain bounds.

$$P_{ij} \doteq k_{ij}/s^{e_{ij}} \quad , \quad k_{ij} \in [a_{ij},b_{ij}] \quad \text{for} \quad \omega > \omega_{x1} \quad . \quad (4.2\text{-}2d)$$

The sub-oh indicates nominal values. The nominal plant values are taken as a_i (with no loss in generality). The problem is to find G_1 or equivalently a nominal L_{10} so that (2.2-1,2) are satisfied. The single loop design was reviewed in Section 1.2, and is not repeated here.

4.3 Design of the Inner Loops

4.3.1. Existence of the Inner Loop.

In order to obtain the most economical outer-loop and thereby minimize the effect of sensor noise N_1 at X, it was assumed that the local feedback G_{12}, G_{22} in Figure 4-1 are able to handle the uncertainties of P_{12}, P_{22}. It is next proven that such G_{12}, G_{22} exist. Assuming $e_{11}+e_{12} = e_{21}+e_{22}$, let

$$g_{12} = b_{11}g_2 \quad , \quad g_{22} = b_{21}g_2 \quad , \quad G_{i2} = g_{i2}s^{e_{i2}} \quad , \quad G_1 = g_1 s^{e_{11}+e_{12}} \quad (4.3\text{-}1)$$

so in hf,

$$L_1 = \frac{(k_{11}k_{12}+k_{21}k_{22})g_1}{1+(k_{12}b_{11}+k_{22}b_{21})g_2} \quad . \quad (4.3\text{-}2)$$

Compare L_1 with

$$L_{1x} \triangleq \frac{(b_{11}k_{12}+b_{21}k_{22})g_1}{1+(k_{12}b_{11}+k_{22}b_{21})g_2} \quad ; \quad (4.3\text{-}3)$$

$$\text{Arg } L_1 = \text{Arg } L_{1x} \quad , \text{ but } \quad |L_1| \leq |L_{1x}| \ \forall \ k_{11},k_{21} \text{ uncertainty.} \quad (4.3\text{-}4)$$

For $\omega > \omega_{x1}$ the problem of violation of specifications is of γ_1 at the top of the template (recall Figures 1-A1a,b). Suppose there exists a G_2 which satisfies the system specifications $\forall\ k_{12},k_{22}$ uncertainty at fixed $k_{11}=b_{11}$, $k_{21}=b_{21}$. The above (4.3-4) guarantees that any other values of k_{11}, k_{21} give points lower down in the template, in

the Nichols chart — further from the γ_1 locus. Hence, such a g_2 is completely satisfactory. So now we need only consider the problem at $k_{11} = b_{11}$, $k_{21} = b_{21}$, at which $L_1 = L_{1x}$ of (4.3-3).

$$\text{Let } L_B \triangleq (b_{11}k_{12} + b_{21}k_{22})g_2 \tag{4.3-5}$$

$$\text{so} \qquad L_{1x} = L_B \frac{g_1}{g_2} \Big/ (1 + L_B) \tag{4.3-6}$$

and the problem is to find a nominal L_{B0} , $\ni L_B/(1+L_B)$ satisfies certain bounds, with

$$L_B = \lambda L_{B0} \quad , \quad \lambda_{max} = \frac{(b_{12}b_{11} + b_{22}b_{21})}{(a_{12}b_{11} + a_{22}b_{21})} \quad . \tag{4.3-7}$$

This is precisely the same problem as in a 2-section cascade design of Section 3.4, using the structure of Figure 4-2, with $L_B = P_B G_B$, $P_B = k_B/s^{e_B}$, $G_B = g_B s^{e_B}$. The problem there is identical to the present problem. Hence, cascade design philosophy with its Desgin Perspective can be used to find L_B here, from which g_2 is obtained, and then g_{12} , g_{22} are available from (4.3-1).

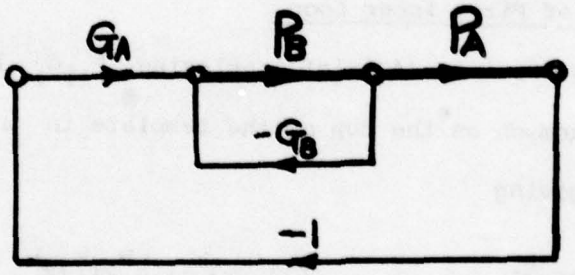

Figure 4-2. A 2-section cascade system.

4.3.2. Trade-off Function $x(\omega)$ between G_{12}, G_{22}.

The above provides a simple design procedure but is based on (4.3-1), giving $G_{12}/G_{22} = b_{11}/b_{21}$. This is not desirable if, for example $b_{11} \sim b_{21}$ while $N_{22} >> N_{12}$ in Figure 4-1. Return to (4.2-1) and let

$$L_2 \triangleq P_{12}G_{12} + P_{22}G_{22} \quad , \quad \alpha_{i2} = \frac{P_{i2}b_{i1}}{P_{12}b_{11} + P_{22}b_{21}} \tag{4.3-8}$$

The effect of sensor noise N_{i2}, at the plant input X, is

$$TN_{i2} = \frac{-X}{N_{i2}} = \frac{G_{i2}}{1 + P_{12}G_{12} + P_{22}G_{22} + PG_1} = \frac{G_{i2}}{(1+L_2)(1+L_1)} = \frac{\alpha_{i2}L_2}{P_{i2}} \tag{4.3-9}$$

for $i = 1,2$. Hence, to minimize this effect reduce $|G_{i2}|$ as fast as possible. But L_2 must cope with the uncertainty in P_{12}, P_{22}, ignored by L_1. So there is a trade-off between G_{12}, G_{22}. Introduce a trade-off function $x(\omega)$ by defining

$$b_{21}g_{12} - b_{11}g_{22} = (b_{11}/b_{22})x(\omega) \quad . \tag{4.3-10}$$

Equation (4.3-1) corresponds to $x = 0$.

4.3.3. Design of First Inner Loop.

Substitute (4.3-10) into (4.2-1c), replacing $P_{11}G_1$ by $b_{11}g_1$, $P_{21}G_1$ by $b_{21}g_1$ inasmuch as the top of the template in $\omega > \omega_{x1}$ need only be considered, giving

$$L_1 = \frac{b_{21}P_{22e}g_1}{1 + P_{22e}g_{22}} \quad , \quad P_{22e} = \frac{b_{22}(k_{12}b_{11} + b_{21}k_{22})}{xk_{12}b_{11} + b_{21}b_{22}} \quad . \tag{4.3-11a,b}$$

To design g_{22}, assume $x(\omega)$ can handle the uncertainty in k_{12}, so replace k_{12} by $k_{120} = a_{12}$ and define

$$L_{22}^{o} = P_{22e}^{o} g_{22} = \frac{b_{22}(a_{12}b_{11} + b_{21}k_{22})g_{22}}{xa_{12}b_{11} + b_{21}b_{22}} \qquad (4.3\text{-}12)$$

with $L_{220}^{o} = L_{22}^{o}$ at $k_{22} = a_{22}$. Thus L_{22}^{o} need handle only the uncertainty in P_{22e}^{o}, in which only k_{22} is uncertain. From (4.3-11b) if $x = 0$, then L_{22} must handle the uncertainty in

$$k_{12}b_{11} + k_{22}b_{21}$$

which gives the design approach of Section 4.3.1.

The ratio of maximum uncertainties, $x = 0$ cf. $x \neq 0$, is

$$\frac{U_{x=0}}{U_{x\neq 0}} = \left(\frac{b_{11}b_{12} + b_{21}b_{22}}{b_{11}a_{12} + b_{21}a_{22}}\right) \Big/ \left(\frac{a_{12}b_{11} + b_{22}b_{21}}{a_{12}b_{11} + a_{22}b_{21}}\right) = \frac{b_{11}b_{12} + b_{21}b_{22}}{b_{11}a_{12} + b_{21}b_{22}} \quad . \qquad (4.3\text{-}13)$$

In view of (4.3-11a), the loop L_{22}^{o} of 4.3-12, is designed analogous to the inner loop design of a 2-section cascade system, with P_B of Figure 4-3 analogous to P_{22e}^{o} of 4.3-12.

4.3.4. Design of Second Inner Loop.

If $x(\omega) \neq 0$ is used for the design of $L_{22}(x)$ in Section 4.3.3, then $x(\omega)$ must handle the uncertainty in k_{12} ignored by L_{22}^{o}. Rewrite (4.3-11,12) as follows:

$$P_{22e} = \left(\frac{b_{11}k_{12}}{b_{21}} + k_{22}\right) \Big/ \left(1 + \frac{xk_{12}b_{11}}{b_{21}b_{22}}\right) \quad , \quad L_{22} = g_{22}P_{22e} \qquad (4.3\text{-}14a,b)$$

which describes precisely the structure of Figure 4-3. Thus, the design procedure for the loop

$$L_x = \frac{k_{12}b_{11}x}{b_{21}b_{22}} \qquad (4.3\text{-}15)$$

in (4.3-14) is precisely the same as that of the first inner loop, in the triangle structure in Chapter 2. The Design Perspective there also applies.

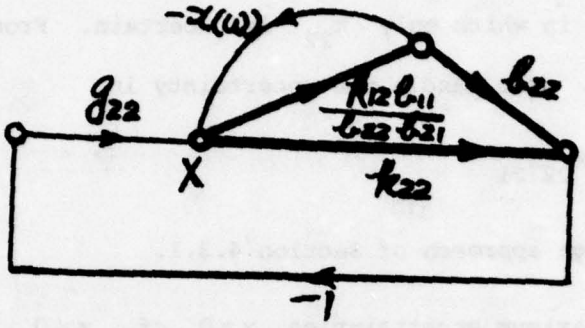

Figure 4-3. An equivalent system for Equation (4.3-14).

4.3.5. Sensor Noise Effects ($x \neq 0$).

In Figure 4-1, at the nominal values of the P_{ij},

$$\frac{-X}{N_{22}} = \frac{G_{22}}{(1 + P_{120}G_{12} + P_{220}G_{22})(1 + L_{10})} \quad . \qquad (4.3\text{-}16)$$

Substituting 4.3-10,11,14 and manipulate to give at hf (at which the sensor noise effects dominate),

$$\frac{-X}{N_{22}} = \frac{L_{220}\Big/\left(P_{120}\,\frac{b_{11}}{b_{21}} + P_{220}\right)}{(1 + L_{220})(1 + L_{10})} \doteq \frac{L_{220}}{P_{120}(b_{11}/b_{21}) + P_{220}} \qquad (4.3\text{-}17)$$

Similarly, $-X/N_{12}$ can be manipulated (at the nominal values of the P_{ij}), at hf into

$$\frac{-X}{N_{12}} = \left(\frac{b_{11}}{b_{21}}\right)\left(\frac{-X}{N_{22}}\right) + \frac{L_{x0}/P_{120}}{(1+L_{x0})(1+L_{220})(1+L_{110})} \quad . \qquad (4.3\text{-}18)$$

If $x = 0$, $L_{x0} = 0$, so (4.3-18) gives the extra effect of N_{12} which one pays for easing the design of L_{22} by means of $x \neq 0$, i.e. by the factor given in (4.3-13).

$$\frac{-X/N_{12}}{-X/N_{22}} = \frac{b_{11}}{b_{21}} \qquad \text{(case } x = 0\text{)} \qquad (4.3\text{-}19)$$

but $\left|-X/N_{22}\right|_{x=0} > \left|-X/N_{22}\right|_{x\neq 0}$ from (4.3-9, 13, 17).

4.4 Design Perspective

As emphasized in previous chapters, "Design Perspective" provides the designer an easy tool for deciding which sensor points to use, and the trade-offs. Since it is so useful, it is again presented here in detail, although the procedures are very similar to that of the previous chapters.

(1) The first step is to design the single-loop L_{s0} to handle the entire uncertainty of P in (4.2-1a). Let α_1 be the overdesign margin of L_{10} . Then the outer loop L_{10} of a multiple-loop design is obtained by shifting the UHF characteristic of L_{s0} upward by Φ_s db , the net saving due to the multiple loop design.

$$\Phi_s = 20 \log \left\{ \frac{P_{11x}P_{12x} + P_{21x}P_{22x}}{P_{11x}P_{120} + P_{21x}P_{220}} \right\} - \alpha_1 \text{ db}$$

for the structure of Figure 4-1a $\sim$ 36 db in the example of 4.5.

(2) Find ω_{m22} (at which L_{220} has its peak value) by placing a transparency of L_{outer} of Figure 1-24a over L_{10} of Figure 4-5a , and noting the arrow.

(3) Locate Q_{22} (the peak position of L_{220}) at ω_{m22}, with value of M_{22} ($\simeq$ -14 db) obtained from Figure 1-22, because L_{220} design is analogous to the inner loop design of cascade system. Point Q_{22} is $|L_{220}(g_{m22})|$. Draw a horizontal line in Figure 4-5a at Δ_{22} magnitude, with $\Delta_{22} = \text{Min}(B_{h22}) - \alpha_{22}$ ($\simeq$ -42,-14,-24 db for different designs in the example of Section 4.5), where $\text{Min}(B_{h22})$ is the point of minimum value of B_{h22}. Lay $L_{i0}(IF)$ of Figure 1-24a over Figure 4-5a, so that Q coincides with Q_{22}. Find the intersection point C_{22} of this $L_{i0}(IF)$ with Δ_{22} horizontal line in Figure 4-5a.

(4) Pick the $L_{i0}(IF)$ curve in Figure 1-24b, according to the Q_{m22} value being used for L_{220}. Lay $L_{i0}(HF)$ on Figure 4-5a, such that C coincides with C_{22}. L_{220} consists of $L_{i0}(IF)$ of Figure 1-24a in the intermediate ω range, and of $L_{i0}(HF)$ of Figure 1-24b in the high frequency range. Use the pattern of $L_{i0}(HF)$ to the left of C to obtain a smooth continuous curve for L_{10}.

(5) Steps (3),(4) are repeated in order to determine L_{x0}. Use the arrow on $L_{i0}(HF)$ of Figure 1-24b to locate ω_{mx}. The peak value M_x of L_{x0} is obtained from Appendix 3 of Chapter 2, because L_{x0} basically is the first inner loop design of structure in Chapter 2. Determine Q_x by ω_{mx} and M_x. Then lay $L_{i0}(IF)$ of Figure 1-24a over Figure 4-5a, so that $Q_x = Q$. A horizontal line of value $\Delta_x = \text{Min}(B_{hx}) - \alpha_x$ ($\simeq$ -42 db in the example) is drawn, etc. Figure 4-5a are the results of the design example in Section 4.5 by using this fast perspective technique. They are in excellent agreement with the actual detail design (in Figure 4-5b), obtained by using the computer to obtain the inner loop bounds, finding a rational $L_{i0}(s)$ to satisfy these

bounds, etc.

(6) After each L_{i0} (i.e. L_{220} , L_{x0}) is obtained, it is a good idea to sketch the effective P values to use for the sensor noise effects. Thus after L_{s0} is obtained, sketch $|P_0| = |P_{110}P_{120} + P_{210}P_{220}|$ in Figure 4-5a. If there is little sensor noise amplification ($|L_{s0}/P_0|$ not large over a large ω range), there may be no point in using more feedback loops. After L_{10} has been obtained, it is easy to see the saving in sensor N_1 noise effect, by comparing the area between $|L_{s0}/P_0|$ and $|L_{10}/P_0|$. Sketch $|P'_{220}| = |P_{120}(P_{11x}/P_{21x}) + P_{220}|$ (= $1.1/s^2$ in the example) to see the hf N_{22} sensor noise effect ($\simeq |L_{220}/[P_{120}(P_{11x}/P_{21x}) + P_{220}]|$). Similarly sketch $|P_{120}|$ (= $1/s^2$ in the example) to get $|L_{x0}/P_{120}|$, then see the hf N_{12} sensor noise effect from (4.3-15b).

This fast design perspective enables the designer to try out various designs very quickly and easily, and thus arrive at a suitable trade-off, after which he can proceed with a careful detailed design.

4.5 Design Example

The structure is shown in Figure 4-1a, with

$$P_{12} = [1,90]/s^2 \quad , \quad P_{11} = [1,10]/s$$
$$P_{22} = [0.1,2]/s^2 \quad , \quad P_{21} = [1,10]/s \qquad (4.6\text{-}1)$$

The time-domain bounds on the acceptable step response and its translation into bounds on $|T(j\omega)|$ are shown in Figures 4-1b,c. The disturbance specification is $\left|\frac{L}{1+L}\right| \leq 2.3$ db.

4.5.1. Outer Loop Design.

For $\omega \leq \omega_{x1}$, we let the outer loop L_1 handle the entire plant of P in (4.2-1a), with uncertainty $U_1 = \frac{90\times10 + 2\times10}{1\times1 + 0.1\times1} = 836.36$. But for $\omega \geq \omega_{x1}$, L_1 handles only the uncertainty U_1^o in P_e^1 of (4.2-2a) with $U_1^o = \frac{1\times10 + .1\times10}{1\times1 + 0.1\times1} = 10$. The saving Φ_s thereby obtained by a multiple loop design, is

$$\Phi_s = 20 \log[\frac{836.36}{10}] - \alpha_1 \text{ db} = (38.45 - \alpha_1)\text{db} \simeq -36 \text{ db} .$$

The design of L_{10} is exactly the problem of single-loop design. The resulting L_{10} is shown in Figure 4-4 on the Nichols chart, and in Figure 4-5b its Bode plot.

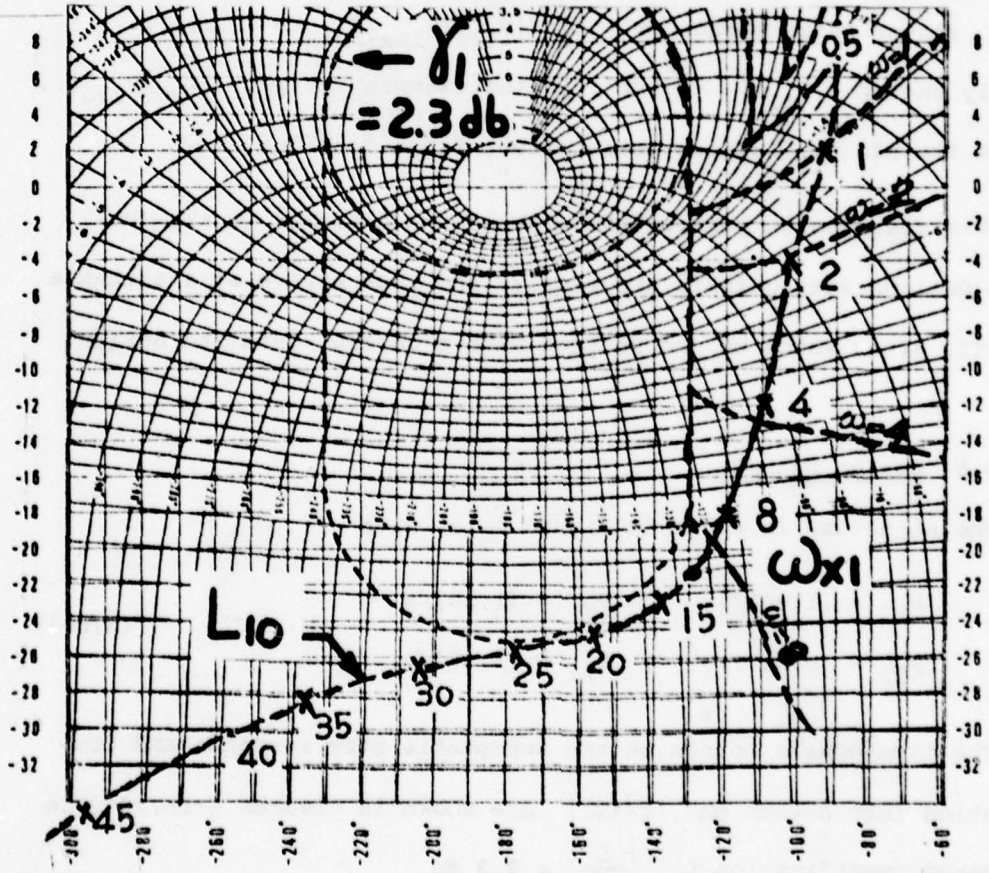

Figure 4-4. Outer loop L_{10} on Nichols chart.

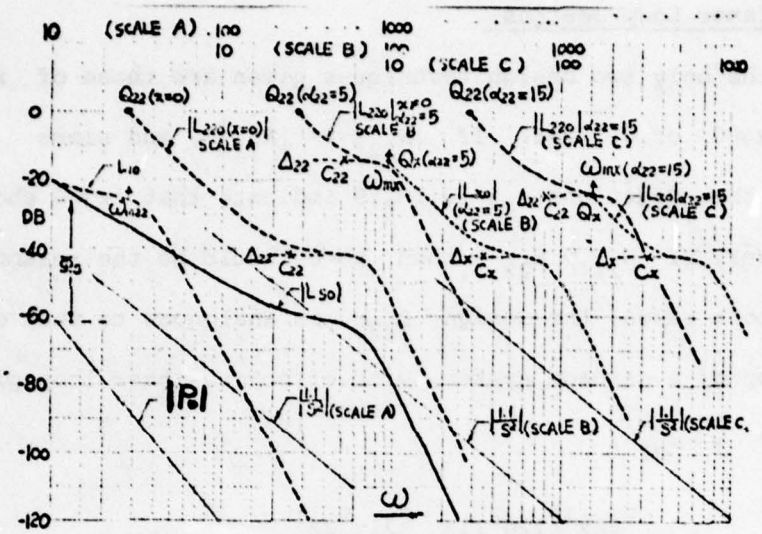

Figure 4-5a. Design Perspective.

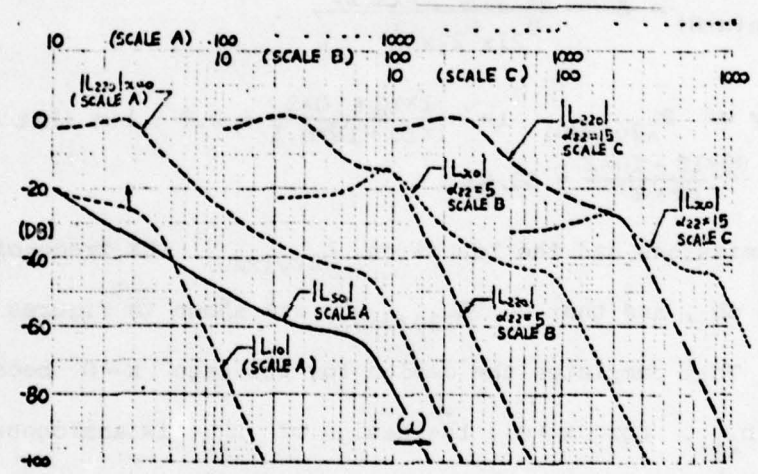

Figure 4-5b. Detailed Design.

4.5.2. Inner Loop Designs.

So far, the only two design techniques given are those of $x = 0$ of 4.3.1 and $x \neq 0$ of 4.3.2-5. If $|N_{22}| >> |N_{21}|$, and since $b_{11} = b_{21} = 10$, then Equations 4.3-13,18,19 indicate that $x \neq 0$ should be used. However, if $N_{21} \sim N_{22}$, then $x = 0$ would be the reasonable approach. In both cases, the design L_{220} is analogous to that of the first inner loop of a cascade system, with effective inner loop plant of (4.3-12) for $\omega > \omega_{x1}$,

$$P_{22e(x\neq 0)} = \frac{P_{22x}[P_{120}P_{11x} + P_{21x}P_{22}]}{xP_{120}P_{11x} + P_{21x}P_{22x}} \quad .$$

If $x = 0$ is used,

$$P_{22e(x=0)} = \frac{P_{22x}[P_{12}P_{11x} + P_{21x}P_{22}]}{P_{21x}P_{22x}} \quad .$$

The uncertainty of $P_{22e(x\neq 0)}$ is $\frac{1\times 10 + 10\times 2}{1\times 10 + 10\times 0.1} = 2.7$, but that of $P_{22e(x=0)}$ is $\frac{90\times 10 + 10\times 2}{10 + 1} = 83.63$.

The loop transmissions and the bounds on $L_{220(x\neq 0)}$ for trade-off value $\alpha_{22} = 5$ db, 15 db, and that on $L_{220(x=0)}$ are shown in Figures 4-6a,b,c respectively. This completes the design for the case $x = 0$ because $g_{12}/g_{22} = b_{11}/b_{21}$. For $x \neq 0$, the design of L_{x0} is analogous to the first inner loop design of Chapter 2. The loop transmission and bounds of the corresponding L_{x0} (for $\alpha_{22} = 5$ db, 15 db) are shown in Figures 4-7a,b. (In this example, the bounds on θ_{m22} were not maintained in the course of finding the bounds on L_{x0}.) Bode plots are shown in Figure 4-5b, including perspective design results in Figure 4-5a for comparison. The rational functions of L_{10}, L_{220}, L_{x0} are given in Appendix 1 of this chapter.

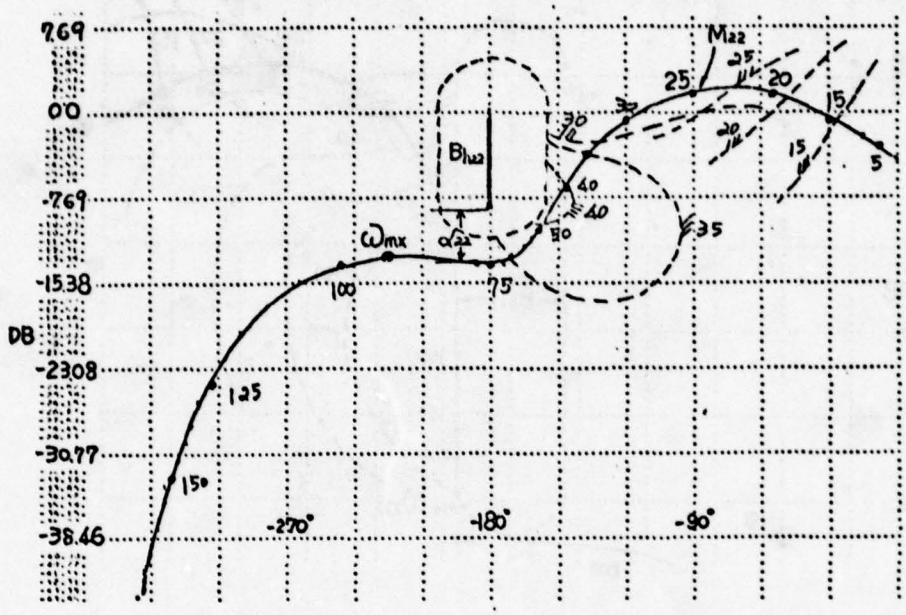

Figure 4-6a. Bounds and loop transmissions of L_{220} for α_{22} = 5 db .

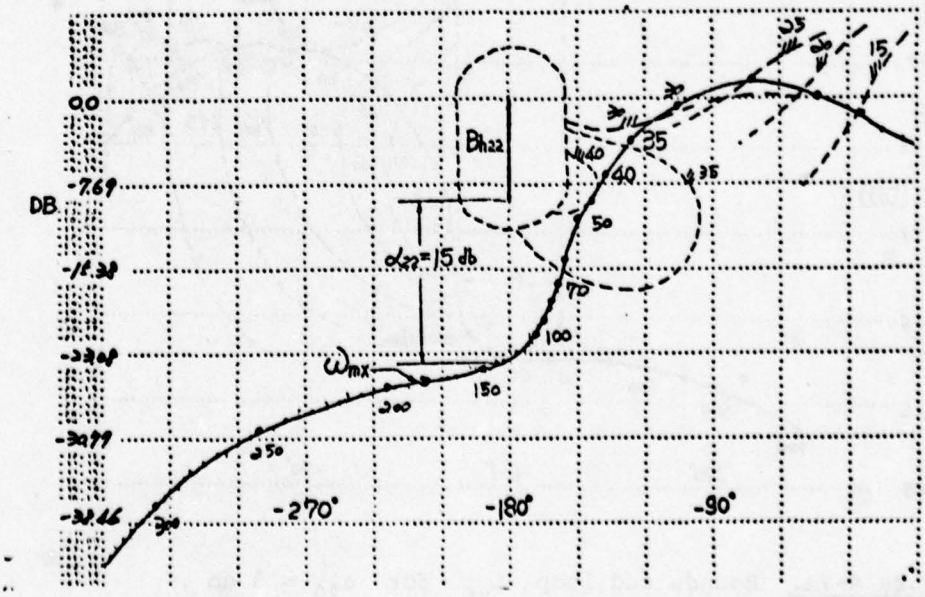

Figure 4-6b. Bounds and loop transmissions of L_{220} for α_{22} = 15 db .

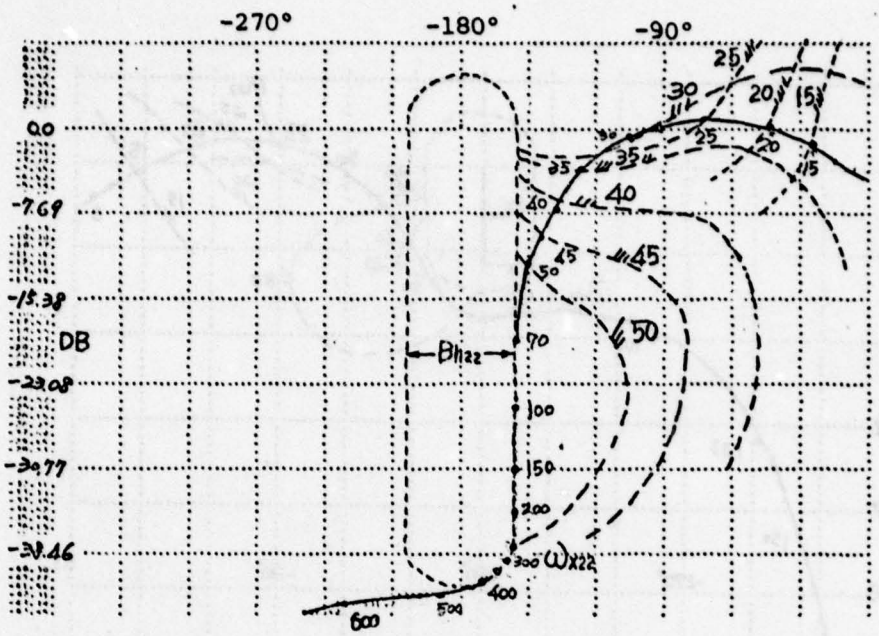

Figure 4-6c. Bounds and loop L_{220} for $x(\omega) = 0$.

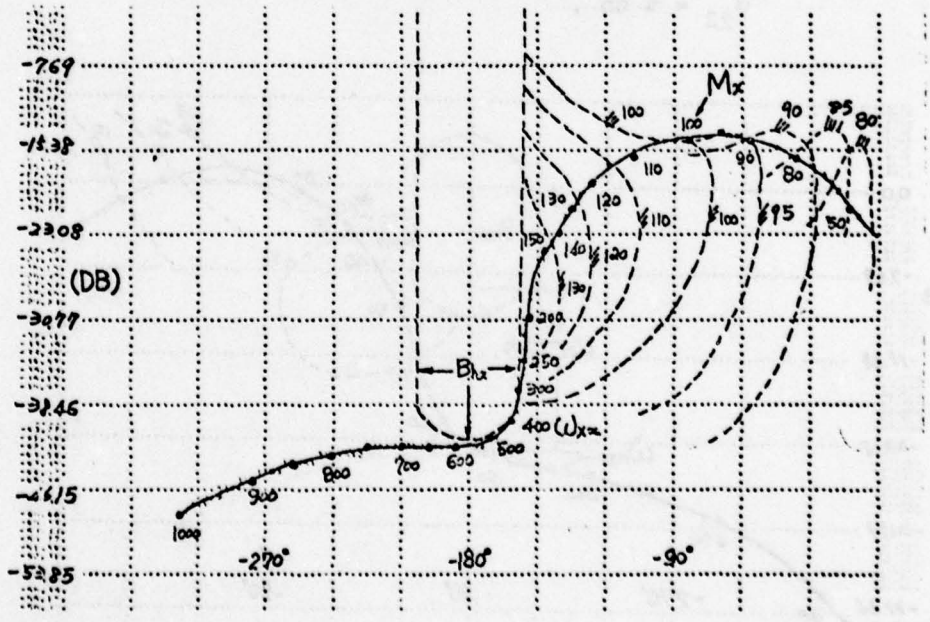

Figure 4-7a. Bounds and loop L_{x0} for α_{22} = 5 db .

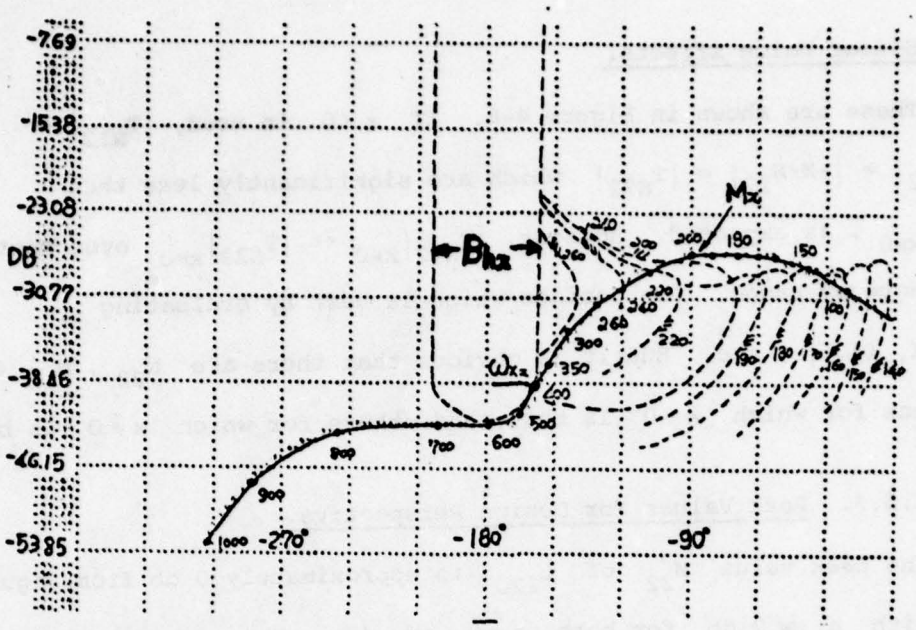

Figure 4-7b. Bounds and loop L_{x0} for α_{22} = 15 db .

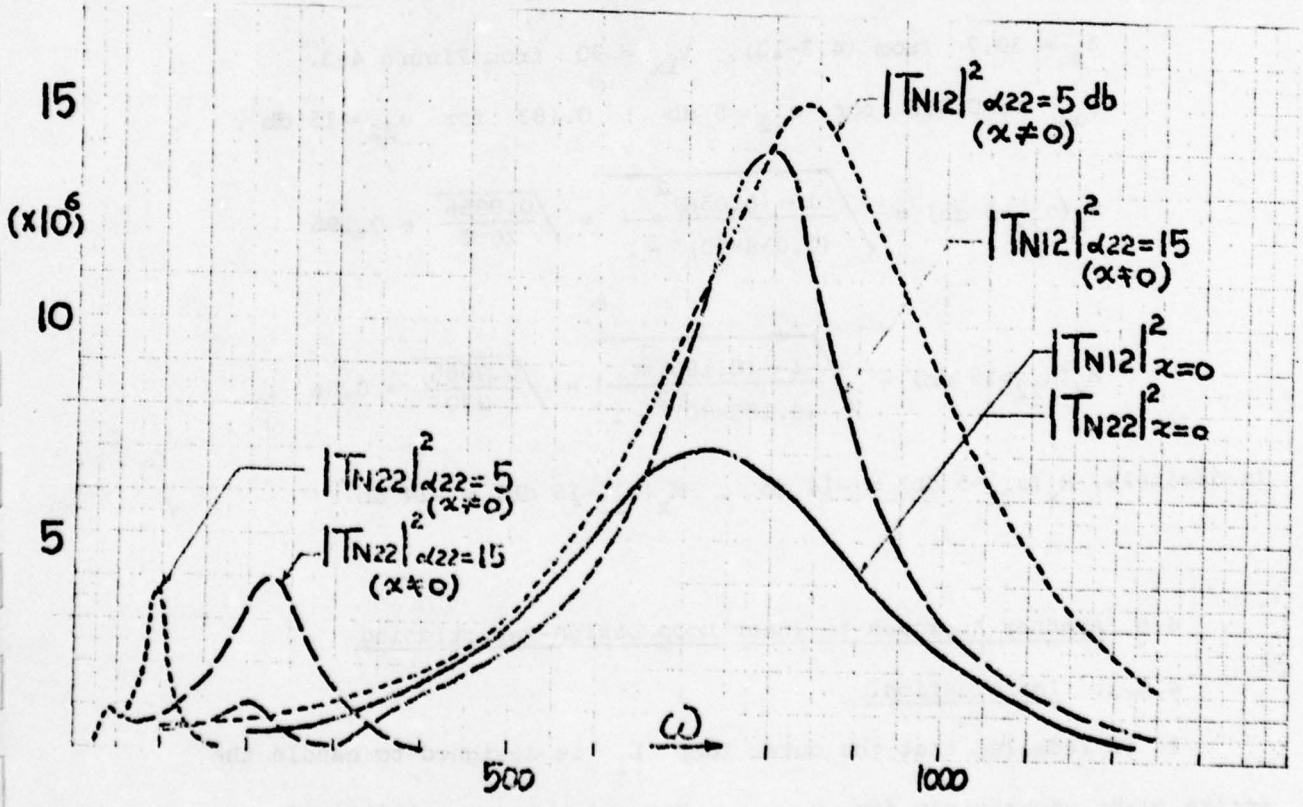

Figure 4-8. Sensor noise effects for different designs.

Sensor Noise Effects.

These are shown in Figure 4-8. If $x=0$ is used, $|T_{N12}| = |-X/N_{12}| = |-X/N_{22}| = |T_{N22}|$ which are significantly less than $|T_{N12}|_{x\neq 0}$, as expected. However, $|T_{N22}|_{x\neq 0} << |T_{N22}|_{x=0}$ over most of the frequency range. One decides which is best by evaluating $|T_{Nij}\ X_{ij}(j\omega)|$, etc. But it is obvious that there are N_{22}, N_{12} functions for which $x=0$ is best, and others for which $x\neq 0$ is best.

4.5.3. Peak Values for Design Perspective.

The peak value M_{22} of L_{220} is approximately 0 db from Figure 1-22, with $\alpha_1 \simeq 2$ db for both $x=0$ or $\neq 0$. The peak values M_x of L_{x0} are calculated from (2.A3-3) for different designs.

$\delta_s = 30.7$ from (4.3-13), $\lambda_{1x} = 90$ from Figure 4-3.

$\delta_{\alpha s}$ is 0.058 for $\alpha_{22}=5$ db ; 0.183 for $\alpha_{22}=15$ db .

$$M_x(\alpha_{22}=5\text{ db}) = \sqrt{\frac{1-(0.058)^2}{(0.058\times 90)^2-1}} = \sqrt{\frac{0.9966}{26.2}} = 0.195$$

$$M_x(\alpha_{22}=15\text{ db}) = \sqrt{\frac{1-(0.183)^2}{(0.183\times 90)^2-1}} = \sqrt{\frac{0.9665}{270}} = 0.06 \quad .$$

In decibels, $M_x(\alpha_{22}=5\text{ db}) \simeq -14$ db , $M_x(\alpha_{22}=15\text{ db}) \simeq -24$ db .

4.6 Another Approach to Inner Loop Design-Partitioning

4.6.1. Introduction.

It is recalled that the outer loop L_1 is designed to handle the entire plant uncertainty for $\omega \leq \omega_{x1}$, but only the uncertainty of

P_{11} , P_{21} for $\omega > \omega_{x1}$. The inner loops handle the uncertainty of P_{12} , P_{22} in $\omega > \omega_{x1}$. It was also shown in Section 4.3.1 that the inner loops may be designed at fixed (largest) values with $P_{11}G_{11} = b_{11}g_{11}$, $P_{21}G_{21} = p_{21}g_{21}$. This is retained in the present section. The new approach of this section is explained by means of Figure 4-9. At b_{11} , b_{21} , the outer loop is denoted by L_{1x} , and sketched in Figure 4-9. This L_{1x} is at fixed nominal values (a_{12} , a_{22}) of k_{11} , k_{22} . Due to the uncertainties $k_{11} \in [a_{11},b_{11}]$, $k_{22} \in [a_{22},b_{22}]$, L_{1x} will vary but g_{12} , g_{22} must be designed so that the resulting L_{1x} does not penetrate into γ_1 of Figure 4-9. We simply partition this reserve (between L_{1x} and γ_1), between L_{12} and L_{22} . $U_1V_1W_1,\ldots,U_4V_4W_4$ show four different partitions. The first inner loop is designed such that due to its plant uncertainty at fixed second inner loop, L_{1x} does not penetrate beyond $U_iV_iW_i$. Then the second inner loop is designed so that due to its uncertainties in both inner loops L_{1x} does not penetrate into γ_1 (and if there is also a constraint γ on the first inner loop, so that this constraint is also not violated). One may choose either (12) or (22) as the first inner loop. The definitions for the inner loops, different from those used previously, are:

$$L_{220} = P_{220}G_{22} \quad , \quad L_{120} = \frac{P_{120}G_{12}}{1 + L_{220}} \quad . \qquad (4.6\text{-}1a,b)$$

The noise effects at plant input X at nominal plant values, due to noise sources N_1 , N_{12} , N_{22} , are

$$-\frac{X}{N_1} = \frac{L_{10}/P_0}{1 + L_{10}} \quad , \quad -\frac{X}{N_{12}} = \frac{L_{120}/P_{120}}{(1+L_{120})(1+L_{10})} \qquad (4.6\text{-}2a,b)$$

$$-\frac{X}{N_{22}} = \frac{L_{220}/P_{220}}{(1+L_{220})(1+L_{120})(1+L_{10})} \quad . \tag{4.6-2c}$$

From (4.6-2b,c), to reduce effect $\left|\frac{X}{N_{i2}}\right|$, minimize the bandwidth of L_{i20}, i=1,2 .

4.6.2. First Inner Loop Design.

To minimize the bandwidth of L_{120}, $P_{22} = P_{220}$ is used, i.e. L_{120} handles the uncertainty in P_{12} only. Let

$$\lambda_{12} = \frac{P_{12}}{P_{120}} \quad , \tag{4.6-3}$$

$$L_1^1 \triangleq \frac{P_{12}P_{11x} + P_{220}P_{21x}}{1 + P_{220}G_{22} + P_{12}G_{12}} G_1 \triangleq P_e^1 \cdot G_1 \quad . \tag{4.6-4}$$

$$P_e^1 = \frac{\lambda_{12}P_{120}P_{11x} + P_{220}P_{21x}}{(1 + P_{220}G_{22})(1 + \lambda_{12}L_{120})} \quad . \tag{4.6-5}$$

Equation (4.6-5) is analogous to (2.3-2), with P_{120} here $\sim P_{a0}$ of (2.3-2), P_{11x} here $\sim P_b$ there, $P_{220}P_{21x}$ here $\sim P_c$ there, and λ_{12} here $\sim \lambda_1$ there. The design of L_{120} is therefore identical to that of L_{10} in Section 2.3.1, except that the constraint on L_1^1 here is the curve $U_iV_iW_iV_1'U_1'$, instead of γ_1 there.

4.6.3. Second Inner Loop Design.

The next step is to design G_{22} to handle the uncertain plant P_{22}, which was ignored in the design of L_{120}. Let

$$\lambda_{22} \triangleq P_{22}/P_{220} \quad , \tag{4.6-6}$$

then
$$L_1^2 \triangleq \frac{P_{21x}P_{22} + P_{12}P_{11x}}{1 + P_{22}G_{22} + P_{12}G_{12}} G_1 = \frac{\lambda_{22}P_{21x}P_{220} + \lambda_{12}P_{120}P_{11x}}{1 + \lambda_{22}L_{220} + \lambda_{12}(1+L_{220})L_{120}} G_1$$

$$\triangleq P_e^2 \cdot G_1 \quad . \tag{4.6-7}$$

L_{220} is designed so that L_1^2 does not penetrate into γ_1 over the range of λ_{12} , λ_{22} .

4.6.4. Design Example.

The same structure and specifications in Section 4.5 are used. The extra margin of the outer loop L_1 below B_{h1} is increased by 2 db, because of the present approach. The resulting L_{1x} (at $k_{11} = b_{11}$, $k_{21} = b_{21}$) is shown in Figure 4-9. L_{12} is taken as the first inner loop. Figures 4-10a-d show the bounds on L_{120} and the designed L_{120} for the 4 different $U_iV_iW_i$ cases in Figure 4-9. The corresponding bounds on L_{220} and resulting L_{220} are shown in Figures 4-11a-d (in which the bounds on θ_{m12} were not considered). Since the bounds on L_{220} for cases 1,3 are very close to those of cases 2,4 respectively, the same L_{220} is used for cases 1,2, and another one for cases 3,4. Bode plots of L_{1x} , L_{120} , L_{220} for all these cases are shown in Figure 4-12. The rational function values are given in Appendix 1 of this chapter. The sensor noise effects are shown in Figure 4-13.

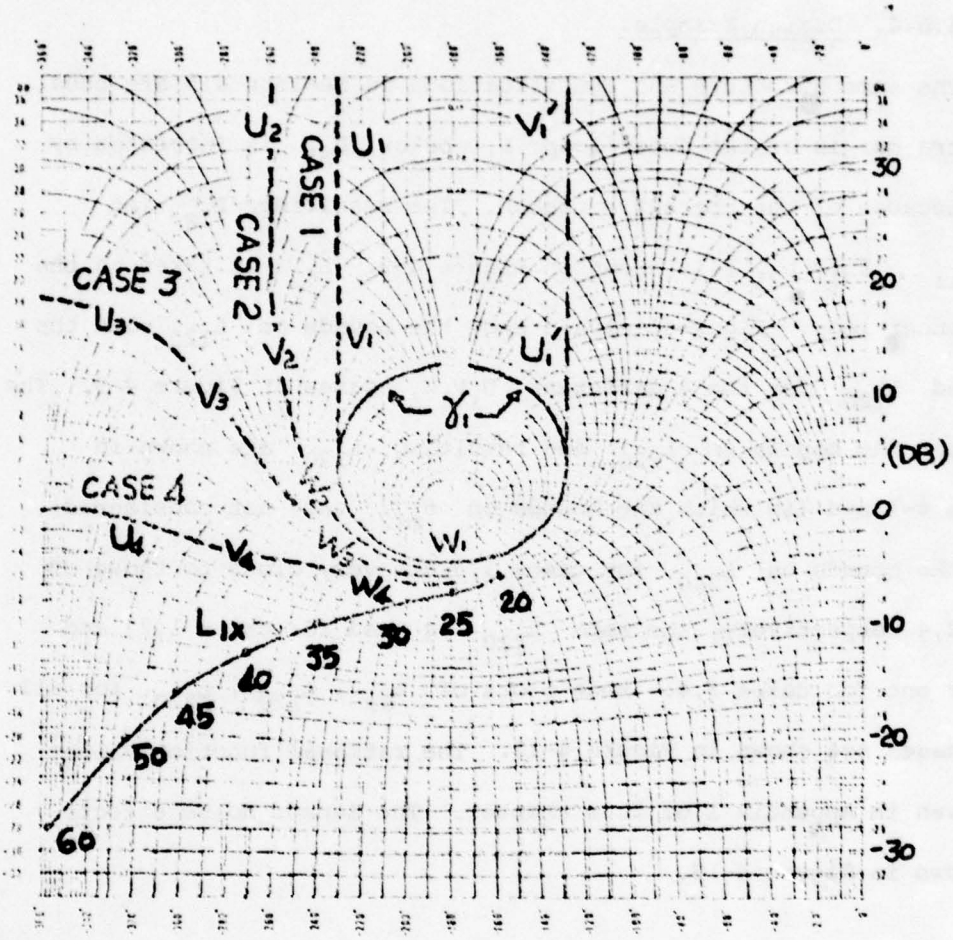

Figure 4-9. Partitioning of reserve between L_{12} and L_{22}.

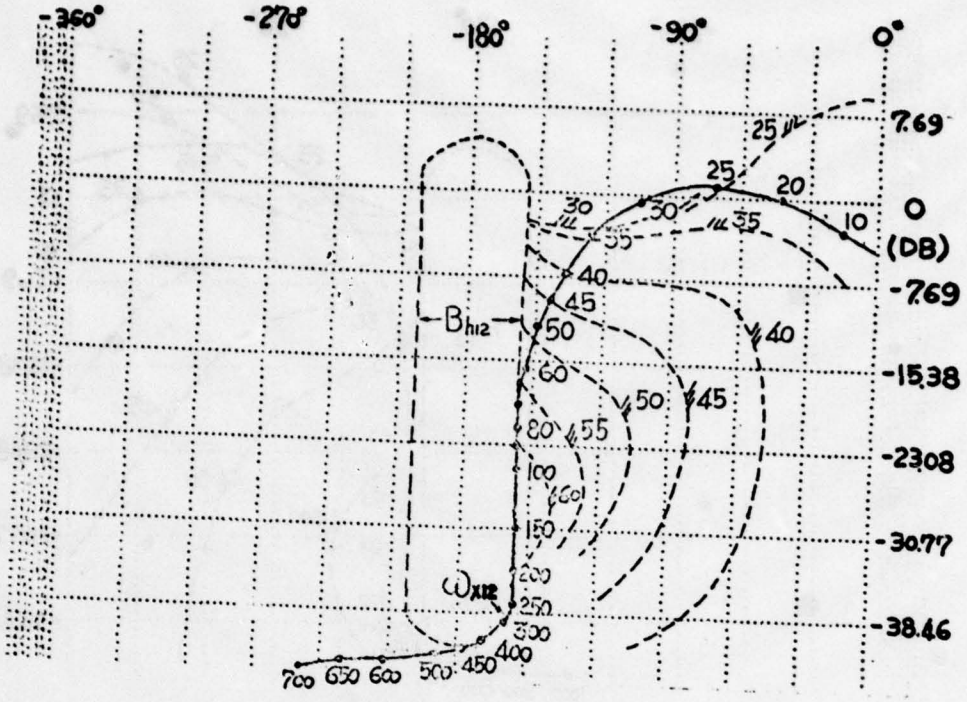

Figure 4-10a. Bounds and loop L_{120} (Case 1).

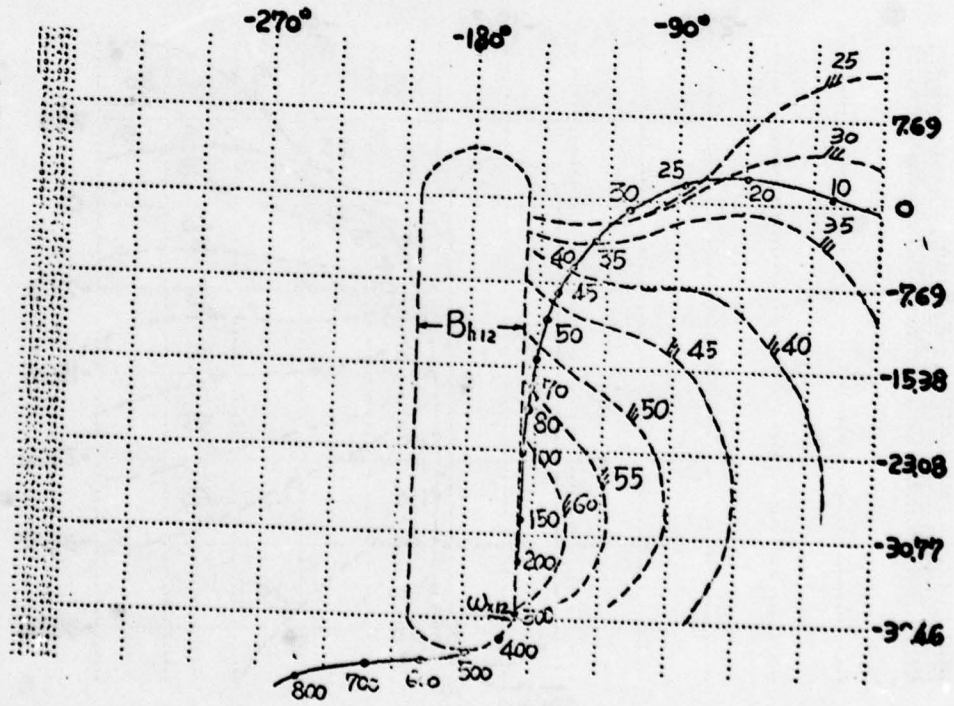

Figure 4-10b. Bounds and loop L_{120} (Case 2).

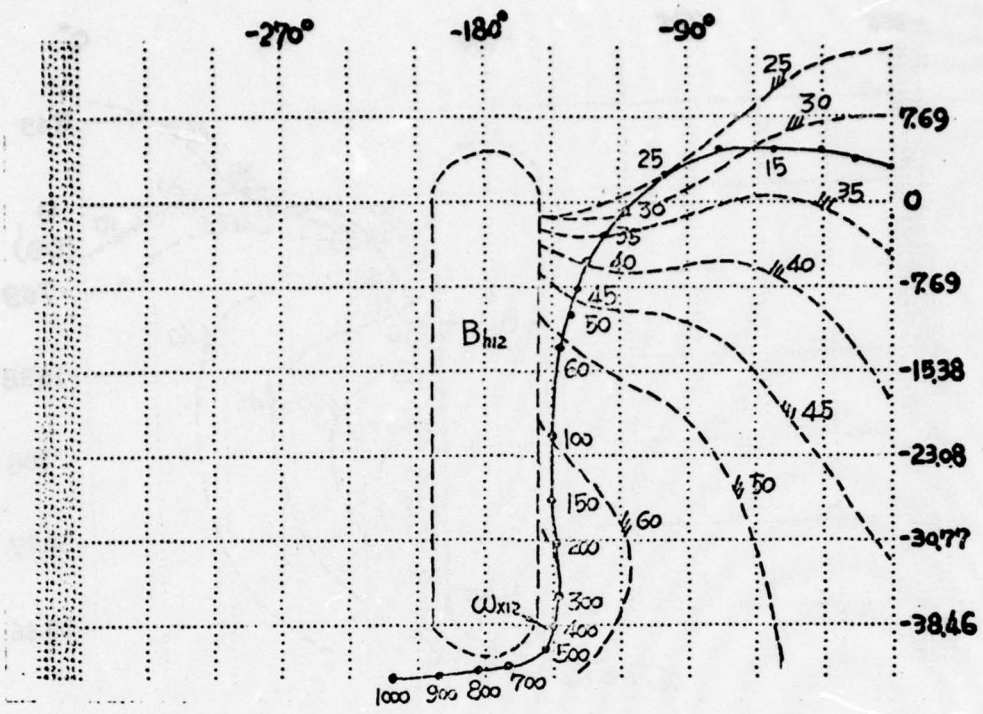

Figure 4-10c. Bounds and loop L_{120} (Case 3).

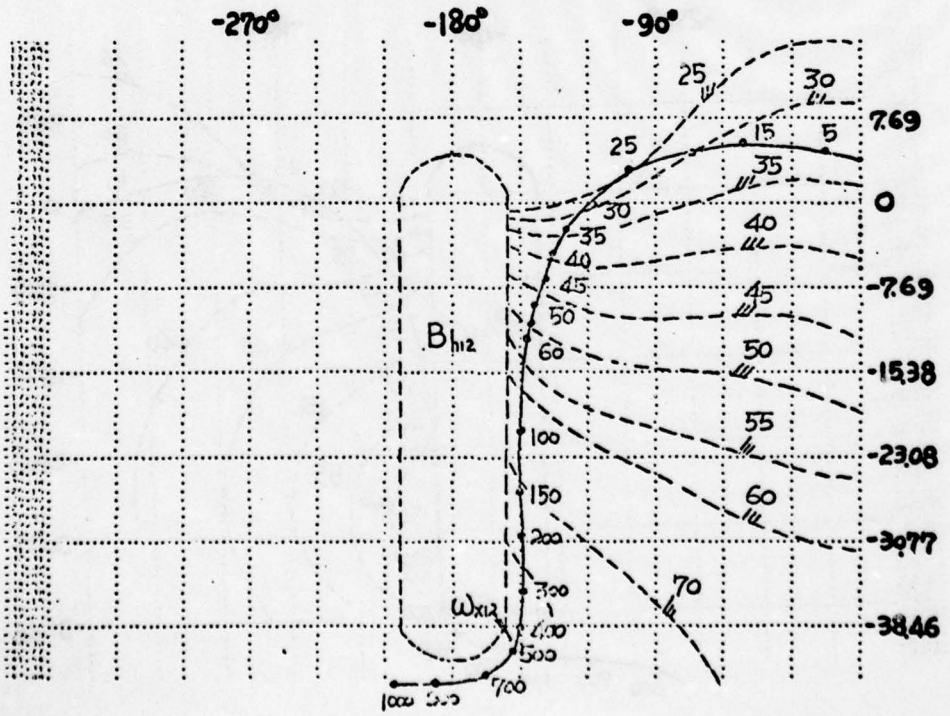

Figure 4-10d. Bounds and loop L_{120} (Case 4).

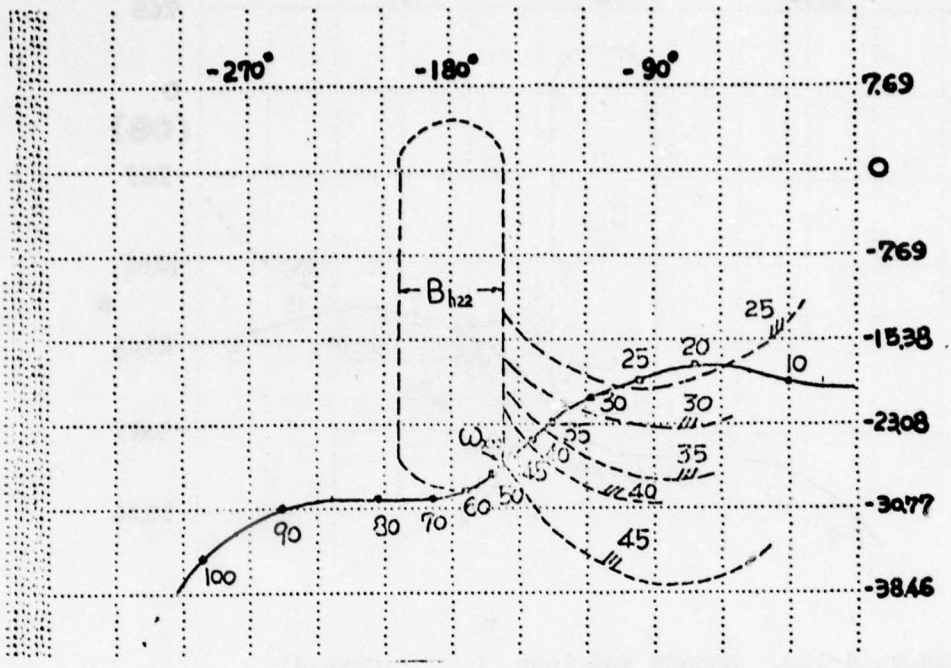

Figure 4-11a. Bounds and loop L_{220} (for Case 1).

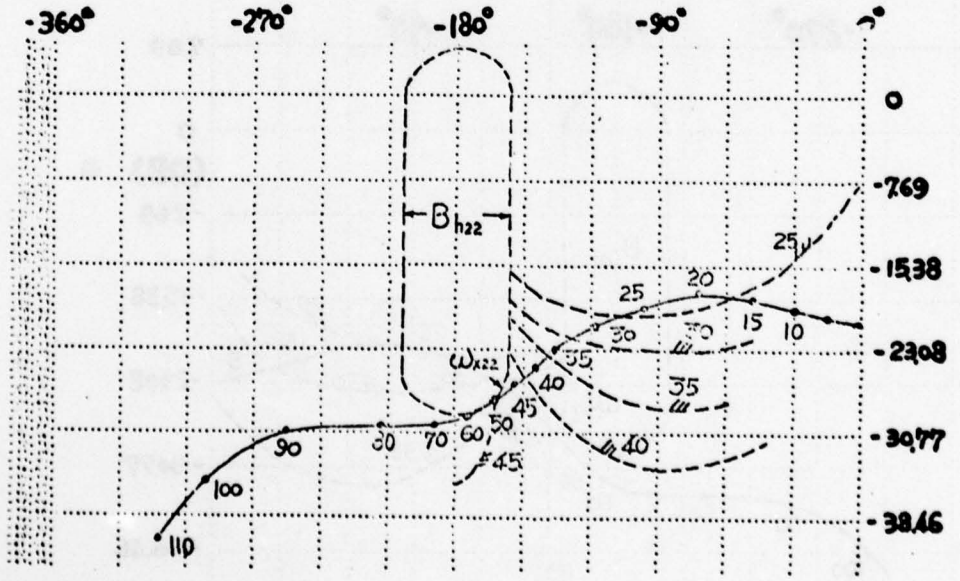

Figure 4-11b. Bounds and loop L_{220} (Case 2).

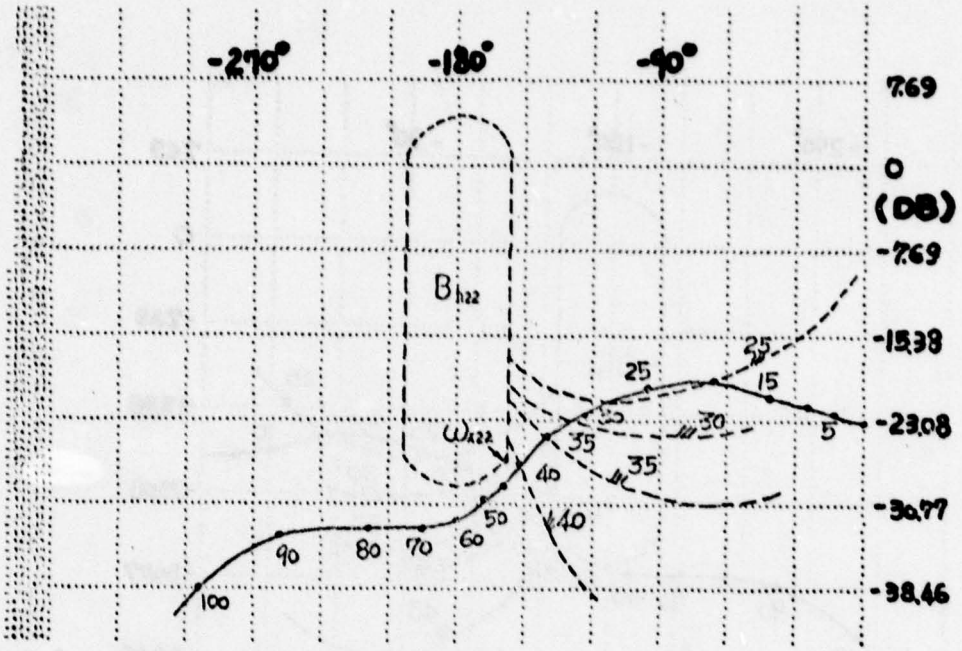

Figure 4-11d. Bounds and loop L_{220} (Case 4).

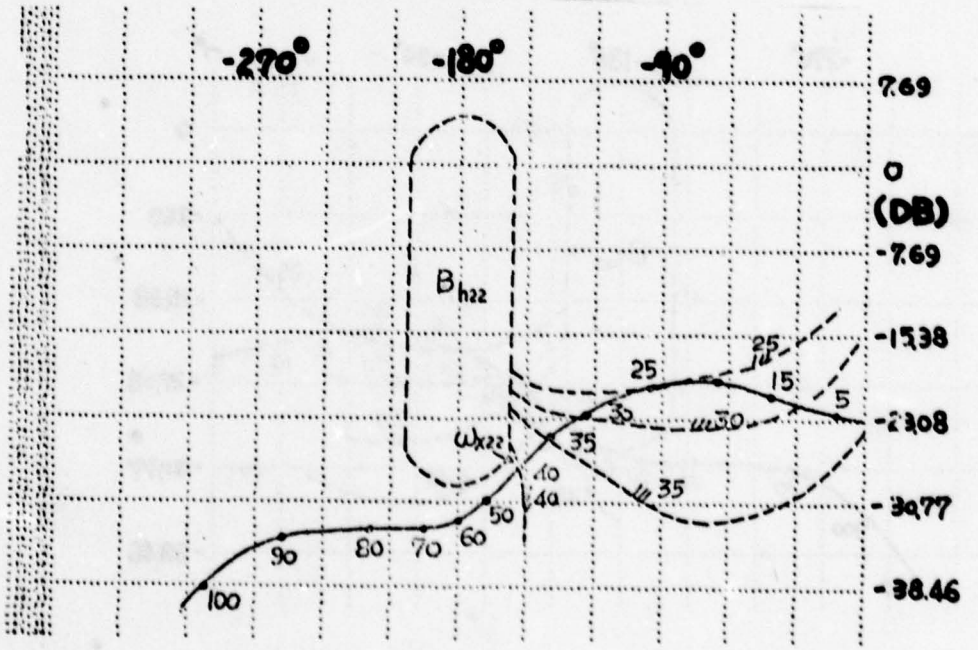

Figure 4-11c. Bounds and loop L_{220} (Case 3).

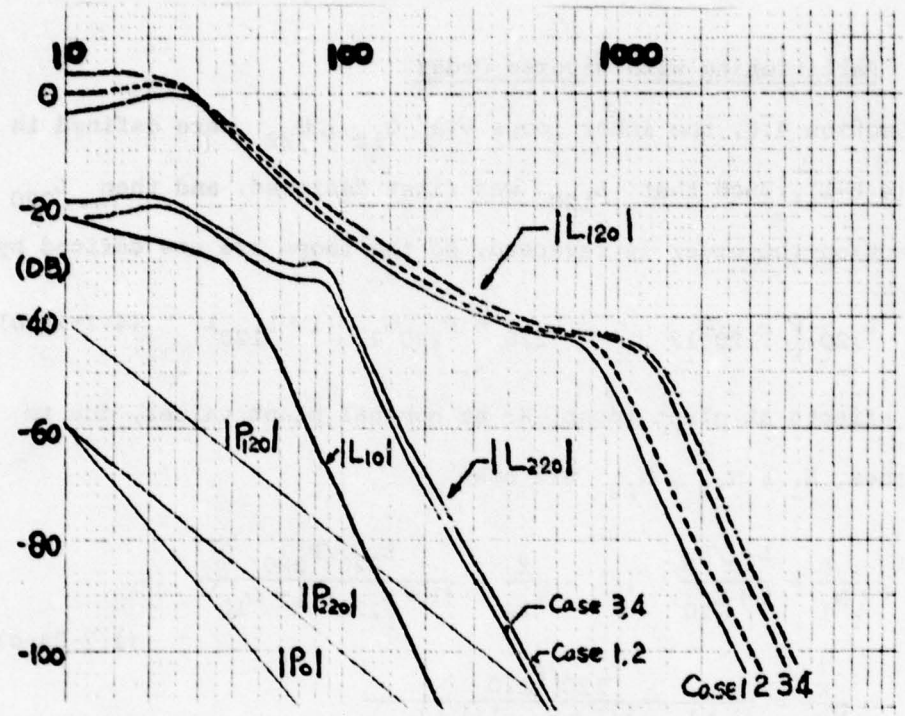

Figure 4-12. Bode plots of L_{10} , L_{120} , L_{220} .

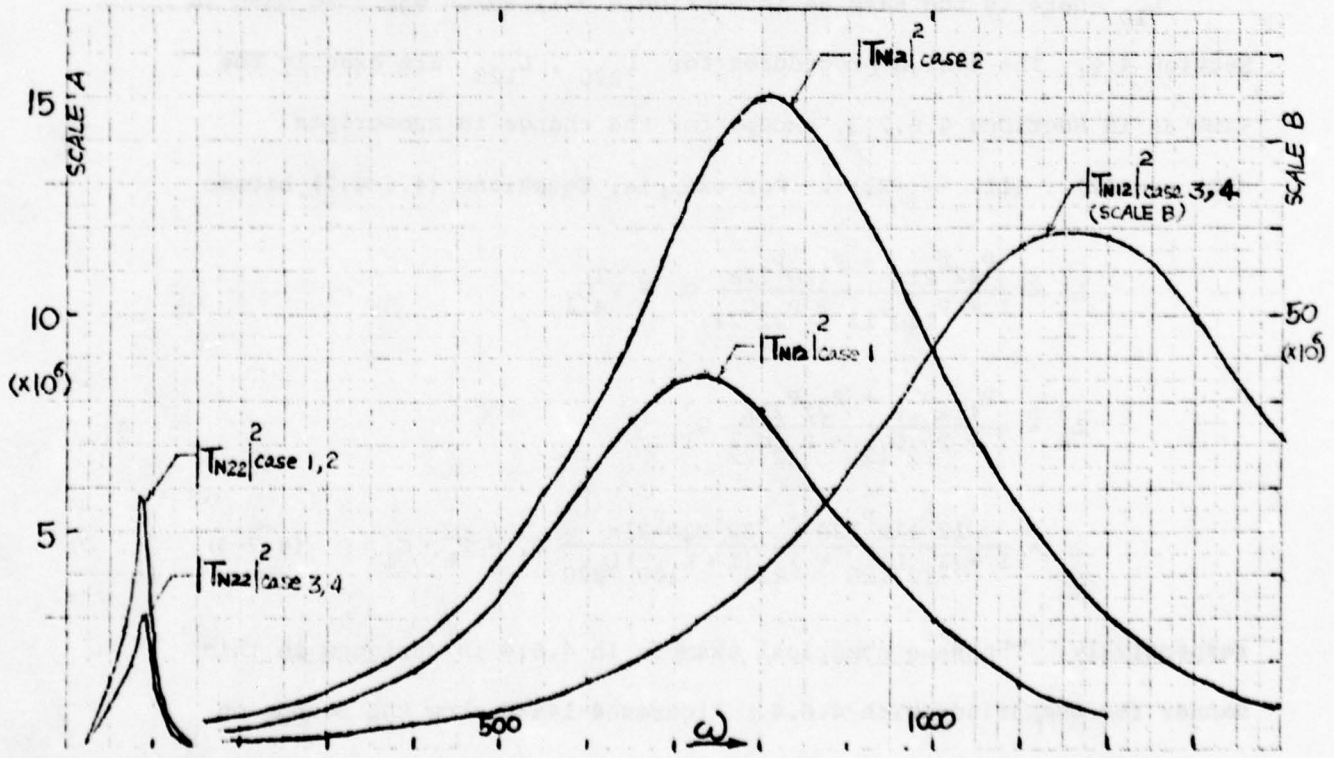

Figure 4-13. Sensor noise responses.

4.7 Partitioning with Reverse Order

In Section 4.6, the inner loops via G_{12} , G_{22} were defined in Equation (4.6-1), such that L_{120} was first designed, and then L_{220} . In this section the order is reversed, so the loops are now defined by

$$L_{120} = P_{120}G_{12} \quad , \quad L_{220} = P_{220}G_{22}/(1 + L_{120}) \qquad (4.7\text{-}1a,b)$$

The noise effects at plant input X at nominal plant values, due to noise sources N_1 , N_{12} , N_{22} are now

$$-\frac{X}{N_1} = \frac{L_{10}/P_0}{1 + L_{10}} \quad , \quad -\frac{X}{N_{22}} = \frac{L_{220}/P_{220}}{(1 + L_{220})(1 + L_{10})}$$

$$-\frac{X}{N_{12}} = \frac{L_{120}/P_{120}}{(1 + L_{120})(1 + L_{220})(1 + L_{10})} \qquad (4.7\text{-}2a\text{-}c)$$

L_{10} here is the same as in Section 4.5.1, which was also used in Section 4.6. The design procedures for L_{220} , L_{120} are exactly the same as in Sections 4.6.2,3, except for the change in subscripts (12) $\leftrightarrow$ (22) , (11) $\leftrightarrow$ (21) . For example, Equations (4.6-4,7) become

$$L_1^1 \triangleq \frac{P_{22}P_{21x} + P_{120}P_{11x}}{1 + P_{120}G_{12} + P_{22}G_{22}} G_1 \triangleq P_e^1 G_1$$

$$L_1^2 \triangleq \frac{P_{11x}P_{12} + P_{22}P_{21x}}{1 + P_{12}G_{12} + P_{22}G_{22}} G_1$$

$$= \frac{\lambda_{12}P_{11x}P_{120} + \lambda_{22}P_{220}P_{21x}}{1 + \lambda_{12}L_{120} + \lambda_{22}(1 + L_{120})L_{220}} G_1 \triangleq P_e^2 \cdot G_1 \qquad (4.7\text{-}3)$$

respectively. The same numerical example in 4.6.4 is designed in this manner for comparison with 4.6.4. Figures 4-14a-d show the bounds on L_{220} (designed first), with the resulting loop L_{220} for the 4 different $U_iV_iW_i$ cases of Figure 4-9. The corresponding bounds on L_{120} and

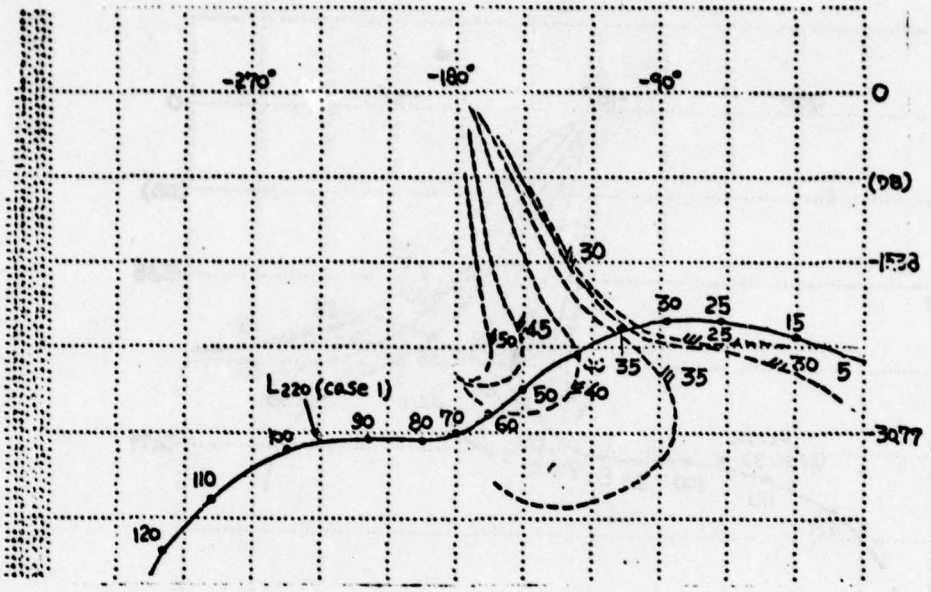

Figure 4-14a. Bounds and loop L_{220} (Case 1).

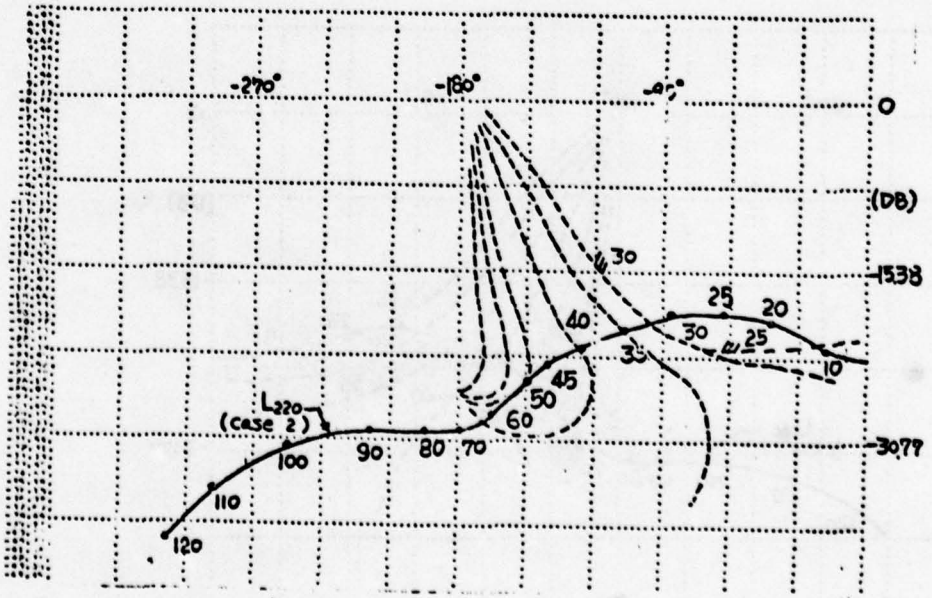

Figure 4-14b. Bounds and loop L_{220} (Case 2).

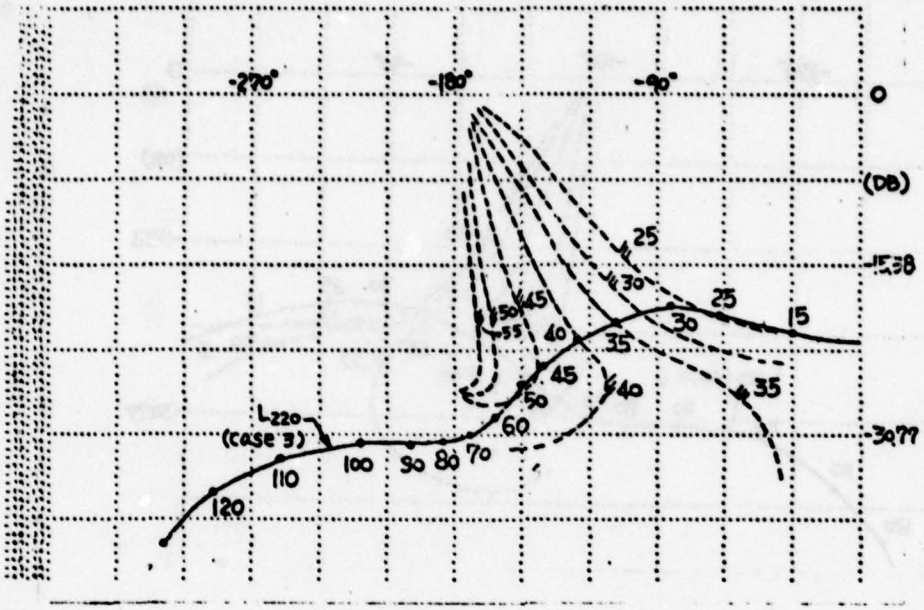

Figure 4-14c. Bounds and loop L_{220} (Case 3).

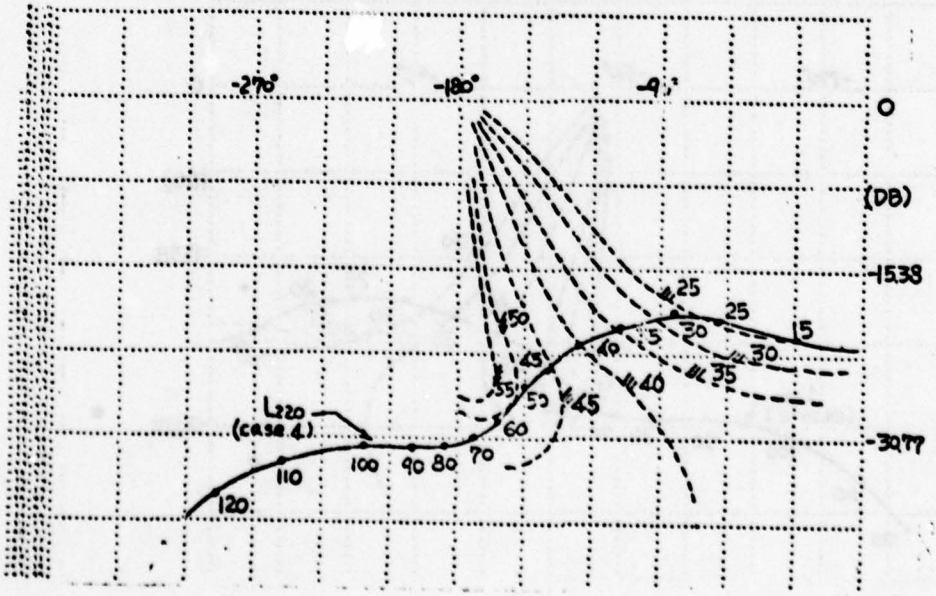

Figure 4-14d. Bounds and loop L_{220} (Case 4).

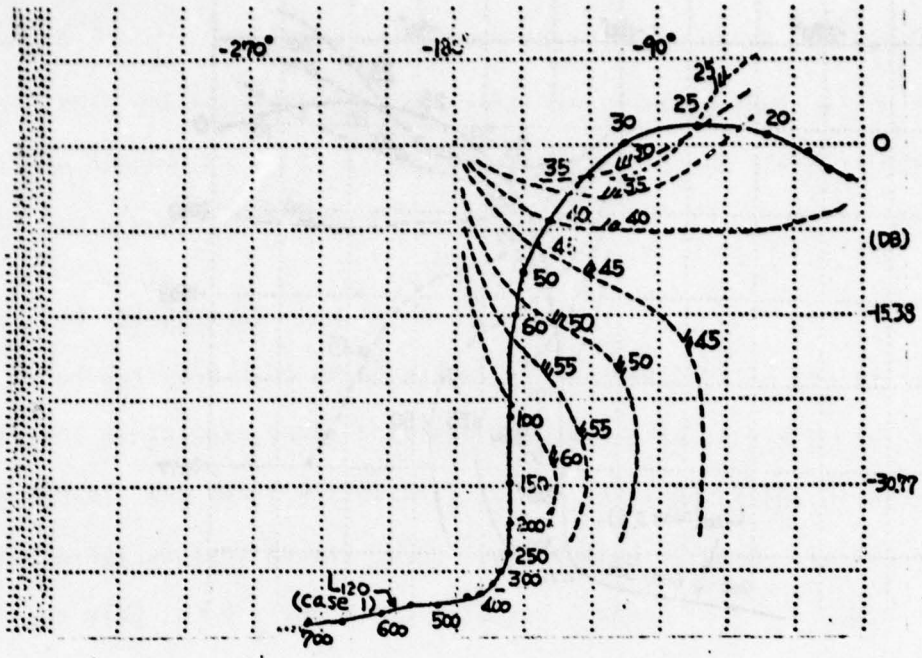

Figure 4-15a. Bounds and loop L_{120} (Case 1).

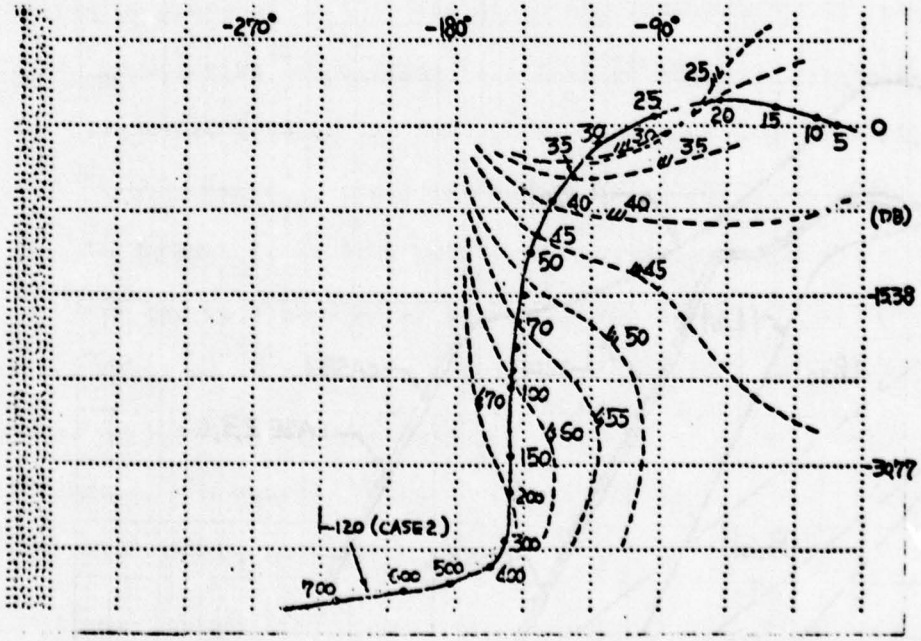

Figure 4-15b. Bounds and loop L_{120} (Case 2).

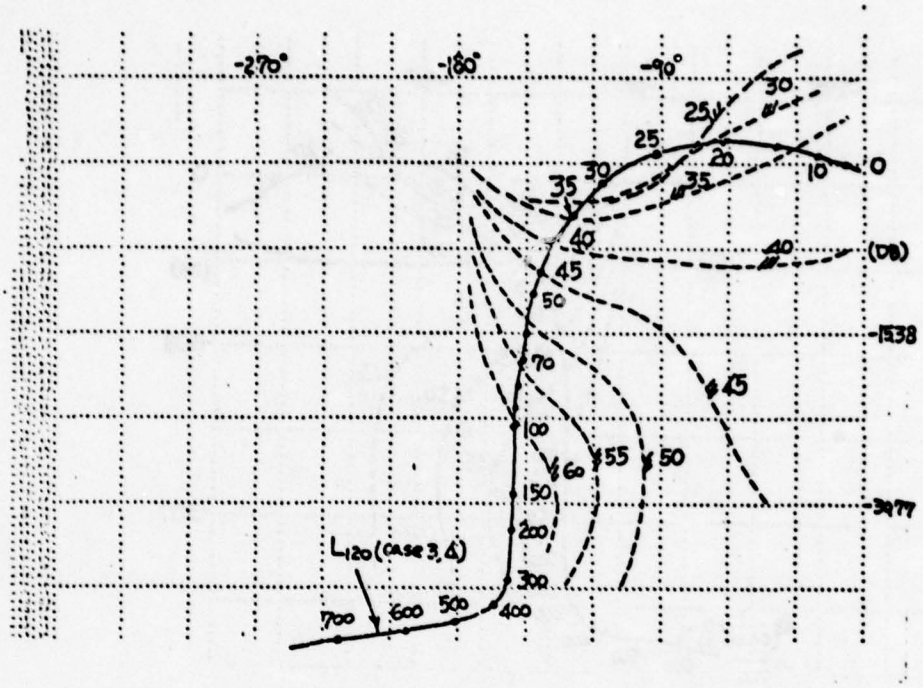

Figure 4-15c. Bounds and loop L_{120} (Cases 3,4).

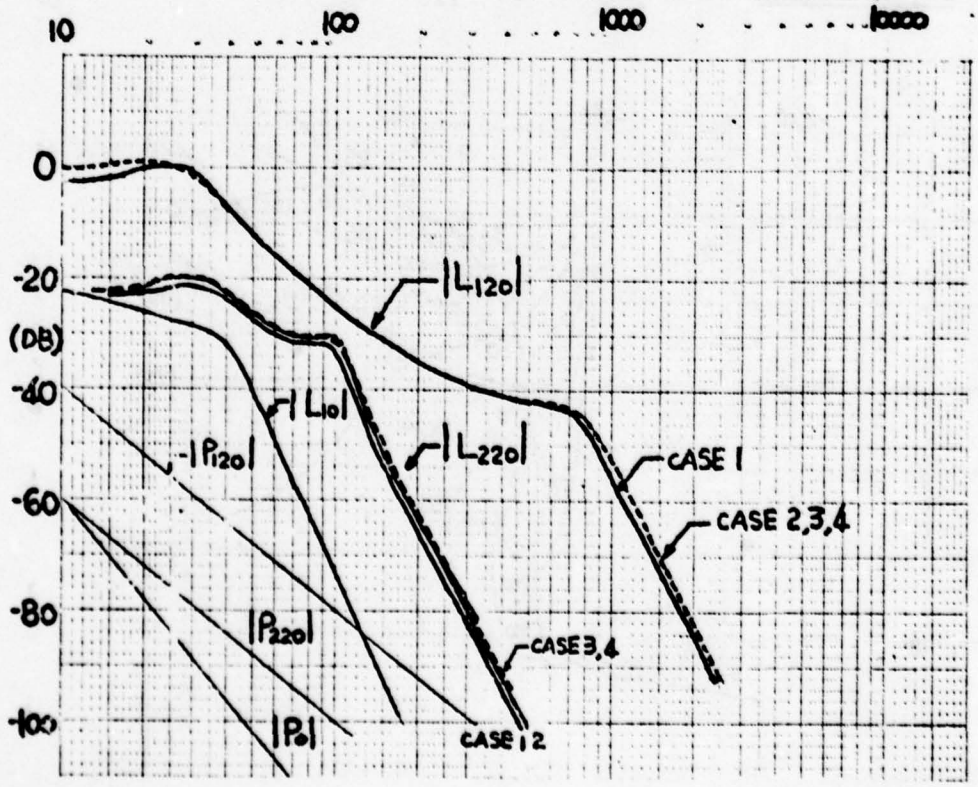

Figure 4-16. Bode plots of L_{10}, L_{120}, L_{220}.

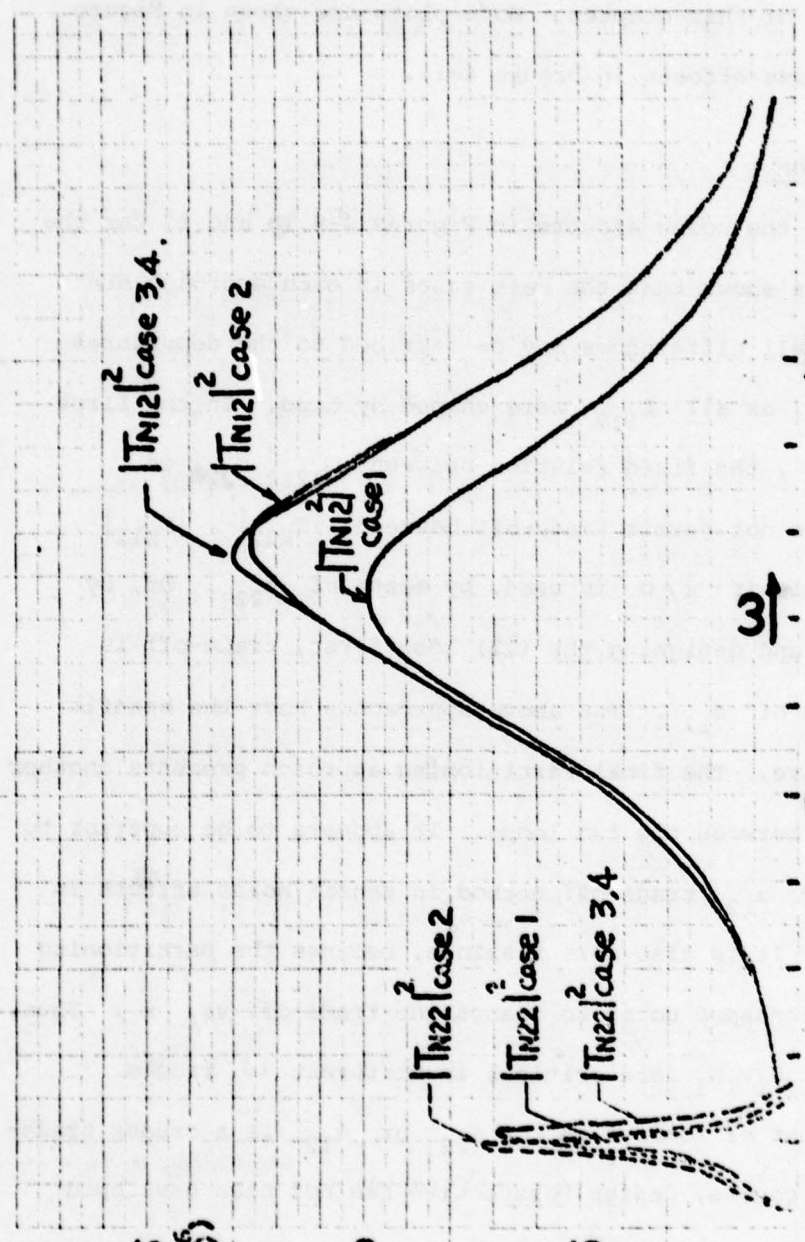

Figure 4-17. Sensor noise effects for different designs.

resulting L_{120} are shown in Figures 4-15a-c (in which the bounds on θ_{m22} were not considered). The rational function expressions are given in Appendix 1 of this chapter. Bode-plots are shown in Figure 4-16, and sensor noise effects in Figure 4-17.

4.8 Discussion

Comparison of the noise effects in Figures 4-8,13 and 17 for the different approaches shows that the best cases in each approach are very close. The small differences may be ascribed to the departures from optimal design, as all L_{ij0} were shaped by hand. In the first approach with $x \doteq 0$, the fixed relation between G_{12}, G_{22} in Equation 4.3-10 does not permit trade-off between $|T_{N22}|$, $|T_{N12}|$. Trade-off is possible if $x \neq 0$ is used, by means of α_{22}. Or, by changing the order and designing the (12) loop first, trade-off is achievable by means of α_{12}. The above approaches have the benefit of Design Perspective. The final Partitioning approach presents another means of trade-off between the two loops. It appears to be superior to the $x \neq 0$, α_{22} or α_{12} trade-off method in sensor noise effects in the example above. It is also more flexible, because the partitioning (Figure 4-9) may be shaped so as to change the trade-off vs. ω. Thus, different parts of $U_i V_i W_i$ are critical in different ω ranges. Obviously assignement of some value to α_{22} or α_{12} is a cruder trade-off technique. Of course, Design Perspective has not been developed for the Partitioning approach.

It must be admitted, however, that a more intensive study is needed of the various techniques in order to determine the best approach for any specific design problem. For example, in the numerical design

problem of Section 4.5, the much larger level of P_{12} vs. P_{22} is undoubtedly an important factor. Nevertheless, the techniques presented, especially Design Perspective, enable the designer to quickly try various designs.

Appendix 1

Rational Functions for the Various Designs.

The prefilter F and the outer loop L_{10} for all the different approaches are:

$$L_{10} = \frac{.2447 \times 10^7 (s^2 + 3.226s + 3.715)(1 + s/8)}{s[s^2 + 2.5682s + 3.1705][s^2 + 36.73s + 1645]^2 (1 + \frac{s}{5.6})}$$

$$F = \frac{.1861 \times 10^5 (s^4 + 29.17s^3 + 217.38s^2 + 764s + 947.33)}{s^7 + 778.16s^6 + 81823.65s^5 + .10123 \times 10^7 s^4 + .6277 \times 10^7 s^2 + \varphi}$$

$$\varphi = .16128 \times 10^8 s^2 + .2467 \times 10^8 s + .1756 \times 10^8$$

The transfer functions L_{220}, L_{x0} for Sections 4.3 to 4.5 are:

$$L_{220}(\alpha_{22}=5) = \frac{0.645(1 + \frac{s}{100})}{[1 + \frac{0.6s}{25} + (\frac{s}{25})^2][1 + \frac{0.3s}{100} + (\frac{s}{100})^2][1 + \frac{2s}{400} + (\frac{s}{400})^2]}$$

$$L_{220}(\alpha_{22}=15) = \frac{0.6(1 + \frac{s}{100})}{[1 + \frac{0.6s}{27} + (\frac{s}{27})^2][1 + \frac{0.8s}{250} + (\frac{s}{250})^2]^2}$$

$$L_{220}(\alpha_{22}=30) = \frac{0.6(1 + \frac{s}{210})(1 + \frac{s}{400})}{[1 + \frac{0.6s}{27} + (\frac{s}{27})^2](1 + \frac{s}{420})[1 + \frac{0.8s}{800} + (\frac{s}{800})^2]^2}$$

$$L_{x0}(\alpha_{22}=5) = \frac{0.07(1 + \frac{s}{800})(1 + \frac{s}{450})}{[1 + \frac{0.4s}{100} + (\frac{s}{100})^2](1 + \frac{s}{1600})[1 + \frac{0.7s}{900} + (\frac{s}{900})^2]^2}$$

The transfer functions L_{120}, L_{220} for Section 4.6 are:

Case 1. $$L_{120} = \frac{0.6(1 + \frac{s}{400})(1 + \frac{s}{210})}{[1 + \frac{0.6s}{27} + (\frac{s}{27})^2][1 + \frac{0.8s}{800} + (\frac{s}{800})^2]^2} \times \frac{1 + \frac{s}{210}}{1 + \frac{s}{420}}$$

$$L_{220} = \frac{0.1}{[1 + \frac{s}{25} + (\frac{s}{25})^2][1 + \frac{0.3s}{90} + (\frac{s}{90})^2]}$$

Case 2. $$L_{120} = \frac{0.9(1+\frac{s}{210})(1+\frac{s}{450})}{[1+\frac{0.8s}{25}+(\frac{s}{25})^2](1+\frac{s}{420})[1+\frac{0.8s}{900}+(\frac{s}{900})^2]^2}$$

$$L_{220} = L_{220} \text{ of Case 1.}$$

Case 3. $$L_{120} = \frac{1.44(1+\frac{s}{170})(1+\frac{s}{500})}{[1+\frac{s}{22}+(\frac{s}{22})^2](1+\frac{s}{340})[1+\frac{0.7s}{1250}+(\frac{s}{1250})^2]^2}$$

$$L_{220} = \frac{0.07}{[1+\frac{0.8s}{25}+(\frac{s}{25})^2][1+\frac{0.3s}{90}+(\frac{s}{90})^2]}$$

Case 4. $$L_{120} = \frac{1.56(1+\frac{s}{170})(1+\frac{s}{550})}{[1+\frac{s}{22}+(\frac{s}{22})^2](1+\frac{s}{340})[1+\frac{0.7s}{1350}+(\frac{s}{1350})^2]^2}$$

$$L_{220} = L_{220} \text{ of Case 3.}$$

The transfer functions L_{220} , L_{120} for Section 4.7 are:

Case 1. $$L_{220} = \frac{0.06}{[1+\frac{0.8s}{32.5}+(\frac{s}{32.5})^2][1+\frac{0.3s}{100}+(\frac{s}{100})^2]}$$

$$L_{120} = \frac{0.645(1+\frac{s}{400})(1+\frac{s}{210})}{[1+\frac{0.6s}{27}+(\frac{s}{27})^2][1+\frac{0.8s}{800}+(\frac{s}{800})^2]^2} \times \frac{(1+\frac{s}{210})}{(1+\frac{s}{420})}$$

Case 2. $$L_{220} = \frac{0.07}{[1+\frac{0.8s}{32.5}+(\frac{s}{32.5})^2][1+\frac{0.3s}{100}+(\frac{s}{100})^2]}$$

$$L_{120} = \frac{0.9(1+\frac{s}{200})(1+\frac{s}{428})}{[1+\frac{0.8s}{24}+(\frac{s}{24})^2](1+\frac{s}{400})[1+\frac{0.8s}{855}+(\frac{s}{855})^2]^2}$$

Cases 3,4. $$L_{220} = \frac{0.07}{[1+\frac{0.8s}{32.5}+(\frac{s}{32.5})^2][1+\frac{0.3s}{110}+(\frac{s}{110})^2]}$$

$$L_{120} = L_{120} \text{ of Case 2.}$$

CHAPTER 5

THE GENERAL PARALLEL CASCADED PLANT STRUCTURE

5.1 Introduction

Previous chapters presented quantitative synthesis techniques for the structures of Figures 2-1, 3-1 and 4-1a, with detailed examples.

The final objective is to develop a quantitative synthesis technique for the more complex and general structure of Figure 1-14, which is redrawn here as Figure 5-1a. There are m parallel branches. Branch one has n_1 cascaded plant sections, etc., and branch m has n_m cascaded sections, so that there is a total of $1 + \sum_{i=1}^{m} (n_i - 1)$ possible independent feedback loops. Each plant P_{ij} has its given parameter uncertainties with the known ranges. The objectives, as before, are to satisfy specifications of the form (2.2-1,2), for each $P_{ij} \in \mathcal{P}_{ij}$. The feedback compensation functions are to be chosen to satisfy those objectives despite the uncertainty, but to do so with minimum net effect of the sensor noise sources N, N_{ij} at the plant input Y. It is obvious that no analytical solution is available for this highly complex problem. A transparent design theory which gives the designer a great deal of insight into the trade-offs has been developed. Furthermore, as before, this insight is available without a detailed design. This design theory will be recognized as based upon the work of previous chapters, especially Chapters 2,4.

5.2 Design of Outer Loop

The design technique is developed by means of a specific example in Figure 5-1a, $m=4$, $n_1=n_2=2$, $n_3=n_4=3$, giving Figure 5-1b. Let

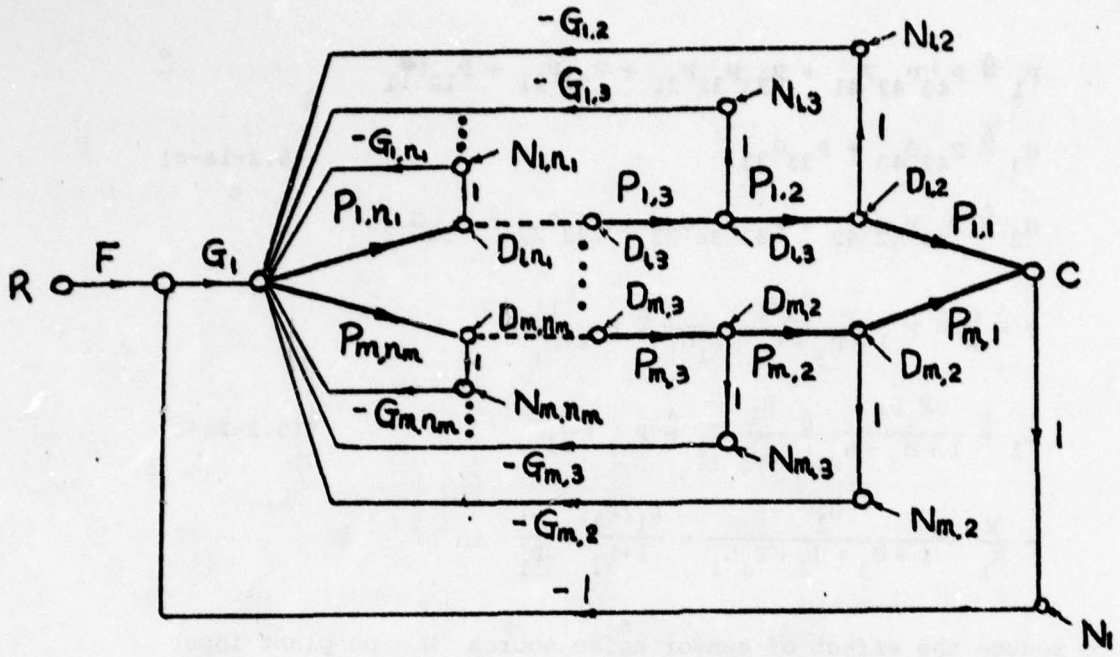

Figure 5-1a. General parallel cascaded plant structure.

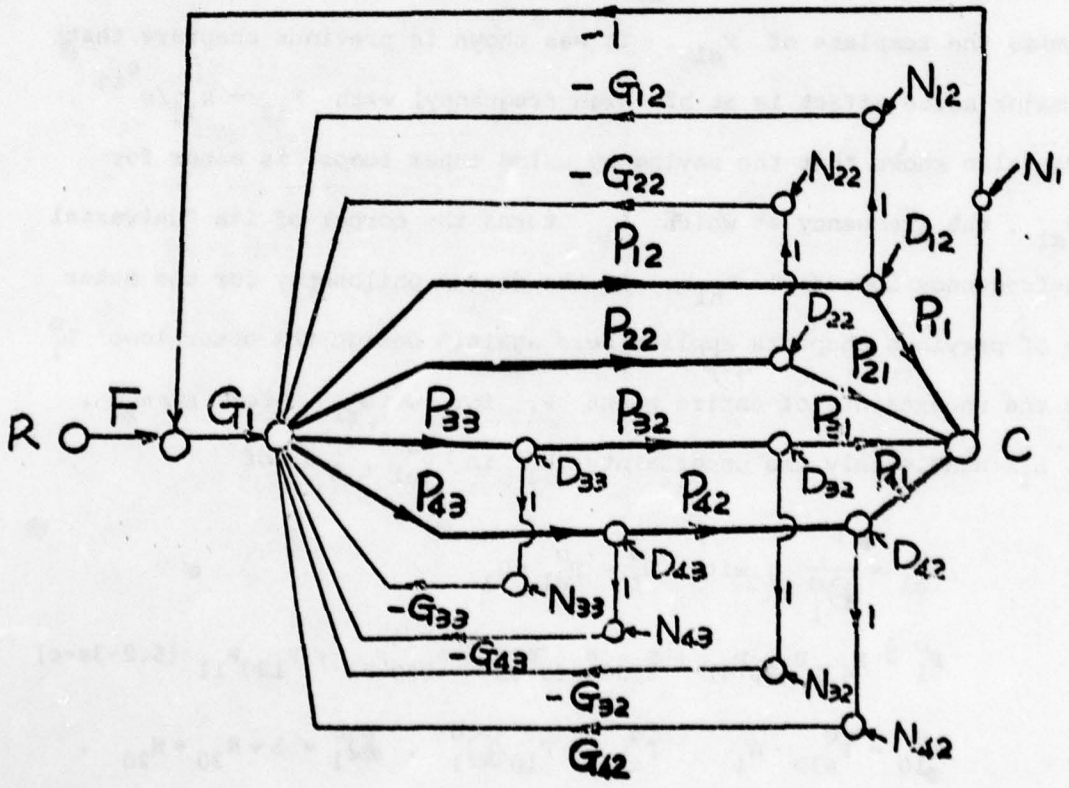

Figure 5-1b. System structure for design example.

$$P_1 \triangleq P_{43}P_{42}P_{41} + P_{33}P_{32}P_{31} + P_{22}P_{21} + P_{12}P_{11}$$

$$H_3 \triangleq P_{43}G_{43} + P_{33}G_{33} \qquad (5.2\text{-}1a\text{-}c)$$

$$H_2 \triangleq P_{43}P_{42}G_{42} + P_{33}P_{32}G_{32} + P_{22}G_{22} + P_{12}G_{12}$$

then $$T \triangleq \frac{C}{R} \triangleq F\,\frac{P_1G_1}{1+H_3+H_2+P_1G_1} \triangleq F\,\frac{L_1}{1+L_1}$$

$$L_1 \triangleq \frac{P_1G_1}{1+H_3+H_2} \triangleq \frac{P_1}{\mathcal{Q}_1}G_1 \triangleq P_{e1}\cdot G_1 \qquad (5.2\text{-}2a\text{-}c)$$

$$-\frac{X}{N_1} = \frac{G_1}{1+H_3+H_2+P_1G_1} = \frac{L_1/P_1}{1+L_1} \doteq \frac{L_1}{P_1} \text{ in hf.}$$

Hence, to reduce the effect of sensor noise source N_1 on plant input X, minimize the bandwidth of L_1. From Equation (5.2-2b), L_1 should cope with the uncertainty of P_{e1}. To minimize the bandwidth of L_1, minimize the template of P_{e1}. It was shown in previous chapters that the major noise effect is at hf (high frequency) with $P_{ij} \to k_{ij}/s^{e_{ij}}$. It was also shown that the saving by using inner loops, is minor for $\omega < \omega_{x1}$, the frequency at which L_{10} turns the corner of its "universal high-frequency boundary" B_{h1}. So the design philosophy for the outer loop of previous chapters applies here again: Design the outer loop L_1^o with the uncertainty of entire plant P_1 for $\omega < \omega_{x1}$. For $\omega \geq \omega_{x1}$, let L_1^o handle only the uncertainty U_1^o in P_{e1}^o, i.e. of

$$P_{e1}^o = \frac{P_1^o}{\mathcal{Q}_1^o}, \text{ with } L_1^o = P_{e1}^o \cdot G_1$$

$$P_1^o \triangleq P_{430}P_{420}P_{41} + P_{330}P_{320}P_{31} + P_{220}P_{21} + P_{120}P_{11} \qquad (5.2\text{-}3a\text{-}c)$$

$$L_{10}^o = P_{e10}^o \cdot G_1, \quad P_{e10}^o = P_{10}/\mathcal{Q}_1^o, \quad \mathcal{Q}_1^o = 1 + H_{30} + H_{20}.$$

This gives a much more economical outer loop L_{10}^o than that (L_{s0}) of

single-loop design, which must handle the entire P_1 uncertainty for all ω. Thus, in the design example below L_{s0} must handle P_1 uncertainty U_1 of 54.5 db, whereas L_{10} need handle uncertainty U_1^o of 5.2-3c only, which is 20 db.

Numerical Example

A) Problem statement

(a) System structure: In Figure 5-1a, let $m=4$, $n_1=n_2=2$, $n_3=n_4=3$, giving Figure 5-1b.

(b) Plant: $P_{12} = \dfrac{k_{12}}{S(1+S/A)}$, $P_{11} = \dfrac{k_{11}}{S}$,

$P_{22} = \dfrac{k_{22}}{S}$, $P_{21} = \dfrac{k_{21}(1+S/z)}{S(S^2+BS+C)}$,

$P_{ij} = \dfrac{k_{ij}}{S}$, $i = 3,4$, $j = 1,2,3$.

(c) Plant Uncertainty: $k_{11}, k_{21} \in [4,40]$

$k_{12}, k_{22} \in [25,750]$

$k_{31}, k_{41} \in [4,20]$

$k_{32}, k_{42} \in [5,40]$

$k_{33}, k_{43} \in [5,75]$

$A \in [1,2]$, $z \in [1,2]$, $B \in [0,1]$,

$C \in [0.04,1]$.

B) Specifications

(a) Bounds on unit step response $C(t)$: The same as shown in Figure 4-1b.

(b) Bounds on $|T(j\omega)|$: Shown in Figure 4-1c were derived from time domain bounds of Figure 4-1b.

(c) Disturbance Response: $\left|\dfrac{L}{1+L}\right| \leq 2.3$ db.

The resulting L_{10}^{o} and L_{s0} in the Nichols chart are shown in Figure 5-2a, their Bode plots are shown in Figure 5-2b. The rational functions of L_{s0}, L_{10} with same prefilter F are:

$$F_1 = \frac{(1 + S/8)}{(1 + S/2)^2 (1 + S/3)}$$

$$L_{s0} = \frac{2.2(1 + S/0.5)(1 + S/100)(1 + S/30)(1 + S/4200)}{S^2(1 + S/20)(1 + S/1000)(1 + S/45)[1 + 0.5s/2800 + (S/2800)^2]^2}$$

$$L_{10} = \frac{2.2(1 + S/0.5)(1 + S/100)(1 + S/30)}{S^2(1 + S/20)[1 + 0.7S/115 + (S/115)^2]^2(1 + S/45)(1 + S/1000)}$$

The noise effects $\left|\frac{X}{N_1}\right|_S$, $\left|\frac{X}{N_1}\right|_{II,III}$ at plant input X at nominal plant values due to noise source N_1 for both single-loop and multiple-loop designs are shown in Figure 5.5.

5.3 Design of Inner Loops

5.3.1. Design of the First Inner Loops.

The next step is obviously to allow for the uncertainty in P_{i2} (i = 1,2,3,4) to be handled by the loops via G_{i2}. For this purpose, let

$$P_2^o \triangleq P_{430}P_{42}P_{41} + P_{330}P_{32}P_{31} + P_{22}P_{21} + P_{12}P_{11}$$

$$H_2^o \triangleq P_{430}P_{42}G_{42} + P_{330}P_{32}G_{32} + P_{22}G_{22} + P_{12}G_{12} \qquad (5.3\text{-}1a\text{-}c)$$

$$H_{30} \triangleq P_{430}G_{43} + P_{330}G_{33}$$

$$L_1^1 = \frac{P_2^o G_1}{1 + H_{30} + H_2^o} = \frac{P_2^o G_1}{(1 + H_{30})(1 + L_2^o)}$$

$$L_2^o \triangleq \frac{H_2^o}{1 + H_{30}} \triangleq \frac{H_2^o}{\Delta_2^o} \quad , \quad L_{20}^o = \frac{H_{20}^o}{1 + H_{30}} \qquad (5.3\text{-}2a\text{-}c)$$

$$-\frac{X}{N_{i2}} = \frac{G_{i2}}{1 + H_{30} + H_{20} + P_{10}G_1} = \frac{P_{i1x}L_{20}^o/P_{2x0}^o}{(1 + L_{20}^o)(1 + L_{10}^o)} \qquad (5.3\text{-}3)$$

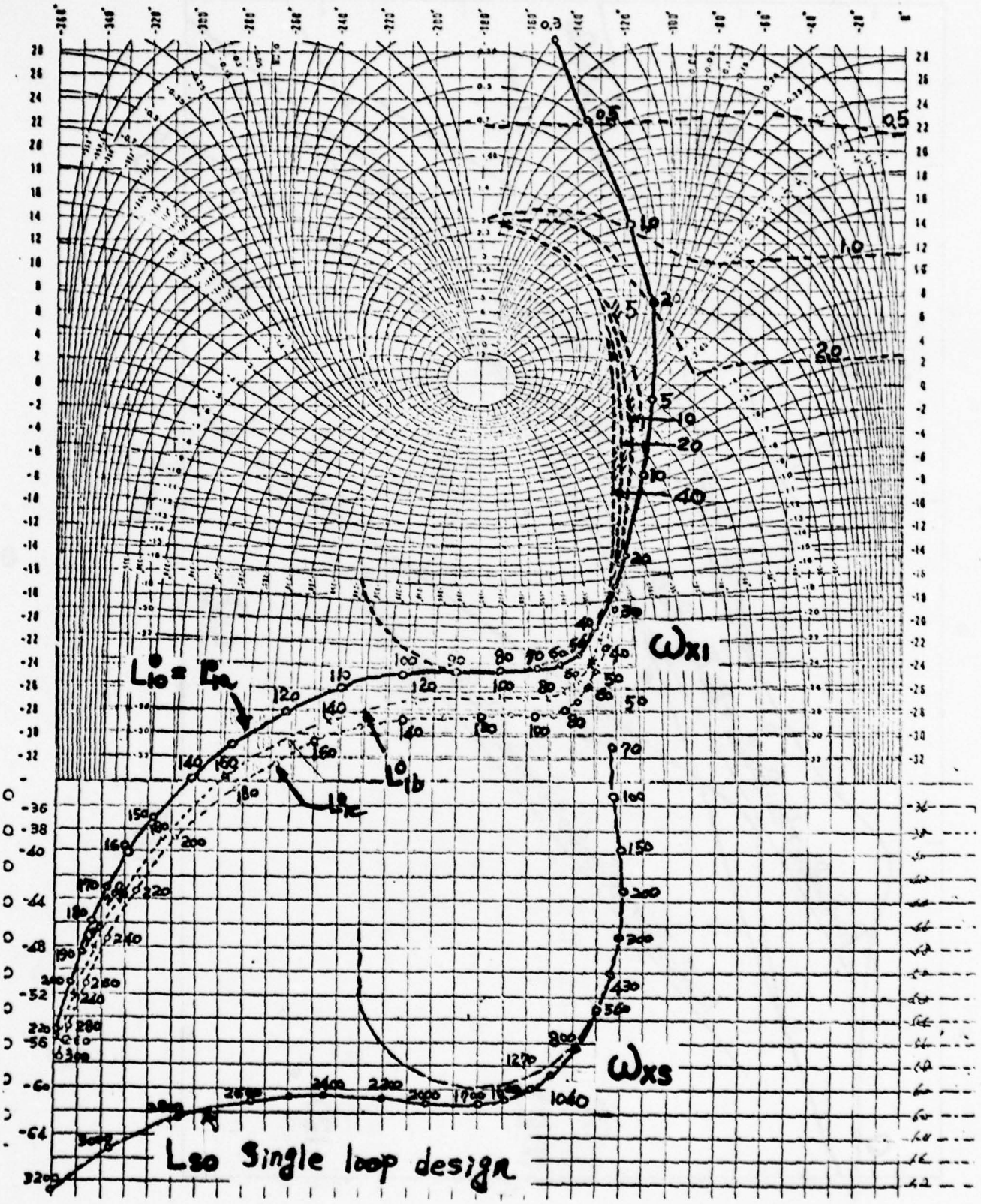

Figure 5-2a. L_{s0} , L_{10} and bounds.

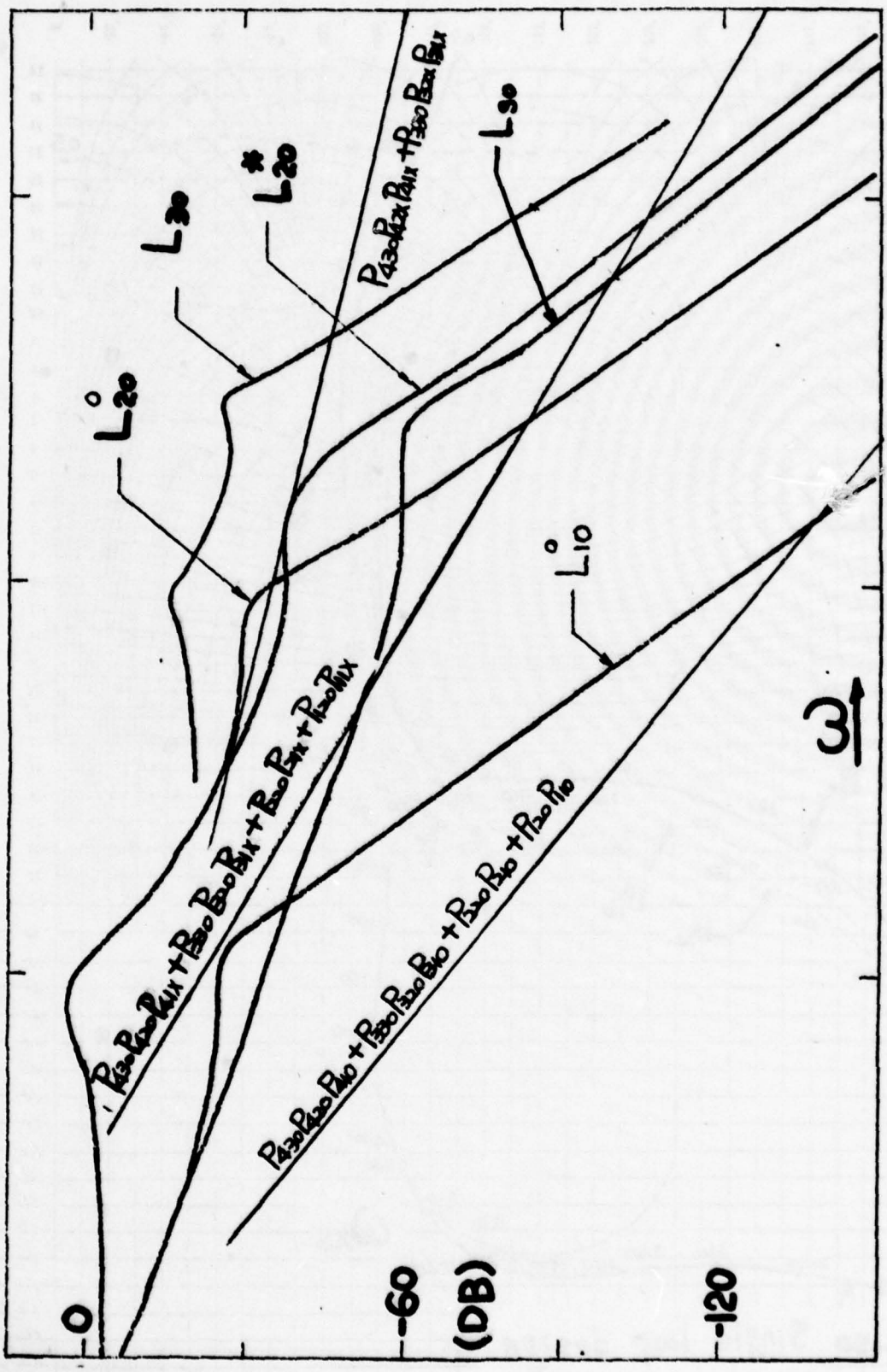

Figure 5-2a. Bode plots of significant loop and plant functions.

(with $P^{o}_{e20} = P^{o}_{e2}$ of Equation 5.3-5 at $P_{i2} = P_{i20}$ for $i \in [1,4]$).

At this point, we can use any of the techniques developed in Chapter 4. We choose, because of its simplicity, the method of Section 4.3.1, i.e. let

$$G_{i2} = P_{i1x}G_2 \quad \text{for} \quad i = 1,2,3,4 \quad , \tag{5.3-4}$$

where at hf, $P_{i1x}G_2 = (b_{i1}/S^{e_{i1}})G_2 \triangleq b_{i1}g_2$. Then

$$L^{o}_2 \triangleq \frac{(P_{430}P_{42}P_{41x} + P_{330}P_{32}P_{31x} + P_{22}P_{21x} + P_{12}P_{11x})G_2}{1 + H_{30}}$$

$$\triangleq P^{o}_{2x}G_2/\mathcal{Q}^{o}_{20} \triangleq P^{o}_{e2}G_2 \quad . \tag{5.3-5}$$

In Chapter 4, Section 4.3.1, it was shown how it suffices to consider the first group of inner loops at the maximum values ($k_{11} = b_{11}$, $k_{21} = b_{21}$) of P_{11} , P_{21} sections of Figure 4-1a. Obviously, the situation is the same here, so we need to examine L^{1}_{1} for uncertainties in P_{i2} only at $P_{i1} = P_{i1x}$ (i.e at $k_{i1} = b_{i1}$) for $i = 1,2,3,4$.

Now L^{1}_{1} at $P_{i1} = P_{i1x}$ becomes

$$L^{1}_{1x} = \frac{P^{o}_{2x}G_1}{(1 + H_{30})(1 + L^{o}_2)} = \frac{P^{o}_{2x}G_1}{\mathcal{Q}^{o}_{20}(1 + L^{o}_2)} = \frac{P^{o}_{e2}G_1}{1 + L^{o}_2} = \frac{(L^{o}_2/G_2)}{1 + L^{o}_2}\,G_1 \tag{5.3-6}$$

Equation (5.3-6) is analogous to (3.4-3) of the 2-section cascaded system. The design of L^{o}_{20} is therefore identical to that of the inner loop of the cascaded system. The bounds on the nominal inner loop L^{o}_{20}, such that those on the outer loop L^{o}_{1x} are satisfied, are precisely of the same type as those on $L_{B0} = P_{B0}G_B$ in (3.4-3), so that those on L_0 are satisfied. In our present example, the bounds on L^{o}_{20} (L^{*}_{20}) and L^{o}_{20} (L^{*}_{20}) are shown in Figures 5-3a,b respectively, with

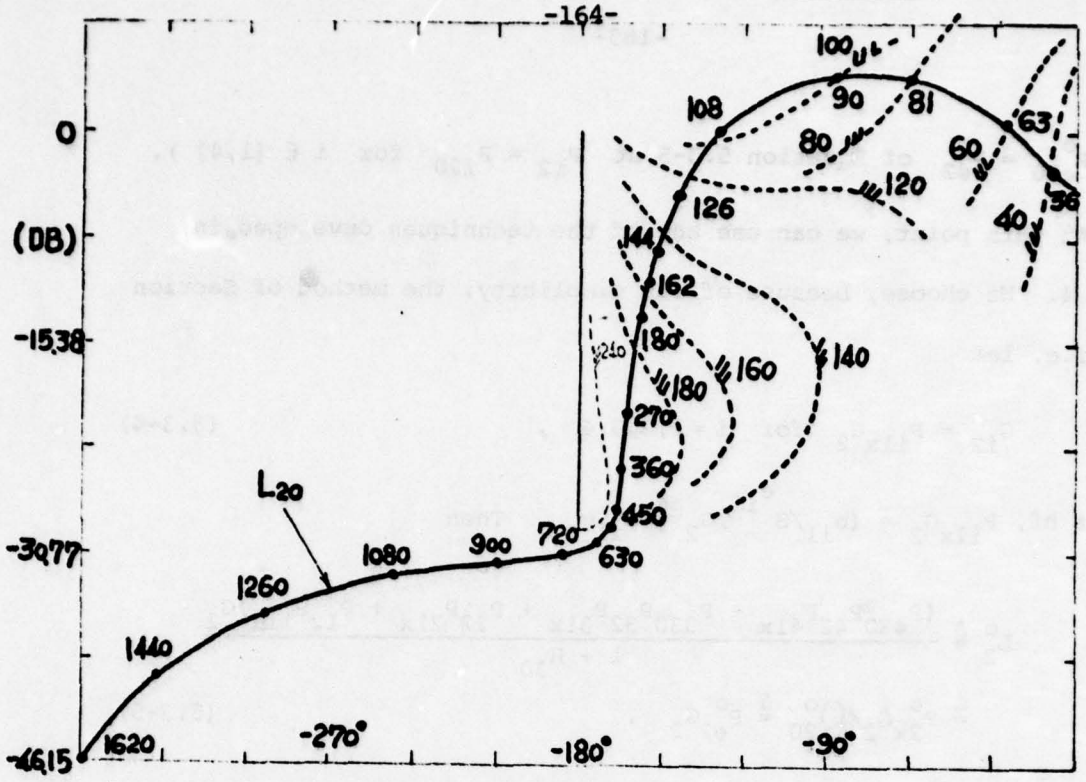

Figure 5-3a. Bounds and loop transmission of L_{20}.

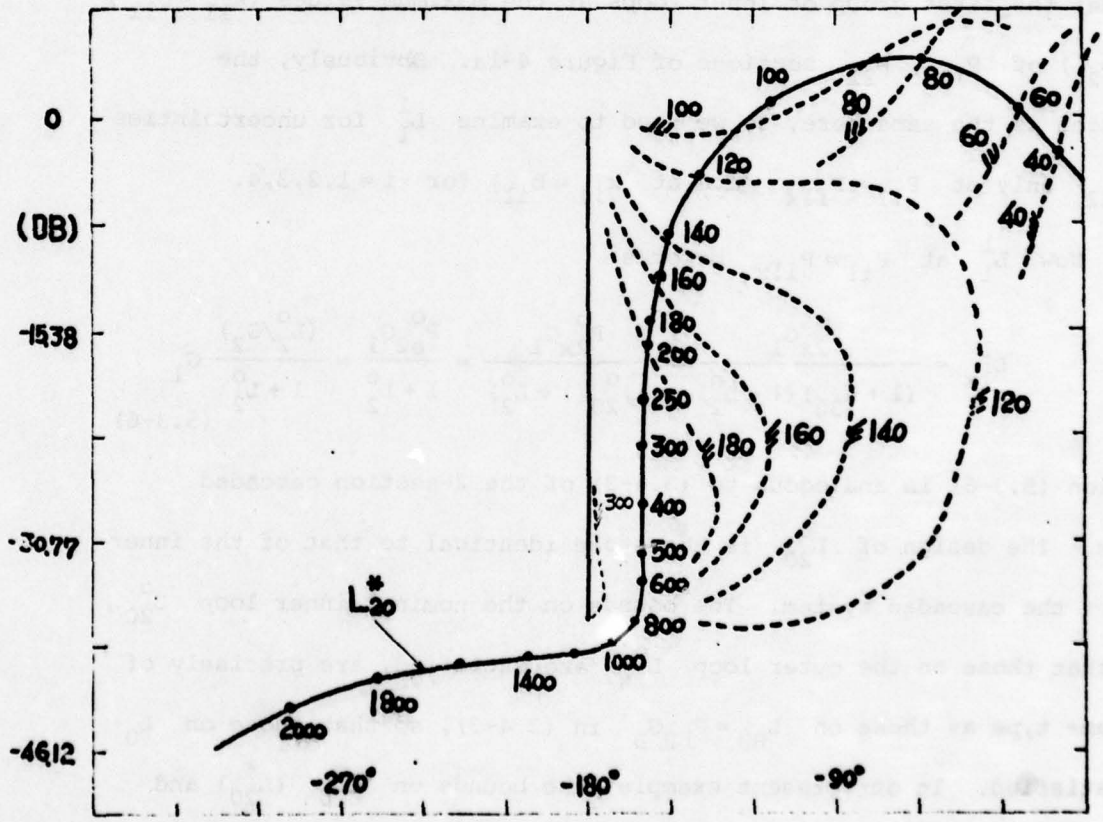

Figure 5-3b. Bounds and loop transmission of L^*_{20}.

$$L_{20}^{*} = \frac{0.59(1 + s/700)}{[1 + 0.4s/90 + (s/90)^2][1 + 0.7s/2000 + (s/2000)^2]^2}$$

$$L_{20} = \frac{0.59(1 + s/500)}{[1 + 0.4s/90 + (s/90)^2][1 + 0.7s/1250 + (s/1250)^2]^2} ,$$

where L_{20}^{*} is used if no inner loops via G_{33}, G_{43} are used, and L_{20}^{o} is used if inner loops via G_{33}, G_{43} are used. The Bode plots of L_{20}^{*}, L_{20}^{o} are also shown in Figure 5-2b. The noise effects at plant input X at nominal plant values for using L_{20}^{*} or L_{20} are shown in Figure 5-5, denoted as $\left|\frac{X}{N_{12}}\right|^2_{II}$, $\left|\frac{X}{N_{12}}\right|^2_{III}$ respectively.

5.3.2. Design of Second Group of Inner Loops.

The function of second group of inner loops via $G_{12}, G_{22}, \ldots, G_{m2}$ in Figure 5-1a is to handle the uncertainties in $P_{12}, P_{22}, \ldots, P_{m2}$. Therefore, in Equation 5.2-3b replace the P_{i30} by P_{i3}, $i = 1, \ldots, m$. Again, as in Section 4.3.1, we need consider the uncertainties of P_{i3} only at the maximum values of P_{ij}, $j < 3$, i.e. at P_{ijx} (corresponding to $k_{ij} = b_{ij}$). Following again, because of its greater simplicity, the design philosophy of Chapter 4, Section 4.3.1 (note that we can switch philosophies at any stage), let

$$G_{i3} = P_{i2x} P_{i1x} G_3 \quad \text{for } i = 3,4 \text{ of Figure 5-1b.} \qquad (5.3\text{-}7)$$

Then for the structure in Figure 5-1b, the "new" outer loop L_1^2 (originally L_1^1 in 5.3-2a) is now

$$L_1^2 \triangleq \frac{(P_{43}P_{42x}P_{41x} + P_{33}P_{32x}P_{31x} + P_{22x}P_{21x} + P_{12x}P_{11x})G_1}{1 + (P_{43}G_{43} + P_{33}G_{33}) + (P_{43}P_{42x}G_{42} + P_{33}P_{32x}G_{32} + P_{22x}G_{22} + P_{12x}G_{12})} ,$$

from 5.3-7,

$$L_1^2 = \frac{(P_{43}P_{42x}P_{41x}+P_{33}P_{32x}P_{31x}+P_{22x}P_{21x}+P_{12x}P_{11x})G_1}{1+(P_{43}P_{42x}P_{41x}+P_{33}P_{32x}P_{31x})G_3+(P_{43}P_{42x}P_{41x}+P_{33}P_{32x}P_{31x}+P_{22x}P_{21x}+P_{12x}P_{11x})G_2}$$

$$= \frac{P_{e2}^1 \cdot G_2}{(1+P_{e2}^1 \cdot G_2)} \frac{G_1}{G_2} = \frac{L_2^1}{1+L_2^1} \frac{G_1}{G_2} \qquad (5.3\text{-}8)$$

with $$L_2^1 \triangleq P_{e2}^1 \cdot G_2 \qquad (5.3\text{-}9a,b)$$

$$P_{e2}^1 \triangleq \frac{P_{43}P_{42x}P_{41x} + P_{33}P_{32x}P_{31x} + P_{22x}P_{21x} + P_{12x}P_{11x}}{1 + (P_{43}P_{42x}P_{41x} + P_{33}P_{32x}P_{31x})G_3}$$

Compare (5.3-8) with (5.3-6). If L_2^1 (with effective plant P_{e2}^1) satisfies the bounds on L_2^o, then L_1^2 also satisfies the bounds of L_{1x}^1. The problem is to choose G_3 to accomplish this. Let

$$L_3 \triangleq (P_{43}P_{42x}P_{41x} + P_{33}P_{32x}P_{31x})G_3 \triangleq P_{3x}^o G_3 = P_{e3} \cdot G_3$$

with $$P_{e30} \triangleq (P_{430}P_{42x}P_{41x} + P_{330}P_{32x}P_{31x}) \quad . \qquad (5.3\text{-}10a,b)$$

We must choose G_3 (or $L_{30} = P_{e30}G_3$) such that $\{L_2^1\} \subseteq \{L_2^o\}$, $\forall P_{43}, P_{33}$. Let $\lambda_3 = P_{e3}^o/P_{e30}^o$, and $L_3 = P_{e3}G_3$, then

$$L_2^1 = P_{e2}^1 G_2 = \left[\frac{P_{e3} + (P_{22x}P_{21x} + P_{12x}P_{11x})}{1 + P_{e3}G_3}\right] G_2$$

$$= \frac{\lambda_3 P_{e30} + (P_{22x}P_{21x} + P_{12x}P_{11x})}{1 + \lambda_3 L_{30}} G_2 \qquad (5.3\text{-}11)$$

$$-\frac{X}{N_{i3}} = \frac{G_{i3}}{1 + H_{30} + H_{20}^o + P_{10}G_1} = \frac{P_{i2x}P_{i1x}L_{30}/P_{3x0}^o}{(1+L_{30})(1+L_{20}^o)(1+L_{10}^o)} \qquad (5.3\text{-}12)$$

with $P_{e30} = P_{e3}$ of 5.3-10a at $P_{43} = P_{430}$, $P_{33} = P_{330}$.

Equation (5.3-11) is precisely the same as Equation (2.3-2) of the first inner loop design of triangular structure in Chapter 2,

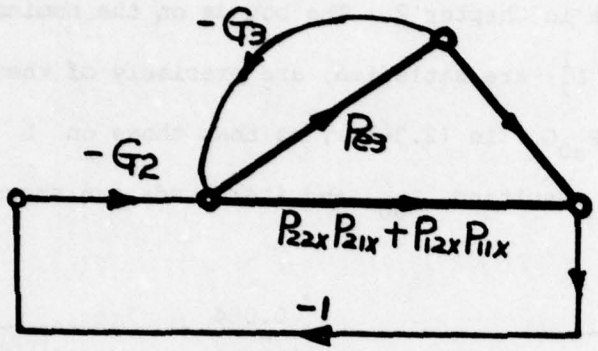

Figure 5-4a. An equivalent structure of Equation (5.3-11).

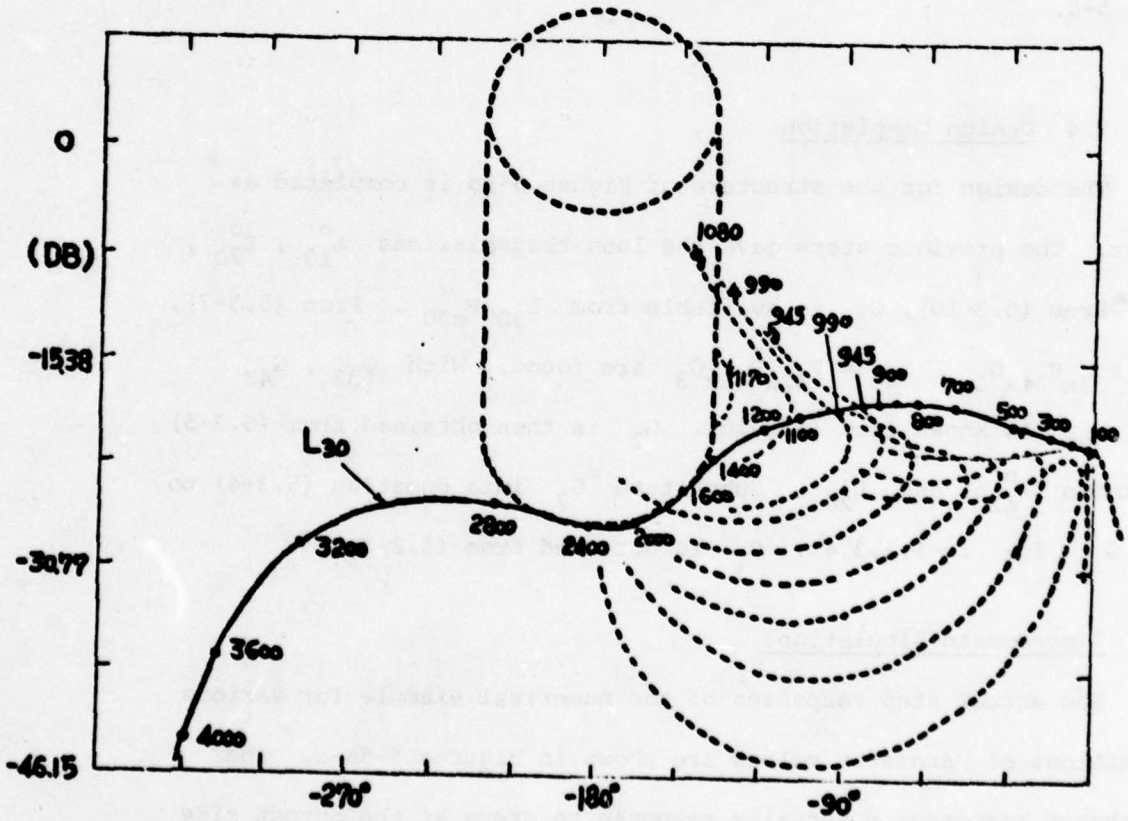

Figure 5-4b. Bounds and loop transmission of L_{30}.

which is redrawn here as Figure 5-4a. The design of L_{30} of (5.3-10) is therefore identical to that of the first inner loop design of the triangular structure in Chapter 2. The bounds on the nominal L_{30}, such that those on L_2^1 are satisfied, are precisely of the same type as those on $L_{10} = P_{a0}G_1$ in (2.3-1b), so that those on L there are satisfied. The resulting L_{30} and its bounds are shown in Figure 5-4b, with

$$L_{30} = \frac{0.084}{[1 + 0.8s/1000 + (s/1000)^2][1 + 0.2s/3000 + (s/3000)^2]^2}$$

The Bode plot of L_{30} is also shown in Figure 5-2b. The noise effect at plant input X at nominal plant value due to N_{33} is shown in Figure 5-5.

5.4 Design Completion

The design for the structure of Figure 5-1b is completed as follows. The previous steps gave the loop transmissions L_{10}^o, L_{20}^o, L_{30}^o. From (5.3-10), G_3 is available from L_{30}/P_{e30}. From (5.3-7), $G_{33} = P_{32x}P_{31x}G_3$, $G_{43} = P_{42x}P_{41x}G_3$ are found. With G_{33}, G_{43} known, H_{30} is known from (5.3-1c). G_2 is then obtained from (5.3-5) from known P_{e20}^o and L_{20}^o. Substitute G_2 into equation (5.3-4) to find G_{i2} for $i = 1,2,3,4$. G_1 is obtained from (5.2-3c).

Time-Domain Simulation.

The actual step responses of the numerical example for various combinations of parameter values are shown in Figures 5-6a-d. The disturbance responses — actually response to steps at the output side of the prefilter, are shown in Figure 5-7a-c.

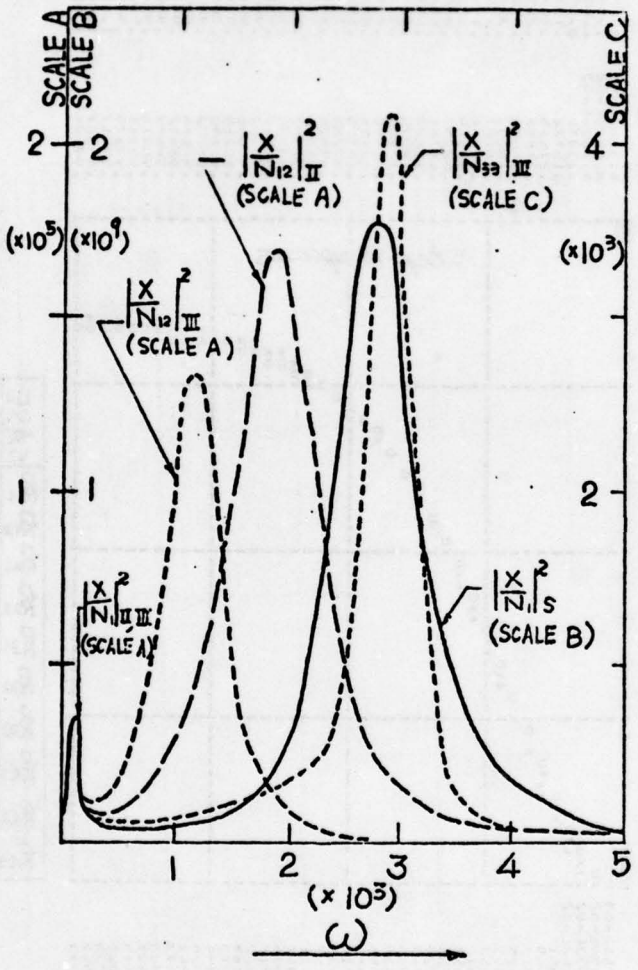

Figure 5-5. Sensor noise effects at plant input x — arithmetic scale.

Figure 5-6a. Simulation results of step response.

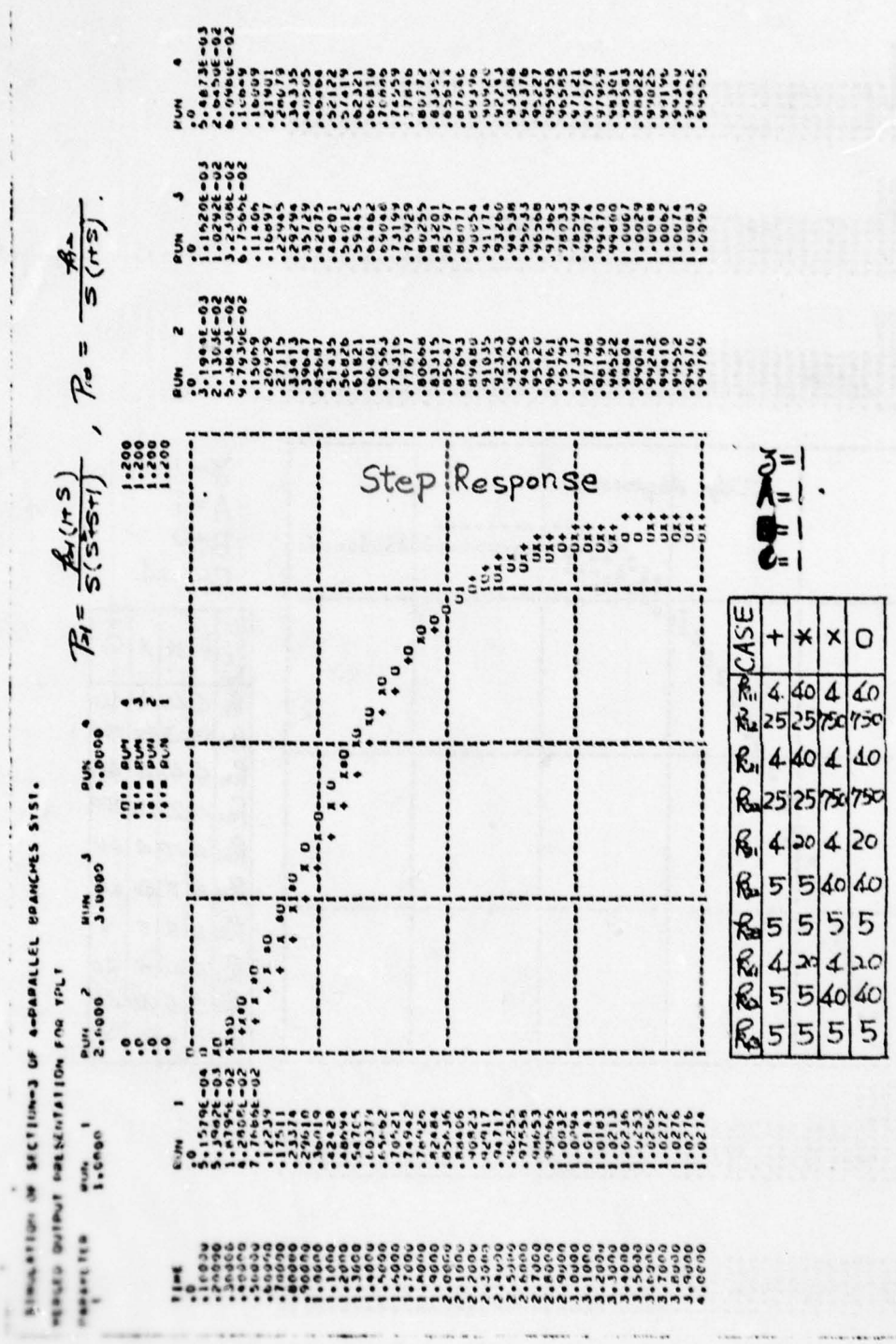

Figure 5-6b. Simulation results of step response.

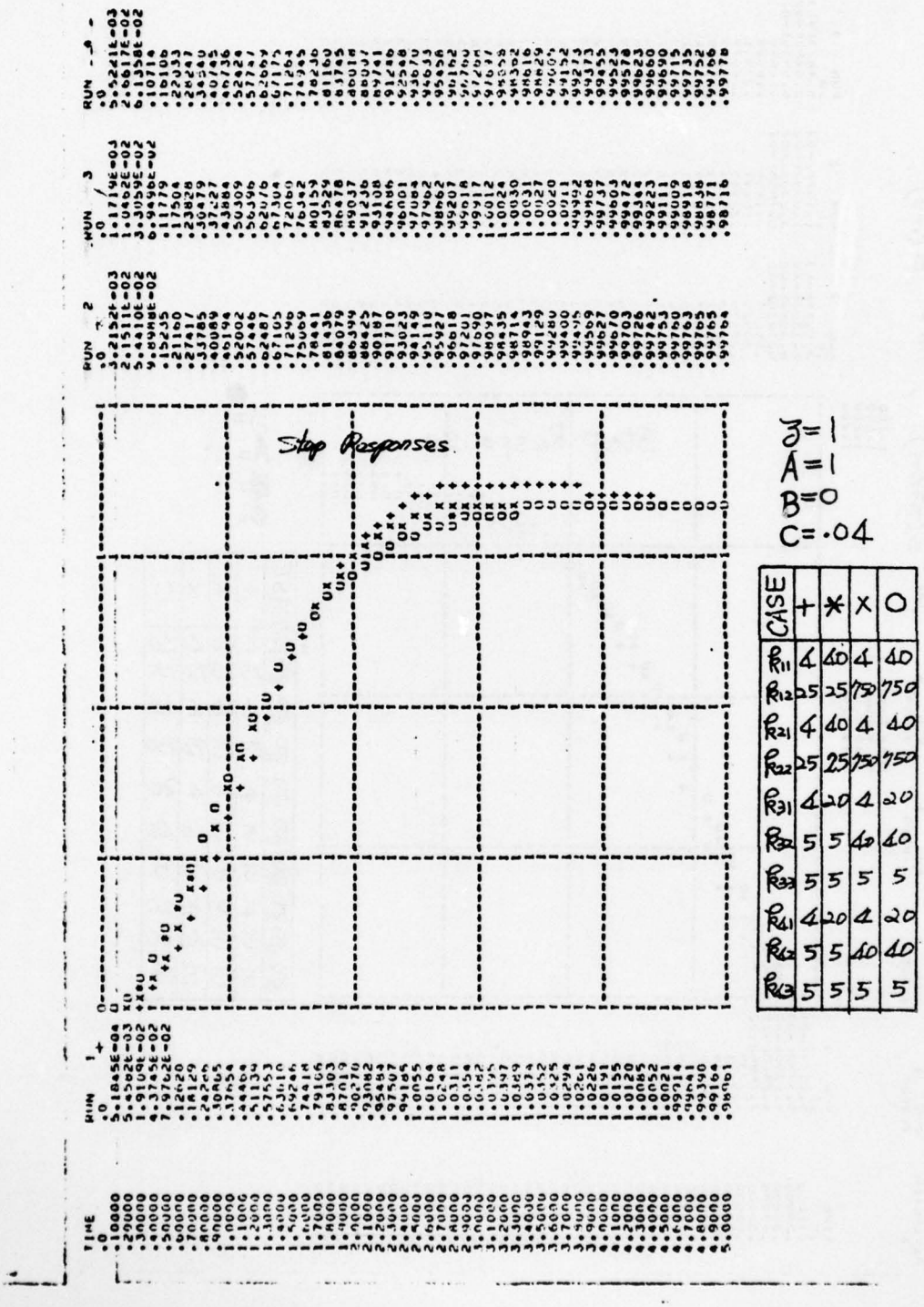

Figure 5-6c. Simulation results of step response.

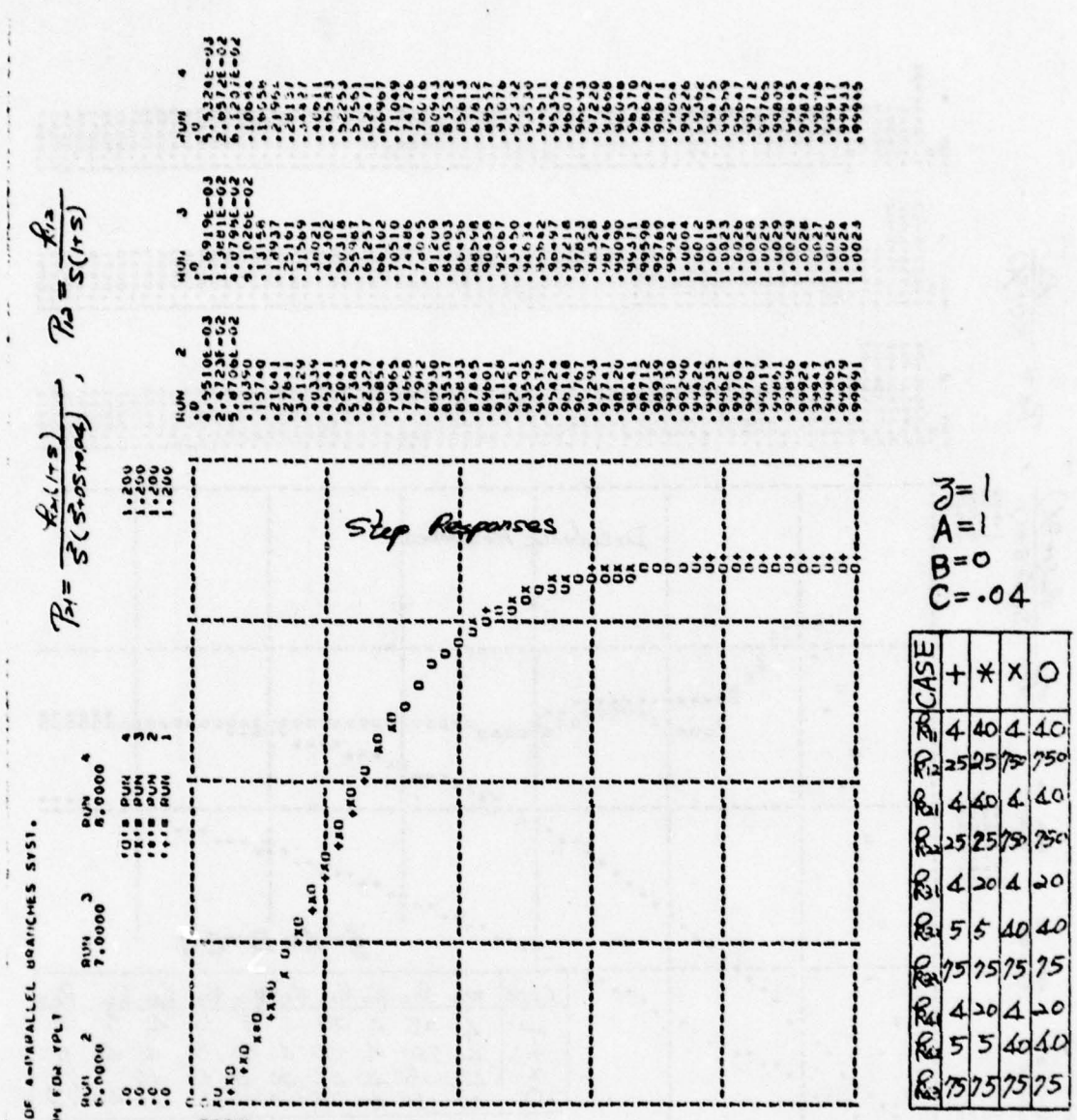

CASE	+	*	X	O
R_{21}	4	40	4	40
R_{12}	25	25	75	750
R_{21}	4	40	4	40
R_{22}	25	25	75	750
R_{31}	4	20	4	20
R_{32}	5	5	40	40
R_{33}	75	75	75	75
R_{41}	4	20	4	20
R_{42}	5	5	40	40
R_{43}	75	75	75	75

Figure 5-6d. Simulation results of step response.

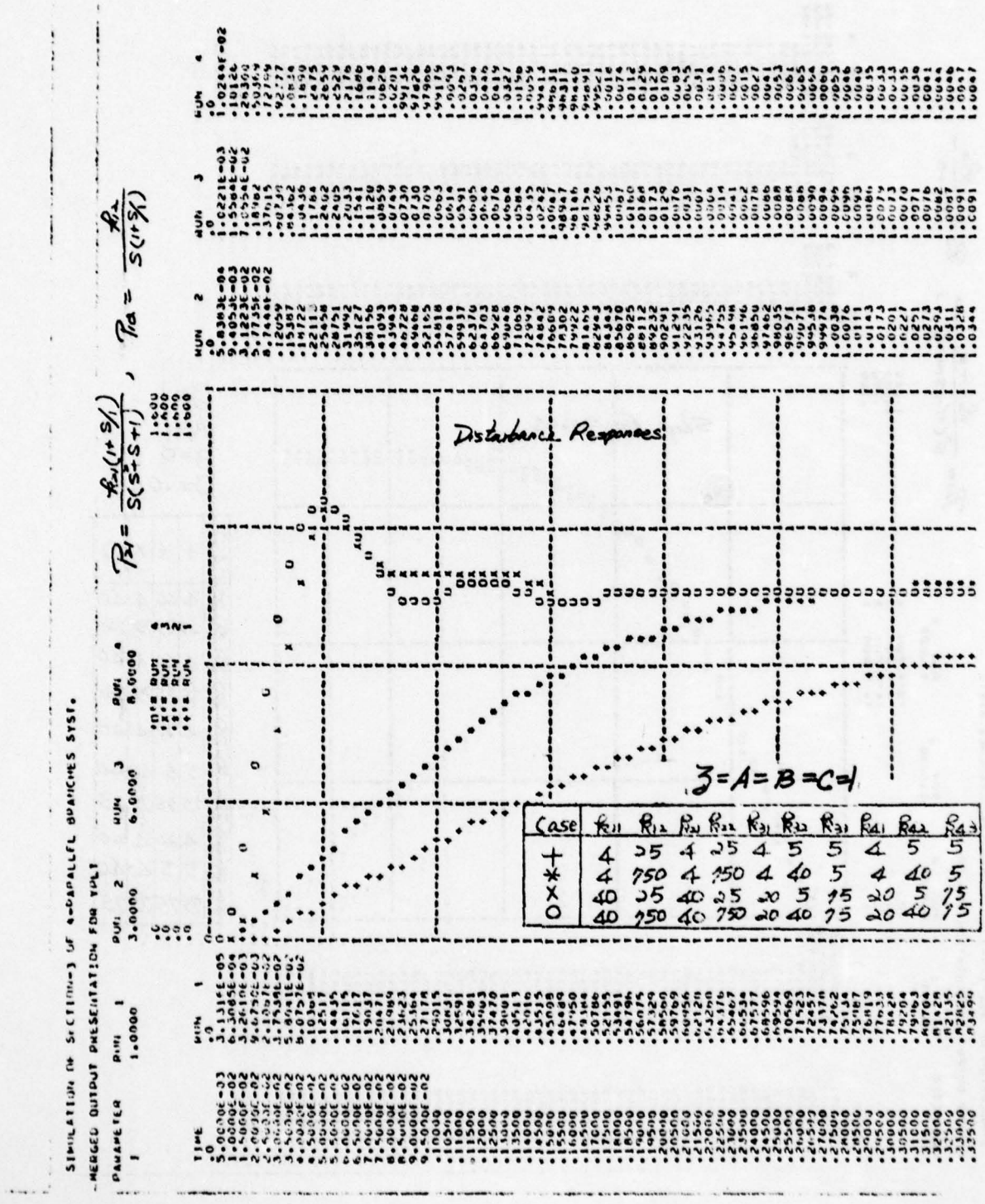

Figure 5-7a. Simulation results of disturbance response.

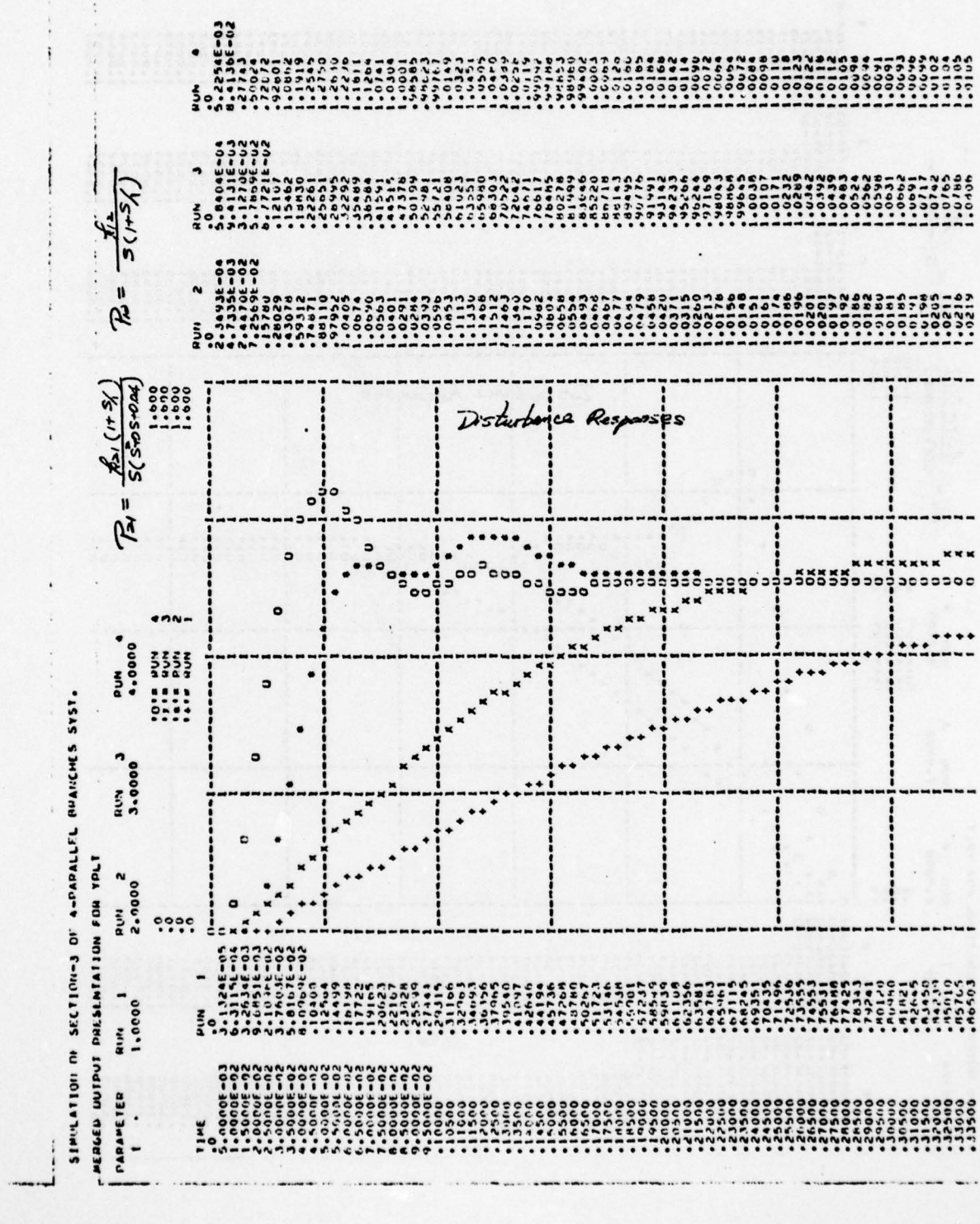

Figure 5-7b. Simulation results of disturbance response (same parameter set as Figure 5-6c).

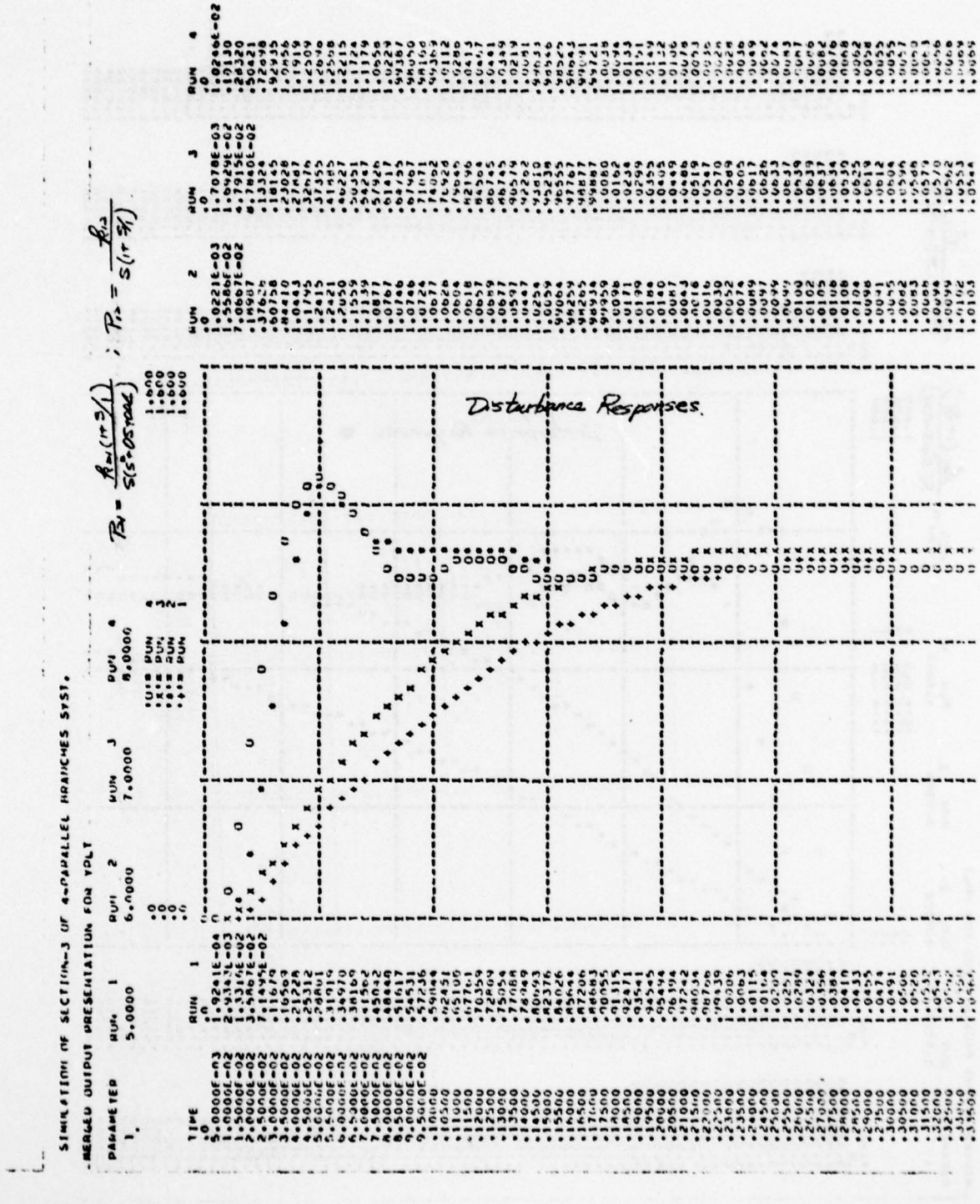

Figure 5-7c. Simulation results of disturbance response (same parameter set as Figure 5-6d).

5.5 Design Perspective

It is very important that one can get good perspective of the design, without performing the detailed design. Since the design philosophy of each loop, as shown in previous sections, is the same as either cascade (in Chapter 1) problem or the problem of Chapter 2, the design perspectives in those two chapters are applicable. Figure 5-8 shows those loops obtained from design perspective, they are in excellent agreement with those obtained from detailed design shown in Figure 5-2b.

5.6 Summary of Design Procedure for General Structure, Based on the Design Philosophy of Chapter 4, Section 4.3.1.

(1) Design the outer loop as in the previous chapters.

(2) Choose $G_{12} = P_{11x}G_2$, $G_{i2} = P_{ilx}G_2$, etc. Define L_2^o in a manner similar to (5.3-5). The design of L_{20}^o is the same as that of the first inner loop in the cascade problem, for which the solution is known. Similarly, choose $G_{i3} = P_{i2x}P_{ilx}G_3$ and define L_3^o as in 5.3-10 (in the example, the process terminated there, so was denoted as L_3). The design of L_{30}^o is equivalent to that of the second inner loop in the cascade design problem, for which the solution is known. This process continues up to n_a , the minimum value of n_i , $i = 1,2,\ldots,m$ in Figure 5-1a, i.e. until at least one of the m branches has been exhausted.

(3) At this point the cascade design philosophy is no longer valid, but by continuing in the same manner the design philosophy of Figure 2-1 (or Figure 5-4a) is henceforth valid step by step, until the last step at the maximum value of n_b of the n_i , $i = 1,2,\ldots,m$.

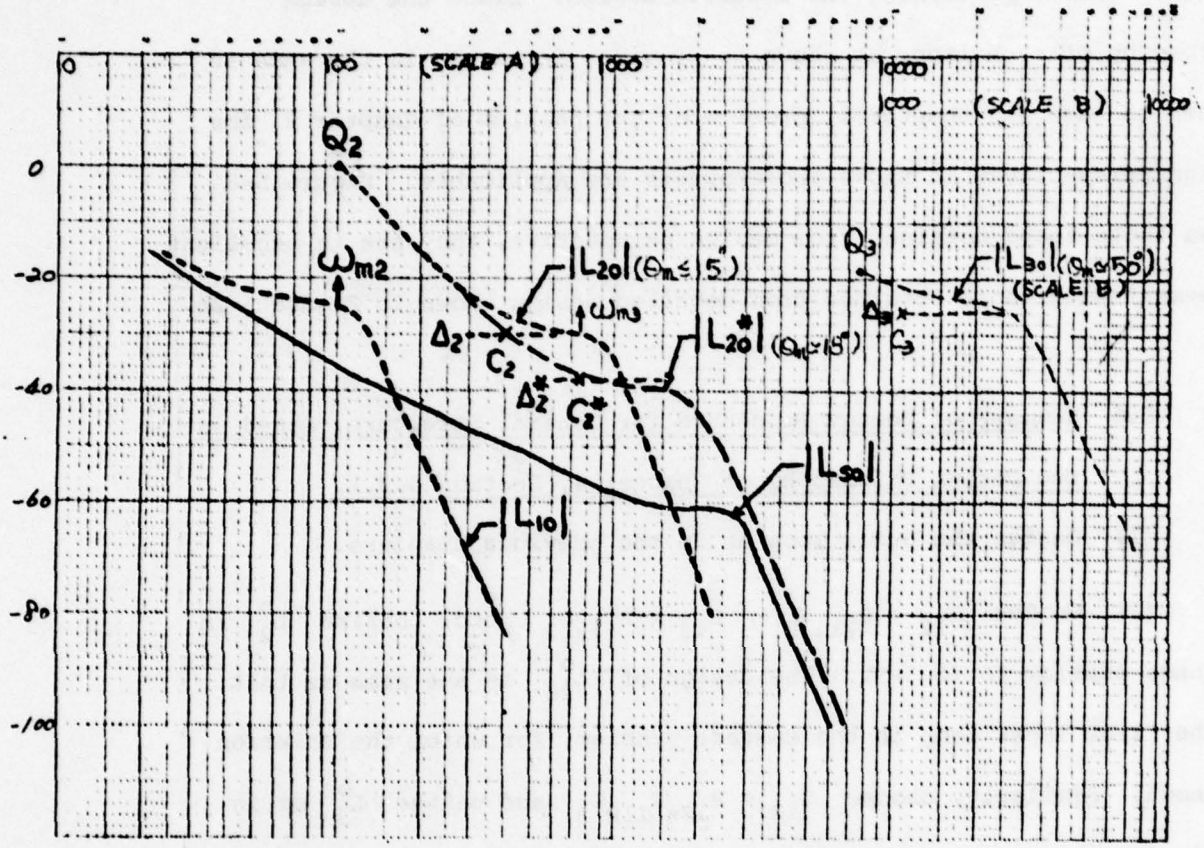

Figure 5-8. Perspective designs.

Suppose for example in Figure 5-1b, there existed an additional section P_{34}, permitting feedback to X via G_{34}. The L_2^1 in (5.3-9) will then be

$$L_2^1 = \frac{[P_{43}P_{42x}P_{41x} + P_{340}P_{33}P_{32x}P_{31x} + P_{22x}P_{21x} + P_{12x}P_{11x}]}{(1+P_{340}G_{34})\left[1 + \frac{(P_{43}P_{42x}P_{41x} + P_{340}P_{33}P_{32x}P_{31x})G_3}{1+P_{340}G_{34}}\right]} G_2 \tag{5.6-1}$$

Let $$L_3^o \triangleq \frac{P_{43}P_{42x}P_{41x} + P_{340}P_{33}P_{32x}P_{31x}}{1+P_{340}G_{34}} G_3 \triangleq \frac{P_{3x}^o}{\Delta_{30}^o} G_3 \triangleq P_{e3}^o G_3 \tag{5.6-2}$$

and $\lambda_3^o = P_{e3}^o/P_{e30}^o$, then

$$L_2^1 = \frac{P_{e3}^o + (P_{22x}P_{21x} + P_{12x}P_{11x})/\Delta_{30}^o}{1+P_{e3}^o G_3} G_2$$

$$= \frac{\lambda_3^o P_{e30}^o + (P_{22x}P_{21x} + P_{12x}P_{11x})/\Delta_{30}^o}{1+\lambda_3^o L_{30}^o} G_2 \tag{5.6-3}$$

$$-\frac{X}{N_{i3}} = \frac{P_{i2x}P_{i1x}L_{30}^o/P_{3x0}^o}{(1+L_{30}^o)(1+L_{20}^o)(1+L_{10}^o)} \quad . \tag{5.6-4}$$

The design of L_{30}^o is exactly the same as the first inner loop design of Chapter 2, as discussed in Section 5.3.2, except the definition L_3^o of (5.6-2) is different from L_3 of (5.3-11).

For the next step of allowing the uncertainty in the additional plant P_{34}, let

$$G_{34} = P_{33x}P_{32x}P_{31x}G_4 \tag{5.6-5}$$

$$P_{3x}^1 = P_{43}P_{42x}P_{41x} + P_{34}P_{33}P_{32x}P_{31x} \quad , \quad P_{e3}^1 = P_{3x}^1/\Delta_{30}^o$$

$$P_{4x}^o = P_{34}P_{33x}P_{32x}P_{31x} \quad , \quad P_{e4}^o = P_{4x}^o/\Delta_{40}^o \quad , \quad L_4 = P_{e4}^o G_4$$

$$\lambda_3^1 = P_{e3}^1/P_{e30}^1 \quad , \quad \lambda_4 = P_{e4}^o/P_{e40}^o = P_{34}/P_{340} \tag{5.6-6a-g}$$

then
$$L_2^2 = \frac{P_{3x}^1 + (P_{22x}P_{21x} + P_{12x}P_{11x})}{1 + \lambda_4 L_{40} + \lambda^1 L_{30}^o (1 + L_{40})} G_2$$

$$= \frac{\lambda_3^1 P_{e30}^1 + (P_{22x}P_{21x} + P_{12x}P_{11x})}{1 + \lambda_4 L_{40} + \lambda_3^1 L_{30}^o (1 + L_{40})} G_2 \qquad (5.6\text{-}7a,b)$$

$$-\frac{X}{N_{i4}} = \frac{P_{i3x}P_{i2x}P_{i1x}L_{40}/P_{4x0}^o}{(1 + L_{40})(1 + L_{30}^o)(1 + L_{20}^o)(1 + L_{10}^o)} \qquad (5.6\text{-}8)$$

Equation (5.6-7) is analogous to (2.3-5). So the design of L_{40} is exactly the same as the second inner loop design of Chapter 2.

5.7 Summary of Design Procedure for General Structure, Based on the Design Philosophy of Chapter 4, Sections 4.3.2-4.

The various techniques of Chapter 4 can be used until one of m branches is exhausted. But thereafter, only the triangular technique of Chapter 2 can be used. Design perspective allows the designer to quickly decide which philosophy to use in the first part. For example, if $N_{42} \gg N_{12}, N_{22}, N_{32}$, one wants to try the philosophy of Sections 4.3.2-4 at the very first inner loop stage. Let

$$b_{41}g_{12} - b_{11}g_{42} = (b_{11}/b_{42})y_{12}$$

$$b_{41}g_{22} - b_{21}g_{42} = (b_{21}/b_{42})y_{22} \qquad (5.7\text{-}1a\text{-}c)$$

$$b_{41}g_{32} - b_{31}g_{42} = (b_{31}/b_{42})y_{32}$$

similar to Equation (4.3-10). Then L_1^1 in (5.3-2a) can be written as

$$L_1^1 = \frac{P_2^o G_1}{1 + H_{30} + H_2^o} = \frac{P_2^o G_1}{\Omega_{20}^o + H_2^o} \qquad (5.7\text{-}2)$$

Suppose $N_{12} \simeq N_{22} \simeq N_{32}$, let $y_{i2} = y(\omega) = y$ for $i = 1,2,3$, and substitute (5.7-1) into the denominator of (5.7-2),

$$\mathcal{D}^o_{20} + H^o_2 = \mathcal{D}^o_{20} + a_{43}k_{42}g_{42} + a_{33}\frac{k_{32}}{b_{41}}\left[b_{31}g_{42} + \frac{b_{31}}{b_{42}}y\right]$$

$$+ \frac{k_{22}}{b_{41}}\left[b_{21}g_{42} + \frac{b_{21}}{b_{42}}y\right] + \frac{k_{12}}{b_{41}}\left[b_{11}g_{42} + \frac{b_{11}}{b_{42}}y\right]$$

$$= \frac{1}{b_{41}b_{42}}\{b_{41}b_{42}\mathcal{D}^o_{20} + y\overbrace{[a_{33}k_{32}b_{31} + k_{22}b_{21} + k_{12}b_{11}]}^{K_2}$$

$$+ b_{42}g_{42}[a_{43}k_{42}b_{41} + \underbrace{a_{33}k_{32}b_{31} + k_{22}b_{21} + k_{12}b_{11}}_{K_2}]\}$$

$$\triangleq \frac{1}{b_{41}b_{42}}\{b_{41}b_{42}\mathcal{D}^o_{20} + yK_2 + b_{42}g_{42}(a_{43}k_{42}b_{41} + K_2)\}$$

Replace K_2 by its nominal value K_{20} , since y will handle the uncertainty in K_2 , so

$$L^1_1(y) = \frac{b_{41}P^o_{42e}g_1}{1 + P^o_{42e}g_{42}} \qquad (5.7\text{-}3)$$

where $$P^o_{42e} = \frac{b_{42}[a_{43}k_{42}b_{41} + K_{20}]}{b_{41}b_{42}\mathcal{D}^o_{20} + y \cdot K_{20}} \quad , \quad L^o_{42} = P^o_{42e} \cdot g_{42} \qquad (5.7\text{-}4a,b)$$

with $K_{20} = K_2$ at $k_{i2} = a_{i2}$, $i = 1,2,3$.

In view of (5.7-3), the loop L^o_{42} of (5.7-4b) is designed analogously to the inner loop design of a 2-section cascade system with P_B of Figure 4-3 analogous to P^o_{42e} of (5.7-4a).

The function $y(\omega)$ is next designed to handle the uncertainty in K_2 ignored by L^o_{42} , such that

$$P^1_{42e} \triangleq \frac{b_{42}[a_{43}k_{42}b_{41} + K_2]}{b_{41}b_{42}\Omega^o_{20} + K_2 y} \subseteq P^o_{42e} \qquad (5.7\text{-}5)$$

Rewrite

$$P^1_{42e} = \frac{\frac{a_{43}k_{42}}{\Omega^o_{20}} + \frac{K_2}{b_{41}\Omega^o_{20}}}{1 + \frac{K_2}{b_{41}b_{42}\Omega^o_{20}}\, y} \qquad (5.7\text{-}6)$$

and define

$$L_y \triangleq \frac{K_2}{b_{41}b_{42}\Omega^o_{20}}\, y \qquad (5.7\text{-}7)$$

Thus, the design procedure for the loop L_y in (5.7-7), such that (5.7-5) is satisfied, is precisely the same as that of the first inner loop in the triangular structure in Chapter 2. The design perspective there also applies.

The procedure is the same if $N_{42} \simeq N_{12} >> N_{22} \simeq N_{32}$, instead of $N_{42} >> N_{12} \simeq N_{22} \simeq N_{32}$, except now take $y_{12} = 0$ in (5.7-1a), and $K_2 = a_{33}k_{32}b_{31} + k_{22}b_{21}$.

REFERENCES

[B1] Bode, H., Network Analysis and Feedback Amplifier Design (New York: Van Nostrand).

[B2] Bhattacharyya, S., The structure of robust observers, IEEE Trans. Autom. Control 21, pp. 581-588, 1976.

[D1] Davidson, E., The robust control of a servomechanism problem for linear time-invariant multivariable systems, IEEE Trans. Autom. Control 21, pp. 25-34, 1976.

[H1] Horowitz, I., A synthesis theory for linear time-varying feedback systems with plant uncertainty, IEEE Trans., AC-20, pp. 454-464, Aug. 1975.

[H2] Horowitz, I., Synthesis of feedback systems with nonlinear time-varying uncertain plants to satisfy quantitative performance specifications, Proceedings of IEEE, 64, No. 1, Jan. 1976.

[H3] Horowitz, I. and Sidi, M., Synthesis of feedback systems with large plant ignorance for prescribed time domain tolerances, Int. J. Control, 16, pp. 287-309, 1972.

[H4] Horowitz, I. and Sidi, M., Synthesis of cascaded multiple-loop feedback systems with large plant parameter ignorance, Automatica, 9, pp. 589-600, 1973.

[H5] Horowitz, I. and Rosenbaum, P., Nonlinear design for cost of feedback reduction in systems with large parameter uncertainty, Int. J. Control, 21, pp. 977-1001, 1975.

[H6] Horowitz, I. and Sidi, M., Optimum Synthesis of non-minimum phase feedback systems with plant uncertainty, Int. J. Control, 27, No. 3, pp. 361-386.

[H7] Horowitz, I., Synthesis of Feedback Systems, Academic Press, 1963.

[H8] Horowitz, I., Optimum loop transfer function in single-loop minimum-phase feedback systems, Int. J. Control, 18, pp. 97-113, 1973.

[H9] Horowitz, I., Smay, J. and Shapiro, A., A synthesis theory for self-oscillating adaptive systems (SOAS), Automatica, 10, pp. 381-392, 1974.

[H10] Horowitz, I., Smay, J. and Shapiro, A., A synthesis theory for the externally excited adaptive system (EEAS), IEEE Trans. AC-19, No. 2, April, 1974.

[H11] Horowitz, I., Synthesis of feedback systems with nonlinear time-varying uncertain plants to satisfy quantitative performance specifications, Proc. IEEE, pp. 123-130, 1976.

[H12] Horowitz, I. and Shaked, U., Superiority of transfer function methods over state variable methods in linear time invariant feedback synthesis, IEEE Trans. Autom. Control 20, pp. 84-97, 1975.

[H13] Horowitz, I. and Wang, T.S., A synthesis theory for a class of multiple-loop systems with plant uncertainty, Int. J. Control, to appear.

[K1] Krishnan, K.R. and Cruickshank, A., Frequency domain design of feedback systems for specified insensitivity of time-domain response to parameter variation, Int. J. Control, 25, pp. 609-620, 1977.

[K2] Krishnan, K.R. and Horowitz, I., Synthesis of a non-linear feedback system with significant plant-ignorance for prescribed system tolerances, Int. J. Control, 19, No. 4, pp. 689-706, 1974.

[L1] Luenberger, D., Observers for multivariable systems, IEEE Trans. Autom. Control 11, pp. 190-197, 1966.

AD-A072 644 COLORADO UNIV BOULDER DEPT OF ELECTRICAL ENGINEERING F/G 13/8
QUANTITATIVE SYNTHESIS OF MULTIPLE LOOP FEEDBACK SYSTEMS WITH L--ETC(U)
JUN 79 T WANG, I HOROWITZ AFOSR-76-2946

UNCLASSIFIED AFOSR-TR-79-0880 NL

3 OF 3
AD A072644

END
DATE FILMED
9-79
DDC

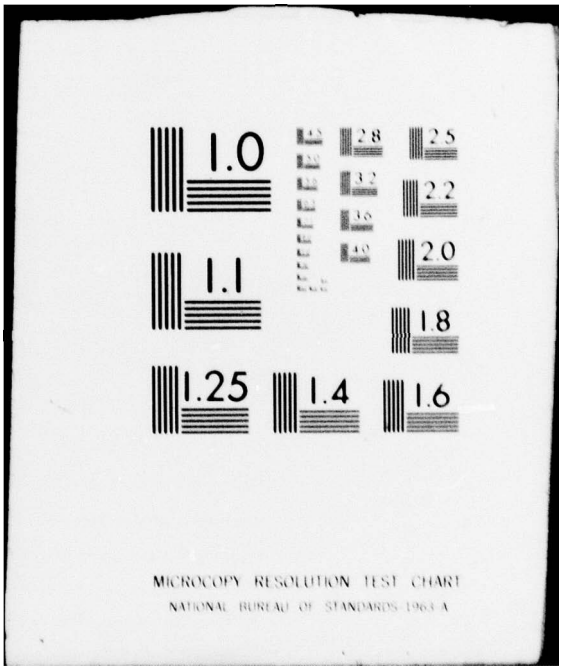
1.0
1.1
1.25
1.4
1.6
2.8
3.2
3.6
4.0
2.5
2.2
2.0
1.8
MICROCOPY RESOLUTION TEST CHART
NATIONAL BUREAU OF STANDARDS 1963-A

[O1] Ostgaard, M., Stear, E. and Gregory, P., Agard Flight Mechanics Tech. Report Sec. III, July 1962, Paris, France.

[P1] Pearson, J., Shields, R. and Staats, Jr., P., Robust solutions to linear multivariable control problems, IEEE Trans. Autom. Control 19, pp. 508-517, 1974.

[P2] Popov, V.M., Hyperstability and optimality of automatic system with several control functions, Rev. Roum. Sci. Tech., Ser. Electrotech. Ener. 9, pp. 629-690, 1964.

[R1] Rosenbaum, P., Reduction of the cost of feedback in systems with large parameter uncertainty, Ph.D. Thesis, Weizmann Institute of Science, Israel, 1977.

[S1] Sidi, M., Synthesis of feedback systems with large plant ignorance for prescribed time-domain tolerance, Ph.D. dissertion, Dept. Applied Math., Weizmann Institute of Science, Rehovot, Israel.

[S2] Safanov, M. and Athans, M., Gain and phase margin for multiloop LQG regulators, IEEE Trans. Autom. Control 22, pp. 173-179, 1977.

[S3] Shaked, U., Horowitz, I. and Golde, S., Synthesis of multivariable, basically non-interacting systems with significant plant uncertainty, Automatica, 12, pp. 61-73, 1976.

[S4] Simon, J. and Mitter, S., Synthesis of transfer function matrices with invariant zeros, IEEE Trans. Autom. Control 14, pp. 420-421, 1969.

[W1] Wang, B.C., Synthesis of Multiple Loop Feedback Systems with Plant Modification, Ph.D. Thesis, University of Colorado, Boulder, Colorado, 1978.

[W2] Wonham, W.M., On pole assignment in multi-input controllable linear systems, IEEE Trans. Autom. Control 12, pp. 660-665, 1967.